STUDIES ON UTILIZATION OF NEW FLUORESCENT COMPOUNDS IN CHIRAL DISCRIMINATION

A THESIS SUBMITTED TO
THE GRADUATE SCHOOL OF NATURAL AND APPLIED SCIENCES
OF
MIDDLE EAST TECHNICAL UNIVERSITY

BY

DUYGU TAN

IN PARTIAL FULFILLMENT OF THE REQUIREMENTS
FOR
THE DEGREE OF DOCTOR OF PHILOSOPHY
IN
CHEMISTRY

JUNE 2020

Approval of the thesis:

STUDIES ON UTILIZATION OF NEW FLUORESCENT COMPOUNDS IN CHIRAL DISCRIMINATION

submitted by **DUYGU TAN** in partial fulfillment of the requirements for the degree of **Doctor of Philosophy in Chemistry, Middle East Technical University** by,

Prof. Dr. Halil Kalıpçılar
Dean, Graduate School of **Natural and Applied Sciences** _____

Prof. Dr. Cihangir Tanyeli
Head of the Department, **Chemistry** _____

Assoc. Prof. Dr. Akın Akdağ
Supervisor, **Chemistry, METU** _____

Prof. Dr. Özdemir Doğan
Co-Supervisor, **Chemistry, METU** _____

Examining Committee Members:

Prof. Dr. Cihangir Tanyeli
Chemistry, METU _____

Assoc. Prof. Dr. Akın Akdağ
Chemistry, METU _____

Prof. Dr. Metin Zora
Chemistry, METU _____

Prof. Dr. Atilla Cihaner
Chemical Engineering, Atılım Uni. _____

Prof. Dr. Adnan Bulut
Chemistry, Kırıkkale Uni. _____

Date: 25.06.2020

I hereby declare that all information in this document has been obtained and presented in accordance with academic rules and ethical conduct. I also declare that, as required by these rules and conduct, I have fully cited and referenced all material and results that are not original to this work.

Name, Last name: Duygu Tan

Signature:

ABSTRACT

STUDIES ON UTILIZATION OF NEW FLUORESCENT COMPOUNDS IN CHIRAL DISCRIMINATION

Tan, Duygu
Doctor of Philosophy, Chemistry
Supervisor: Assoc. Prof. Dr. Akın Akdağ
Co-Supervisor: Prof. Dr. Özdemir Doğan

June 2020, 250 pages

In modern age, time is becoming an increasingly valuable parameter. Advances in science and technology are triggered by using time more effectively. The reflection of this in chemistry is towards developing computer-aided setups that allow performing multiple experiments at the same time and developing analysis techniques that can give results within a short time period. For many years, scientists have been trying to modify some spectroscopic techniques (mass, nmr, fluorescence, etc.) to develop alternative methods that will give faster results. Among these techniques, fluorescence spectroscopy is the most remarkable and open to development in recent years. For this purpose, fluorescence spectroscopy is used in various fields such as DNA folding, protein dynamics, drug detection, and enantiomeric excess determination in asymmetric reactions. Among these applications, asymmetric reactions are of great importance for the pharmaceutical industry, as they allow chiral substances to be obtained in high purity. However, a widely used method for the practical determination of the results of such reactions has not yet been developed. Studies on this subject have been growing rapidly in recent years. In this dissertation, in order to contribute to the applications of fluorescence

spectroscopy in the field of chiral recognition, new chiral fluorescence sensors based on coumarin, naphthalene and 7,7,8,8-tetracyanoquinodimethane (TCNQ) were developed and characterized by NMR, HRMS and FTIR techniques. Fluorescence studies have been performed to distinguish tartaric acid, α-methylbenzyl amine, 1-phenyl ethanol and 2-butanol enantiomers with these new fluorescence sensors by fluorescence technique. From these new chiral sensors synthesized, coumarin-derived ones did not show selectivity against any of the above- mentioned substances, while they were successful in sodium and potassium determination and showed selectivity towards sodium. Naphthalene derivative sensor shows affinity for all carboxylic acids; however, it has not been able to separate the enantiomers of those carboxylic acids. Our TCNQ based sensors showed selectivity against α-methylbenzyl amine enantiomers. For all sensors, experimental results were supported by theoretical calculations. This dissertation covers all the details of synthetic, spectroscopic, chromatographic and theoretical studies.

Keywords: Fluorescence spectroscopy, fluorescence sensing, chiral sensing, fluorescence sensors

ÖZ

YENİ FLORESAN BİLEŞİKLERİN KİRAL TANIMADA KULLANILMASI ÜZERİNE ÇALIŞMALAR

Tan, Duygu
Doktora, Kimya
Tez Yöneticisi: Doç. Dr. Akın Akdağ
Ortak Tez Yöneticisi: Prof. Dr. Özdemir Doğan

Haziran 2020, 250 sayfa

Modern çağda zaman giderek daha da kıymetli bir parametre haline gelmektedir. Bilim ve teknolojideki tüm gelişmeler zamanı daha etkili kullanmaya yönelik gerçekleşmektedir. Bunun kimyadaki yansıması ise birçok deneyin aynı anda kurulup takip edilebildiği bilgisayar destekli düzenekler ve kısa zaman dilimi içerisinde sonuç verebilen analiz teknikleri geliştirmek üzerinedir. Bilim insanları uzun yıllardan beri bazı spektroskopik teknikleri (kütle, nmr, floresans vb) daha çabuk sonuç verecek alternatif yöntemler geliştirerek değiştirmeye çalışmaktadır. Floresans spektroskopisi bu teknikler arasında son yıllarda en çok dikkat çeken ve geliştirilmeye en açık olanıdır. Bu amaçla floresans spektroskopisi DNA katlama, protein dinamikleri, ilaç tayini, asimetrik tepkimelerde enantiomerik fazlalık belirleme gibi çeşitli alanlarda kullanılmaktadır. Bu uygulamalar arasında en dikkat çekici olan asimetrik tepkimeler, kiral maddelerin yüksek saflıkta elde edilmesine olanak sağladığından ilaç endüstrisi için çok büyük önem arz etmektedir. Fakat bu tip tepkimelerin sonuçlarının da pratik bir şekilde belirlenmesi için yaygın kullanımı olan bir yöntem henüz geliştirilememiştir. Bu konuda çalışmalar son yıllarda hızla devam etmektedir.

Bu tezde floresans spektroskopisinin kiral tanıma alanındaki uygulamalarına katkıda bulunabilmek amacı ile kumarin, naftalin ve 7,7,8,8-tetrasiyanokuinodimetan (TCNQ) bazlı yeni kiral floresans sensörleri geliştirilmiş ve NMR, HRMS ve FTIR teknikleri ile karakterize edilmiştir. Bu yeni floresans sensörleri ile enantiosaf tartarik asit, α-metilbenzil amin, 1-fenil etanol ve 2-bütanol enantiomerlerini floresans yöntemiyle ayırt edebilmek için çalışmalar yapılmıştır. Sentezlenen bu yeni kiral sensörlerden kumarin türevi olanlar bahsedilen hiçbir maddeye karşı seçicilik göstermez iken sodyum ve potasyum tayini uygulamasında başarılı sonuç vermiş ve sodyuma karşı seçicilik göstermiştir. Naftalin türevi olan sensörümüz karboksilik asitlere karşı ilgi gösterir iken bu karboksilik asitlerin enantiomerlerini ayırmayı başaramamıştır. TCNQ bazlı sensörlerimiz ise α-metilbenzil amin enantiomerlerine karşı seçicilik göstererek ayırmayı başarmıştır. Bütün sensörler için deneysel sonuçlar teorik hesaplamalar ile desteklenmiştir. Bu tez, bahsi geçen tüm sensörlere ait sentetik, spektroskopik ve teorik çalışmalarının tüm detaylarını kapsamaktadır.

Anahtar Kelimeler: Floresans spektroskopisi, floresans tayini, kiral tayin, floresans sensörleri

To my most precious one, İpek

ACKNOWLEDGEMENTS

"A PhD is so much more than a degree. It can break you down into your most vulnerable form, but has the potential to build you back together to become a resilient, determined, humble, and knowledgable researcher. It's not just about getting the degree. It'is about becoming who you are meant to be."

Anonymous

I would like to emphasize my gratitude to my supervisor Assoc. Prof. Dr. Akın Akdağ since he brought me into the position where I am right now. Thanks to him, I learned how to deal with several difficulties that I have faced not only in my PhD studies but also in real life. He has the greatest impact on making me the person who I am today. Herein, I wish to acknowledge him.

I would like to thank my coadvisor Prof. Dr. Özdemir Doğan for his valuable advices and stimulating discussions.

I would like to thank Prof. Dr. Metin Zora and Prof. Dr. Atilla Cihaner since they accepted to be my thesis monitoring commitee members, and Assist. Prof. Dr. Tarık Baytekin as being my former thesis monitoring commitee member.

I would like to thank Prof. Dr. Ahmet Önal since he gave me the opportunity to use spectrofluorometer in his laboratory.

I would like to thank BAP for financial support.

Furthermore, I wish to thank Perihan Öztürk, Gizem Ünay, Sadia Tull Munna, Bengi Şentürk, Ece Ayça Yücel and all other Akın Akdağ Research Group members since they have always created a supportive and warm environment in our laboratory.

My special gratidues go to Asude Çetin. I am so afraid that no matter what I write here about her, it will be incomplete. We have faced with a lot of difficulties and overcome all of them together throughout the years. We "grew up" together with a lot of good memories kept in many beautiful photos that we cannot spare to share

with anyone else. I have also felt the support of Gönül Hızalan Özsoy, Derya Özhava, Nurhan Çiçek and Pelin Paşabeyoğlu behind me, and I really appreciate their valuable friendship.

My most special and deepest appreciations and gratitude are devoted to my family members. Indeed, I am indepted to my mother Sema Aksakal who really strived and fostered me to finish my journey despite many challenges I have faced with. I would like to thank my other family members Turgut Aksakal, Kadir Oğuz Aksakal, Esra Aksakal and my lovely little boy Ege Aksakal for their unconditional supports and being understanding throughout this long time period. I would also like to thank my second family, Necla Tan and İbrahim Tan for their constant moral support. I cannot express my feelings about how they are special to me.

Last but not least, I would like to appreciate the most special ones who have the greatest impact on my life; my lovely husband Serkan Tan and my precious, little girl İpek Tan. Serkan was always by my side and lived every single minute of all obstacles with me, and continued to support me for focusing my passion on what I really desire. İpek has given me an amazing power after which I believe that I can do everything even they initially seem to be impossible. My ultimate aim is to be worthy of their endless love, patience, encouragement, support, etc…, in the absence of which I would do nothing.

TABLE OF CONTENTS

ABSTRACT v

TABLE OF CONTENTS xii

LIST OF TABLES xvii

LIST OF FIGURES xviii

LIST OF ABBREVIATIONS xxiii

LIST OF SYMBOLS xxiv

CHAPTERS……..…1

1 INTRODUCTION 1

1.1 Nature of Light 1

1.1.1 Absorption and Emission of Light 4

1.2 Absorption and Emission Spectra 6

1.3 Selection Rules 7

1.3.1 Fermi's Golden Rule 7

1.3.2 Probabilty of transitions 8

1.4 Luminescence Spectroscopy 10

1.5 Fundamentals of Fluorescence Spectroscopy 12

1.6 Applications of Fluorescence Spectroscopy 13

1.6.1 Clinical Diagnosis 13

2 CHARACTERIZATION OF CHIRAL COMPOUNDS BY FLUORESCENCE SPECTROSCOPY 17

2.1 Chirality 17
2.2 Importance of Chirality 18
3 AIM OF STUDY 25
4 RESULTS AND DISCUSSION 27
4.1 Coumarins 27
4.2 New Chiral Coumarin Derivatives 29
4.3 Amino acid derivatives of coumarin-3-carboxylic acid 36
4.4 Synthesis of Other Coumarin Sensors 40
4.4.1 Why alkali metal ions are important? 43
4.4.2 Studies related to cation sensing with filexible coumarin dimers 44
4.5 New fluorescent sensor for complexation with Zn^{2+} 53
4.6 Studies with 7,7,8,8-tetracyanoquinodimethane derivatives 68
5 CONCLUSION 91
6 EXPERIMENTAL 95
6.1 General Information 95
6.2 Synthesis of 2,4-dihydroxybenzaldehyde[95,142] 96
6.3 Synthesis of 7-hydroxy-2*H*-chromene-3-carboxylic acid[93] 97
6.4 Synthesis of 7-hydroxy-2*H*-chromene-3-carbonyl chloride 97
6.5 Synthesis of (*S*)-7-hydroxy-N-(1-phenylethyl)-2*H*-chromene-3-carboxamide 98
6.6 Synthesis of 2*H*-chromene-3-carboxylic acid[93] 98
6.7 Synthesis of 2*H*-chromene-3-carbonyl chloride 99
6.8 Synthesis of (*S*) -N-(1-phenylethyl)-2*H*-chromene-3-carboxamide 99
6.9 Synthesis of (*R*) -N-(1-phenylethyl)-2*H*-chromene-3-carboxamide .. 100

6.10 Synthesis of 3-(*1H*-Benzotriazol-1-yl-carbonyl)-*2H*-chromen-2-one[96] 101

6.11 Synthesis of (*S*)-2-(2-oxo-*2H*-chromene-3-carboxamido) propanoic acid[93] 102

6.12 Synthesis of (*R*)-2-(2-oxo-2*H*-chromene-3-carboxamido) propanoic acid 102

6.13 Synthesis of (*S*)-2-(2-oxo-*2H*-chromene-3-carboxamido)-3-phenylpropanoic acid.....103

6.14 Synthesis of (*R*)-2-(2-oxo-*2H*-chromene-3-carboxamido)-3-phenylpropanoic acid.....104

6.15 General procedure for synthesis of compounds 15-19[83].....104

6.15.1 Synthesis of ethane-1,2-diyl bis(2-oxo-2*H*-chromene-3-carboxylate).....105

6.15.2 Synthesis of oxybis(ethane-2,1-diyl) bis(2-oxo-2*H*-chromene-3-carboxylate).....105

6.15.3 Synthesis of (ethane-1,2-diylbis(oxy))bis(ethane-2,1-diyl) bis(2-oxo-2*H*-chromene-3-carboxylate).....106

6.15.4 Synthesis of ((oxybis(ethane-2,1-diyl))bis(oxy))bis(ethane-2,1-diyl) bis(2-oxo-2*H*-chromene-3-carboxylate).....106

6.15.5 Synthesis of octane-1,8-diyl bis(2-oxo-2*H*-chromene-3-carboxylate).....107

6.16 Synthesis of methyl ester of coumarin-3- carboxylic acid[143].....107

6.17 Synthesis of Sodium 4-(2-hydroxybenzylideneamino)-3-hydroxynaphthalene-1-sulfonate[120].....108

6.18 Synthesis of 2-(4-(bis(((*S*)-1-phenylethyl)amino)methylene)cyclohexa-2,5-dien-1-ylidene)malononitrile.....109

6.19 Synthesis of 2-(4-(bis(((*R*)-1-phenylethyl)amino)methylene)cyclohexa-2,5-dien-1-ylidene)malononitrile 110

6.20 2-(4-(bis(((*R*)-1-(naphthalen-1-yl)ethyl)amino)methylene)cyclohexa-2,5-dien-1-ylidene)malononitrile 110

6.21 2-(4-(bis(((*S*)-1-(naphthalen-2-yl)ethyl)amino)methylene)cyclohexa-2,5-dien-1-ylidene)malononitrile 111

6.22 2-(4-(bis(((*R*)-1-cyclohexylethyl)amino)methylene)cyclohexa-2,5-dien-1-ylidene)malononitrile 112

7 REFERENCES 113

8 APPENDICES 131

A. Characterization data for chiral coumarin derivarives 131

8.1 NMR spectra 131

8.2 IR spectra of chiral coumarins 149

8.3 HRMS spectra of chiral coumarins 153

B. Characterization data for coumarin dimers 156

8.4 NMR Spectra 156

8.5 IR Spectra 175

8.6 Mass Spectra 178

8.7 DSC Thermograms 180

8.8 UV-Vis Spectra 183

8.9 XY Coordinates of Optimized Structures 186

8.9.1 Optimized structure of 16 186

8.9.2 Optimized structure of 16 + Na^+ 188

8.9.3 Optimized structure of 16 + K^+ 191

C. Characterization and Fluorescence data for Schiff base 195

8.10 NMR spectra 195

8.11 XY Coordinates of Optimized Structures 196

8.11.1 For 21-C1 196

8.11.2 For 21-C2 198

8.11.3 For 21-C3 200

8.11.4 For 21-C4 202

8.11.5 For 21-C5 203

D. Characterization and Fluorescence data for chiral diaminodicyanoquinones 206

8.12 NMR spectra 206

8.13 IR spectra 224

8.14 HRMS spectra 226

8.15 Fluorescence Spectra 229

8.16 XY Coordinates of Optimized Structures 231

8.16.1 For 25-C1 231

8.16.2 For 25-C2 234

8.16.3 For 25-C3 237

8.16.4 For the complex between compound 25 and (*S*)-α-methylbenzyl amine 241

8.16.5 For the complex between compound 25 and (*R*) -α-methylbenzyl amine 245

CURRICULUM VITAE 249

LIST OF TABLES

TABLES

Table 4.1 Results of solvent screening studies with 1-phenylethanol enantiomers* 37
Table 4.2 Results of solvent screening studies for α-methylbenzyl amine enantiomers* 38
Table 4.3 Amino acid derivative coumarin sensors and analytes that are experimented 39
Table 4.4 Chiral amine derivative coumarin sensors and analytes that are experimented 40
Table 4.5 Results of fluorescence studies conducted for determination of the sensor that gives best selectivity* 45
Table 4.6 Results of fluorescence studies with Schiff base-zinc complex* 57
Table 4.7 Different conformations of compound **21*** 62
Table 4.8 Effect of dye concentration in SDS micelle on Stokes shift 73
Table 4.9 Results of solvent screening studies with compound **22*** 75
Table 4.10 Fluorescence studies of compound **22** in the presence of selected enantiopure compounds (Sensor concentration was 0.1 mM, excitation slit width was 5 nm, emission slit width was 2.5 nm, scan rate was 200 nm/min). 77
Table 4.11 Fluorescence studies of compound **24** in the presence of selected enantiopure compounds (Sensor concentration was 0.1 mM, excitation slit width was 5 nm, emission slit width was 2.5 nm, scan rate was 200 nm/min). 79
Table 4.12 Optimized geometries of different conformations of compound **25** 89

LIST OF FIGURES

FIGURES

Figure 1.1. Pictorial representation of electric and magnetic fields 2
Figure 1.2. Potential energy curves for ground state and first singlet excited state in which vibrational levels are represented as wavefunctions to illustrate Franck-Condon principle (modified from reference 15)[15] 9
Figure 1.3. Perrin-Jablónski diagram for the illustration of photophysical processes 11
Figure 1.4. Block diagram of a fluorescence spectrometer 12
Figure 1.5. Anthracene and BINOL based boronic acid receptors synthesized for sensing saccharides 14
Figure 1.6. Boronic acid-based chiral receptors for saccharide binding 14
Figure 1.7. Metal sensitive biaryl fluorophores 15
Figure 1.8. Metal sensitive biaryl acetylene fluorophores 16
Figure 1.9. Dual responsive and metal sensitive fluorescent probe 16
Figure 2.1. Boronic acid derivative PET sensor synthesized by James *et al.* 20
Figure 2.2. Dendrimer synthesized by Pu *et al.* 21
Figure 2.3. 1,8-bis(2-isopropyl-4-quinolyl) naphthalene *N, N′*- dioxide, synthesized by Tumambac *et al.* 22
Figure 2.4. 1,8-diheteroacridylnaphthalene sensor synthesized by Mei *et al.* 23
Figure 2.5. 1,8-diheteroacridylnaphthalene sensor synthesized by Wolf *et al.* 23
Figure 3.1. Web of Science records in 2019 25
Figure 3.2. Fluorescent starting materials that are focused on in this dissertation .. 26
Figure 4.1. Structure of coumarin and numbers are assigned for each position 27
Figure 4.2. 3rd and 7th positions on coumarin for synthetic modifications 30
Figure 4.3. First target compound to be used in chiral recognition studies 30
Figure 4.4. Proposed interaction with our potential sensor (compound **4**) and chiral amine 31
Figure 4.5. Sensor and analytes to be experimented in our initial studies 31

Figure 4.6. Fluorescence spectra of compound **4** in the presence of (a) enantiopure *(R) and* (b) *(S)*-α-methylbenzyl amine (sensor concentration 1.6×10^{-7} M, in DCM, excess amine was added, excited at 365 nm, slit widths were 5 nm, scan rate was 400 nm/min and 0.1 ml Et_3N was used as an additive). 32
Figure 4.7. Overlapped fluorescence spectra of compound **4** in the presence of enantiopure (*R*) and (*S*)-α-methylbenzyl amine (sensor concentration 1.6×10^{-7} M, in DCM, excess amine was added, excited at 365 nm, slit widths were 5 nm, scan rate was 400 nm/min and 0.1 ml Et_3N was used as an additive). 33
Figure 4.8. Methoxide derivative of compound **4**..... 34
Figure 4.9. Coumarin- derived new chiral sensors 35
Figure 4.10. Synthesized amino acid derivatives and their isolated yields..... 36
Figure 4.11. Triethylene glycol functionalized coumarin dimer 40
Figure 4.12. ^1H NMR spectrum of compound **17 (**in $CDCl_3$)..... 41
Figure 4.13. Optimized geometry for compound **17**..... 42
Figure 4.14. Flexible coumarin dimer series..... 44
Figure 4.15. Fluorescence spectra of compound **16** in case of different sodium cation concentrations (sensor concentration 5×10^{-5} M, in CH_3CN, excited at 335 nm, slit widths were 5 nm, scan rate was 600 nm/min). 47
Figure 4.16. Stern-Völmer plot for titration studies with compound **16** in the presence of sodium and potassium cations 48
Figure 4.17. Benesi-Hildebrand plot for titration studies with compound **16** in the presence of sodium cations 49
Figure 4.18. The optimized structures of Na^+ and K^+ bound to **16**..... 50
Figure 4.19. The structure of 1,8-octane diol derivative coumarin dimer, **19** 50
Figure 4.20. Fluorescence spectra of compound **19** in the presence of Na^+ and K^+ ions (sensor concentration 5×10^{-5} M, in CH_3CN, 100 equiv. metal salt was added, excited at 335 nm, slit widths were 5 nm, scan rate was 600 nm/min)..... 51
Figure 4.21. Methyl ester of coumarin-3-carboxylic acid 51

Figure 4.22. Fluorescence spectra of compound **20** in the presence of Na^+ and K^+ ions (sensor concentration 5×10^{-5} M, in CH_3CN, 100 equiv. metal salt was added, excited at 335 nm, slit widths were 5 nm, scan rate was 600 nm/min). 52
Figure 4.23. Proposed structure of the cation-sensing complex 52
Figure 4.24. First trials for Zn^{2+} complexation 54
Figure 4.25. ^1H NMR spectrum of Schiff base, **21** (in DMSO-d_6) 55
Figure 4.26. (a) UV-Vis and (b) fluorescence spectra of Schiff base in the absence and presence of Zn^{2+} salt in MeOH:2% DCM 56
Figure 4.27. Fluorescence spectra of compound **21** in the presence of tartaric acid enantiomers (Sensor concentration was 0.1 mM in MeOH:2% DCM, excited at 345 nm, slit widths were 5 nm, scan rate was 600 nm/min). 61
Figure 4.28. Optimized structure of Schiff base 64
Figure 4.29. ^1H NMR spectrum of compound **21** in the presence of Hünig's base (in DMSO-d_6) 65
Figure 4.30. HPLC chromatogram of compound **21** (Chiralcel OD-H, eluent 95:5 n-Hexane:^{i}PrOH, flow rate 1.0 ml/min, t_R: 3.0, 5.2 min). 66
Figure 4.31. Structure of DADQs 68
Figure 4.32. New chiral diaminodicyanoquinone derivatives 69
Figure 4.33. Fluorescence absorption and emission spectra of compound **22** in micelle solution (SDS concentration was 10 mM, dye concentration was 0.1 mM, excited at 400 nm, slit widths were adjusted as 5.0/2.5 and scan rate was 200 nm/min) 71
Figure 4.34. Effect of dye concentration on absorption and emission spectra (SDS concentration was 10 mM, excited at 400 nm, slit widths were adjusted as 5.0/2.5 and scan rate was 200 nm/min). 72
Figure 4.35. Comparison of micelle solution with organic solvents in terms of fluorescence intensity (Sensor concentration was 0.1 mM, excitation slit width was 5 nm, emission slit width was 2.5 nm, scan rate was 200 nm/min). 73
Figure 4.36. New chiral DADQ derivatives 78

Figure 4.37. Overlapped UV-Vis spectra of compounds **24** and **25** (0.1 mM in DCM) 80
Figure 4.38. Overlapped fluorescence spectra of compounds **24** and **25** in DCM when excited at (a) 465 nm (b) 280 nm 81
Figure 4.39. Fluorescence spectra of compound **24** in the presence of enantiopure (*R*) or (*S*)- α- methylbenzyl amine (Sensor concentration was 0.1 mM in ACN, excited at 280 nm, excitation slit width was 5 nm, emission slit width was 2.5 nm, scan rate was 200 nm/min)..... 82
Figure 4.40. Fluorescence spectra of compound **26** in the presence of enantiopure (*R*) or (*S*)- α- methylbenzyl amine (Sensor concentration was 0.1 mM in ACN, excited at 280 nm, excitation slit width was 5 nm, emission slit width was 2.5 nm, scan rate was 200 nm/min)..... 82
Figure 4.41. Fluorescence spectra of compound **24** in the presence of enantiopure (*R*) or (*S*)- α- methylbenzyl amine (Sensor concentration was 0.1 mM in ACN, excited at 280 nm, excitation slit width was 10 nm, emission slit width was 5 nm, scan rate was 200 nm/min)..... 84
Figure 4.42. Fluorescence spectra of compound **25** in the presence of enantiopure (*R*) or (*S*)- α- methylbenzyl amine (Sensor concentration was 0.1 mM in ACN, excited at 280 nm, excitation slit width was 10 nm, emission slit width was 5 nm, scan rate was 200 nm/min)..... 85
Figure 4.43. Maximum intensity vs equiv. of chiral amine added graph for the titration of compound **25** with α-methyl benzyl amine enantiomers 86
Figure 4.44. Stern-Völmer graph for the titration of compound **25** with α-methylbenzyl amine enantiomers..... 87
Figure 4.45. Benesi-Hildebrand graph for the titration of compound **25** with (*S*)-α-methylbenzyl amine 88
Figure 4.46. Optimized geometry for the complex between compound **25** and (a) (*S*)-α-methylbenzyl amine (b) (*R*)-α-methylbenzyl amine..... 90

LIST OF SCHEMES

SCHEMES

Scheme 4.1 Synthesis of coumarin via Perkin reaction 28
Scheme 4.2 Knoevenagel condensation for the synthesis of coumarins 28
Scheme 4.3 Pechmann reaction for the synthesis of coumarins 28
Scheme 4.4 Synthesis of coumarin-3-carboxylic acid 29
Scheme 4.5 Proposed mechanism for the synthesis of coumarin-3-carboxylic acid 29
Scheme 4.6 Synthesis pathway of target compound 30
Scheme 4.7 Reaction conditions experimented for the synthesis of compound **5** .. 34
Scheme 4.8 Proposed mechanism for hydrolysis 35
Scheme 4.9 Synthesis pathway of compounds **8** and **9** 35
Scheme 4.10 Reaction scheme for the synthesis of amino acid derivatives **11**-**14** . 36
Scheme 4.11 Synthesis pathway of compound **17** 41
Scheme 4.12 Synthesis of Schiff base, **21** 54
Scheme 4.13 Synthesis of acetophenone derivative of Schiff base 67
Scheme 4.14 Conditions tried to get O-alkylation product 67
Scheme 4.15 Synthesis of chiral DADQs 69

LIST OF ABBREVIATIONS

ABBREVIATIONS

OD	Optical Density
FC	Franck-Condon
HPLC	High Performance Liquid Chromatography
DSC	Differential Scanning Calorimetry
FTIR	Fourier Transform Infrared
NMR	Nuclear Magnetic Resonance
HRMS	High Resolution Mass Spectroscopy
DCC	Dicyclohexyl carbodiimide
DCM	Dichloromethane
ACN	Acetonitrile
DMSO	Dimethylsulfoxide
DMF	Dimethylformamide
MeOH	Methanol
MBA	Methylbenzylamine
DTA	*D*-tartaric acid
LTA	*L*-tartaric acid
NICS	Nucleus Independent Chemical Shift

LIST OF SYMBOLS

SYMBOLS

T	Temperature
λ	Wavelength
E	Energy of a photon
ν	Frequency
h	Planck's constant
F	Force exerted on a molecule
E	Electric field strength
H	Magnetic field strength
c	Speed of light
υ	Velocity of an electron
e	Charge on an electron
α	Polarizability
μ_i	Transition dipole moment
f	Oscillator strength
ε	Extinction coefficient
ν	Wavenumber
I_0	Intensity of incident light
I_t	Intensity of transmitted light
I_e	Emission intensity
Φ^A	Quantum yield
S	Singlet manifold
T	Triplet manifold

CHAPTER 1

INTRODUCTION

"*We cannot solve our problems with the same thinking we used when we created them."*

Albert Einstein

1.1 Nature of Light

Antipodal to simply accepting scientific hypotheses as they are is to continue questioning for creating new explanations to contribute to the development of science. A good reflection of this was furnished by the efforts of many scientists' and philosophers' on understanding of nature of light. Throughout the history, one of the greatest challenges of scientists has been to understand the properties of light. Studies regarding the definition of light and its interaction with matter with our today's grasping dated back to 1700s. Historically, there were four fundamental definitions of light (i.e. corpuscular theory, wave theory, electromagnetic theory and quantum theory) each of which can be assumed as a cornerstone, and led to a paradigm shift for science in their own credit.

During 1700s, Newton postulated that the light consisted of particles (corpuscular theory) that move through the space or transparent media. However, in the early 1800s, it was realized that Newton's theory failed to explain diffraction, constructive or destructive interference, and polarization of the light.[1–3] This was the beginning of the first paradigm shift.

Newton's particle theory lost its popularity in favor of Huygens' speculations about wave nature of light.[4] Huygens postulated that the light consist of longitudinal and transverse waves. The investigations of Thomas Young and Robert Hooke supported

the wave theory of Huygens so that phenomena of diffraction, polarization and especially interference were explained in following years.[3–5]

In the mid-1800s, Maxwell claimed that light was described as a wave brought about oscillating electromagnetic field surrounded by oscillating charged particles (i.e. electrons and nucleus).[2,4,6] He tried to accommodate magnetism and electricity, and described light as consisting of oscillating electrical, $\vec{\mathbf{E}}$ and magnetic, $\vec{\mathbf{H}}$ fields aligned perpendicular to each other (Figure 1.1).[4]

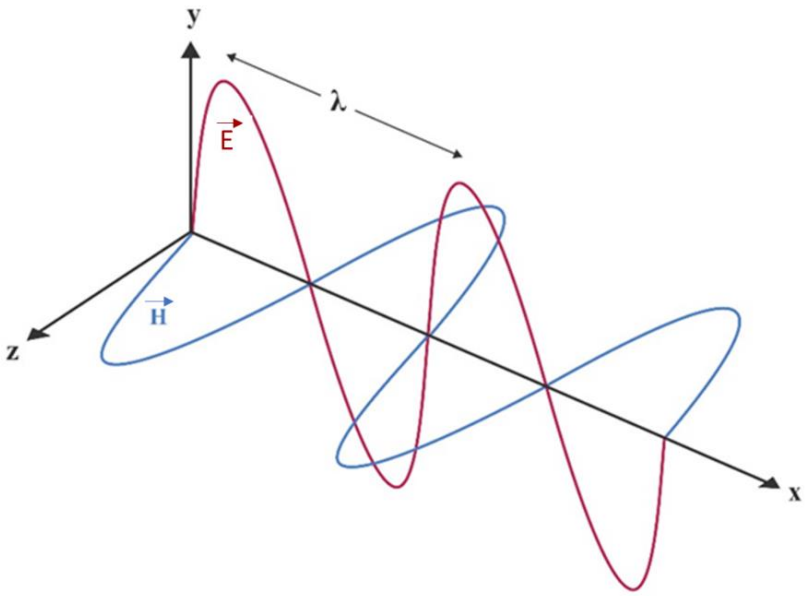

Figure 1.1. Pictorial representation of electric and magnetic fields

Maxwell's definition of light was accepted universally and referred as "classical paradigm of light as electromagnetic waves".[2] Although, Maxwell's theory of light was able to explain interference, scattering, reflection and refraction phenomena, quantitatively, it could not explain absorption, emission of light by matter, and *"photoelectric effect"*. The former can be simply explained by experiments related with blackbody radiation. According to classical theory, emission intensity was predicted to be proportional to T/λ^4 where T is temperature in K and, λ is wavelength in m. This means at a given temperature, as λ gets smaller, the intensity of light should approach infinity. This implies that the emitted light would have enormous energy and able to destroy the universe (i.e. UV catastrophe).[2] Planck resolved this

complexity in absorption and emission intensities. At the end of 1800s, he postulated that light has particles, *photons*, endowed with an energy equal to *E* in his famous equation:[2,4]

$$E = h\upsilon \qquad \text{Equation 1}$$

where E corresponds to energy of photon, and υ corresponds to frequency

According to this equation, energy of light is quantized, and light cannot be absorbed continuously so that the intensity of blackbody radiation can have a maximum value of hυ. This explanation by Planck eliminated the idea of infinite intensity and UV-catastrophe.[2]

"Photoelectric effect" was explained by Einstein after Planck's proposals.[4] According to the classical theory, energy of absorbed light depends only on the amplitude, not the frequency. Einstein stated that the light itself is quantized and consisted of photons which also makes photon a quantized particle (quantum theory). When a photon strikes metal surface, an electron is ejected by absorbing the photon's energy which is directly related to the frequency of the light. Together with Planck's explanations, the idea that Einstein put forward contributed to the third paradigm shift with two new concepts of quantization of energy and photons.[2,7] Later on, de Broglie correlated these two ideas by postulating that the light has both wave and particle characteristics, and suggested following equation:[8]

$$\lambda = h/m\upsilon \qquad \text{Equation 2}$$

where λ corresponds to wave property, and mυ corresponds to particle property of light.

In summary, classical theory was useful to explain the important phenomena like wavelength, interference, and scattering while the quantum mechanical explanations gave rise to understanding photons' quantization. Classical theory contributes to wave characteristics of light while the quantum mechanics enlightens the particle nature as well.[2]

1.1.1 Absorption and Emission of Light

Maxwell's classical wave theory is explained the initial interaction between the light and electrons physically. According to the classical theory, electromagnetic field and the electrons in a molecule can be viewed as two oscillating dipole systems. If their oscillation frequencies match, they can be coupled as energy donor (photon) and acceptor (electrons in molecule), and participate in a common resonance that results in absorption of photons from electromagnetic field. The excited oscillating electron of a molecule gained the energy that is lost by electromagnetic field; as a result, the molecule becomes electronically excited.[2,4,9]

Emission is the reverse process of absorption. The energy of an oscillating electron in excited state is transferred to electromagnetic field. The energy of electromagnetic field increases while the energy of an electron decreases with the same amount. As a result, excited molecule returns to ground state.[2,4,9]

The fundamental requirement for absorption and emission is the conservation of energy and angular momentum. From the Einstein's resonance relation (Equation 3), the energy separation between two electronic states equals to the frequency of oscillation.[2,4,9]

$$\upsilon = \Delta E/h \qquad \text{Equation 3}$$

At this frequency, energy exchange occurs by resonance between oscillating electrons and electromagnetic field. This is the "*resonance condition*" for absorption and emission of light.[2,9]

Electrical and magnetic perturbations are applied on a molecule when light is passing through. Total force (F) that is exerted on a molecule by light equals to the sum of both the electrical and magnetic forces (Equation 4).[2,10]

$$F = eE + e[Hv]/c \qquad \text{Equation 4}$$

where e corresponds to charge on an electron, E: electric field strength, H: magnetic field strength, c: speed of light, v: velocity of an electron

The electrons travel much slower than the light (i.e. v << c). Thus, the magnetic term on Equation 4 can be neglected and one can say that the electrical force operating on electrons is dominant (F≅eE).[2]

Electromagnetic field exerts forces on nucleus, too. However, nucleus is so massive and according to harmonic oscillator model, the frequency of oscillation is inversely proportional to the mass, nucleus cannot be set into resonance at frequencies that drives the electrons into resonance (see section 1.3.2.1 for Born-Oppenheimer approximation).[2,11]

1.1.1.1 Polarizability

The strength of interaction between the electrons and electric field depends on two important parameters at the resonance condition:

1) The ability of electrons to couple with electromagnetic field,
2) The magnitude of charge separation between positive and negative centers, Δr (dipole)

When an electrical force is applied on an electron, a "*transition dipole moment"* (μ_i, which equals to er) is generated in the electron cloud. This perturbation in electron cloud is defined as "polarizability" (α)[2,12]

$$\alpha = \mu_i / E \qquad \text{Equation 5}$$

The equation is interpreted as the larger the value of transition dipole moment, the larger the polarizability, and the larger the probability of transition.[2]

1.1.1.2 Oscillator Strength

Oscillator strength (*f*) is the measure of the probability of an electronic transition affecting the intensity. Basically, it gives quantitative intuition of the effect of each

transition on absorption spectra. In other words, it can be assigned as a factor for emphasizing the strength of a transition.[2,13]

In a one-dimensional harmonic oscillator, the oscillator strength will be expressed as:

$$f = 4.3 \times 10^{-9} \int \varepsilon dv \qquad \text{Equation 6}$$

where ε: extinction coefficient, υ: wavenumber

Oscillator strength is directly related to the transition dipole moment (i.e. $f \sim \mu_i^2$).[2]

1.2 Absorption and Emission Spectra

Beer's law and Lambert's law are two basic principles for the experimental measurement of electronic absorption spectra.[2,4,9,12] The concentration dependence of the light absorbed is explained by Beer's law, and it is valid for concentrations that are low enough to eliminate the risk of aggregation. Lambert's law states that the initial intensity of the light has no effect on the degree of the light absorption by medium. However, Lambert's law is not valid when high-intensity sources such as lasers are utilized.[2]

Optical density (OD) is the experimental parameter that is related to the quantity of absorption (Equation 7)

$$OD = \log(I_0/I_t) \qquad \text{Equation 7}$$

where I_0 is the intensity of incident light, and I_t is the intensity of transmitted light

Absorption spectra are generally plotted as OD versus wavelength (λ, in nm).

Emission spectrum is a plot of emission intensity (I_e) versus wavelength (λ, in nm) for which the corresponding data are obtained at a fixed excitation wavelength and constant intensity for the incident light (I_0).[2] The relation between these parameters can be formulized as in Equation 8:[2]

$$I_e = 2.3l[A]I_0\varepsilon_A\Phi^A \qquad \text{Equation 8}$$

where l: path length [A]: concentration of molecule A ε_A: extinction coefficient Φ^A: quantum yield

Emission is advantageous over absorption in terms of sensitivity. Luminescence constitutes an important class of emission techniques. In luminescence, intensity of emitted light is directly measured while only the ratio of the intensity of incident light to transmitted light is measured in absorption. Direct measurement of intensity allows recording the spectra at very low concentrations. As a result, luminescence techniques are more sensitive than the absorption.

To understand emission phenomena in more details, one must understand selection rules that are summarized below.

1.3 Selection Rules

1.3.1 Fermi's Golden Rule

Fermi's golden rule is an approximation that relates the rates of electronic, vibrational and/or spin transitions from φ_1 to φ_2 upon perturbation by "weak" interactions. These interactions correspond to either interactions with oscillating electromagnetic field[14] or HOMO-LUMO interactions that are accompanied by a chemical change or electron transfer (Equation 9):[2]

$$k_{obs} \sim \rho[< \varphi_1 | P'_{1\to2} | \varphi_2 >]^2 \qquad \text{Equation 9}$$

where ρ: density of states $P'_{1\to2}$: perturbation

The matrix element is generally considered as transition dipole moment. If the above-mentioned "weak" interactions triggers the generation of a large transition

dipole moment, the value of k_{obs} will be greater. As a result, the rate of transition increases which appears as a strong absorption band.

1.3.2 Probabilty of transitions

Probability of a vibronic transition can be explained by Franck-Condon principle. In order to understand Franck-Condon principle, one must understand Born-Oppenheimer approximation. Born-Oppenheimer approximation helps us to gather a quantum intuition for the basis of Franck-Condon principle.

1.3.2.1 Born-Oppenheimer Approximation

Born-Oppenheimer approximation is the most important idea used for determining molecular wave functions of molecules. According to Born-Oppenheimer approximation, nuclei are so massive that the electrons move much more rapid. As a result of this approximation, electronic and nuclear motions are treated independently so that the electronic wave function can be solved assuming that the nuclei are fixed (i.e. frozen nuclei approximation).[2,10–12]

1.3.2.2 Franck-Condon Principle

Franck-Condon (FC) principle corresponds to the adaptation of Born-Oppenheimer approximation into absorption phenomena. FC principle can be assigned as a selection rule to understand the relative probabilities of vibronic transitions. The idea behind FC principle is the conservation of energy and momentum for both radiative and nonradiative transitions.[2,10]

FC principle states that when an electron interacts with the electromagnetic field, a vertical transition occurs between two states to obtain a net positive overlap in between the vibrational wavefunctions.[2]

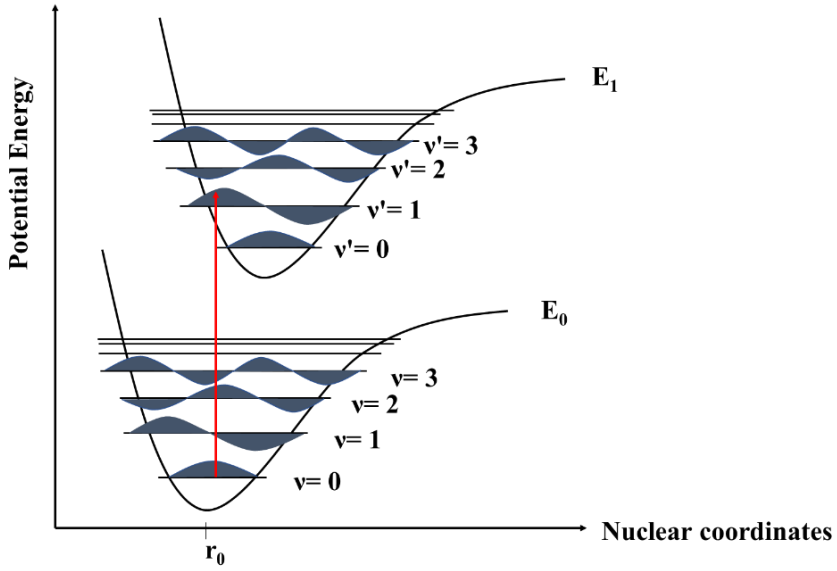

Figure 1.2. Potential energy curves for ground state and first singlet excited state in which vibrational levels are represented as wavefunctions to illustrate Franck-Condon principle (modified from reference 15)[15]

The measure of transition probability between two states is given by overlap integral (FC integral), $<\chi_1|\chi_2>$. The larger FC integral value implies that there is a net constructive overlap of wavefunctions; as a result, the probability of transition is high. The square of FC integral is called FC factor, $<\chi_1|\chi_2>^2$, which is a measure of "reorganization energy". FC factor can be regarded as a parameter that allows analysis of the absorption or emission spectra in a qualitative and quantitative manner. Qualitatively, the large FC factor means that the reorganization energy is small and the probability for electronic transition is high. Quantitatively, the intensities of the vibrational bands in the spectra are regulated by FC factor.[2,10]

FC principle can also be applied to nonradiative transitions in which conservation of energy and momentum rule is satisfied. Indeed, the energy is easily conserved at the crossing points of the wavefunctions on the potential energy curves, (i.e. conical intersections). In these curve-crossing regions, the overlap integral is larger, which means there is a net positive overlap of wavefunctions and transition probability is

high. Moreover, initial and final electronic states resemble to each other in terms of structure and energy at these curve crossing regions.[2,10]

1.3.2.3 Kasha's rule

Excited state is generated after a vertical transition from ground state to the upper states where the orbital overlap is high. In solution, the excited molecules can be brought to the ground state by collisions. In a molecule, energy can be rapidly distributed within the vibrational modes. Thus, excitation to higher energy states (singlet or triplet) results in deactivation to S_1 or T_1. The deactivation of higher excited states occurs so fast that energy is generally removed within time scales on the order of few picoseconds or less. As a result, the lowest excited states (S_1 or T_1) generally become the only candidates for emission process. This generalization is known as Kasha's rule.[2,16] Azulene and its derivatives are the exceptions to Kasha's rule. The small energy difference between S_1 and S_0 of azulene leads to the rapid internal conversion while the large energy gap between S_2 and S_1 results in relatively slow internal conversion, so the significant fluorescence occurs from S_2 state. It is called "anomalous fluorescence".[12]

1.4 Luminescence Spectroscopy

Molecule at its electronically excited state is not favorable due to the excess energy it posseses at these states. To liberate this excess energy, molecules may undergo certain photophysical processes to return to ground state within a very short time period. These deactivation processes are well summarized in a state-energy diagram named as Perrin-Jablónski (Figure 1.3) for the honor of well-known physicists Francis Perrin and Alexander Jablónski.[17–19] The basic form of this diagram was drawn by Herzberg in 1947.[20]

The deactivation processes can be classified as radiative and nonradiative. Radiative transitions are formally divided into two categories depending on the multiplicity of

the excited state from which the emission occurs. In other words, if the corresponding excited state is a singlet manifold, the radiative deactivation process is called fluorescence, and if it is a triplet manifold, the process is called phosphorescence. Internal conversion, intersystem crossing (intramolecular) and vibrational relaxation (intermolecular) constitute the nonradiative decay processes.[9,12,21]

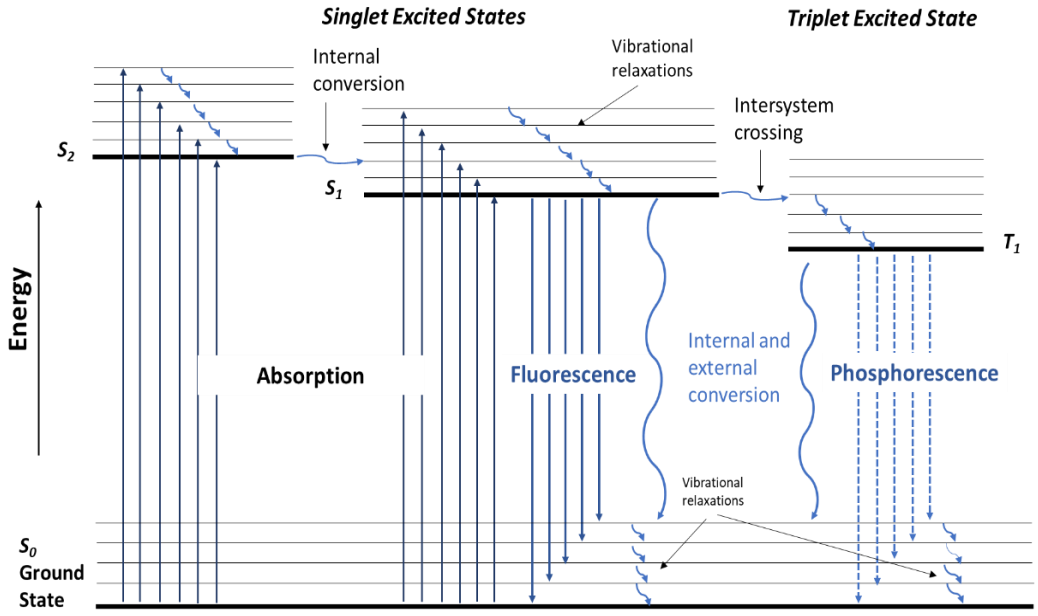

Figure 1.3. Perrin-Jablónski diagram for the illustration of photophysical processes

Fluorescence is a spin-allowed radiative process in which emission of a photon occurs between the states of same multiplicity, normally from the lowest vibrational level of the first singlet excited state (S_1). Phosphorescence is a spin-forbidden radiative process in which emission of a photon occurs from lowest triplet state (T_1) to the signlet ground state (S_o). Since this is a forbidden process involving a spin interconversion (i.e. spin-orbit coupling), the phosphorescence lifetimes are much longer (10^{-3} to 100s) compared to the fluorescence lifetimes (10^{-10} to 10^{-7} s).[2,12,21,22]

Nonradiative relaxation from upper excited states to lower excited states occurs faster than any other measurable processes and the excess energy is released in the form of heat. When the relaxation occurs between the isoenergetic (i.e. having same

total energy) vibronic states of the same multiplicity, the process is named as internal conversion and it takes place in a time period on the order of 10^{-14} to 10^{-11}s. When the intramolecular nonradiative decay takes place between the isoenergetic vibronic states of different multiplicities, the process is called intersystem crossing. The lifetime of intersystem crossing is longer (10^{-11} to 10^{-8} s) compared to internal conversion. The transition from singlet state to triplet state promoted by a process called spin-orbit coupling which is the coupling of electron spin and orbital angular momentum. As a result of this interaction, there is some mixing of states which means singlet state has some triplet character and vice versa.[9] Vibrational relaxation is an intermolecular deactivation process in which release of energy is driven by collisions with other molecules.[2,12,21,22]

1.5 Fundamentals of Fluorescence Spectroscopy

Fluorescence spectroscopy is a spectroscopic technique that enables the qualitative and quantitative analysis of a compound which is excited at a fixed wavelength (excitation wavelength) and resulting emission spectrum is recorded with a detector placed at right angle to the incident light (Figure 1.4).[22]

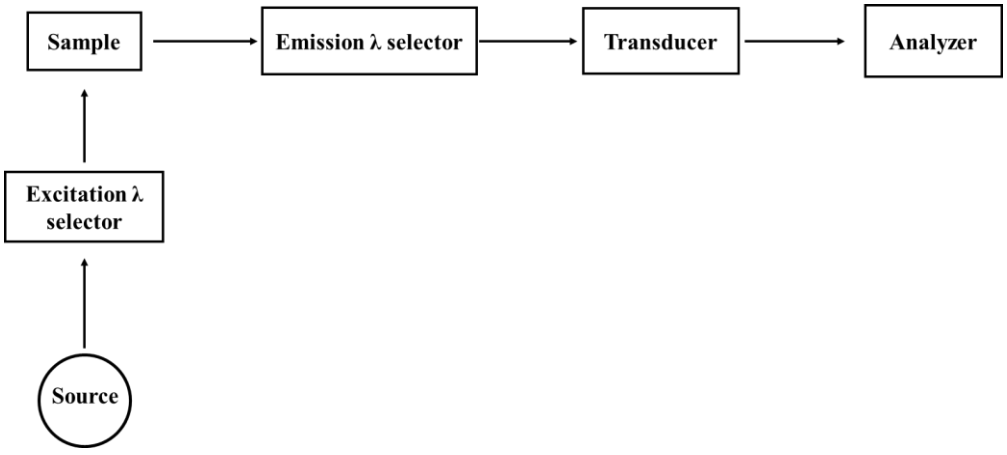

Figure 1.4. Block diagram of a fluorescence spectrometer

The shapes of vibrational bands, emission wavelength, and quantum yields are mainly determined by molecular structure. Rigid, planar, aromatic hydrocarbons

with high symmetry have well-resolved fluorescence spectra with relatively high quantum yields while the nonplanar molecules have less resolved fluorescence spectra with low quantum yields. The explanation is that the rigidity suppresses the internal conversion or intersystem crossing which are triggered by molecular motion in relatively less rigid molecules.[2,23]

One of the significant outcomes of Kasha's rule is the fact that the emission spectrum is independent of excitation wavelength in fluorescence. The reason is that when excited to higher levels, the molecule dissipates its excess energy very quickly to return to S_1 level through nonradiative decay. Moreover, Vavilov had also investigations on the effect of excitation wavelengths on quantum yields. [24–26] For fluorescence, the excitation wavelength independency of quantum yield has been acknowledged as Kasha-Vavilov rule.

Due to these properties, fluorescence spectroscopy found many applications.

1.6 Applications of Fluorescence Spectroscopy

The inherent sensitivity, low detection limit, different analysis modes are among the most important factors that make fluorescence spectroscopy a valuable and attractive technique for analysis of various types of species (i.e. anions, cations, small neutral molecules, supramolecules).[27,28] The applications of fluorescence spectroscopy in RNA folding and dynamics,[29] protein-protein interactions,[30] protein- DNA interactions,[31] drug detection,[32] clinical diagnosis[33,34] and chiral recognition[35–37] are gaining considerable attention of many researchers over the last decades.

1.6.1 Clinical Diagnosis

The chemical composition of the body fluids, intracellular and extracellular space is of great importance since any small deviation can be indication of important illnesses such as hypertension, cardiovascular diseases, cancer, diabetics, Parkinson's disease,

Alzheimer's disease, and Cushing syndrome. Therefore, the maintenance of certain amounts of the composition is strictly required for our health. Problems related to qualitative and quantitative analysis of biologically important species have been addressed by the fluorescent signaling molecules.[38–40]

One of the most intriguing applications of fluorescence spectroscopy in clinical diagnosis involves the use of boronic acid receptors which have been known to bind sugar acids which can be used for the treatment of diabetics.[41–43] Yoon *et al.* have used anthrylboronic acid receptor in Figure 1.5 for polyol binding whose fluorescence response is decreased upon polyol binding due to chelation enhanced quenching (CHEQ).[41]

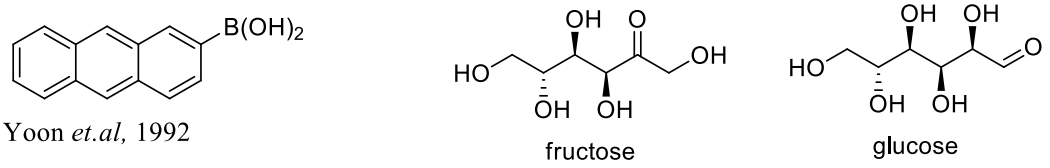

Figure 1.5. Anthracene and BINOL based boronic acid receptors synthesized for sensing saccharides

Zhao et al. have synthesized chiral boronic acid receptors and studied enantioselective fluorescence sensing of a series of sugar acids including *D*- and *L*-tartaric acid due to photoinduced electron transfer (PET) mechanism (Figure 1.6).[42]

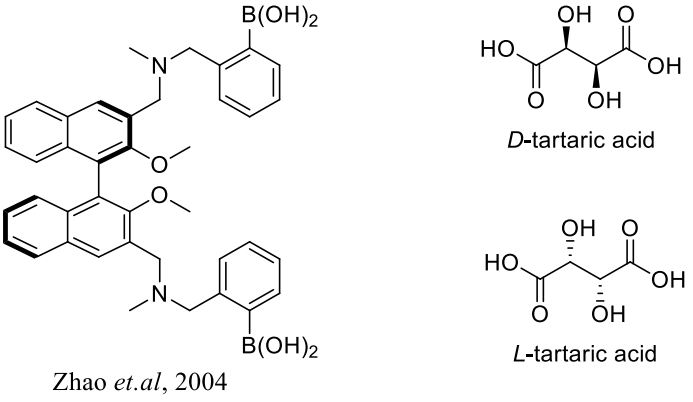

Figure 1.6. Boronic acid-based chiral receptors for saccharide binding

Another application of fluorescence is the detection of biologically relevant metal ions. For this purpose, crown ethers were facilitated as they have been known to complex with certain metal ions, especially alkali metal ions.[44] It was reported in the literature that more rigid fluorophores are more fluorescent compared to the nonrigid similar compounds.[45] Thus, the crown ethers have been utilized as rigid, metal-sensitive chemosensors that change fluorescence response upon complexation. For that, McFarland *et al.* designed flexible biaryl fluorophores (Figure 1.7) for which cation binding (Li^+, Na^+, K^+ and Ca^{2+}) brings about conformational restriction by hindering the rotation in the excited state; thus suppressing the intersystem crossing as a result of which the fluorescence response has enhanced.[45,46]

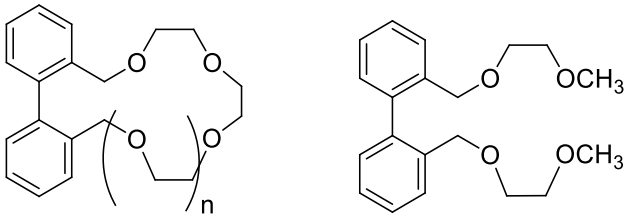

n=1,2,3 4

McFarland *et.al*, 2001

Figure 1.7. Metal sensitive biaryl fluorophores

In another study, McFarland *et al.* synthesized the fluorophores **1** and **2** in Figure 1.8 to evaluate the influence of covalent conformational restriction.[47] Compounds **3-5** were synthesized to study the metal binding and concluded that metal binding (Li^+) enhances the fluorescence intensity.

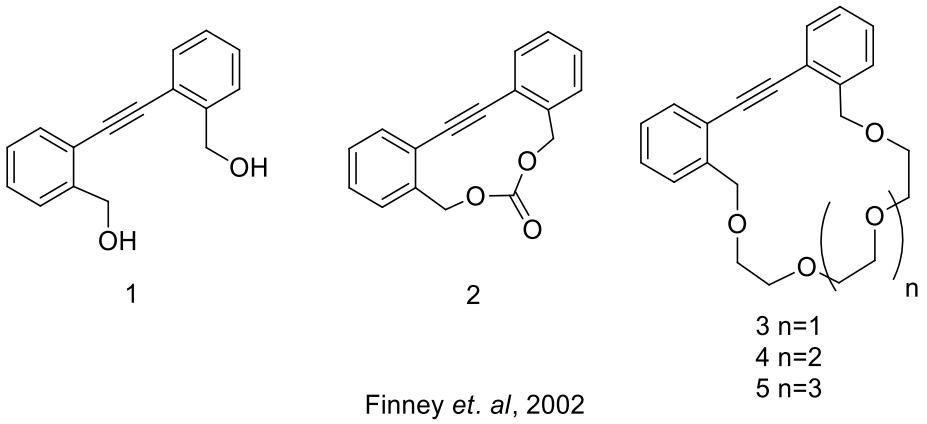

Figure 1.8. Metal sensitive biaryl acetylene fluorophores

An anthracene-based fluorophore was synthesized by Xu *et al.,* shown in Figure 1.9 as a dual-responsive sensor which detects potassium ions in basic solution whereas it detects sodium ions in acidic solutions. The sensor consists of two receptor moieties; benzo-15-crown-5, which is a good host for sodium ions and the other is aza-18-crown-6, which is for potassium ions.[48]

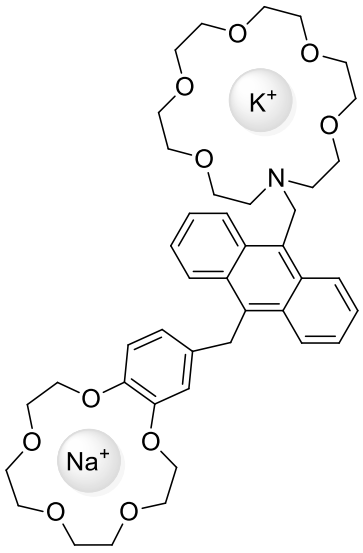

Figure 1.9. Dual responsive and metal sensitive fluorescent probe

CHAPTER 2

CHARACTERIZATION OF CHIRAL COMPOUNDS BY FLUORESCENCE SPECTROSCOPY

''I can call any geometrical figure, or group of points, chiral, and say that it has chirality, if its image in a plane mirror, ideally realized, cannot be brought to coincide with itself.''

Lord Kelvin, 1893

2.1 Chirality

Based on the chirality definition of Lord Kelvin which is widely accepted by scientific community, a molecule can be defined as chiral if it has asymmetric grouping of atoms around a central atom so that it cannot coincide with its mirror image. From a group theory point of view, chirality can be defined as a property of any rigid molecule which lack an improper rotation axis. The simplest improper rotation operation is S_1 which equals to taking mirror image of a molecule so that it gives the enantiomer.[12,49]

Chiral molecules do not need to be *"asymmetric"*. "*Asymmetric*" means having no symmetry element and corresponding molecules belong to C_1 point group. Indeed, "*dissymmetric*" is a more general term for chiral molecules; moreover, asymmetric molecules are classified as a subclass of dissymmetric molecules. In other words, all asymmetric molecules are dissymmetric while the reverse is not true.[12,49]

2.2 Importance of Chirality

Chirality has been the most important aspect of the nature since the very first living being existed. The biological world has been originated due to this important phenomenon. The most important biopolymers were made up of chiral monomers such as *L*-aminoacids and *D*-sugars. Regardless of their origin, the presence of *L*-aminoacids and *D*-sugars on earth indicates that the asymmetric synthesis has been inherently present in nature.[50,51] However, the nature's chiral pool provides limited range of enantiopure compounds. Therefore, to obtain chiral compounds in enantiopure forms has been a major challenge of synthetic organic chemists.[50] Starting from the discovery of Louis Pasteur, who separated the enantiomers of *D*- and *L*-tartaric acid, the demand for enantiopure substances has been ever increasing.[52]

With the increasing demand for enantiopure substances, the need for characterization and separation of enantiomers has emerged. When the polarimeter was first developed by Biot in 1816, it was shown that natural products have had optical activities, meaning that they were able to rotate plane polarized light.[53] However, this technique has some disadvantages. While using polarimetry, sample must be purified from chiral impurities without causing unintended enantiomeric enrichment by crystallizing the sample in chiral medium. Moreover, if the compound has low optical rotatory power, large amount of sample is required for optical purity measurement. More importantly, specific rotation value of the pure enantiomer must be known certainly which is not possible for newly synthesized compounds that are not present in the literature.[54,55] As a result, polarimetry was not a sufficient technique for determination of enantiomeric purity when it's used alone. Indeed, it should be used in corporation with other techniques.

Chiral HPLC columns are most widely used for the determination of enantiomeric excess in corporation with polarimetry.[56] In 1951, Munio Kotake was able to differentiate amino acid racemates through the use of natural cellulose.[57] This study can be assigned as the basis for chiral HPLC. However, in some cases, the retention

times are too long that the analysis becomes time-consuming which in turn results in too much waste production of organic solvents. Moreover, if the analyte is not known in the literature, one has to set the optimum conditions for analysis which is very challenging. Chiral HPLC has been mentioned by its very expensive chiral columns which loses applicability upon frequent use.[35] It has been widely used since there is no alternative technique with such general applicability; however, there have been many efforts to find a cheaper and more practical technique which can be able to replace chiral HPLC.

Nuclear magnetic resonance spectroscopy is another technique used to characterize enantiomers. But it requires the use of special chiral shift reagents or chiral solvating agents.[58] Analysis of enantiomers through NMR spectroscopy was first realized by Harry Mosher in 1969, after his advent of Mosher acid.[59] The chiral derivatizing agents, such as Mosher acid, has many disadvantages. They require too many specifications before use. Moreover, covalent modification of the parent molecule is required (for diastereomer formation). Furthermore, they are very expensive. These disadvantages limit the use of NMR spectroscopy in chiral recognition.

In 1977, mass spectrometry-based techniques have emerged (such as dissociation induced collisions).[60] However, they couldn't become popular due to expensive instrumentation, their being time-consuming and sample consuming, and low resolution in the spectra.[56,61–63]

Over the years, the demand for faster and more reliable analysis techniques that can be a superior alternative to the older ones is getting increasing attention. In the recent years, determination of optical purity via fluorescence spectroscopy has become very attractive since it is easy to use, highly sensitive, less time-consuming, and greener in terms of the reduced organic wastes. Fluorescence spectroscopy enables easier and faster detection of enantioselectivity, provides real-time analysis and meets the need for high-throughput screening efforts of synthetic organic chemists.[64]

Detailed survey of the literature revealed that the most remarkable contributions on chiral fluorescence sensing come from research groups of James,[42,43,65–67] Pu[36,68–72]

and Wolf.[37,64,73–79] To the best of our knowledge, although there were many reports on the fluorescent detection of organic molecules, the report of James *et al.* was the very first report on "*chiral sensing"* by fluorescence in the literature.[65] In this study, James and coworkers have synthesized the boronic acid (Figure 2.1) for selective binding of saccharides. Addition of saccharides results in the formation of cyclic borate esters, and the acidity of boronic acid sensor is increased. This increase in the acidity gives rise to increase in the Lewis acid-base interactions, and formation of stronger boron-nitrogen bonds by fixing nitrogen in a certain orientation. Moreover, they proposed that binaphthyl unit can also twist upon saccharide binding so that the steric factors of the sensor are also believed to play important roles in differentiation of enantiomers. Despite that this study made a great contribution to the concept of chiral sensing through fluorescence, it has a disadvantage of multistep synthesis of corresponding boronic acid (Figure 2.1).

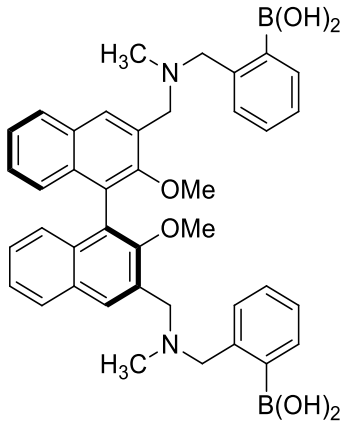

Figure 2.1. Boronic acid derivative PET sensor synthesized by James *et al.*

Pu and coworkers have synthesized the dendrimer in Figure 2.2.[80] They reported that the dendrimer consists of high migration energy from phenylacetylene dendrons to the chiral binaphthyl core. In addition to this migration energy, the increase in the number of light-absorbing units resulted in the considerable improvement of fluorescence response of the dendrimer compared to the binaphthol. Moreover, the dendrimer was found to differentiate the enantiomers of chiral alcohols and chiral amines such as 2-amino-1-propanol, 3-methyl-1-butanol, *trans*-1,2-

diaminocyclohexane. They found out that the fluorescence response of the dendrimer is quenched in the presence of amino alcohols due to the hydrogen bonding interactions at the ground state and the excited-state deprotonation of binaphthol molecules itself. They reported that the enantioselective sensing can be performed with this dendrimer due to different quenching rates of individual enantiomers.

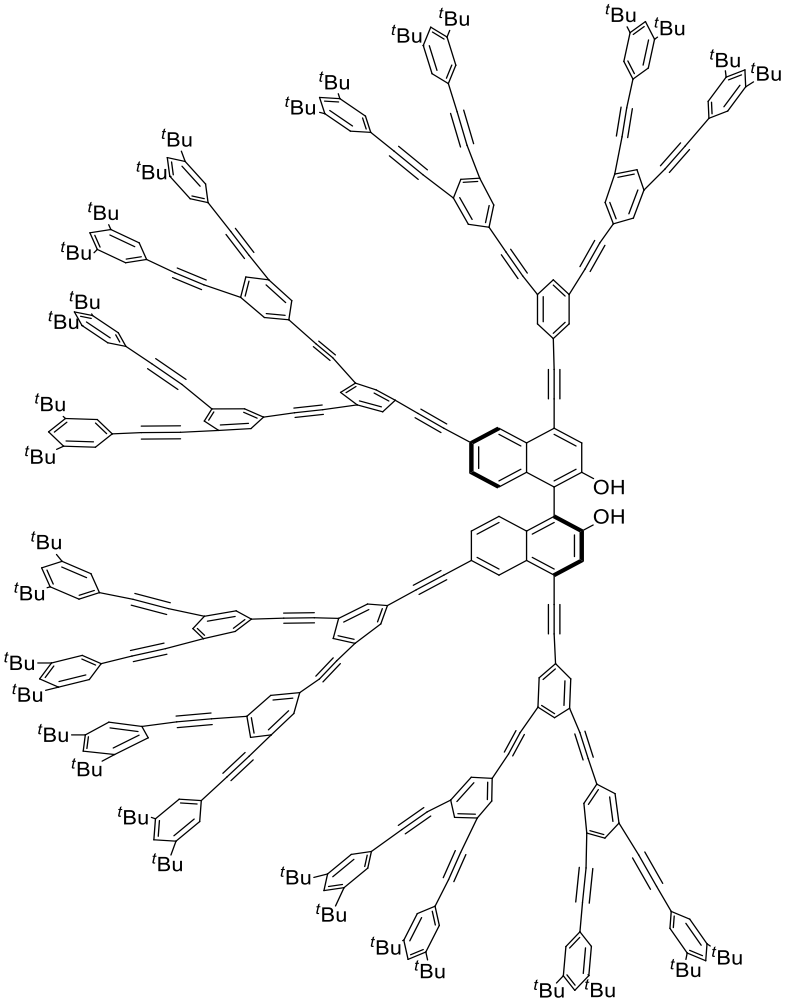

Figure 2.2. Dendrimer synthesized by Pu *et al.*

Wolf group have utilized sterically hindered diheteroarylnaphthalenes that participate in interactions with enantiomers of wide variety of compounds (especially carboxylic acids) selectively giving rise to changes in fluorescence spectra with different detection modes (enhancement and quenching).

In their study, Tumambac *et al.* have adopted the use of fluorescence sensors in enantioselective analysis of an asymmetric reaction,[64] rather than chiral sensing of isolated samples. They used sensor given in Figure 2.3 for the analysis of enzyme-catalyzed kinetic resolution of *trans*-1,2-diaminocyclohexane. Their chiral sensor seemed to be responsive towards *(R, R)* enantiomer since the addition of this enantiomer increased the intensity of fluorescence signal of the sensor significantly compared to the other enantiomer. This study was important for being the first study in which a fluorescent sensor is employed in enantioselective analysis of an asymmetric reaction but indeed it's limited in terms of the presence of multiple steps in the synthetic pathway of the sensor and it's limited to only kinetic resolution of *trans*-1,2-diaminocyclohexane, and cannot be used for the general purpose in enantioselective fluorescence sensing of asymmetric reactions.

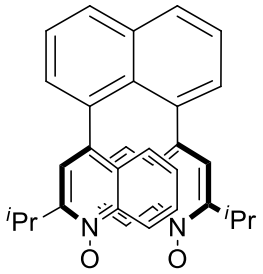

Figure 2.3. 1,8-bis(2-isopropyl-4-quinolyl) naphthalene *N, N′*- dioxide, synthesized by Tumambac *et al.*

They have also reported that 1,8-diacridylnaphthalene sensor given in Figure 2.4 exhibits dual mode of detection.[79] In other words, it shows both enantioselective static and dynamic quenching in the presence of amino acids (serine, glutamine and proline). They reported this as the first study in which a sensor operates in two different detection modes, and fluorescence sensing is based on lifetime measurements.

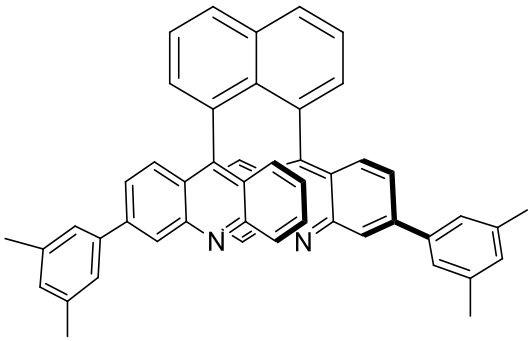

Figure 2.4. 1,8-diheteroacridylnaphthalene sensor synthesized by Mei *et al.*

Another great contribution of Wolf group is to enable direct measurement of both concentration and enantiomeric excesses of carboxylic acid derivatives with sensor given in Figure 2.5. With the racemic form of this sensor, they were able to determine the concentration of analytes while the enantiopure form of the sensor showed selectivity towards (*R*)- enantiomers so the quenching experiments with enantiopure sensor provided enantiomeric excesses with high reproducibility and accuracy.[75]

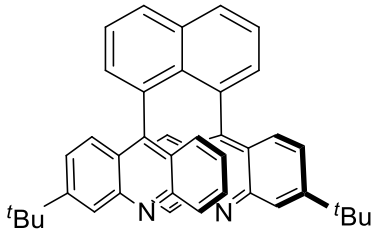

Figure 2.5. 1,8-diheteroacridylnaphthalene sensor synthesized by Wolf *et al.*

Wolf group has also extensive contributions to recognition of enantiomeric composition of wide variety of compounds by UV-Vis[75] and CD[78,81,82] spectroscopy techniques. The studies of Wolf group have impressed us in terms of their wide range of substrate scopes, giving excellent results in terms of reproducibility and accuracy, and their being prime examples of literature.

CHAPTER 3

AIM OF STUDY

According to the Web of Science records (2019), fluorescence sensing has been gathering more and more attention over the last 25 years (Figure 2.6).

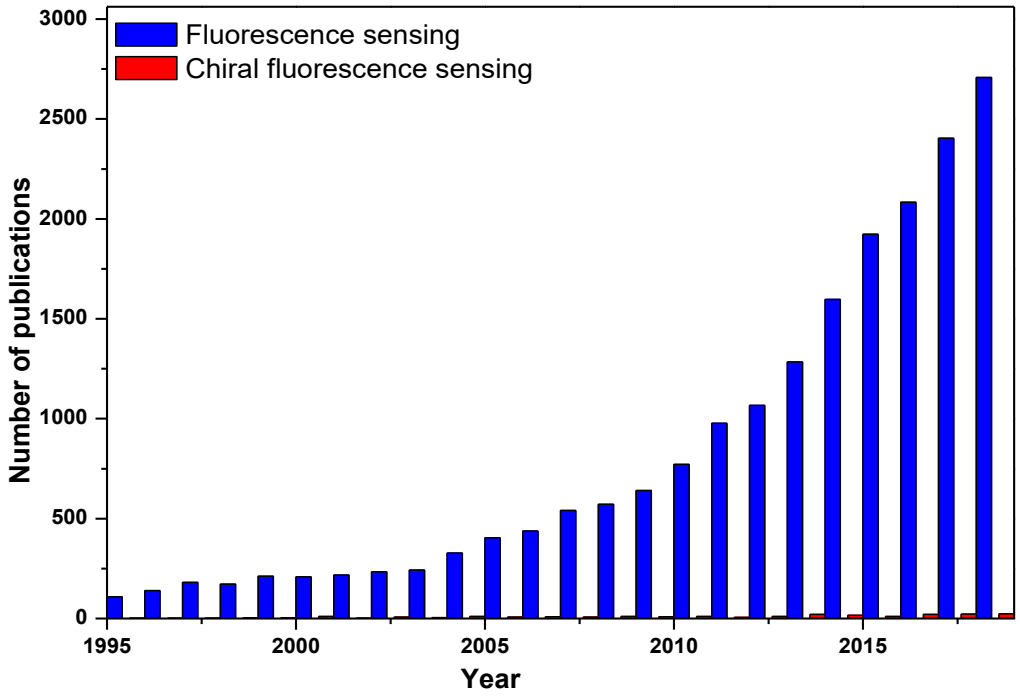

Figure 3.1. Web of Science records in 2019

Among the 22,203 papers published on fluorescence sensing, only approximately 1% have been related to chiral sensing by fluorescence spectroscopy. In other words, fluorescence detection of many species such as metal ions, organic or inorganic molecules has been well-documented; however, chiral sensing by fluorescence spectroscopy is still infant.

Despite the impressive works in the literature mentioned in previous chapters of this dissertation, most of the fluorescence sensors for chiral sensing have been based on

BINOL and its derivatives due to the unique features of this compound. Thus, it was thought that new sensors should be designed based on other fluorescent molecules (Figure 3.2). By this way, we believed that we can expand the substrate or reaction scope for chiral fluorescence sensing.

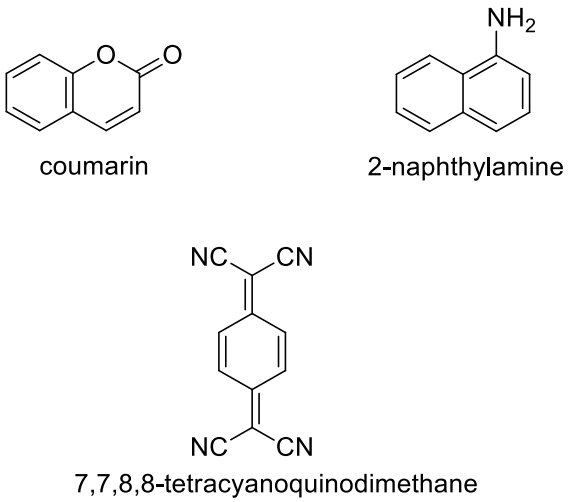

Figure 3.2. Fluorescent starting materials that are focused on in this dissertation

In the literature, already studied fluorophores have a disadvantage of presence of multiple steps in their synthesis. Through fluorescence spectroscopy, it's aimed to simplify the sensing of chiral compounds. However, by synthesizing fluorescent compounds in multiple steps, actually we are moving away from the ultimate desire. As a result, we thought that we could design new sensors which can be easily synthesized or modified and utilized in enantioselective sensing by fluorescence. To the best of our knowledge, designing new, easy-to-synthesize fluorescent molecules from easily-accessible and cheaper precursors are in high demand for the sake of simple and practical sensing of chirality by fluorescence spectroscopy.

CHAPTER 4

RESULTS AND DISCUSSION

4.1 Coumarins

For cultivation of our passion and desire for the synthesis of new fluorescent molecules, the literature was digged and fluorescent molecules utilized for chiral recognition were surveyed. As summarized in previous chapters, already studied fluorescent sensors are disadvantageous in terms of having multiple steps in their synthesis. To overcome this disadvantage and contribute to the literature for further simplification of the fluorescence recognition of chiral molecules, we preferred to choose easy-to-modify synthons with high fluorescence quantum yields and high photostabilities. For this purpose, coumarin has been chosen as a candidate since it has been rendered as an important structural motif present in various types of compounds having biological activities such as anticoagulant, anticancer and antifungal activities.[83–85]

According to IUPAC, coumarins are mentioned as 2*H*-chromen-ones, and they consist of a pyrone ring fused to benzene. Carbonyl group of pyrone ring is situated at second position (Figure 4.1).

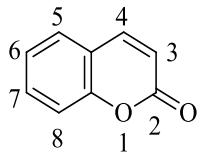

Figure 4.1. Structure of coumarin and numbers are assigned for each position

Coumarins are found in nature, and extracted from *Tonka bean (dipteryx odorata* or *cumaru)*, but they can also be obtained synthetically. This ubiquitous nature of coumarins makes them easily available. The synthesis of coumarin (Scheme 4.1) was first achieved by Perkin in 1868 (Perkin reaction).[86]

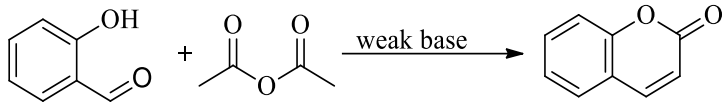

Scheme 4.1 Synthesis of coumarin via Perkin reaction

The Knoevenagel condensation[87] and Pechmann reaction[88] constitute other well-known classical routes for synthesis of coumarins.

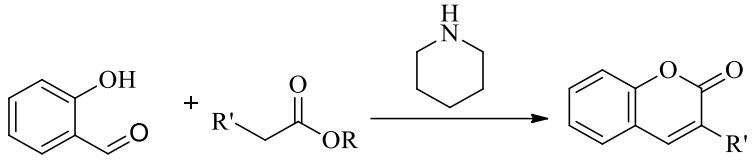

Scheme 4.2 Knoevenagel condensation for the synthesis of coumarins

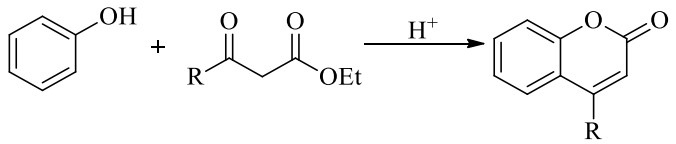

Scheme 4.3 Pechmann reaction for the synthesis of coumarins

The general strategy for functionalization of coumarins is de novo synthesis of new coumarins using starting materials accordingly. In other words, direct modification of coumarin skeleton is very rare despite the high reactivity of the double bond between C3 and C4 carbons.[89,90]

Although coumarin itself exhibits very weak fluorescence, its photophysical properties can be easily improved to obtain high fluorescence quantum yield and high photostability.[89,91] Modification of coumarin from 7th position with electron donating groups or 3rd position with electron withdrawing groups enhances its spectral properties due to inductive and mesomeric effects (i.e. push and pull effect) for desired applications.[92]

With all these important information in hand, we incorporated carboxyl moiety to the third position using salicylaldehyde and diethyl malonate (Scheme 4.4),[93] and used this carboxylic acid derivative as a synthon of our fluorescent sensors.

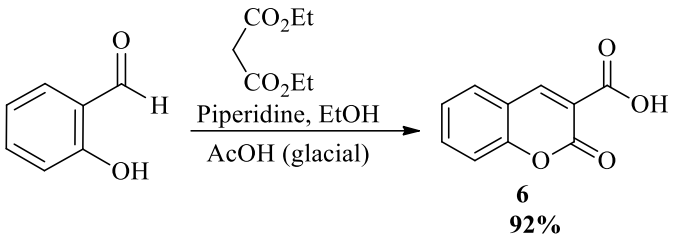

Scheme 4.4 Synthesis of coumarin-3-carboxylic acid

Although coumarin-3-carboxylic acid is commercially available, it was synthesized under given conditions (Scheme 4.4) easily in very high yields. The mechanism is proposed to be a simple Knoevenagel condensation of salicylaldehyde and active methylene compound generated by diethyl malonate (Scheme 4.5).[94]

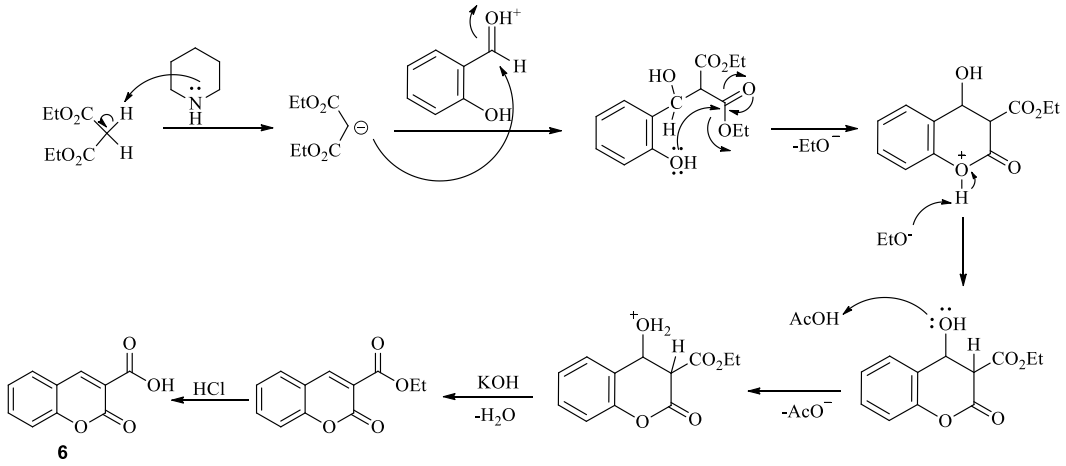

Scheme 4.5 Proposed mechanism for the synthesis of coumarin-3-carboxylic acid

4.2 New Chiral Coumarin Derivatives

The photophysical properties of coumarin can be enhanced through modifying it from third and seventh positions due to inductive and resonance effects (Figure 4.2).[92]

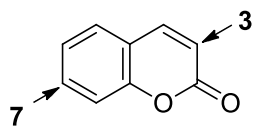

Figure 4.2. 3rd and 7th positions on coumarin for synthetic modifications

To begin with, compound **4** (Figure 4.3), which bears hydroxyl group at its 7th position, was first synthesized:

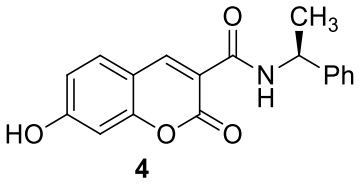

4

Figure 4.3. First target compound to be used in chiral recognition studies

The starting material, 7-hydroxycoumarin-3-carboxylic acid (compound **2**, Scheme 4.6) was commercially available but it was not easily accessible economically. Thus, it was easily synthesized through Vilsmeier-Haack reaction and Knoevenagel condensation reaction starting from resorcinol.[93,95] The target compound is synthesized in an acceptable yield by chlorination followed by the reaction with chiral amine (Scheme 4.6).

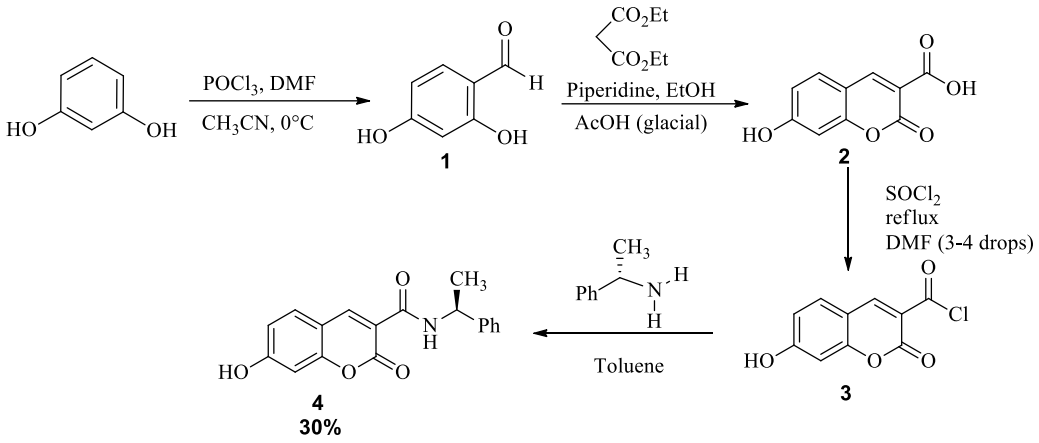

Scheme 4.6 Synthesis pathway of target compound

Noncovalent interactions such as hydrogen bonding interaction between this fluorescent chiral coumarin derivative and chiral amines, chiral alcohols, chiral amino acids, or chiral carboxylic acids were thought to trigger the differentiation of enantiomers via fluorescence spectroscopy. A chiral pocket between carbonyl group on pyrone ring and amide moiety will be generated after incorporation of chiral

amine on coumarin skeleton. It was postulated that only one enantiomer will be able to reach the chiral pocket of the compound for hydrogen bonding interactions due to steric reasons (Figure 4.4), and will result in a change in the electron density of the corresponding compound as a result of which fluorescence spectrum is expected to change. Since the fluorescence spectroscopy provides multiple modes of detection, the either of the following changes can be expected to arise in the fluorescence spectrum of parent fluorescent sensor:

- Hyperchromic (intensity increase)
- Hypochromic (intensity decrease/quenching)
- Hypsochromic shift (blue shift, shorter λ)
- Bathochromic shift (red shift, larger λ)

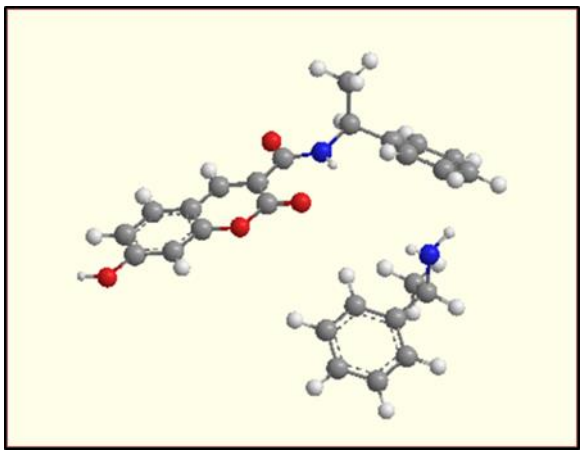

Figure 4.4. Proposed interaction with our potential sensor (compound **4**) and chiral amine

To test our proposal, preliminary fluorescence studies in the presence of enantiopure (*R*) and (*S*)-α- methylbenzyl amine were performed (Figure 4.5).

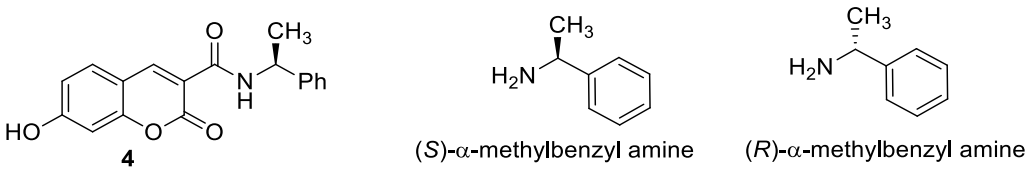

Figure 4.5. Sensor and analytes to be experimented in our initial studies

According to fluorescence spectra in Figure 4.6, compound **4** seemed to respond to both enantiomers which is concluded from the increase in the fluorescence intensity of the parent compound upon addition of either enantiomer.

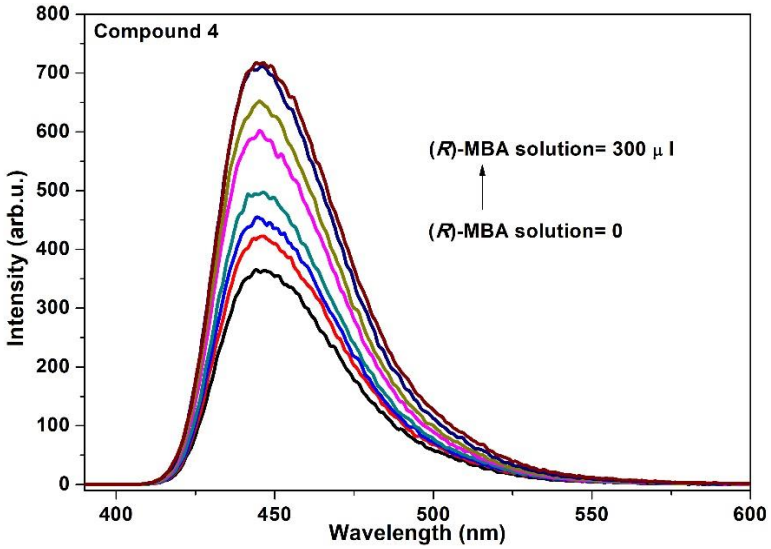

(a)

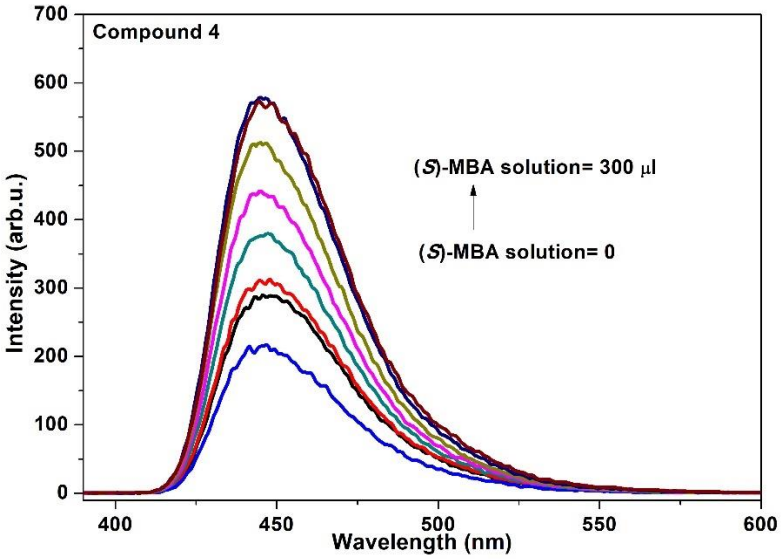

(b)

Figure 4.6. Fluorescence spectra of compound **4** in the presence of (a) enantiopure *(R) and* (b) *(S)*-α-methylbenzyl amine (sensor concentration 1.6×10^{-7} M, in DCM, excess amine was added, excited at 365 nm, slit widths were 5 nm, scan rate was 400 nm/min and 0.1 ml Et_3N was used as an additive).

To evaluate fluorescence titration data in more details, graph in Figure 4.7 in which maximum fluorescence intensity is plotted against the volume of chiral amine added was drawn. The graph consists of two curves drawn for (*R*)- or (*S*)- α-methylbenzyl amine which are overlapped almost one-to-one. In other words, it can be deduced that the compound **4** cannot differentiate the enantiomers since the addition of either enantiomer has the same effect on the fluorescence intensity of the sensor.

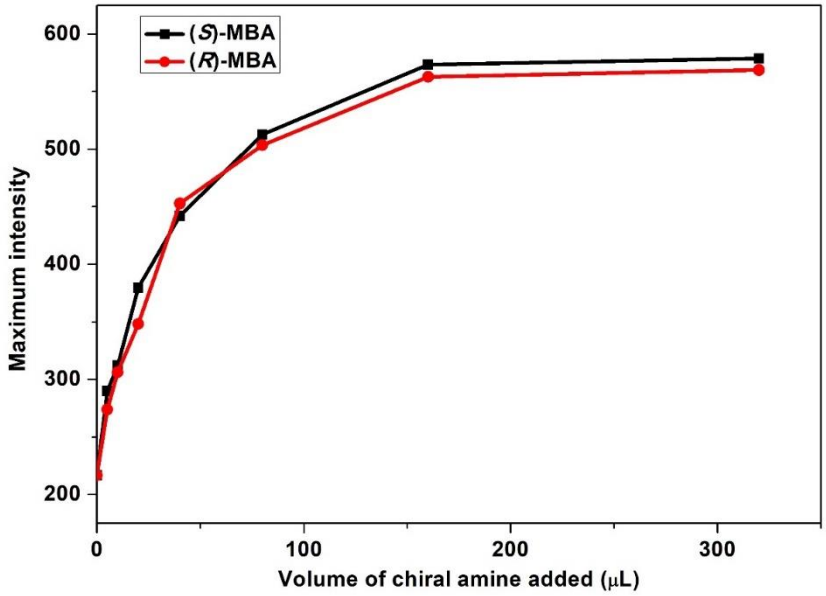

Figure 4.7. Overlapped fluorescence spectra of compound **4** in the presence of enantiopure (*R*) and (*S*)-α-methylbenzyl amine (sensor concentration 1.6×10^{-7} M, in DCM, excess amine was added, excited at 365 nm, slit widths were 5 nm, scan rate was 400 nm/min and 0.1 ml Et_3N was used as an additive).

While working with compound **4**, it was realized that hydroxyl group at 7th position may participate in acid-base reactions with chiral amines which was deduced from the dramatic increase in the fluorescence intensity (i.e. optical saturation was observed) in the absence of Et_3N additive. Thus, use of some basic additives such as Et_3N during fluorescence studies was needed. This seemed to be complicated. For this purpose, a new compound was decided to be synthesized (compound **5**, Figure 4.8) which does not have the risk of participating in acid-base reactions with analytes.

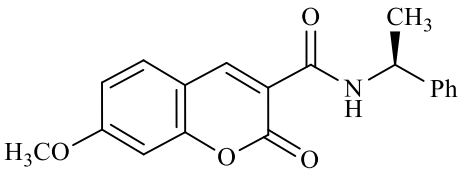

5

Figure 4.8. Methoxide derivative of compound **4**

For the synthesis of corresponding compound, three different synthetic routes involving different reaction conditions were tested (Scheme 4.7).

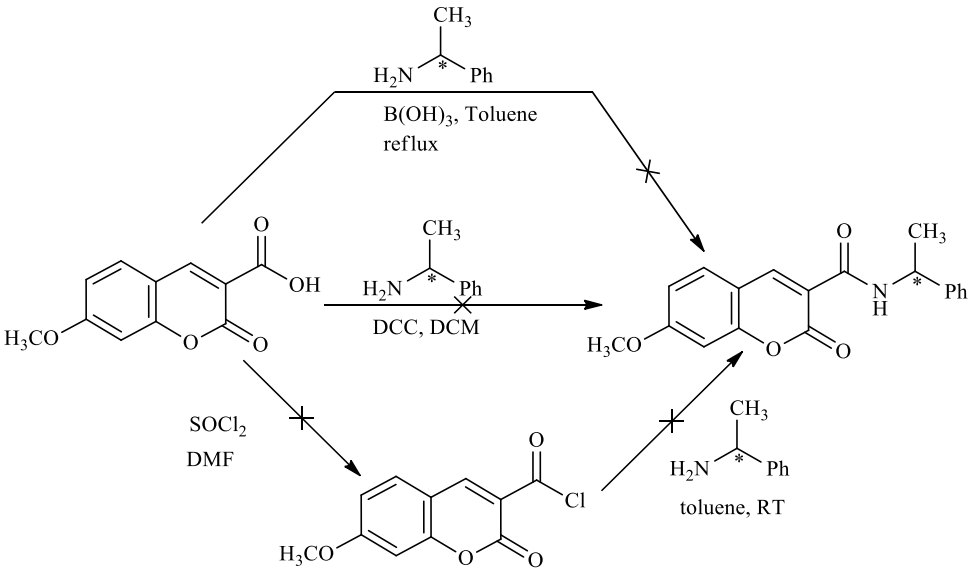

Scheme 4.7 Reaction conditions experimented for the synthesis of compound **5**

Reactions with boric acid and DCC did not result in product formation. However, from the last method, which involves chlorination and reaction with chiral amine, a product was isolated. After full analysis of the isolated product, it was realized that due to the acidic reaction medium because of thionyl chloride, the compound was hydrolyzed to compound **4**. Mechanism for the hydrolysis was proposed to be as in Scheme 4.8:

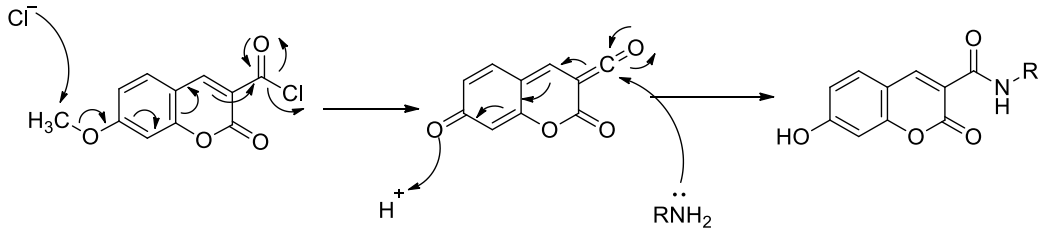

Scheme 4.8 Proposed mechanism for hydrolysis

Due to the complicated nature of the synthesis of compound **5**, it was decided to further simplify our compound, and synthesized following compounds **8** and **9** in Figure 4.9 using the same synthetic pathway that was used before (Scheme 4.9).[95] The only expected spectroscopic change was that the simple coumarin derivatives will absorb light by a blue shift of the above-mentioned compounds.

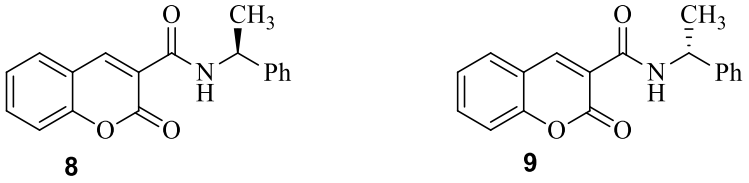

8 **9**

Figure 4.9. Coumarin- derived new chiral sensors

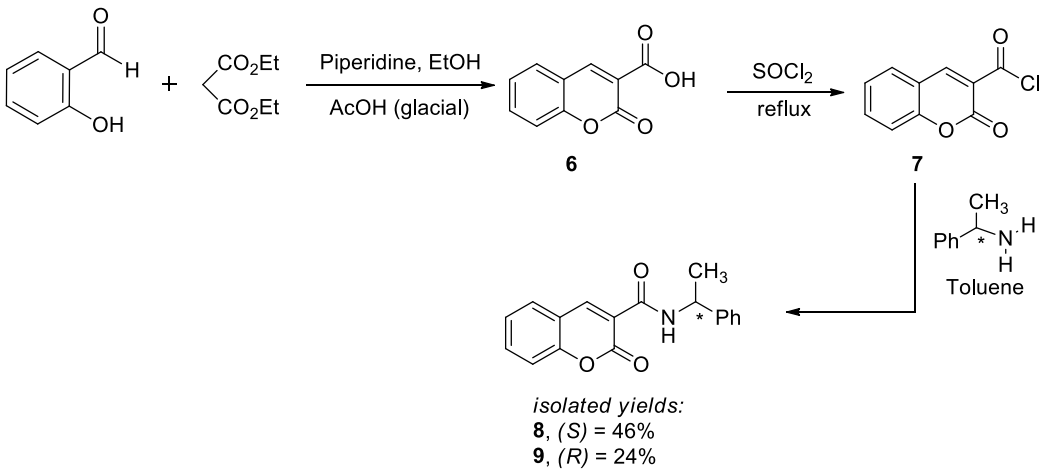

Scheme 4.9 Synthesis pathway of compounds **8** and **9**

4.3 Amino acid derivatives of coumarin-3-carboxylic acid

Amino acid derived coumarins were also synthesized. Adapting a literature procedure,[96] chiral alanine and phenylalanine derivatives (Figure 4.10) were synthesized in high yields through a benzotriazole intermediate (compound **10**, Scheme 4.10).

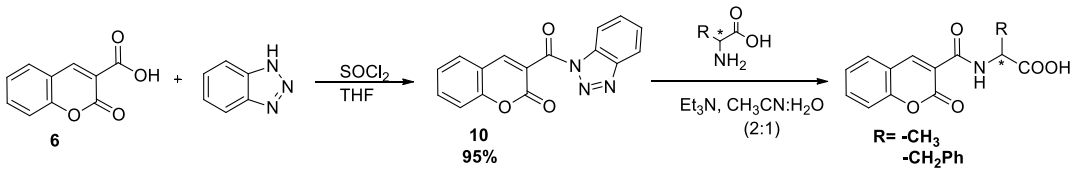

Scheme 4.10 Reaction scheme for the synthesis of amino acid derivatives **11**-**14**

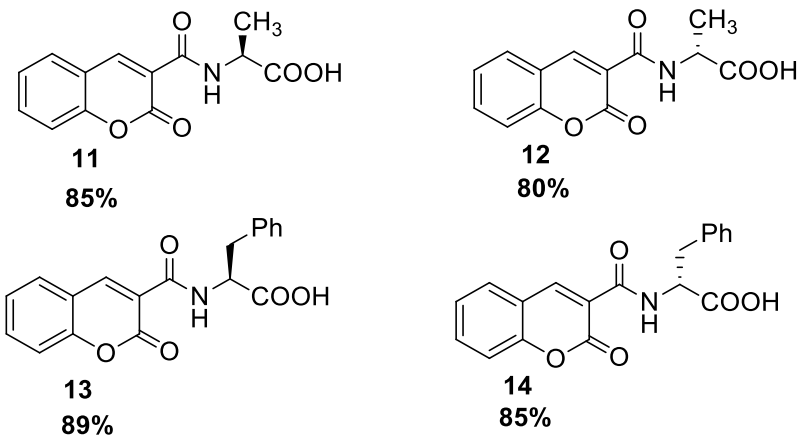

Figure 4.10. Synthesized amino acid derivatives and their isolated yields

With six new chiral coumarin derivatives in hand, fluorescence studies were carried out using enantiopure 1-phenylethanol, α-methylbenzyl amine and tartaric acid. Solvent screening studies were performed with alanine derivative (compounds **11** and **12**) at 10^{-4}M sensor concentration and using 20 equivalents chiral amine/alcohol. The solvents DCM, CH_3CN, $CHCl_3$ were screened since the use of these solvents are widely reported in the literature in this type of studies.

The results of the solvent screening studies with enantiopure (*R*) and (*S*)-1-phenylethanol were summarized in Table 4.1 below. In CH_3CN and $CHCl_3$, no

intensity change was observed upon the addition of 1-phenylethanol enantiomers. In DCM, a small selectivity was observed towards *R* enantiomer with compound **12** while compound **11** showed a reverse selectivity as expected. However, these minute selectivities did not motivate us for further investigations.

Table 4.1 Results of solvent screening studies with 1-phenylethanol enantiomers*

Solvent	Compound 11	Compound 12
DCM	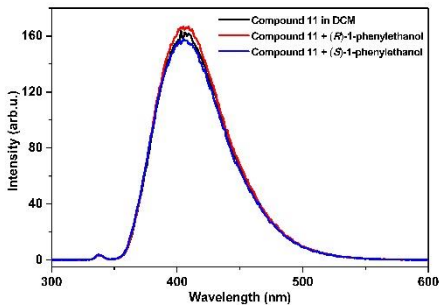	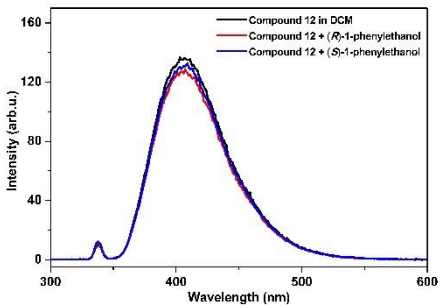
CH_3CN	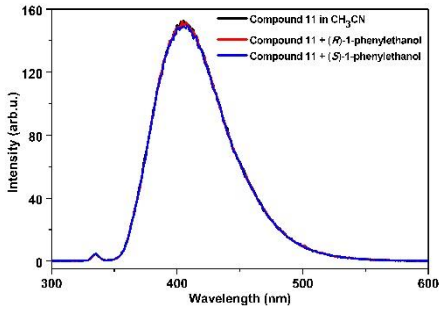	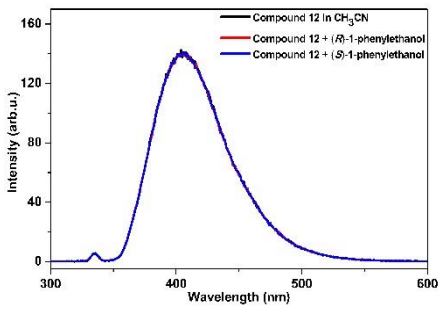
$CHCl_3$	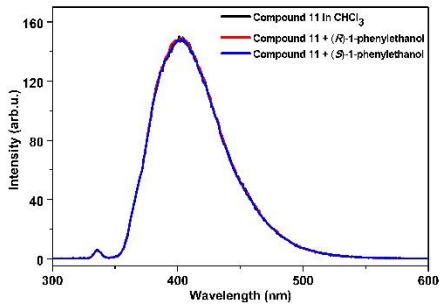	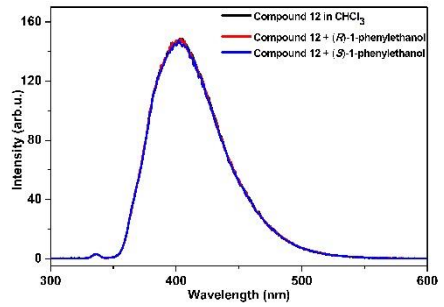

*Sensor concentration was 0.1 mM, 20 equiv. analyte was added in each case, excited at 337 nm, slit widths were 5 nm, scan rate was 600 nm/min).

The results of the solvent screening studies with enantiopure (*R*) and (*S*)-α-methylbenzyl amine were summarized in Table 4.2 below. From the fluorescence spectra recorded using solutions in CH_3CN and $CHCl_3$, intensity changes upon the addition of α-methylbenzyl amine enantiomers were observed. Indeed, there is also selectivity; however, none of them were specific to one enantiomer that is why they could not have a practical utility in our studies. In DCM, a selectivity towards (*S*)-amine was observed with compound **12**, but despite the many trials, the same results couldn't be reproduced. Moreover, the reverse selectivity must be observed with compound **11** while it was not the case in our studies. Owing to the susceptibility of fluorescence spectroscopy, the reproducibility of the results can sometimes be questionable.[97] These two reasons prevented us from further investigations on these results.

Table 4.2 Results of solvent screening studies for α-methylbenzyl amine enantiomers*

Solvent	**Compound 11**	**Compound 12**
DCM	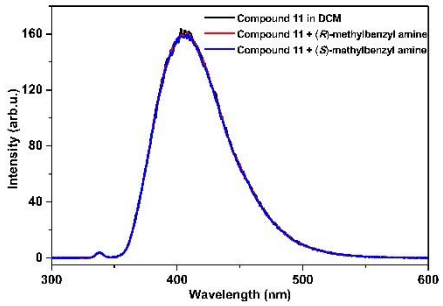	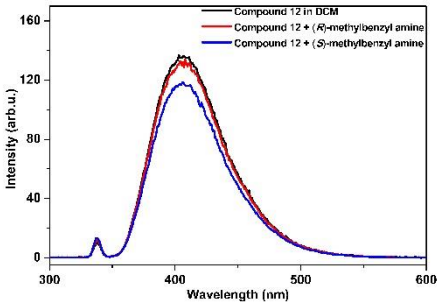
CH_3CN	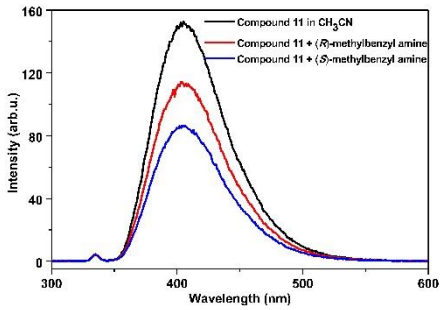	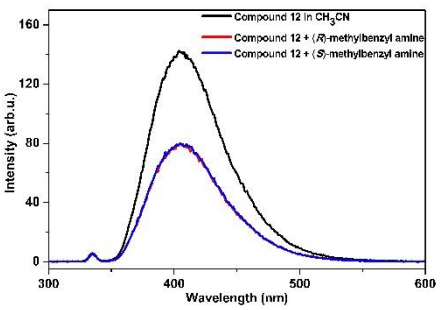

Table 4.2 (continued)		
$CHCl_3$	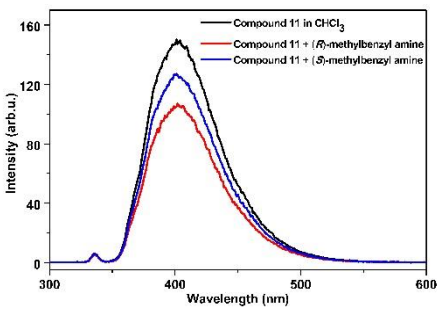	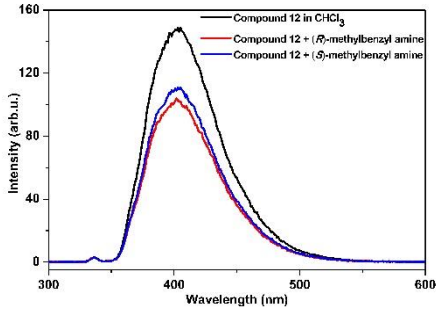

*Sensor concentration was 0.1 mM, 20 equiv. analyte was added in each case, excited at 337 nm, slit widths were 5 nm, scan rate was 600 nm/min).

The performances of all synthesized chiral sensors (compounds **8**, **9**, **11**-**14**) were tested with different substrates in chiral recognition through fluorescence spectroscopy (Tables 4.3 and 4.4). It was decided to look for alternative approaches to achieve an enantioselective differentiation.

Table 4.3 Amino acid derivative coumarin sensors and analytes that are experimented

Compounds	**11**	**12**	**13**	**14**
(R)-methylbenzyl amine	+	+	+	+
(S)-methylbenzyl amine	+	+	+	+
(R)-1-phenylethanol	+	+	+	+
(S)-1-phenylethanol	+	+	+	+
D-tartaric acid	+	+	+	+
L-tartaric acid	+	+	+	+

Table 4.4 Chiral amine derivative coumarin sensors and analytes that are experimented

Compounds	**8**	**9**
(R)-methylbenzyl amine	+	+
(S)-methylbenzyl amine	+	+
(R)-1-phenylethanol	+	+
(S)-1-phenylethanol	+	+

4.4 Synthesis of Other Coumarin Sensors

To achieve chiral recognition with coumarin derivatives, we have decided to synthesize new sensors based on this precursor since it has outstanding photophysical properties. After a detailed survey of the literature, it was realized that fluorescent sensors with point or axial chirality are widely utilized in chiral recognition studies; however, the sensors helical chirality are very rare in fluorescence spectroscopy. With this information and extensive experience in coumarin derivatives in hand, it was decided to functionalize coumarin-3-carboxylic acid with triethylene glycol (compound **17**, Figure 4.11) to investigate whether there is a gauche effect, that is believed to endow a helical form to the structure, or not.[98] If there is helicity, it was wondered that whether this helical chirality can be used for chiral sensing or not.

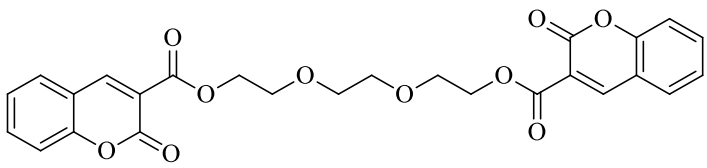

17

Figure 4.11. Triethylene glycol functionalized coumarin dimer

A literature procedure was adapted for the synthesis of compound **17**.[83] The desired compound is obtained in just a single step (Scheme 4.11).

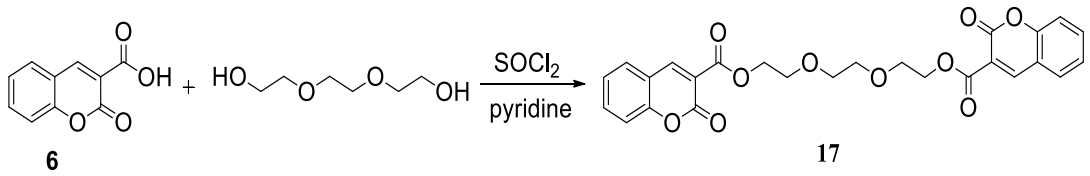

6 17

Scheme 4.11 Synthesis pathway of compound **17**

^{1}H NMR analysis was performed to prove the formation of the compound **17** and also we thought that the splitting pattern of methylene protons would give us some indication about helicity of the compound. In other words, there would be different interactions between methylene protons due to different electronic environment around each of them caused by helicity. Owing to this difference in electronic environment, splitting pattern of methylene protons were expected to differ from each other. However, the simplicity and symmetric nature of those signals (Figure 4.12) indicated that the structure was not locked in the gauche conformation at room temperature. Rather, it seems to be an average of different conformations.

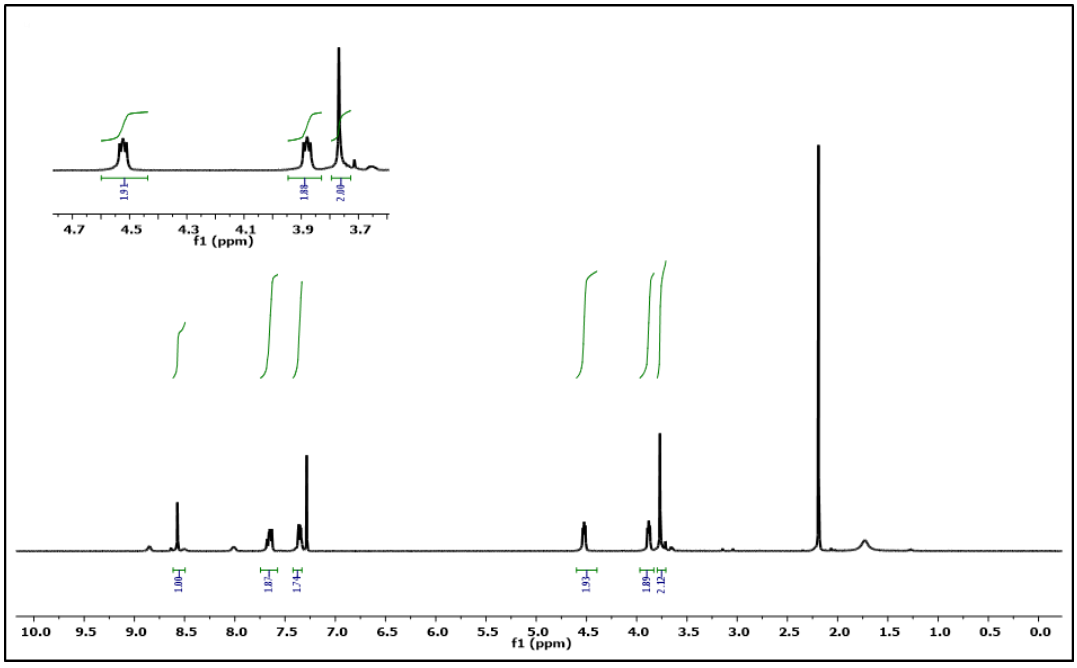

Figure 4.12. ^{1}H NMR spectrum of compound **17 (**in $CDCl_3$)

Theoretical calculations were performed for further investigations on helicity. M06/6-311g(d) level was implemented in Gaussian 09 package program[99] to carry out the calculations since m06 level was known to give results closer to the experimental values. The results indicated that the structure consists of alternating gauche and anti conformations (Figure 4.13) with a small energy difference which was calculated to be approximately 2 kcal/mol which is readily provided at room temperature. Calculations with similar but simpler molecules revealed that the presence of ester units favors the gauche arrangement by decreasing the energy compared to anti conformation while the alcohol units favors the anti conformation. As a result, due to the low energy difference between two conformations, we have concluded that the compound **17** has a dynamic chemical structure which satisfies the results of ^{1}H NMR study. Indeed, the compound did not give us the desired helicity.

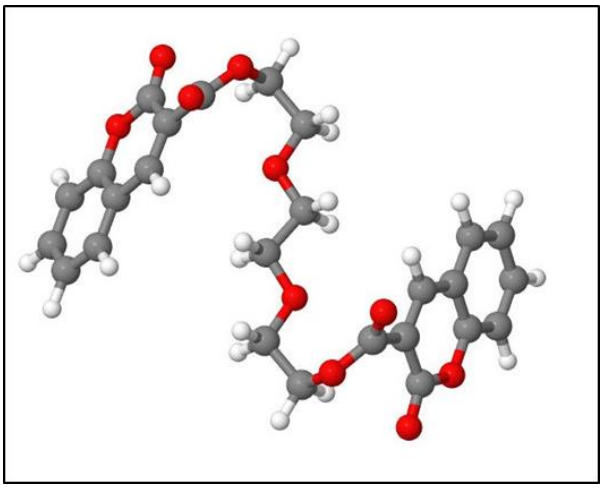

Figure 4.13. Optimized geometry for compound **17**

The compound **17** did not endow with the helical chirality; thus, it was thought that it couldn't have utility in chiral recognition studies. As a result, it was decided to look for an alternative application for it. Compound **17** resembles to crown ether-type podands in terms of its structure. This structural similarity made us think that compound **17** can behave similarly with crown ethers. Crown ethers have been known to be sensitive towards alkali metal ions. Jean-Marie Lehn, Donald Cram and

Charles Pederson got Nobel Prize in 1987 for their contributions to the detection of alkali metal ions with crown ethers. Although the crown ethers have witnessed considerable attentions over the last decades in tems of their ability to bind metal cations,[100–102] they have some inherent disadvantages. Simple crown ethers are associated with being lack of binding Na cations at clinically important concentrations (0.3-300 mM).[101] Moreover, crown ethers are expensive and not easily accessible. Apart from crown ethers,[103,104] calixarenes[105] and rhodamine derivatives[106] were also investigated in sodium and potassium detection. However, they mostly require multiple steps in their synthesis. To the best of our knowledge, designing new, easy-to-synthesize fluorescent molecules from easily-accessible and cheaper precursors are in high demand for the sake of simple and practical nature of fluorescence spectroscopy. It was thought that our sensor would serve as a better alternative.

4.4.1 Why alkali metal ions are important?

The chemical composition of the body fluids, intracellular and extracellular space is of great importance since even any small deviation can be the indication of important illnesses; and therefore, the maintainance of certain amounts of the composition is strictly required for our health. Problems related to qualitative and quantitative analysis of biologically important species have been adressed by the fluorescent signalling molecules.[38] Our further motivation is that sodium is among the most important elements for human body since it regulates blood volume, blood pressure, osmotic equilibrium and pH.[102] Moreover, it's known in the literature that cancer cells have higher sodium/potassium ratio than normal, healthy cells.[107,108] The analysis of sodium and potassium ions was gathered our attention since there is an optimum sodium/potassium ratio that human body can tolerate and the deviations from this optimum ratio can be indication of many important diseases such as:[39,40,109]

- Hypertension
- Cardiovascular diseases

- Cancer
- Parkinson
- Alzeihmer
- Cushing syndrome

4.4.2 Studies related to cation sensing with filexible coumarin dimers

A series of coumarin dimers linked through ethylene glycol units having different chain lengths (compounds **15-18**, Figure 4.14) was synthesized. The glycols that were used as linkers in the synthesis of fluorophores are also known to be biocompatible and biodegradable.[85] Especially ethylene glycol has been of particular importance for biomedical applications.[110] Our foresight in the study was that there would be a size-matching between the sensor's cavity and size of the metal ions. Indeed, this size-matching effect was thought to be the driving force for complexation with cations and selectivity towards one of them.

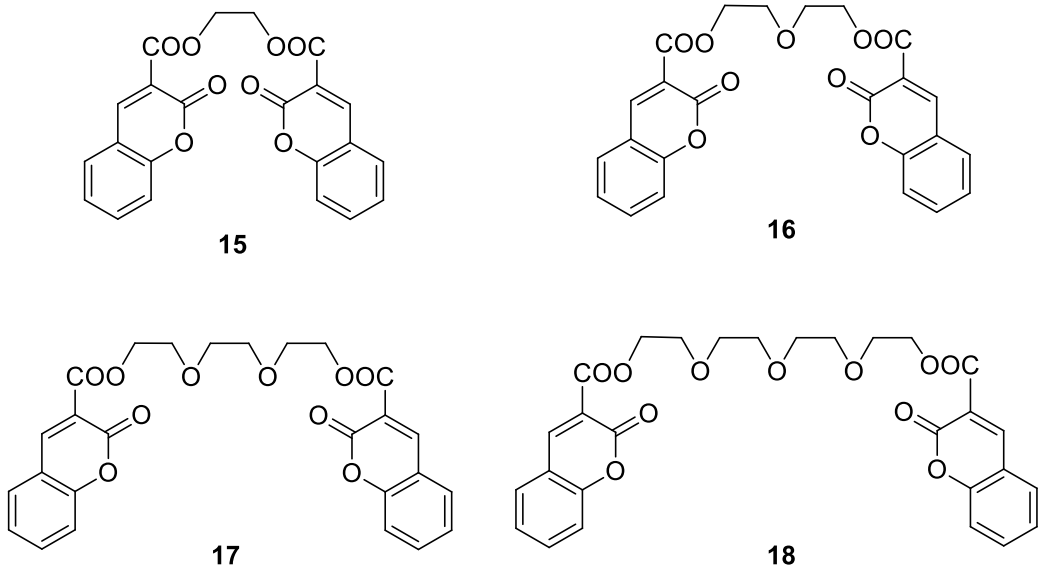

Figure 4.14. Flexible coumarin dimer series

During fluorescence recognition studies, perchlorate salts of corresponding cations were used. Although perchlorates are known to be explosive, they were used since it

is a weakly coordinating anion and believed to act as an inert counterion.[111,112] In other words, perchlorate anion is separated from the cations in solution easily as if they are ‘’naked’’ so that there is no risk of anion interference. Moreover, the corresponding perchlorate salts are soluble in CH_3CN. Acetonitrile was selected as the solvent in this study since it can be assigned as a relatively ‘’*green*’’ organic solvent since its oxidation product is acetic acid.

With these fluorescent compounds in hand, preliminary fluorescence studies were carried out to investigate whether any of these sensors would respond to the presence of either cation or not. Results are summarized in Table 4.5:

Table 4.5 Results of fluorescence studies conducted for determination of the sensor that gives best selectivity*

Sensor	**Fluorescence spectra**
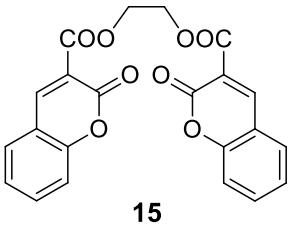 **15**	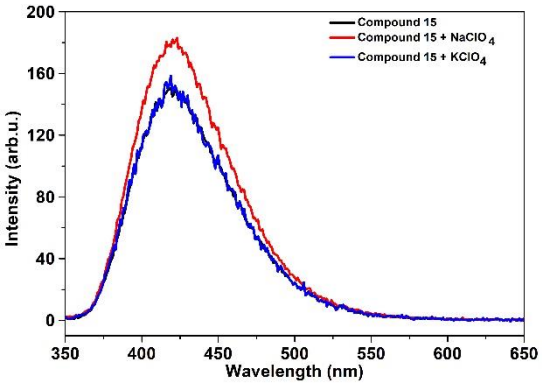
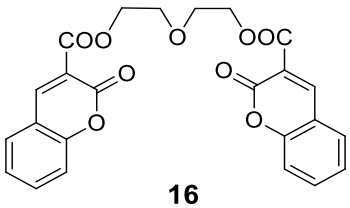 **16**	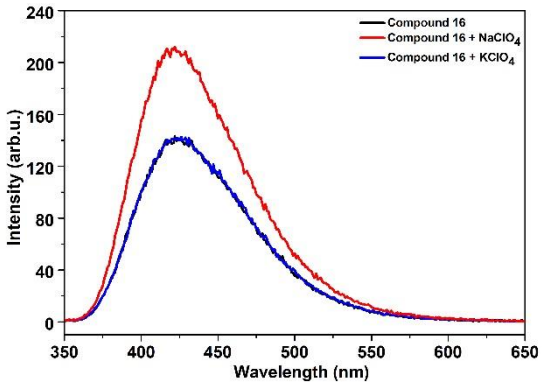

Table 4.5 (continued)

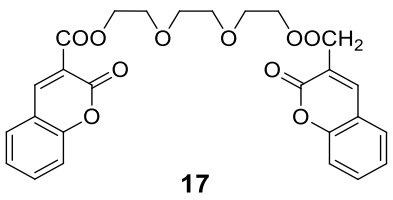 **17**	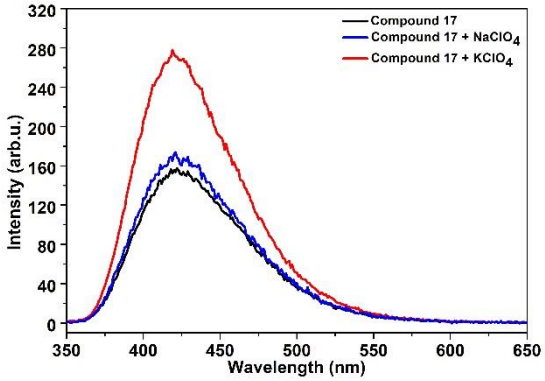
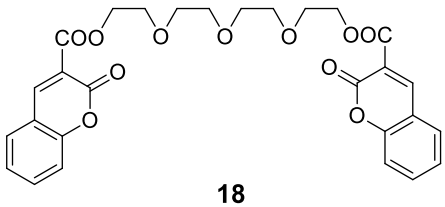 **18**	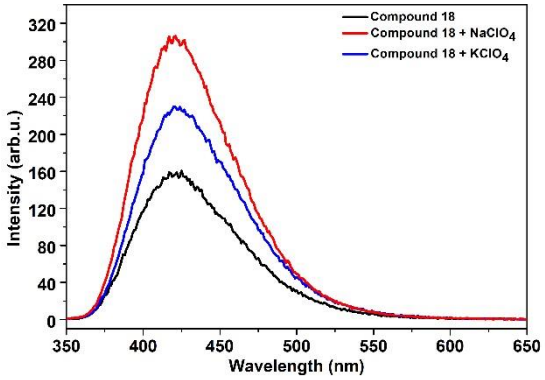

*Sensor concentration 5×10^{-5} M, in CH_3CN, 100 equiv. metal salt was added in each case, excited at 335 nm, slit widths were 5 nm, scan rate was 600 nm/min).

From the fluorescence spectra that were recorded to identify the best sensor in the series, it was realized that our fluorescent molecules seemed to be selective towards sodium cation and the driving force for this selectivity is size-matching effect as expected. According to the fluorescence spectra, the compound **15** gave us a small selectivity towards Na^+; however, a better selectivity was observed with compound **16**. Moreover, with the compounds **17** and **18**, the chain lengths are increased as a result of which the cavity size of the sensors are increased. It can be seen from the fluorescence spectra that the increase in the cavity size has lead to the interference of potassium cation and decrease in selectivity towards sodium cation. There is also

a selevtivity towards Na^+ with compounds **17** and **18**; however, due to the interference of K^+, the compounds **17** and **18** cannot be used for practical purposes. As a result, we have decided to continue our further investigations with compound **16** as it's the best sensor in this series.

As the second step of our investigations, concentration screening study was performed in which the concentration of Na^+ was increased from 0 mM to 45 mM (Figure 4.15). Up to 35 mM, the fluorescence intensity has increased linearly and then it remained constant. Thus, the dynamic range was determined to be in between 0-35 mM which corresponds to intracellular sodium cation concentration range,[113] and is also in between clinically important concentrations reported for sodium cation.[101]

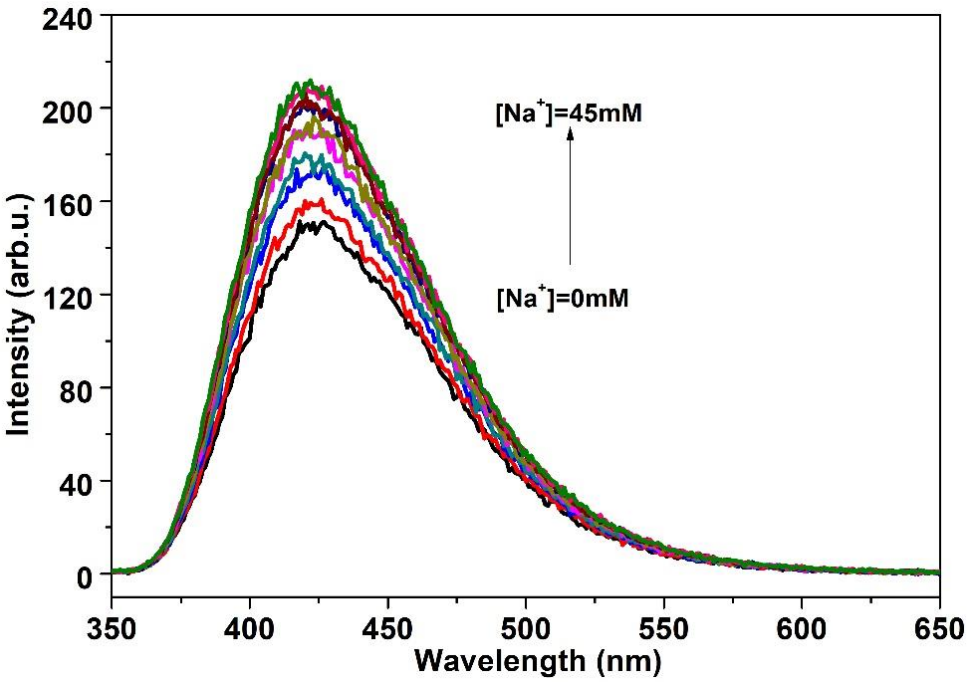

Figure 4.15. Fluorescence spectra of compound **16** in case of different sodium cation concentrations (sensor concentration 5×10^{-5} M, in CH_3CN, excited at 335 nm, slit widths were 5 nm, scan rate was 600 nm/min).

To further process of our experimental data, two theoretical plots were utilized. The first one was the Stern-Völmer plot (Figure 4.16). A modified Stern-Völmer

equation[74] (Equation 4.1) was used to further examine the fluorescence enhancement of the sensor **16** in the presence of Na^+ and K^+. Stern-Völmer plot indicates that addition of increasing concentration of Na^+ increases the intensity of sensor while K^+ addition has almost no effect. The information on this plot can be used in terms of qualitative and quantitative analysis. Qualitatively, the large difference between the slopes of these curves ensures the selectivity towards Na^+. Quantitatively, the slopes of two curves gave us the Stern-Völmer binding constants of the complexes formed between the sensor and the cation. A "*selectivity factor"* can be defined by dividing the SV binding constants of two cations, and it was found to be 51.25 which is a promisingly high value. Thus, it can be concluded that fluorescence enhancements were selective.

$$\frac{I}{I_o} = 1 + K_{SV}[M^+] \qquad \text{Equation 4.1}$$

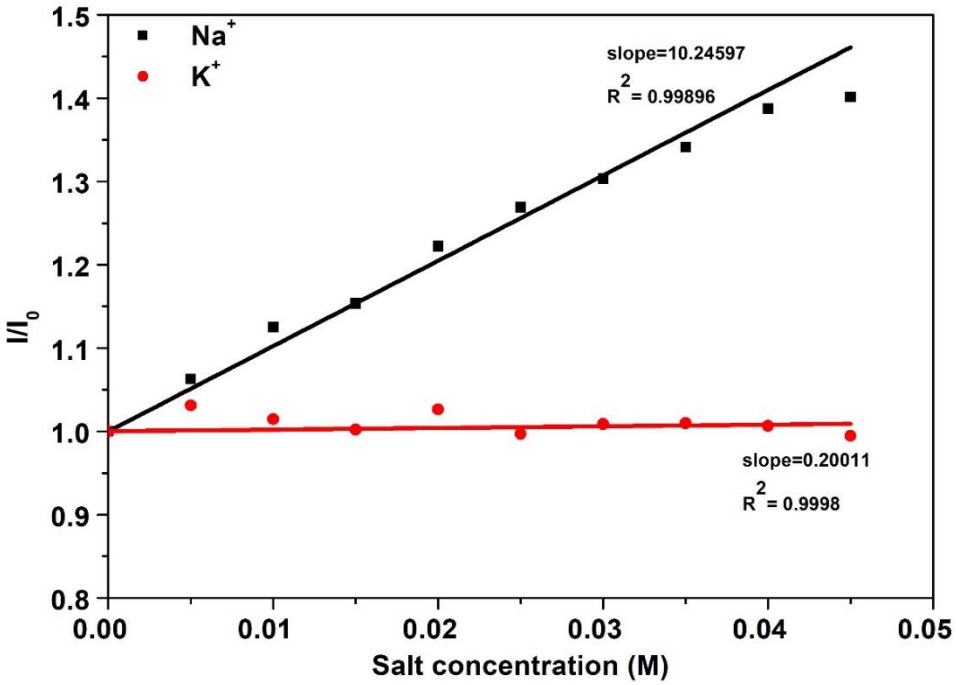

Figure 4.16. Stern-Völmer plot for titration studies with compound **16** in the presence of sodium and potassium cations

Titration data for Na^+ were further analyzed by Benesi-Hildebrand plot (Equation 4.2) to calculate binding stoichiometry.[114,115] The linear fitting was found to be more

correlated with our experimental data. As a result, the Benesi-Hildebrand plot indicates that our sensor forms 1:1 complexes with Na^+ ions (Figure 4.17) and the association constant was calculated from the slope of the curve (K_{BH}=5,7 M^{-1}).

$$\frac{1}{I-I_o} = \frac{1}{I_1-I_o} + \frac{1}{(I_1-I_o)K[M^+]} \qquad \text{Equation 4.2}$$

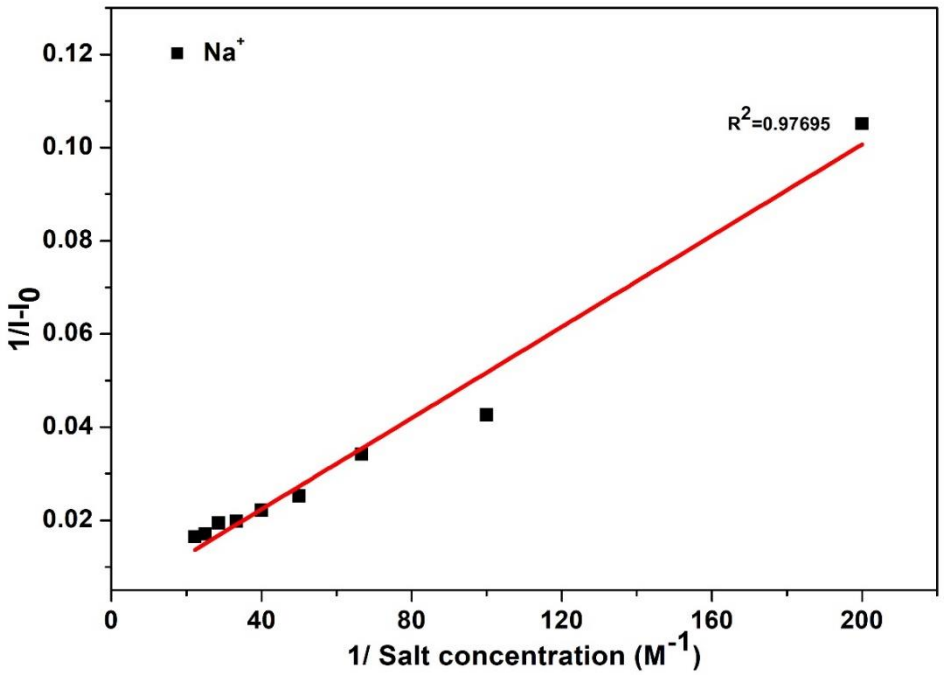

Figure 4.17. Benesi-Hildebrand plot for titration studies with compound **16** in the presence of sodium cations

It was postulated that metal ions are placed in the cavity between coumarin units coordinating through carbonyl oxygens and oxygen atoms of the linker groups. The metal complexes and the dimer **16** were optimized at the B3LYP/SVP level of theory as implemented in Gausian 09.[99] The gas phase calculations showed that the sodium cation complexation is 24.74 kcal/mol more exergonic than the potassium cation complexation is. The stability of the sodium complex with **16** is contributing to the rigidity; thus, the differentiation is observed (Figure 4.18).

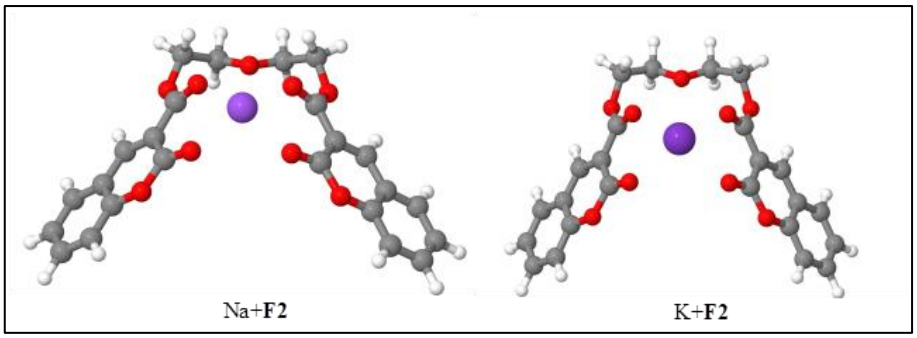

Figure 4.18. The optimized structures of Na^+ and K^+ bound to **16**

To further clarify whether the oxygens in the linker part have a role in this complex formation or not, 1,8- octanediol derivative **19** (Figure 4.19) was synthesized by the same synthetic route given in Scheme 4.6.

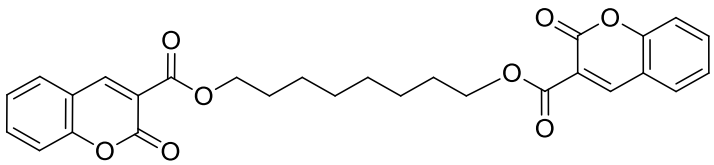

19

Figure 4.19. The structure of 1,8-octane diol derivative coumarin dimer, **19**

Fluorescence studies under the same conditions gave us the following spectra given in Figure 4.20. Compound **19** shows no selectivity towards either cations. This suggests that the oxygen atoms in the linker unit contribute to complex formation and facilitate the electronic coupling between two coumarin units.

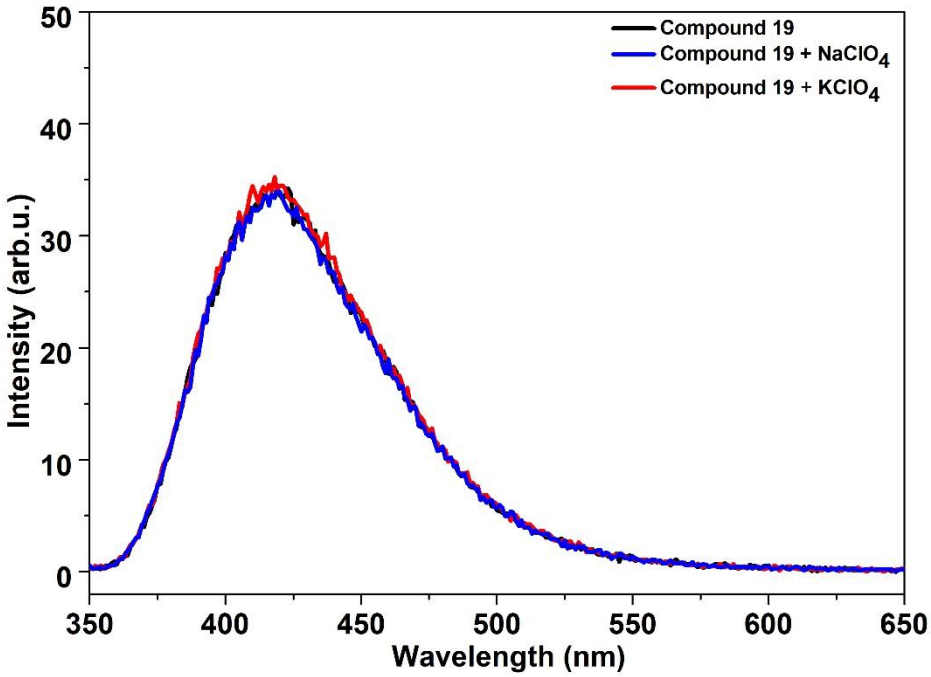

Figure 4.20. Fluorescence spectra of compound **19** in the presence of Na^+ and K^+ ions (sensor concentration 5×10^{-5} M, in CH_3CN, 100 equiv. metal salt was added, excited at 335 nm, slit widths were 5 nm, scan rate was 600 nm/min).

The compound **20** (Figure 4.21) was synthesized to see whether the dimeric structure of the sensor is necessary for cation sensing or not.

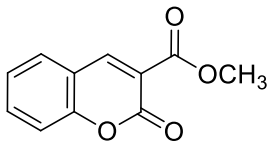

20

Figure 4.21. Methyl ester of coumarin-3-carboxylic acid

It can be deduced from the fluorescence spectra of this compound in the presence of metal ions (Figure 4.22) that the addition of metal ions has no effect on the fluorescence intensity of the sensor. This indicated us that there is no interaction between cations and the sensor. Thus, it was realized that the dimeric structure is required for cation sensing.

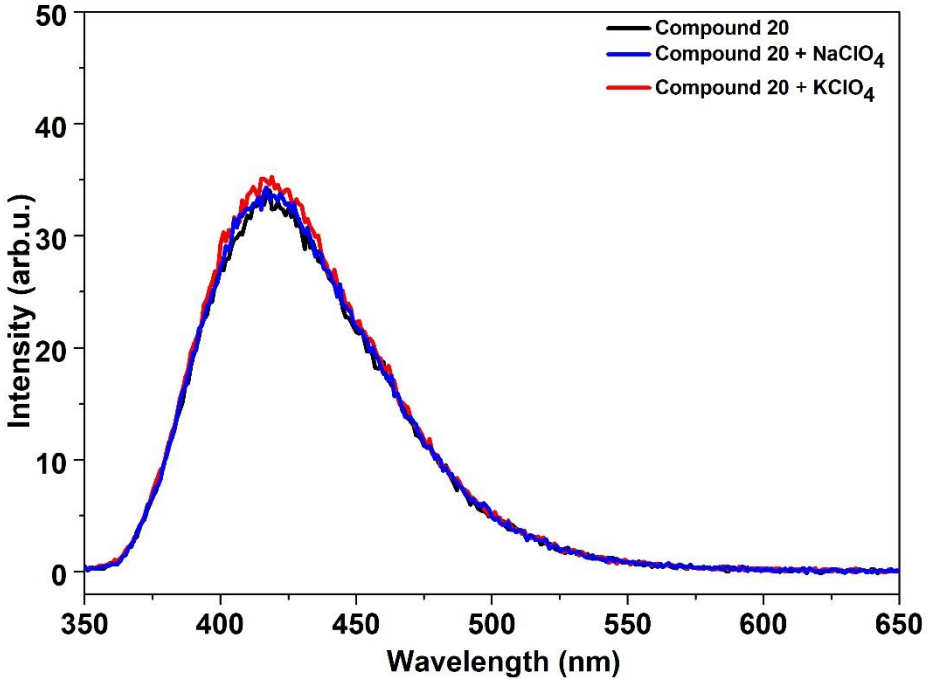

Figure 4.22. Fluorescence spectra of compound **20** in the presence of Na^+ and K^+ ions (sensor concentration 5×10^{-5} M, in CH_3CN, 100 equiv. metal salt was added, excited at 335 nm, slit widths were 5 nm, scan rate was 600 nm/min).

In the literature, the tendency of coumarin units to reside in close proximity due to π-π stacking is known.[116] With all these important information in hand, a structure for the cation-sensing complex was proposed to be as in Figure 4.23:

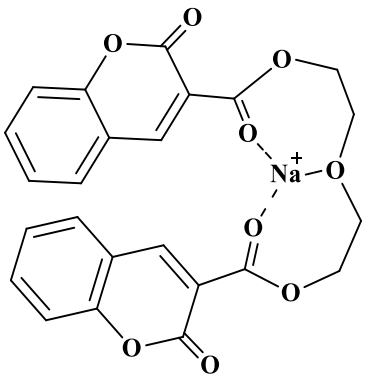

Figure 4.23. Proposed structure of the cation-sensing complex

In this study, new coumarin-based flexible fluorescent molecules linked through ethylene glycol units of different chain lengths were synthesized in just a single step. It was believed that these sensors will serve as a better alternative of crown ethers which are expensive and not easily accessible. The compounds **15**, **16**, **18** and **19** were not reported in the literature and the compound **16** was able to differentiate Na^+ and K^+ ions through fluorescence spectroscopy succesfully. Moreover, it was known that coumarin and ethylene glycol derivatives are biocompatible precursors. By choosing a relatively green organic solvent, we also tried to make it more environmentally friendly. In this study, our intentions and efforts on designing a sensor which can be easily synthesized are met successfully. We have successfully performed a study under simpler, cheaper and greener conditions compared to the studies reported in the literature.

Although the study of cation-sensing with flexible coumarin dimers has satisfied us in terms of the fact that facilitating easily accessible ethylene glycol units contribute to this area of interest, we could not achieve our goal in chiral recognition. However, with this study, an extensive experience on coumarin and its derivatives were attained.

4.5 New fluorescent sensor for complexation with Zn^{2+}

Previously, the design principle of our fluorescent molecules was based on the generation of hydrogen bonding pathways and formation of a chiral pocket through insertion of a chiral moiety on a highly fluorescent molecule. However, a differentiation couldn't be observed with this strategy. Thus, it was decided to utilize a new strategy for chiral recognition studies through fluorescence spectroscopy.

Imperiali has reported that Zn^{2+} can form chiral complexes since Zn^{2+} has ability to bind peptides and proteins (in an analogy to zinc finger domains).[117] It was thought that differentiation of enantiomers could be achieved through Zn^{2+} complexes. Moreover, Wolf group has a report on chiral recognition with zinc complexes via

CD spectroscopy.[118] For this purpose, the amino acid derivatives of coumarin (compounds **11**-**14**) were used and their fluorescence spectra were recorded in the prescence of two different Zn^{2+} salts. It was postulated that coordination with zinc cation would change the electron density of parent sensor; as a result, a change in the fluorescence spectrum (in intensity or wavelength) associated with the change in electron density and/or electronic structure should be observed. However, we couldn't see any difference in the fluorescence spectra of our compounds. This showed that there is no interaction between Zn^{2+} and our chiral coumarin derivatives.

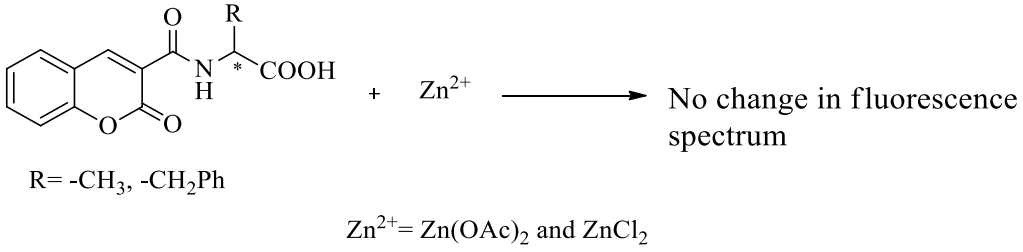

Figure 4.24. First trials for Zn^{2+} complexation

To test the ideas of zinc complexation, a new compound (compound **21**) was designed. 2-hydroxynaphthyl amine-based Schiff bases are known to be versatile coordinating agents. They are utilized in the preparation of various fluorescent sensors.[119] The compound **21** is believed to act as a bidentate ligand, and expected to form complexes with Zn^{2+} through hydroxyl groups. The compound **21** was easily synthesized in high yields by adapting a procedure from the literature (Scheme 4.12).[120]

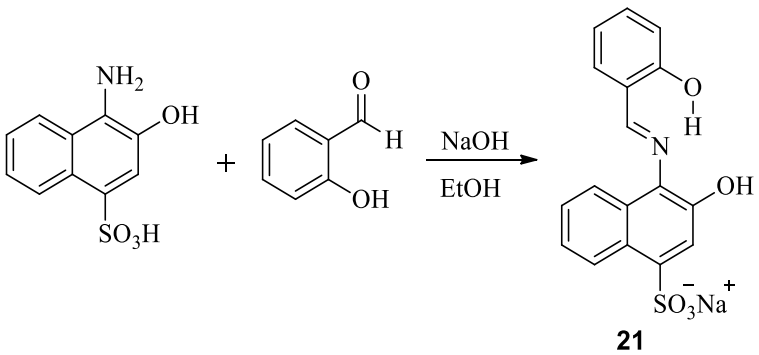

Scheme 4.12 Synthesis of Schiff base, **21**

The ^{1}H NMR spectrum of the compound **21** indicated that the hydroxyl proton on phenyl unit is shifted to lower field (13.5 ppm) compared to hydroxyl proton on naphthalene unit (10 ppm) due to the hydrogen bonding interaction with imine nitrogen (Figure 4.25).

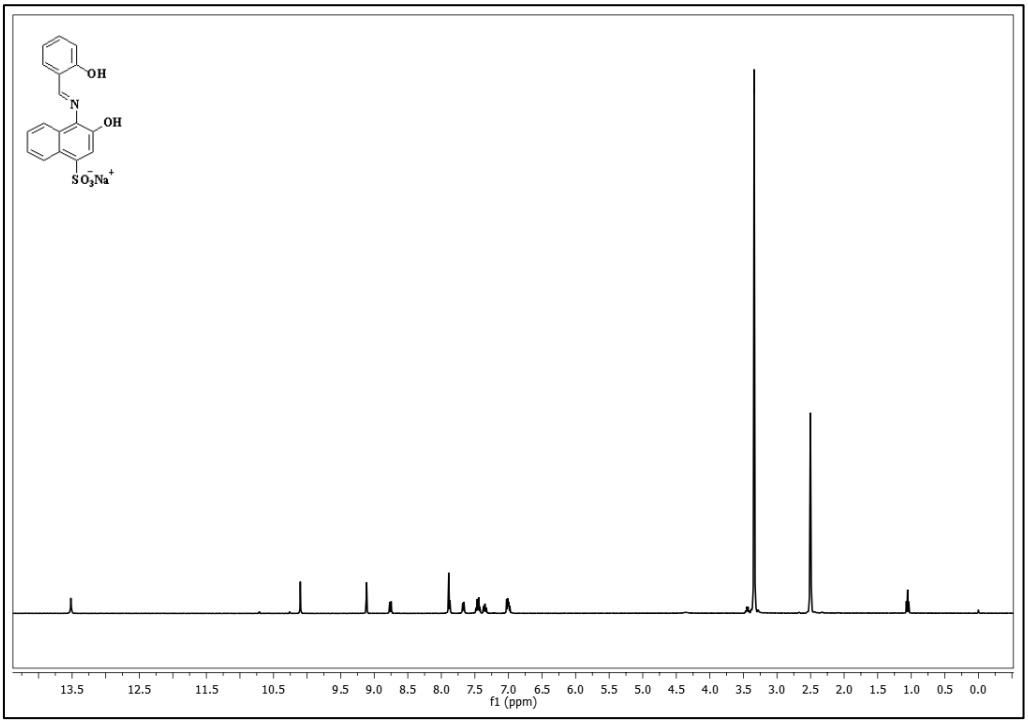

Figure 4.25. ^{1}H NMR spectrum of Schiff base, **21** (in DMSO-d_6)

Investigations on the complex formation between our compound **21** and Zn^{2+} revealed following UV-Vis and fluorescence spectra (Figure 4.26). The large red shift in UV-Vis spectra and the decrease in the intensity of fluorescence signal made us think that at least there is an interaction between Zn^{2+} and compound **21**. Most probably, the conjugation is increased upon Zn^{2+} binding, as a result of which the HOMO-LUMO energy difference is decreased and a red shift is observed in UV-Vis spectrum. Moreover, it was thought that after the Zn^{2+} coordination, the compound becomes somehow twisted. In other words, planarity is decreased as a result, fluorescence intensity is decreased.

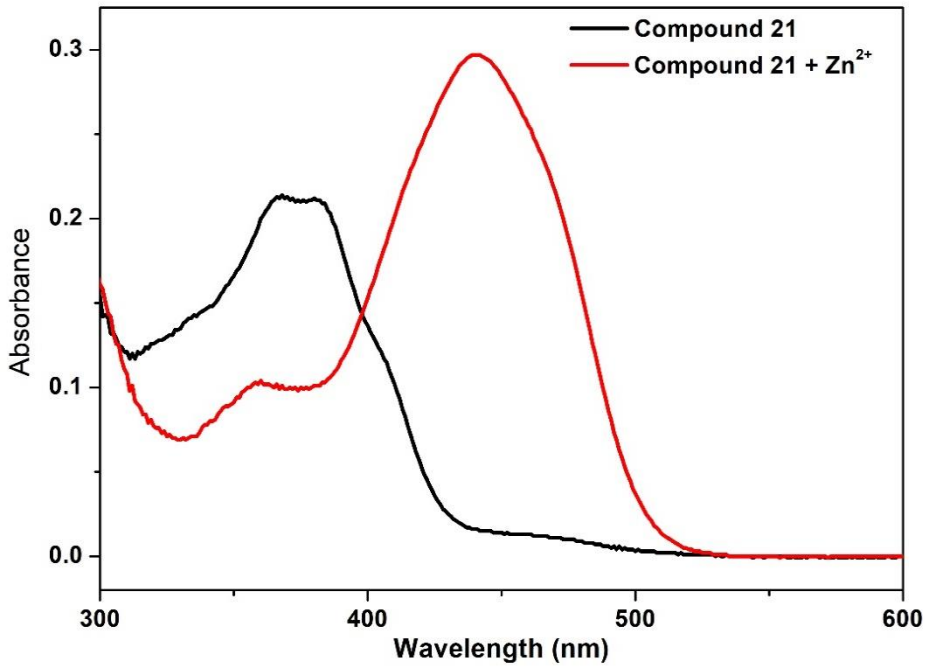

(a)

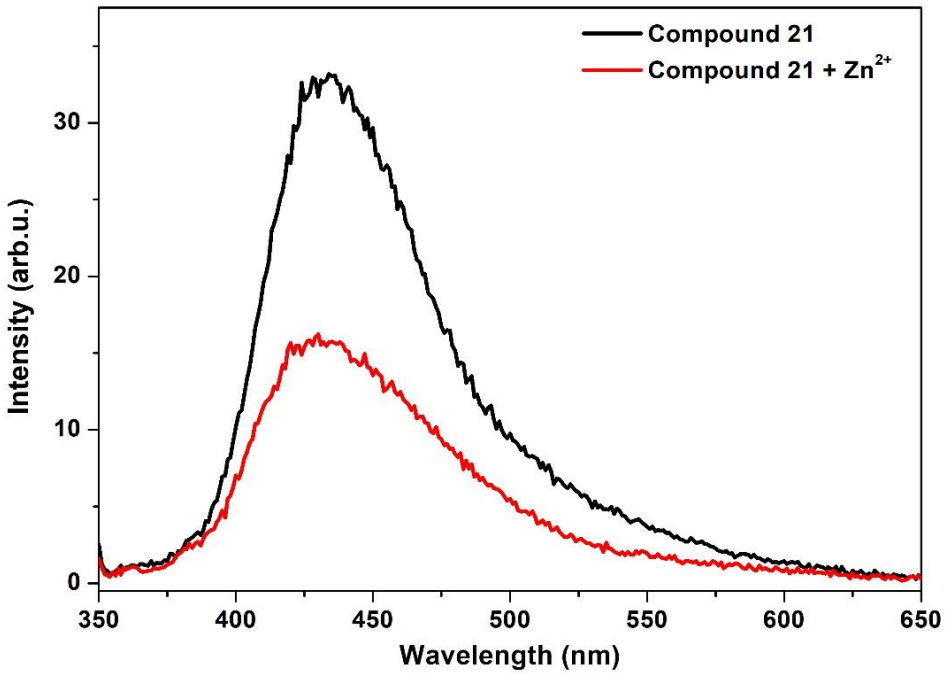

(b)

Figure 4.26. (a) UV-Vis and (b) fluorescence spectra of Schiff base in the absence and presence of Zn^{2+} salt in MeOH:2% DCM

Compound **21** was tested towards wide variety of substrates involving carboxylic acid derivatives, amino acids, alcohols, and diols. The fluorescence spectroscopy results showed that our sensor is responsive to all carboxylic and α-hydroxycarboxylic acid derivatives which is characterized by change in the fluorescence signal intensity. The results are summarized in Table 4.6.

Table 4.6 Results of fluorescence studies with Schiff base-zinc complex*

Analyte	**Fluorescence Spectra**
Tartaric acid	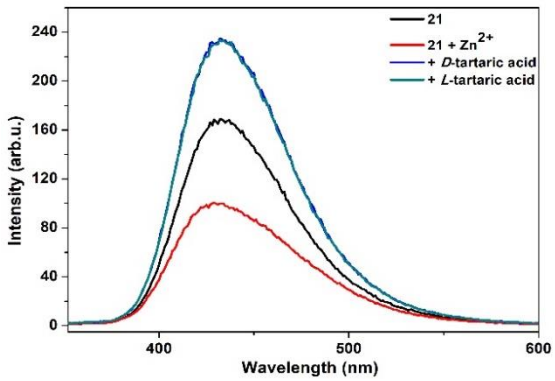
Mandelic acid	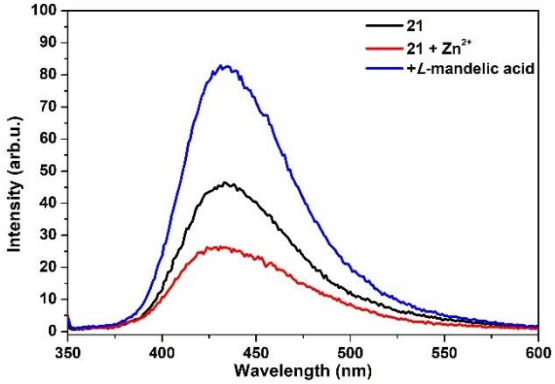
Lactic acid	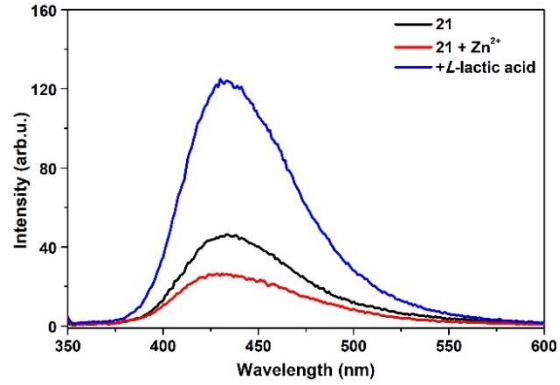

Table 4.6 (continued)	
Propionic acid	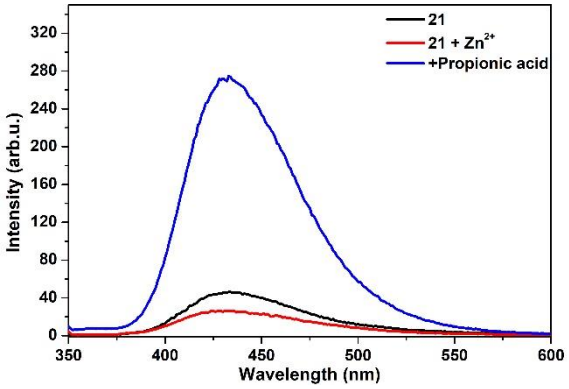
Alanine	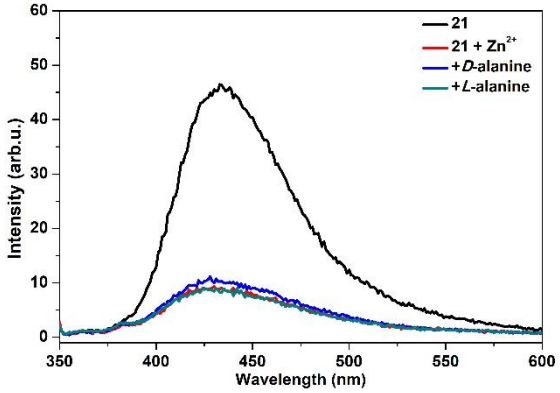
Phenylalanine	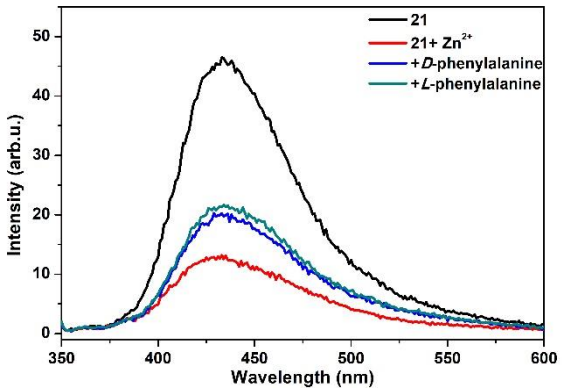

Table 4.6 (continued)

Glucose	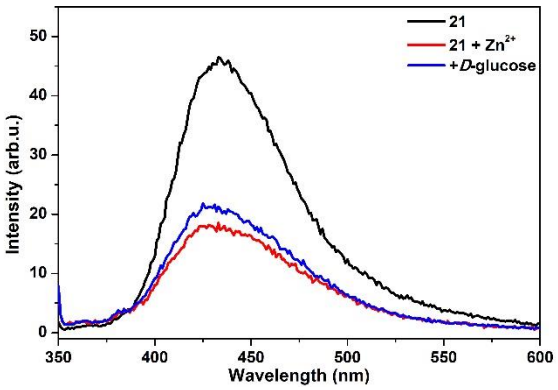
2-Butanol	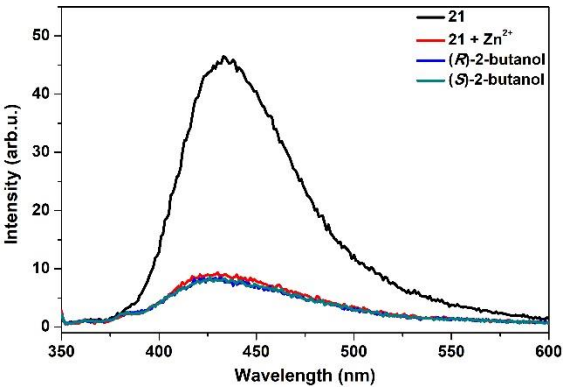
trans-1,2-cyclohexanediol	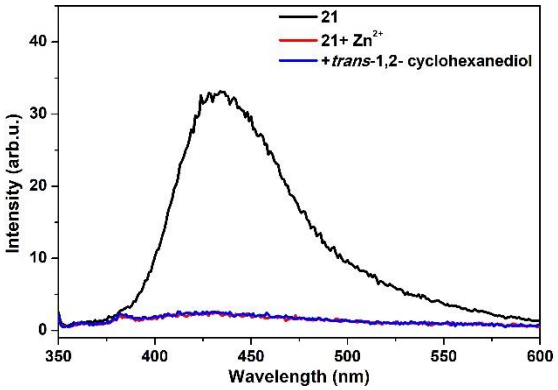

Table 4.6 (continued)	
Ethylene glycol	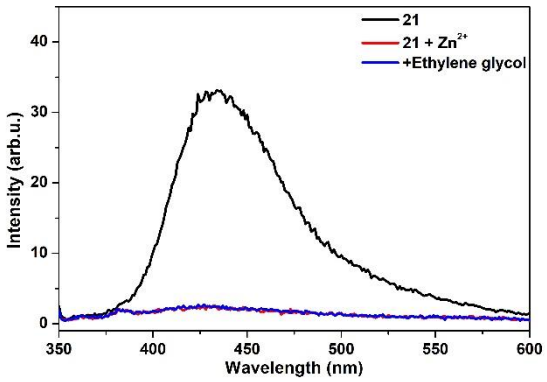

* Fluorescence spectra of the compound **21** in the presence of different compounds (Sensor concentration was 0.1 mM in MeOH:2% DCM, 7.5 equiv. analyte was added in each case, excited at 345 nm, slit widths were 5 nm, scan rate was 600 nm/min).

The results of the fluorescence studies related to determination of substrate scope were summarized in Table 4.6. The Schiff base-zinc complex responded to all carboxylic acid and α-hydroxy carboxylic acid derivatives and phenylalanine, and not responded to alcohols or diols or alanine. In other words, the changes in the intensities indicate that our sensor is able to detect the presence of such compounds. However, during these studies related to Zn^{2+} complexes, it was realized that they are very unstable and not easy to handle. It was also reported in the literature that Zn^{2+} complexes are so fragile that they should be freshly prepared and used immediately after preparation.[70] Thus, the experiments were repeated in the absence of Zn^{2+}. It was realized that compound **21** was able to detect tartaric acid enantiomers even in the absence of Zn^{2+}, gladly. However, the concentration screening studies showed that the addition of either tartaric acid enantiomer has nearly the same effect on the fluorescence intensity of the sensor (Figure 4.27).

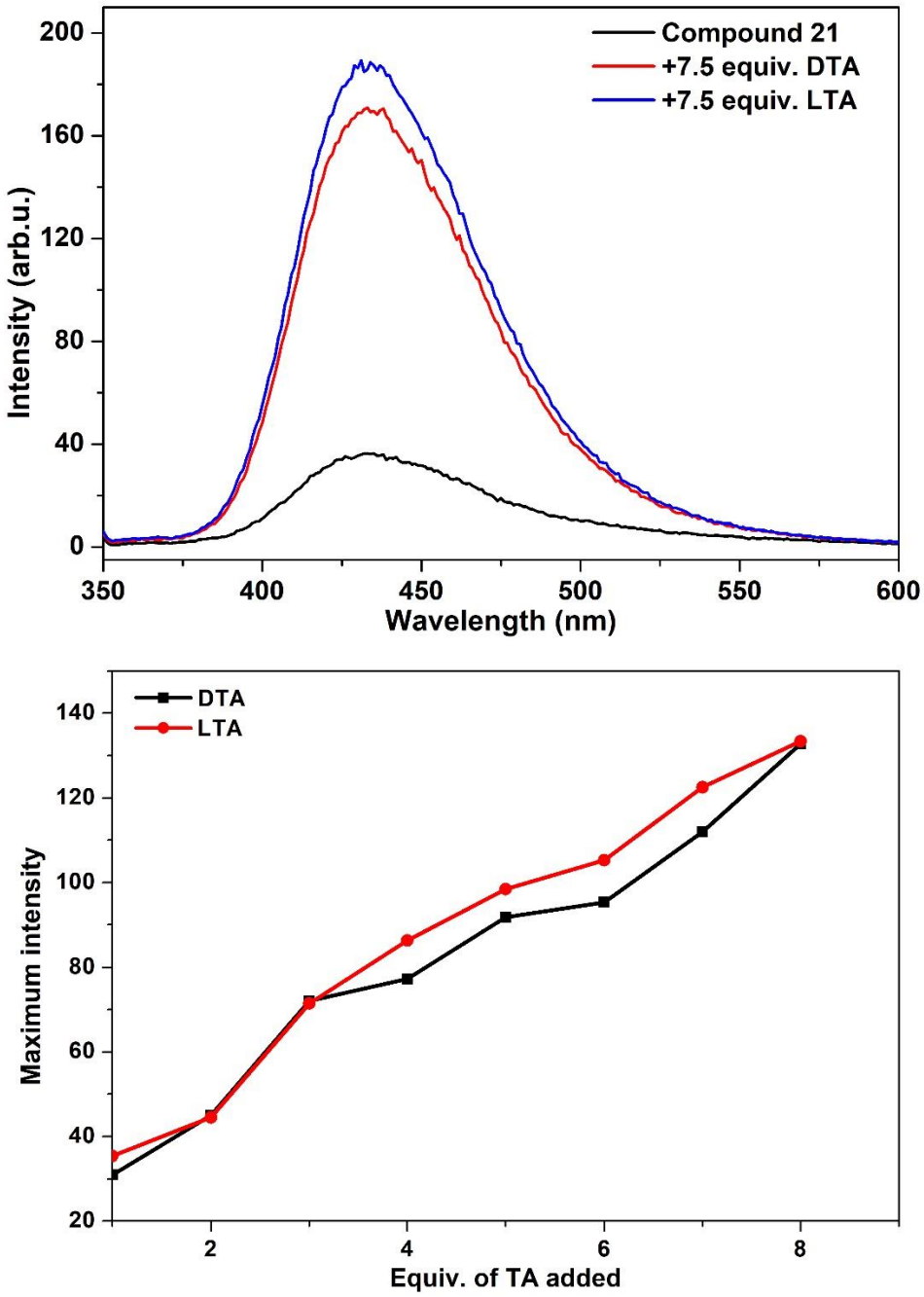

Figure 4.27. Fluorescence spectra of compound **21** in the presence of tartaric acid enantiomers (Sensor concentration was 0.1 mM in MeOH:2% DCM, excited at 345 nm, slit widths were 5 nm, scan rate was 600 nm/min).

For further investigations about the fluorescence intensity changes, theoretical calculations[99] were performed for conformational analysis. For the simplicity,

different conformations of acid form were submitted for calculations. The ground state geometries for six different conformations of acid form were optimized by m06/6-311+g(d) level as implemented in Gaussian 09.[99] The structures and relative energies of optimized conformations are summarized in Table 4.7 below:

Table 4.7 Different conformations of compound **21***

Conformer	Optimized structure	2D structure	Dihedral angle	Relative energy (kcal/mol)
21-C1	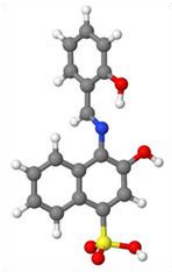	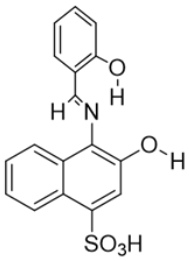	**-67°**	**1.8**
21-C2	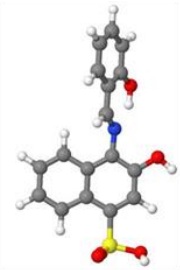	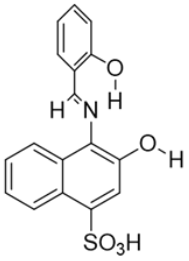	**64°**	**2.8**
21-C3	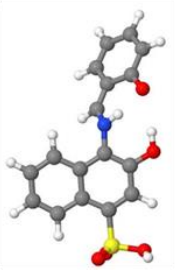	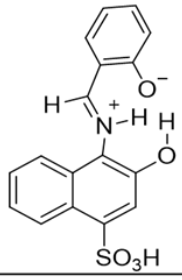	**-68°**	**5.9**
21-C4	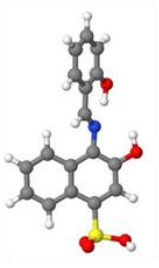	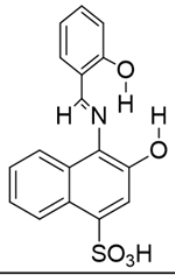	**54°**	**0**

Table 4.7 (continued)				
21-C5	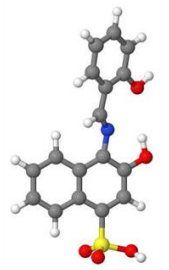	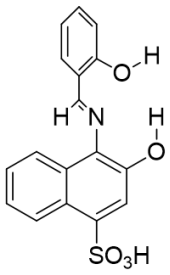	**41°**	**7.1**

* The graphics in Table 4.7 were created by using Jmol[121] which is an open-source Java viewer for chemical structures in 3D.

Different conformers were named from **21-C1** to **21-C5**. They consist of twisted forms of compound **21** as reflected by their dihedral angles (angle between naphthyl plane and phenyl plane). The conformers **21-C1** and **21-C2** are enantiomers, and they have slightly higher energy compared to **21-C4**. In conformation named as **21-C3**, it was realized that the hydroxyl proton on phenyl unit was shifted to imine nitrogen due to the close proximity; however, **21-C3** has the second highest energy among these conformations. In **21-C3**, the proton on imine nitrogen becomes more acidic, while this result was not observed experimentally. It can be inferred from the Table 4.7 that the conformer **21-C4** has the lowest energy among all for geometrical reasons. Besides that hydrogen bond formation is favored in this conformation, six-membered ring formation occurs in this geometry. For hydrogen bonding interaction to occur, six-membered ring formation is preferred over five-membered ring formation since it better fulfills the geometrical criteria for hydrogen bonding interaction. The conformer **21-C5** was found to have the highest energy among all since the hydrogen bonding is not favored in this conformation.

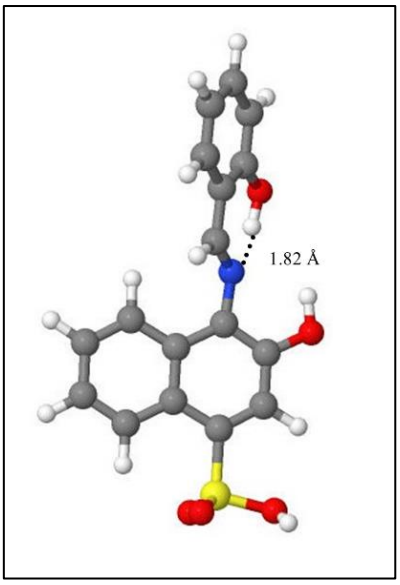

Figure 4.28. Optimized structure of Schiff base

Moreover, the hydrogen bonding interaction between the hydroxyl proton on phenyl unit and imine nitrogen which is also deduced from ^{1}H NMR spectrum of the compound **21** recorded in the presence of Hünig's base. The ^{1}H NMR spectrum (Figure 4.29) showed that the Hünig's base abstracts the hydroxyl proton on naphthalene unit despite the hydroxyl proton on phenyl unit is more acidic. This is believed to be due to the strong hydrogen bond interaction. This hydrogen bonding interaction triggers six-membered ring formation.

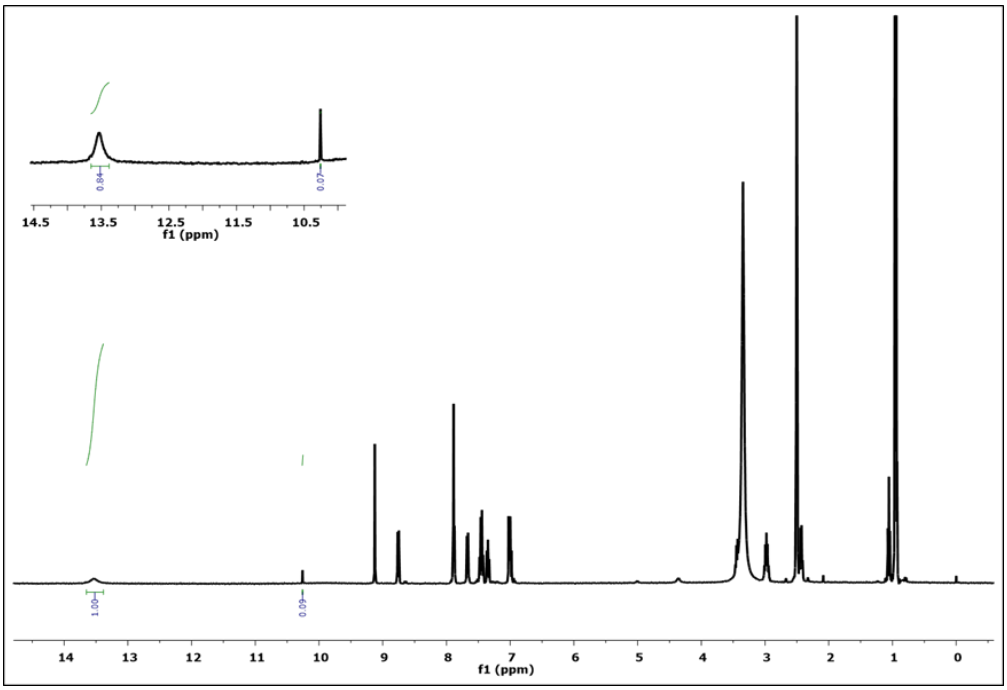

Figure 4.29. ^{1}H NMR spectrum of compound **21** in the presence of Hünig's base (in DMSO-d_6)

It was thought that the lower energy and higher stability of conformer **21-C4** compared to the other conformers can be indication of aromaticity in that conformation. Calculation of NMR spectrum in Gaussian 09[99] revealed a negative NICS(1) value of -0.46. This negative NICS(1) value implies the aromaticity in six-membered ring.[122–124] Thus, as a result of this six-membered pseudo aromatic[125] ring formation, the compound has "*atropisomers*".

For further characterization of atropisomers, chiral HPLC studies were performed which satisfies the results of spectroscopy studies (*vide supra*). In HPLC chromatogram (Figure 4.30), two distinct peaks with slightly different intensities (7%) were observed. This supports the presence of atropisomers. The origin of different areas under these peaks was postulated to be related to a change in the conformation in chiral environment.

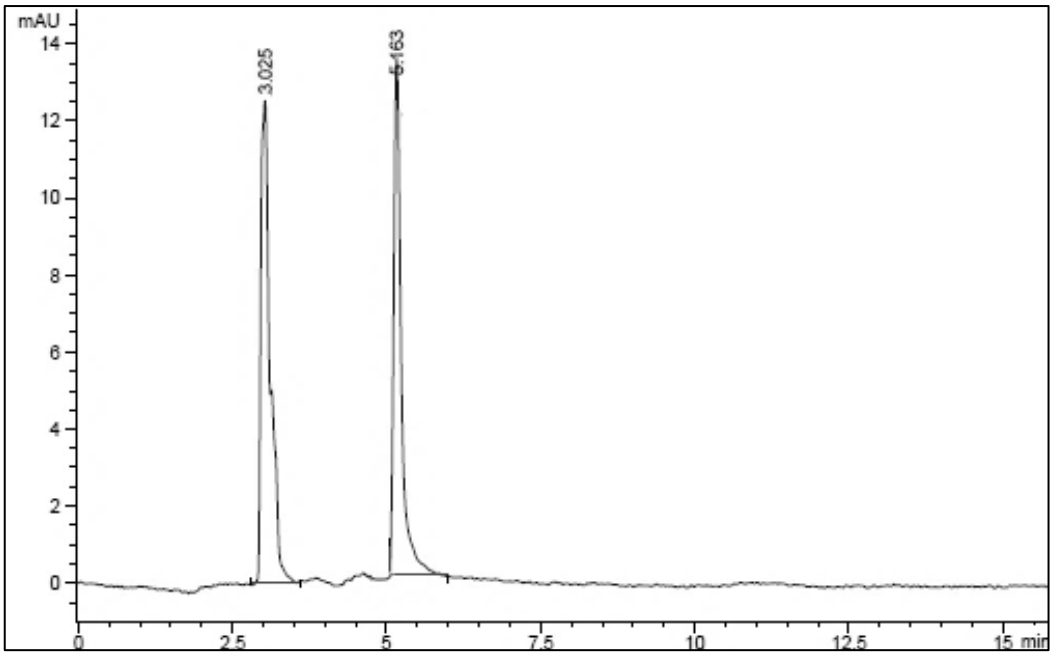

Figure 4.30. HPLC chromatogram of compound **21** (Chiralcel OD-H, eluent 95:5 n-Hexane:^{i}PrOH, flow rate 1.0 ml/min, t_R: 3.0, 5.2 min).

Despite the compound **21** is a mixture of atropisomers and it's racemic, it was believed to recognize and differentiate the enantiomers through diastereomeric interactions. However, this was not the case in our studies. It was thought that the atropisomers should be separated. For this purpose, two main strategies were determined. The first one is to increase the rotation barrier by incorporating bulky substituents; and thus, steric hinderence. It was thought that increasing rotation barrier will render the atropisomers more stable and isolable. For this purpose, it was decided to synthesize ketimines. Acetophenone derivative of Schiff base was tried to be synthesized using same synthetic pathway of compound **21**. However, the product couldn't be obtained out of this reaction (Scheme 4.13). Using acetophenone rather than salicylaldehyde for the synthesis of Schiff base does not favor the formation of product. As it is known that aromatic aldehydes are highly reactive that imines form readily under mild reaction conditions. However, the reactions of ketones with amines requires harsh conditions such as high temperature or pressure, or may require use of acid catalysis.[126]

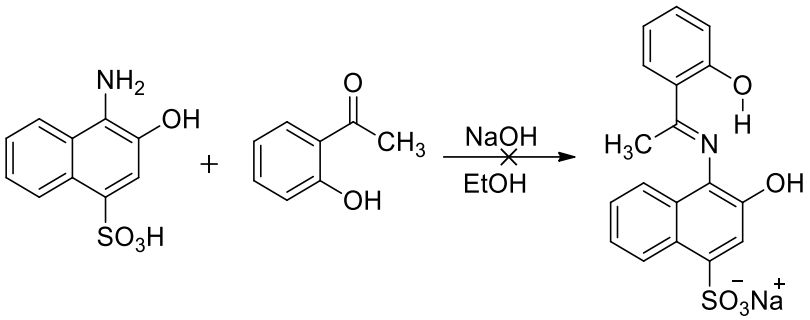

Scheme 4.13 Synthesis of acetophenone derivative of Schiff base

The second strategy was the formation of diastereomers. For this purpose, two different procedures were adapted (Scheme 4.14). The aim was to get O-alkylation product. If the O-alkylation product would be obtained, and if the corresponding compound had atropisomers, the methylene protons of benzyl group will be diastereotopic, and will appear as an AB system in ^{1}H NMR. Moreover, if that reactions would work, the next strategy would be trying to incorporate a chiral moiety on the same position to get diastereomers. By this way, the atropisomers of parent molecule would be isolated in a diasteromeric form. However, none of these reactions worked. O-alkylation products couldn't be obtained from these reactions which is most probably due to steric reasons caused by twisted structure.

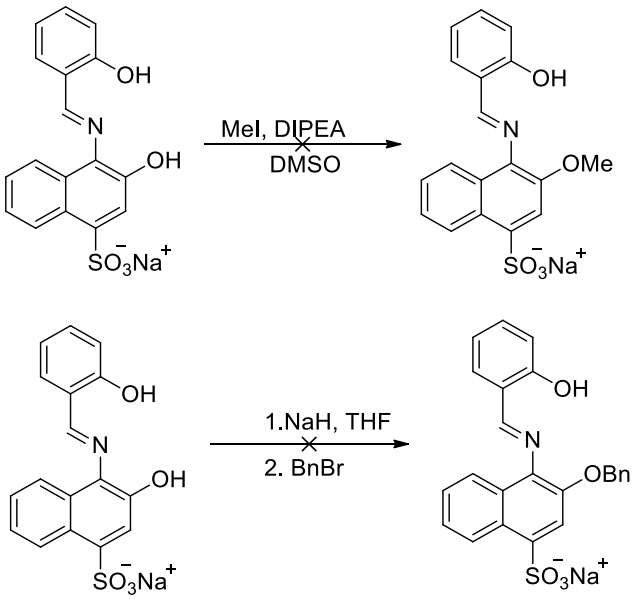

Scheme 4.14 Conditions tried to get O-alkylation product

In literature, it has been widely reported that the atropisomers can be separated by an asymmetric reaction in which a suitable catalyst is utilized.[127–129] Simple chemical modifications seemed to be not enough for this separation; in contrast, the asymmetric reactions are also beyond the scope of this thesis.

4.6 Studies with 7,7,8,8-tetracyanoquinodimethane derivatives

7,7,8,8-Tetracyanoquinodimethane (TCNQ) is an interesting structural motif that has been widely used as a building block of organic electronics, organic semiconductors and nonlinear optics owing to its unique electron acceptor properties.[130,131] Although it is known to be weakly fluorescent,[130] its photophysical properties can be improved through functionalization with primary or secondary amines. Diaminodicyanoquinone (DADQ) framework possesses electron-donating and electron-accepting moieties connected through a benzenoid ring, and has a zwitterionic structure due to the push-and-pull effect in this extended π sytem (Figure 4.31).[131,132] The torsional angle (τ) between the diamino group and benzenoid ring affects the electronic structure of DADQs. These molecules are known to have low quantum yields due to nonradiative relaxations followed by increasing torsional angle up to 90° in the excited state.[133]

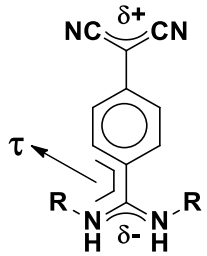

Figure 4.31. Structure of DADQs

After a detailed literature survey, it was realized that photophysical properties of achiral DADQs have been well investigated for different types of applications as mentioned above. However, to the best of our knowledge, there are no reports on the synthesis of chiral DADQ derivatives and applications of them on chiral recognition.

For this purpose, we have functionalized TCNQ by using enantiopure α-methylbenzyl amine (compounds **22** and **23**, Figure 4.32) to incorporate hydrogen bonding pathways, and utilized it in chiral recognition of alcohols, amines and amino acids. It was thought that functionalizing TCNQ with chiral amines will produce a chiral pocket consisting of multiple hydrogen bonding sites which can engage in enantioselective interactions with chiral compounds. As a result of these interactions, the electronic structure of DADQs will be changed which is believed to result in a change in the absorption and emission spectra. The extent of these interactions is expected to differ for each enantiomer due to steric reasons, so that different fluorescence spectra (different wavelength or intensity) will be obtained for each enantiomer. By this way, chiral recognition will be achieved.

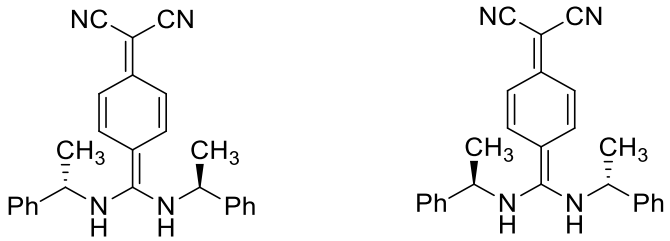

Figure 4.32. New chiral diaminodicyanoquinone derivatives

The synthesis of compounds **22** and **23** were simply performed by refluxing TCNQ and corresponding chiral amine in acetonitrile overnight (Scheme 4.15). The mechanism of this conversion is proposed to be a simple addition-elimination reaction with the removal of HCN.[134]

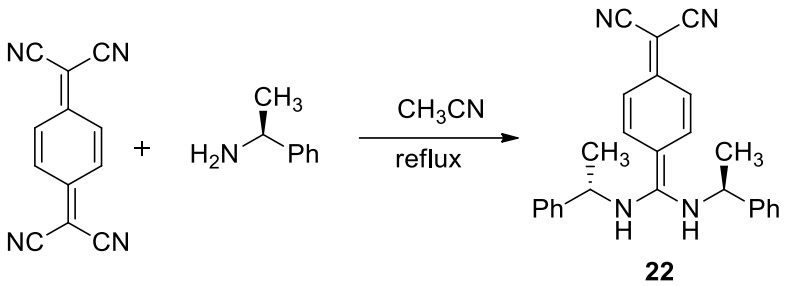

Scheme 4.15 Synthesis of chiral DADQs

The investigations on photophysical properties of different DADQs have been well documented in literature.[131–133,135,136] These novel compounds exhibit very weak fluorescence in solution due to extensive nonradiative relaxations and intramolecular rotations which result in a large Stokes shift. Their photophysical properties have generally showed matrix dependence (solvent).[137] In other words, the local environment of DADQs are important when studying their photophysical properties.[135] DADQs were reported to exhibit strong fluorescence emission in viscous matrices due to the decrease in the conformational flexibility, inhibition of torsional motion and decrease in nonradiative relaxations.[133,135–137] In other words, Stokes shift is decreased and fluorescence emission is enhanced in viscous media.

Micelle solutions are of great importance to study photophysical properties of dyes. Photophysics in micellar environment has widespread applications in pharmaceutical science, luminescence, and biochemistry. The microenvironment inside a micelle solution is expected to be very different from the bulk solutions. In other words, the viscosity inside these thermodynamically stable molecular systems is higher compared to the solutions. The driving force for micelle formation is hydrophobic effect, so they are formed in water spontaneously. The hydrophilic tail is directed towards water molecules and hydrogen bond network is reorganized, while a hydrophobic core is formed due to van der Waals forces so that free energy of the system decreases. Micelles can participate in interactions with water-insoluble molecules in its hydrophobic core. As a result of these astonishing properties of micelles, it was postulated that our chiral DADQs can be encapsulated in micelle solutions. By this way, their photophysical properties will be enhanced due to inhibition of nonradiative relaxations and decrease in conformational flexibility as a result of increased viscosity of hydrophobic core inside the micelle. Moreover, a chiral medium will be generated inside this hydrophobic core when chiral DADQs are trapped in this region so that chiral recognition studies of water-insoluble alcohols and amines can be performed using micelle solutions.

An anionic surfactant, sodium dodecyl sulfate (SDS) was utilized as a micelle solution and photophysical properties of compound **22** were investigated in this

micellar microenvironment. Normally, compound **22** is water-insoluble. However, when SDS micelle solution (above its critical micelle concentration which is 8 mM) was used, it was realized that this fluorescent dye is incorporated into the hydrophobic core of micelle as the color change of the solution implies (i.e. color of the micelle solution changes from colorless to yellow). The fluorescence excitation and emission spectra of the dye in this microenvironment were recorded (Figure 4.33).

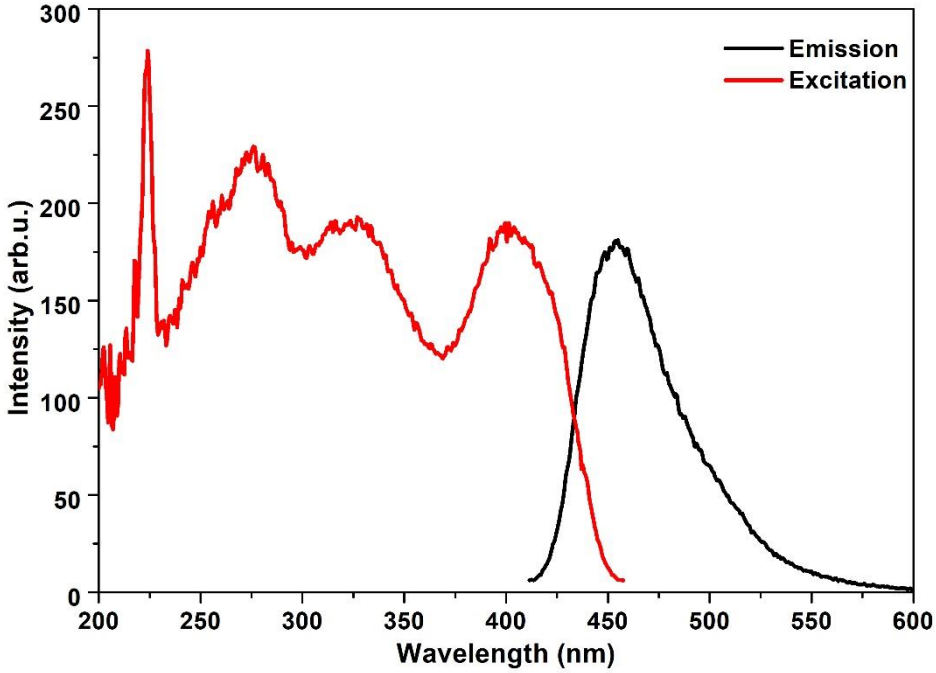

Figure 4.33. Fluorescence absorption and emission spectra of compound **22** in micelle solution (SDS concentration was 10 mM, dye concentration was 0.1 mM, excited at 400 nm, slit widths were adjusted as 5.0/2.5 and scan rate was 200 nm/min)

It was also known that the steric reasons have an impact on the rate of nonradiative relaxations.[135] To increase the steric crowding in micellar environment, the concentration of dye was increased, and fluorescence absorption and emission spectra were recorded.

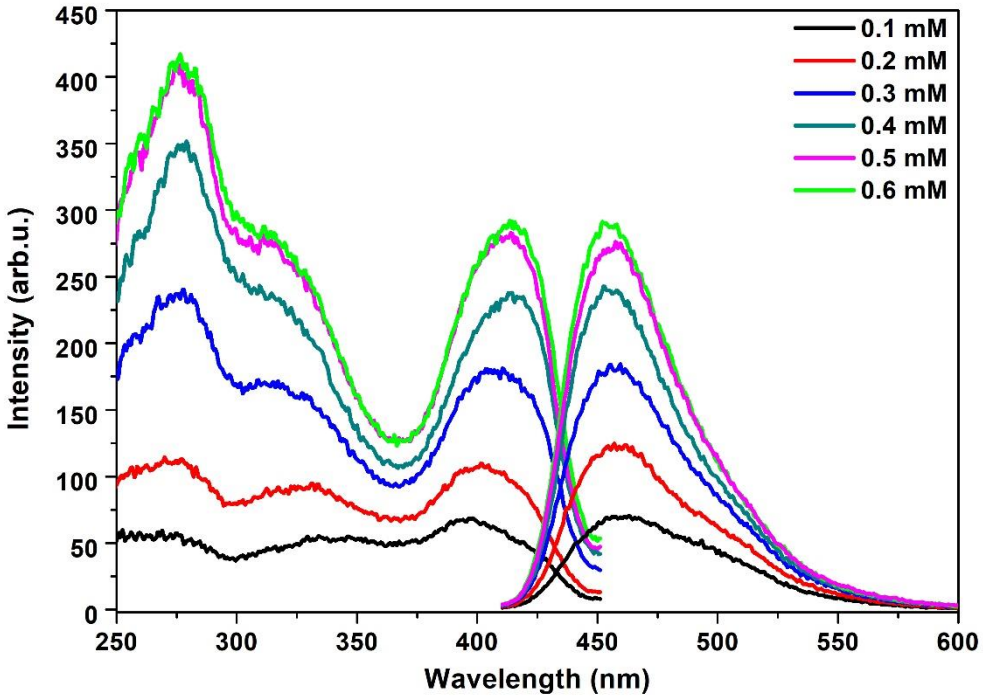

Figure 4.34. Effect of dye concentration on absorption and emission spectra (SDS concentration was 10 mM, excited at 400 nm, slit widths were adjusted as 5.0/2.5 and scan rate was 200 nm/min).

As can be inferred from the spectra in Figure 4.34, the intensities of 0→0 bands were increased upon increasing dye concentration. Stokes shifts were decreased in the same manner (Table 4.8). The effect of concentration can be correlated with increasing crowdence in the hydrophobic core of the micelle which affects the rate of nonradiative relaxation processes. Fluorescence intensities increase as a result of decrease in the rate of nonradiative relaxations.

Table 4.8 Effect of dye concentration in SDS micelle on Stokes shift

Dye concentration	Stokes shift, nm
0.1 mM	65
0.2 mM	60
0.3 mM	55.5
0.4 mM	52
0.5 mM	50
0.6 mM	48

The intensity of fluorecence absorption band was increased when the compound **22** was trapped in micellar environment. The comparison of fluorescence intensity in micelle solutions and various solvents is summarized in Figure 4.35. As can be inferred from fluorescence plots, micelle solution provided a superior environment for compound **22** to reduce nonradiative relaxations and conformational flexibility compared to organic solvents having a range of different viscosities.

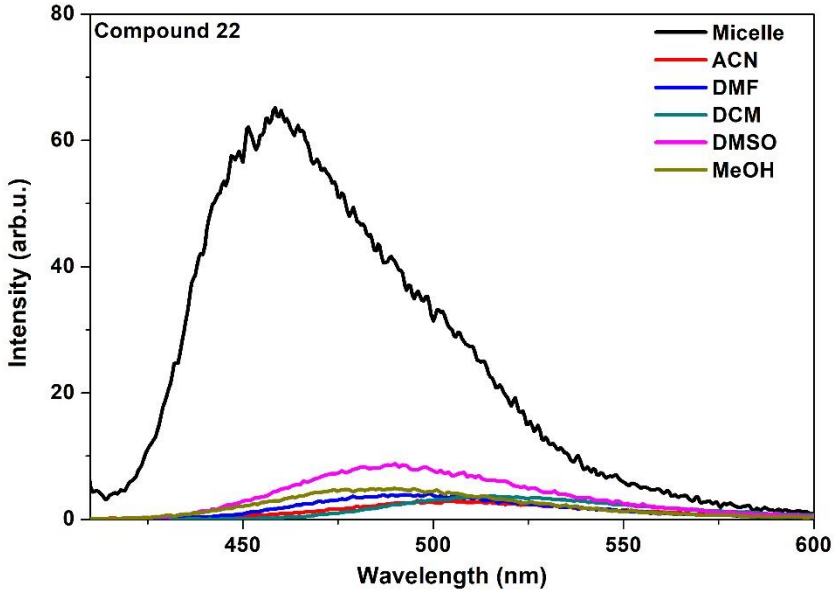

Figure 4.35. Comparison of micelle solution with organic solvents in terms of fluorescence intensity (Sensor concentration was 0.1 mM, excitation slit width was 5 nm, emission slit width was 2.5 nm, scan rate was 200 nm/min).

With these information in hand, it was decided to utilize these novel DADQ derivatives (compounds **22** and **23**) in chiral recognition studies of water-insoluble chiral alcohols and chiral amines. Fluorescence titration studies were performed using enantiopure 2-butanol, 1-phenylethanol and α-methylbenzyl amine. Although selectivities were observed toward one enantiomer of each of these compounds, the selectivities were not reproducible. It couldn't be clarified whether the micelle formation and dye encapsulation were thermodynamically or kinetically driven. Many different time and preparation conditions were applied during micelle preparation, dye addition, and addition of chiral impurities; however, the results couldn't be reproduced, unfortunately.

Due to the complicated nature of photophysical studies in micelle solutions and lack of reproducibility in the spectra, it was decided to study the photophysical properties of these novel DADQ derivatives in various solvents to investigate the effect of solvent polarity on UV-Vis absorption, fluorescence absorption and emission spectra (Table 4.9). The solvent polarities were compared according to normalized Dimroth-Reichardt parameters (E_T^N).[138] Dimroth Reichardt parameter (E_T or $E_T(30)$) has been the most comprehensively used empirical solvent polarity scale. This parameter was measured based on the wavelength of the maximum of long intramolecular charge transfer band of Reichardt's betaine dye (pyridinium N-phenolate) which was used as a standart by virtue of its large negative solvatochromic behaviour.[138–140] High E_T value means high polarity of the solvent. Dimroth Reichardt parameter was normalized with respect to the highest polarity solvent (water, E_T=63.1) and the lowest polarity solvent (TMS, E_T=30.7) to get a scale which has a better correlation with other empirical solvent polarity scales. Normalized E_T scale (E_T^N) can be calculated as follows:[138,141]

$$E_T^N = \frac{E_T(\text{solvent}) - E_T(SiMe_4)}{E_T(\text{water}) - E_T(SiMe_4)} \qquad \text{Equation 4.3}$$

where E_T is the transition energy of maximum absorption band of Reichardt's betaine dye in given solvent (E_T(kcal/mol)=28591/λ_{max} in nm)

Table 4.9 Results of solvent screening studies with compound **22***

Solvent	E_T^N**	UV-Vis	Fluroescence*		Stokes shift, nm
		λ_{abs}	λ_{exc}	λ_{em}	
ACN	0.460	392	427	510	83
DCM	0.309	427	450	516	66
DMF	0.386	388	431	499	68
DMSO	0.444	381	427	490	63
MeOH	0.762	371	413	490	77
$CHCl_3$	0.259	426	445	505	60

* See Appendix D for corresponding fluorescence spectra

** values obtained from reference 138

The effect of solvent on the absorption and emission spectra (shape, wavelength or intensity of bands) is called "solvatochromism" which is a concept that first reported by Hantz-Schlater, and is observed in fluorescent molecules that have large difference in dipole moments in ground and excited states such as DADQs. [131,138] Solvatochromism can be negative or positive and its sign can be identified by a shift in the position of emission bands. If a hypsochromic (blue) shift is observed upon increase in solvent polarity, it is called "negative solvatochromism" or if a batochromic (red) shift is observed, it called "positive solvatochromism". In Table 4.7, it can be easily deduced that there is a negative solvatochromism when the positions of emission bands are compared for the solvents ACN, DCM, DMF and DMSO and $CHCl_3$. However, the polarity of the solvent is not the only factor that tunes the emission spectrum of a fluorescent molecule. Since our DADQ derivatives (compounds **22** and **23**) are endowed with hydrogen bonding pathways in their structures, hydrogen bonding between our fluorescent molecule and solvent also affects the sign and extent of solvatochromism.[138] Thus, when we look at the

emission wavelengths obtained with ACN and MeOH, we can realize that the extent of negative solvatochromism is decreased due to the use of solvents having strong hydrogen bond donor properties. To sum up, we can say that these chiral DADQ derivatives (compounds **22** and **23**) possess negative solvatochromism and our experimental data are in accordance with those reported for achiral DADQ derivatives.[131]

In addition to polarity, viscosity of the medium is another important factor that has an influence on absorption or emission spectra of DADQ derivatives.[135] DADQ derivatives have low quantum yields due to the nonradiative relaxation processes that take place within a very short time period in solution. In a viscous environment, these nonradiative pathways slow down, or blocked; as a result, Stokes shift decreases and emission properties of these dyes are enhanced.[131,135] The lower Stokes shift obtained in DMSO can be explained by higher viscosity of the solvent compared to the others.

The utility of compound **22** in chiral recognition studies were tested in the presence of both enantiopure forms of 2-butanol, 1-phenylethanol, α-methylbenzyl amine and tartaric acid. For this purpose, DCM and $CHCl_3$ were selected as the solvents due to the lowest Stokes shifts obtained in these solvents (Table 4.9). However, we couldn't observe a selectivity for the enantiopure compounds given above. Moreover, tartaric acid enantiomers have very low solubility in these solvents; thus, we didnot continue to use tartaric acid enantiomers on purpose. The results of fluorescence studies with compound **22** are summarized in Table 4.10 below. Selectivity with compound **23** was not expected so that the studies were not repeated for compound **23** since they are enantiomers of each other.

Table 4.10 Fluorescence studies of compound **22** in the presence of selected enantiopure compounds (Sensor concentration was 0.1 mM, excitation slit width was 5 nm, emission slit width was 2.5 nm, scan rate was 200 nm/min).

DCM	**$CHCl_3$**
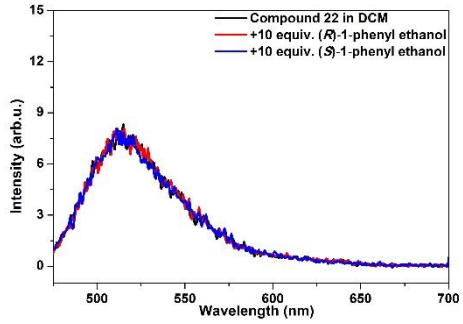	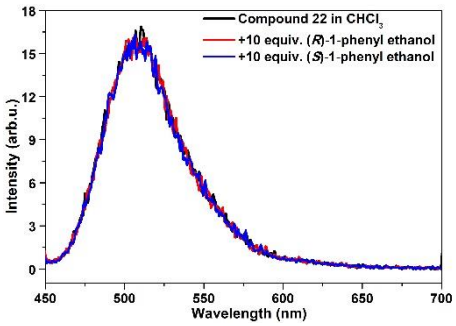
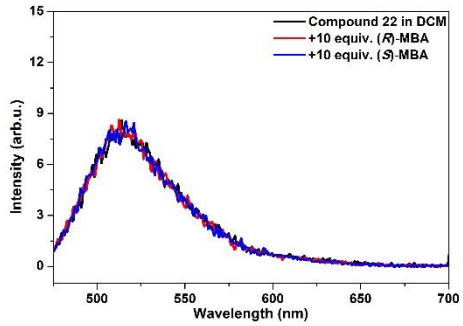	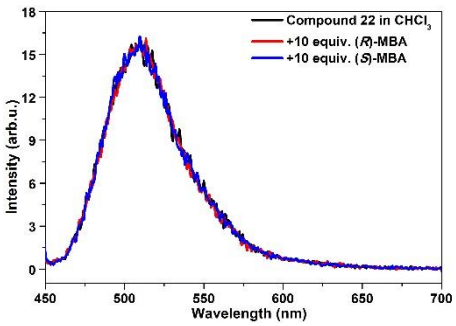
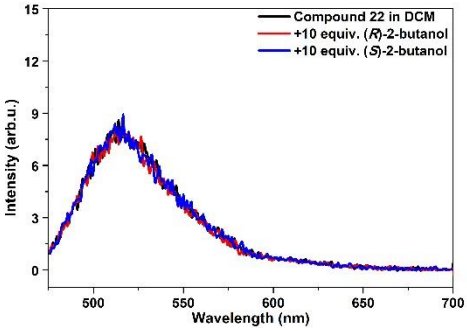	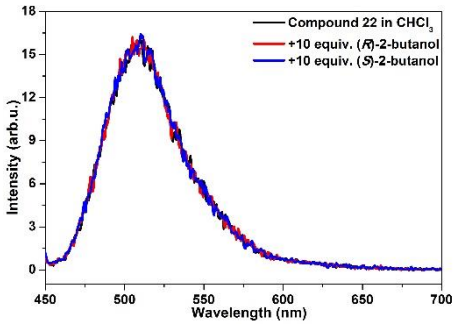

To investigate the effect of subtituents on the photophysical properties and enantioselective recognition, we have synthesized the compounds in Figure 4.36.

Substitution of naphthyl group (compounds **24** and **25**) instead of phenyl ring in compounds **22** and **23** did not improve the photophysical properties (i.e. intensity and Stokes shift) of DADQs.

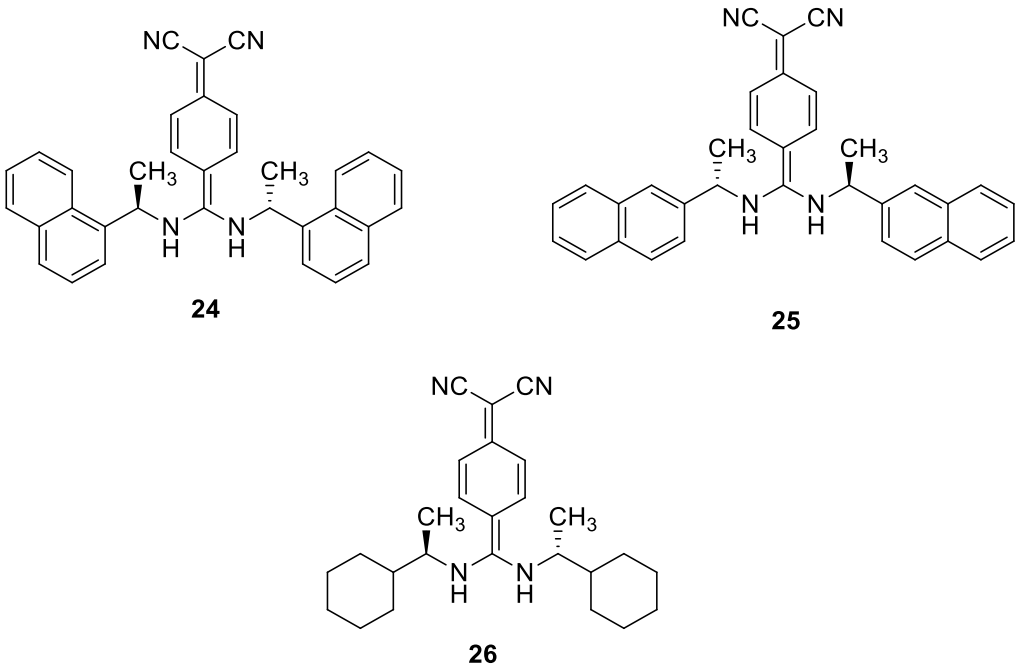

Figure 4.36. New chiral DADQ derivatives

To test the potential of compound **24** in chiral recognition studies, same fluorescence studies, that were performed for compound **22**, were performed. The results are given in Table 4.11:

Table 4.11 Fluorescence studies of compound **24** in the presence of selected enantiopure compounds (Sensor concentration was 0.1 mM, excitation slit width was 5 nm, emission slit width was 2.5 nm, scan rate was 200 nm/min).

DCM	**$CHCl_3$**
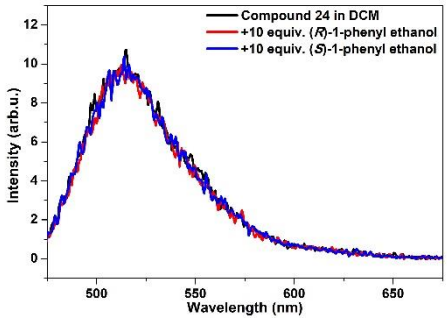	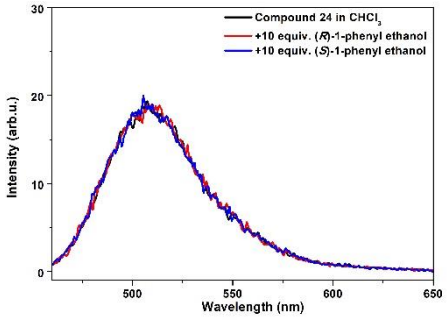
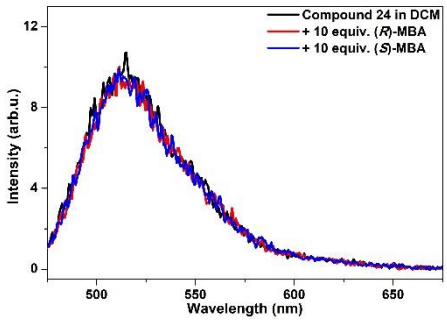	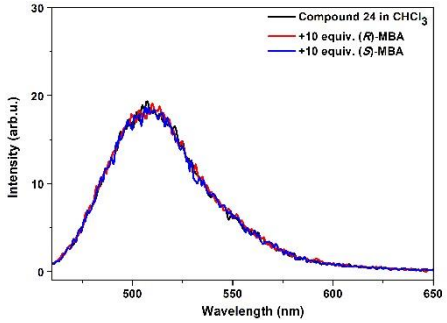
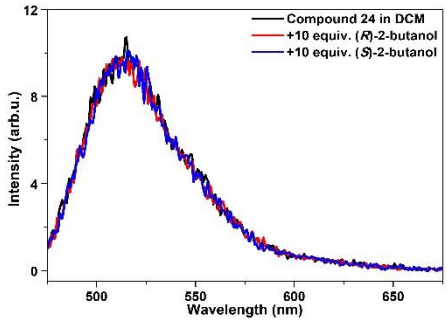	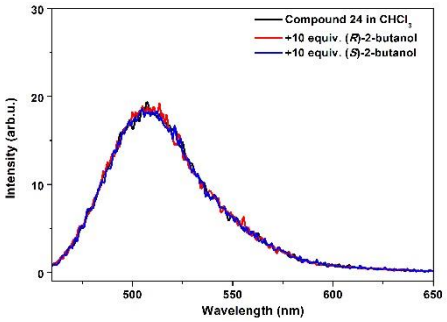

The compounds **25** and **26** were also tested for the same purpose. No selectivity was observed with compounds **25** and **26** under given conditions, too.

With compounds **24** and **25**, a new absorption band in blue region of electromagnetic spectrum was observed in UV-Vis spectra which corresponds to the naphthalene unit (Figure 4.37).

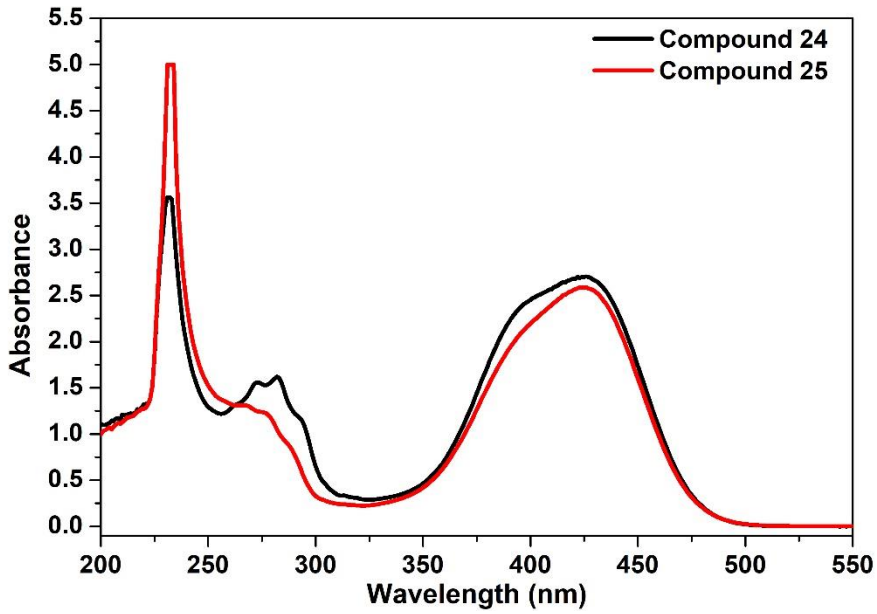

Figure 4.37. Overlapped UV-Vis spectra of compounds **24** and **25** (0.1 mM in DCM)

It was decided to excite these sensors at 280 nm, since the naphthalene unit is closer to chiral center. This was thought to generate a differentiation in fluorescence spectra of sensors in the presence of different enantiomers. When excited at 280 nm, new bands appeared in both blue and red regions of electromagnetic spectrum (Figure 4.38 (b)). The fluorescence absorption and emission spectra of compounds **24** and **25** seemed to be similar; therefore, it was concluded that substitution of 1-naphthyl or 2-naphthyl amines makes almost no difference in the photophysical properties and excited state dynamics of both compounds (Figure 4.37).

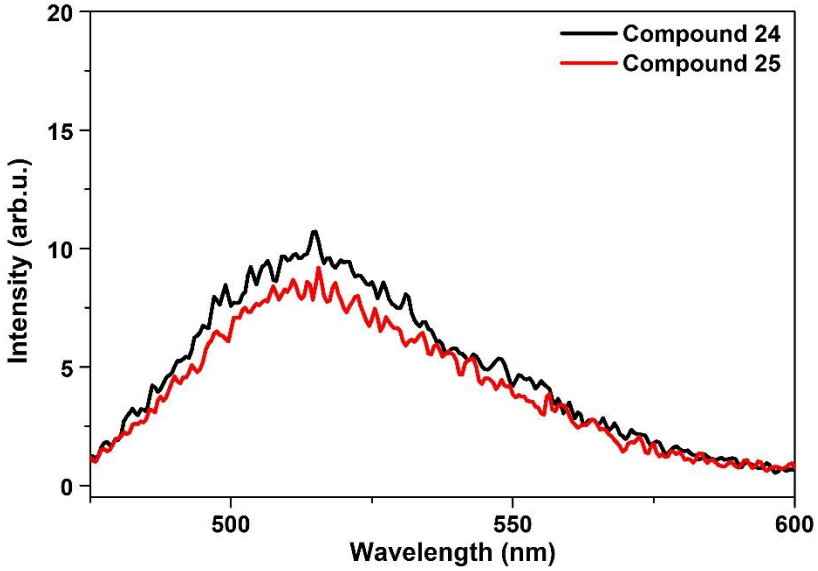

(a)

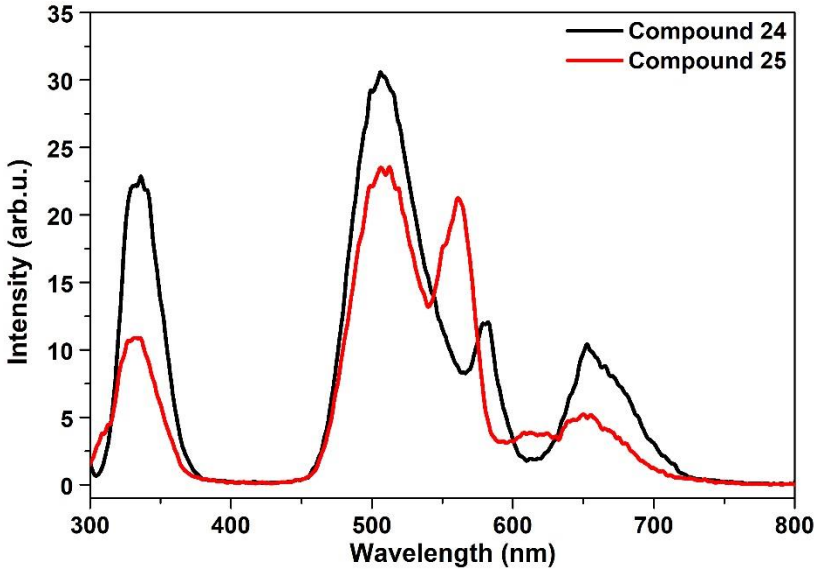

(b)

Figure 4.38. Overlapped fluorescence spectra of compounds **24** and **25** in DCM when excited at (a) 465 nm (b) 280 nm

During chiral recognition studies with fluorescence spectroscopy, exciting these molecules at the wavelength of core unit, which corresponds to 7,7,8,8-tetracyanoquinodimethane (around 400 nm), did not provide an enantioselective recognition while exciting the same molecules at the wavelength that corresponds to

the naphthalene (280 nm), selectivities towards (*S*)-α-methylbenzyl amine were observed (Figures 4.39 and 4.40).

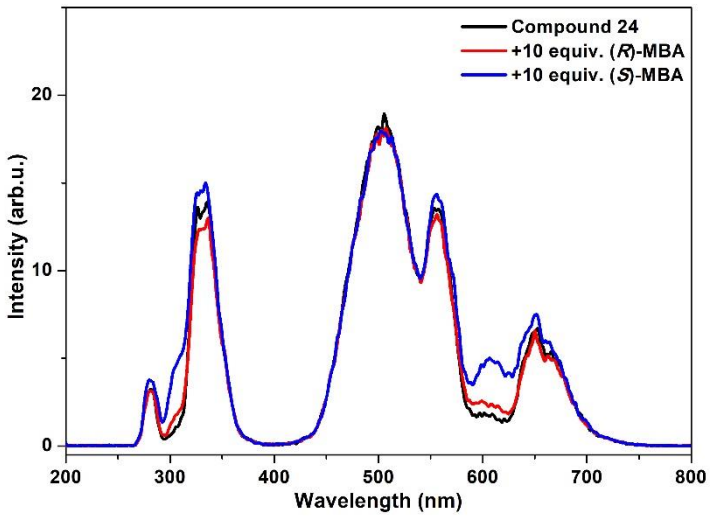

Figure 4.39. Fluorescence spectra of compound **24** in the presence of enantiopure (*R*) or (*S*)- α- methylbenzyl amine (Sensor concentration was 0.1 mM in ACN, excited at 280 nm, excitation slit width was 5 nm, emission slit width was 2.5 nm, scan rate was 200 nm/min).

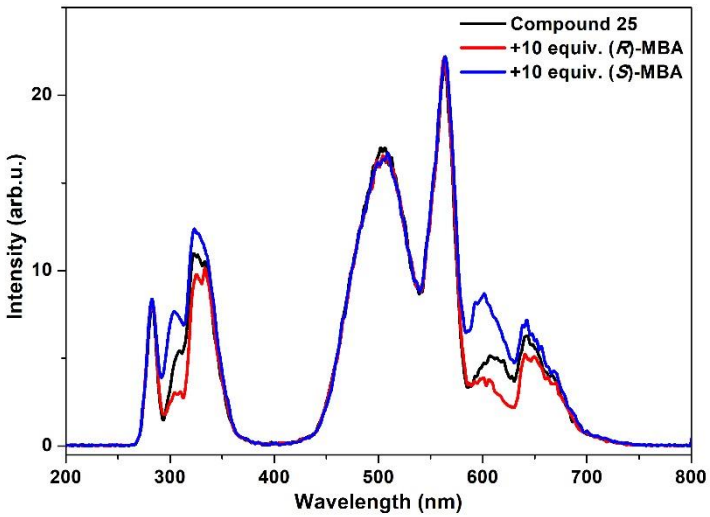

Figure 4.40. Fluorescence spectra of compound **25** in the presence of enantiopure (*R*) or (*S*)- α- methylbenzyl amine (Sensor concentration was 0.1 mM in ACN, excited at 280 nm, excitation slit width was 5 nm, emission slit width was 2.5 nm, scan rate was 200 nm/min).

It can be clearly seen in Figure 4.39 and Figure 4.40 that addition of (*S*)- α-methylbenzyl amine increases the fluorescence intensity of emission band around 300-350 nm, while (*R*) enantiomer has the reverse effect for both compunds **24** and **25**. Moreover, after exciting at 280 nm, a new emission band was appeared in the red region of electromagnetic spectrum.

The mechanism behind the recognition was thought to be a hydrogen bonding interaction between sensor and (*S*)- α- methylbenzyl amine. In addition, naphthalene is close to the chiral center, so that exciting the sensor from a fluorophore unit which is close to the chiral center, brought about a selectivity towards one enantiomer as expected.

To further investigate the complex formed between sensor and chiral amines, fluorescence titration studies were performed with compounds **24** and **25** in which the concentration of chiral amine was increased from 0 mM to 65 mM and effect of this concentration on fluorescence spectra was monitored. Acetonitrile was preferred to be used in these studies since it's a relatively green organic solvent and it's highly preferred in chiral recognition studies in the literature. The fluorescence titration curves are given in Figure 4.40 and Figure 4.41 below:

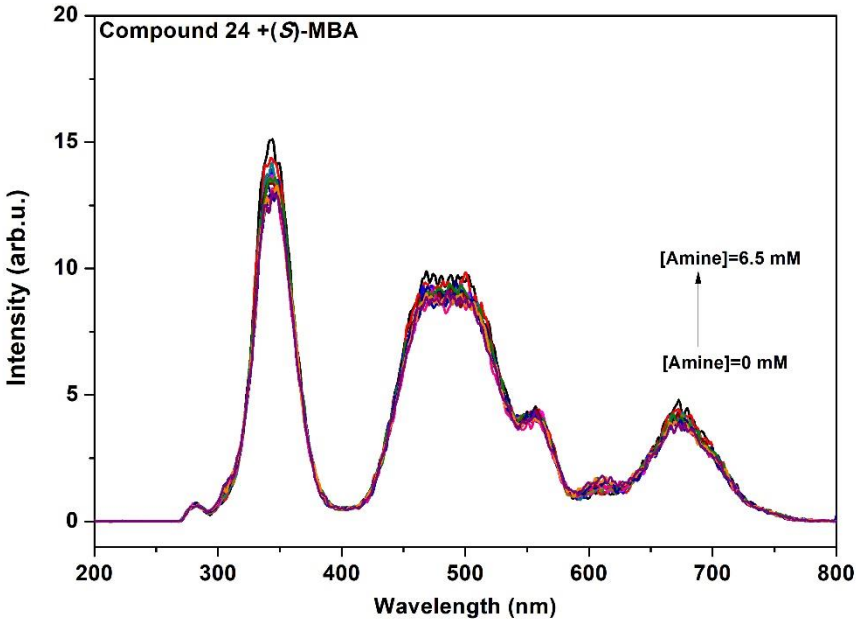

(a)

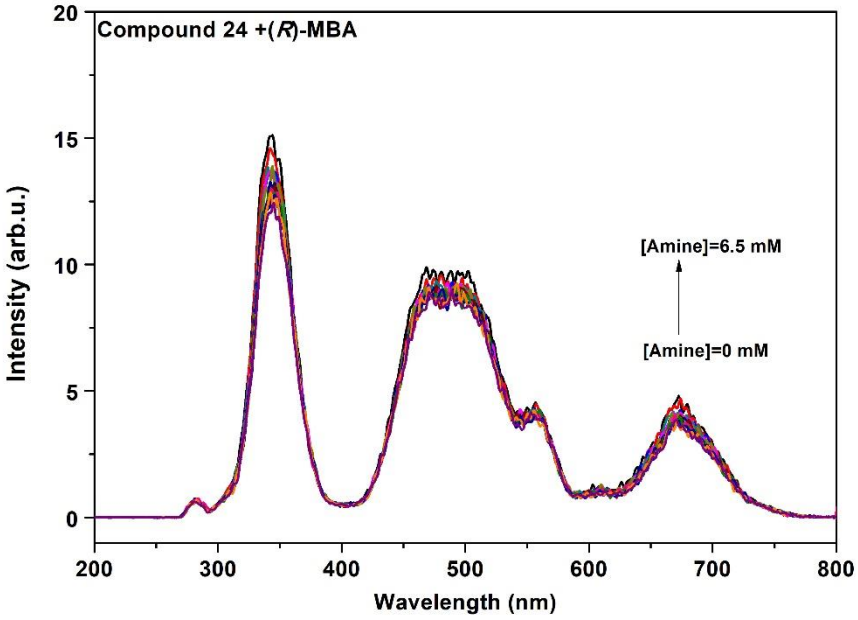

(b)

Figure 4.41. Fluorescence spectra of compound **24** in the presence of enantiopure (*S*) or (*R*)- α- methylbenzyl amine (Sensor concentration was 0.1 mM in ACN, excited at 280 nm, excitation slit width was 10 nm, emission slit width was 5 nm, scan rate was 200 nm/min).

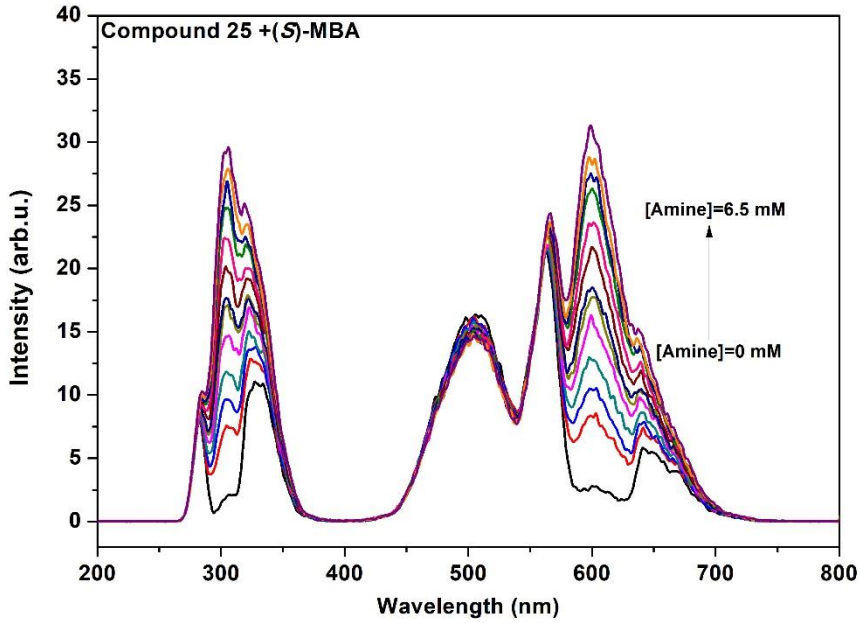

(a)

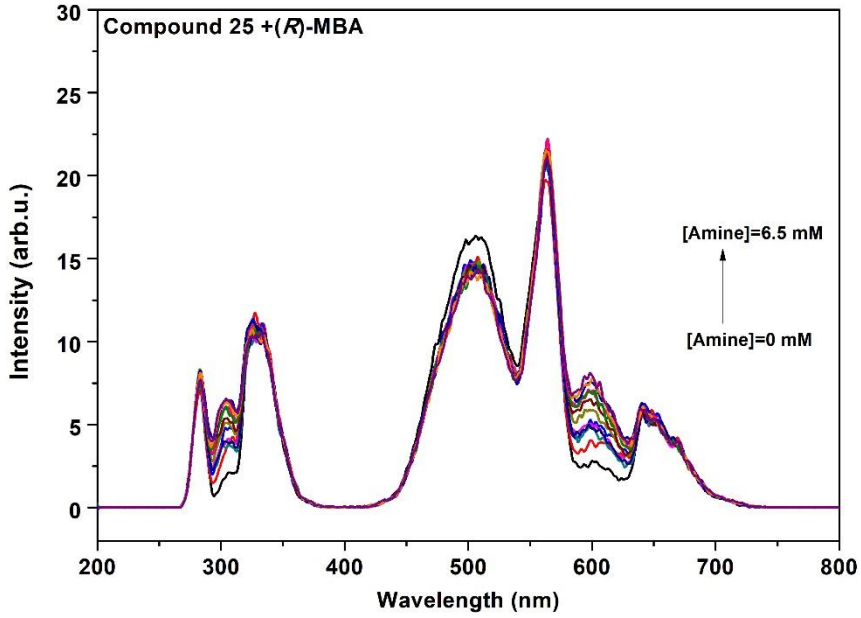

(b)

Figure 4.42. Fluorescence spectra of compound **25** in the presence of enantiopure (*S*) or (*R*)- α- methylbenzyl amine (Sensor concentration was 0.1 mM in ACN, excited at 280 nm, excitation slit width was 10 nm, emission slit width was 5 nm, scan rate was 200 nm/min).

The selectivity of compound **24** towards (*S*)-α-methyl benzyl amine was very low and limited to the very low concentrations only. However, compound **25** showed a much more promising selectivity towards (*S*)- α-methyl benzyl amine.

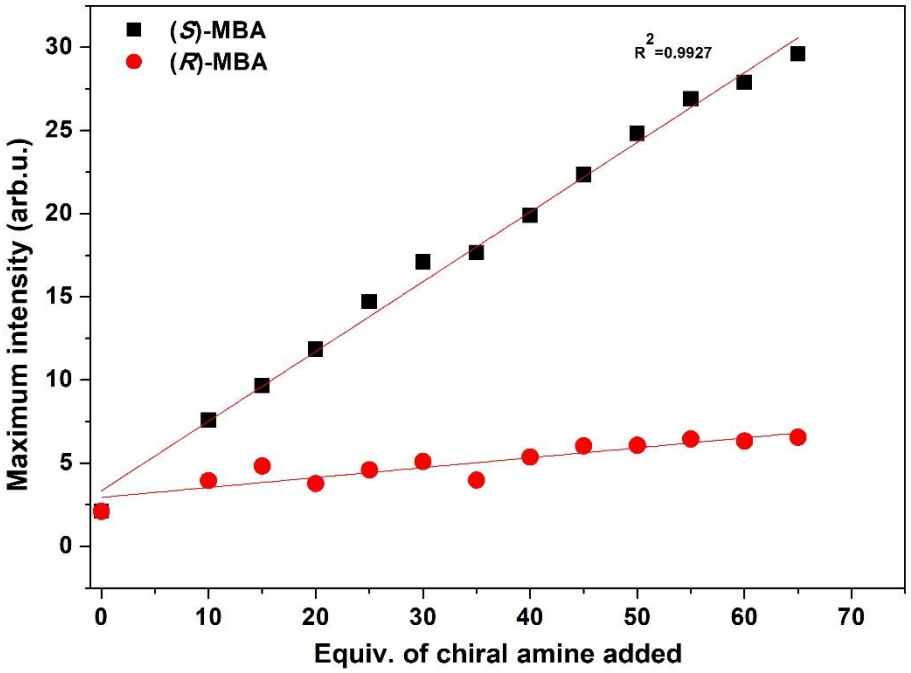

Figure 4.43. Maximum intensity vs equiv. of chiral amine added graph for the titration of compound **25** with α-methylbenzyl amine enantiomers

Experimental data were further processed to propose a structure for the complex and mechanism for selectivity. Stern-Völmer plot[74] indicated that the large difference between the slopes of two curves supports the selectivity towards (*S*) enantiomer.

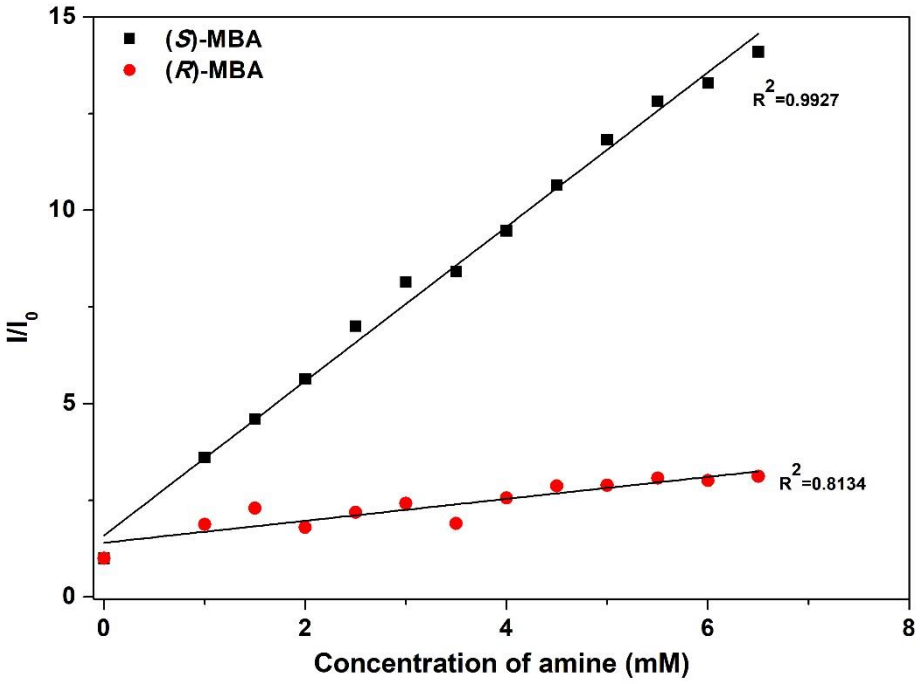

Figure 4.44. Stern-Völmer graph for the titration of compound **25** with α-methylbenzyl amine enantiomers

Benesi-Hildebrand curve[114,115] was plotted to determine the binding stoichiometry of the complex formed between compound **25** and (*S*)-α-methylbenzyl amine. Linear slope of this curve indicated that the complex formed between compound **25** and (*S*)-α-methylbenzyl amine is a 1:1 complex.

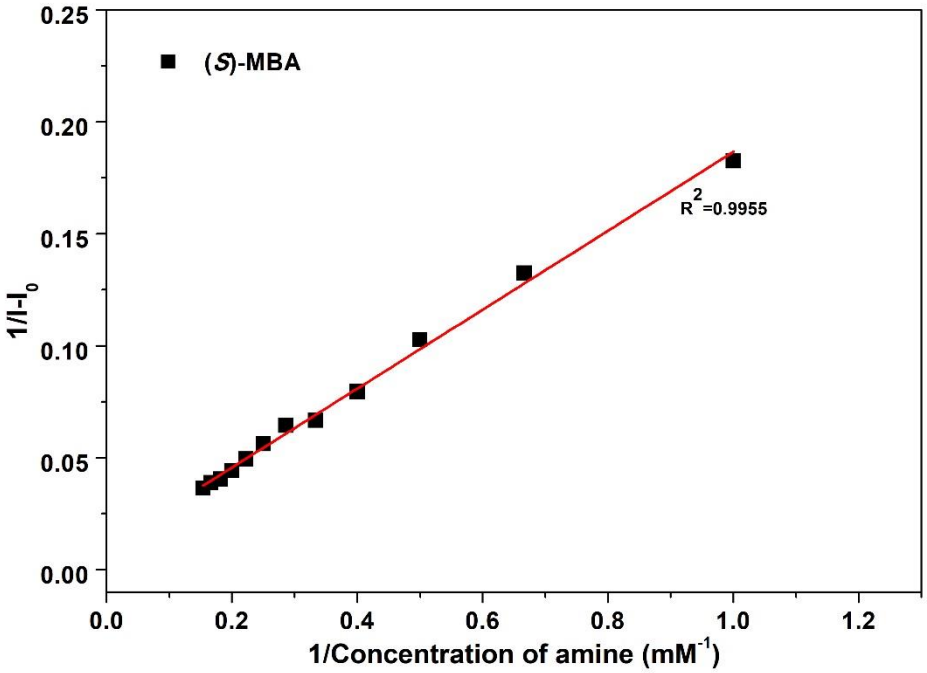

Figure 4.45. Benesi-Hildebrand graph for the titration of compound **25** with (*S*)-α-methylbenzyl amine

To attain a better understanding of mechanism of the recognition and selectivity, ground states of predicted conformations were optimized implementing B3LYP/SVP level was implemented in Gaussian 09 program.[99] The results of these calculations are summarized in Table 4.12.

Table 4.12 Optimized geometries of different conformations of compound **25**

Conformer	Optimized structure	2D structure	Relative energy (kcal/mol)
25-C1	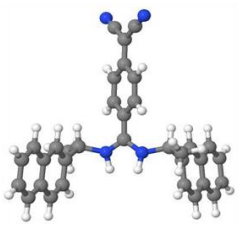	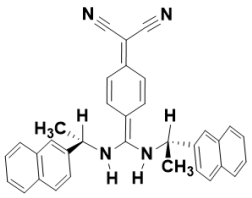	**0**
25-C2	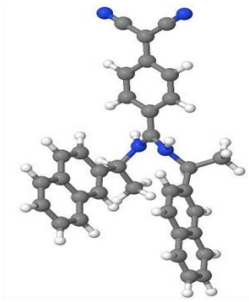	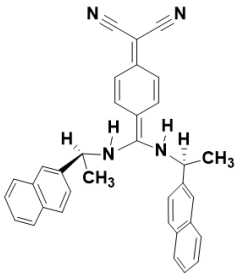	**5.1**
25-C3	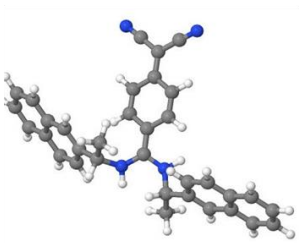	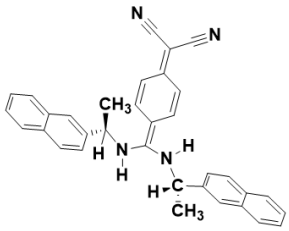	**7.1**

* The graphics in Table 4.12 were created by using Jmol[121] which is an open-source Java viewer for chemical structures in 3D.

When energies of conformations given in Table 4.12 were compared, it was realized that the conformer **25-C1** was seemed to have a relatively lower energy. Moreover, hydrogen bonding interaction is the primary interaction for the observed selectivity. With these information in hand, theoretical calculations were run at the level of B3LYP/SVP as implemented in Gaussian 09.[99] As a result of experimental and theoretical studies, the structures in Figure 4.46 were proposed as the structures of the complexes between compound **25** and both enantiomers of α-methylbenzyl amine.

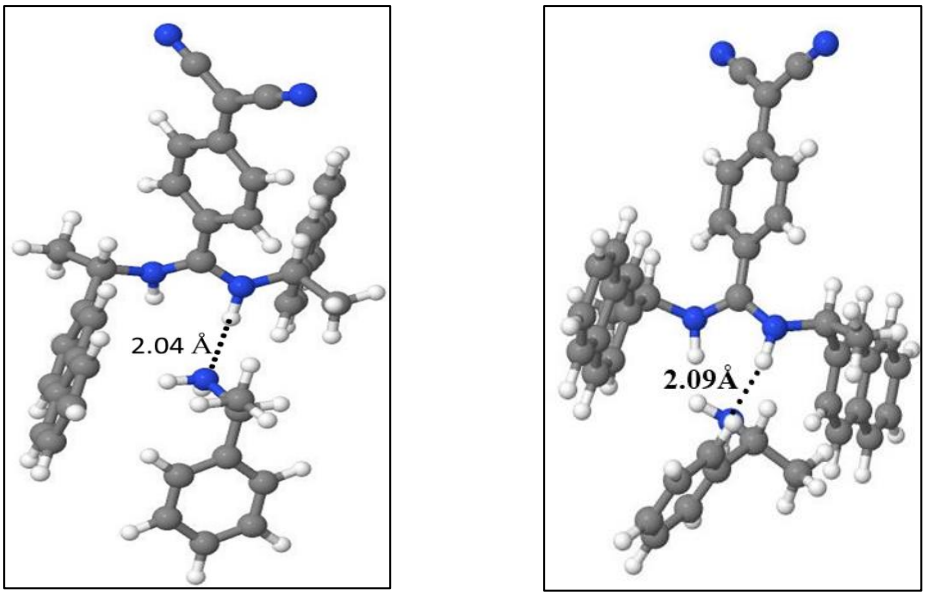

(a) (b)

Figure 4.46. Optimized geometry for the complex between compound **25** and (a) (*S*)-α-methylbenzyl amine (b) (*R*)-α-methylbenzyl amine

The optimized structure of the complex between compound **25** and (*R*)-α-methylbenzyl amine has a relative energy of +0.74 kcal/mol compared to the complex between compound **25** and (*S*)-α-methylbenzyl amine. Moreover, it can be observed from the structure in Figure 4.46 (b) that (*R*)-α-methylbenzyl amine cannot become closer to the compound **25** due to steric repulsion between methyl groups on amine and compound **25**. Thus, complex formation with (*S*)-α-methylbenzyl amine was more favorable under these conditions. The results of these studies support the results of spectroscopy studies and explain the selectivity towards (*S*)-amine.

CHAPTER 5

CONCLUSION

In this thesis, the aim was to design and synthesize new chiral fluorescence sensors that are expected to participate in chiral interactions with enantiomers in different extents in their chiral pockets through hydrogen bonding pathways. With the help of these chiral interactions, it was aimed to set up a chiral recognition methodology through fluorescence spectroscopy. For this purpose, easy-to-modify fluorescent molecules were main focuses of this study as state of art.

In summary, fluorescent compounds that belong to coumarin, naphthalene and 7,7,8,8-tetracyanoquinodimethane families were designed. When carefully thought, the sensors based on these compounds may consist of multiple hydrogen bonding pathways and a chiral pocket, and their photophysical properties may be improved through simple chemical modifications. All fluorescence sensors were synthesized in just one or two steps under very mild reaction conditions with easily accessible and cheap precursors. These fluorescence sensors were fully-characterized by different techniques including NMR, HRMS, IR spectroscopy. In addition, R_f values, melting point measurements and specific rotations were reported for the ones that are not reported in literature.

To attain the aim of this study, the potential utilities of all synthesized sensors towards isolated enantiomers were tested in fluorescence and UV-Vis spectroscopies.

In the first part, coumarin-derived sensors were tested in the presence of enantiopure α-methyl benzyl amine, 1-phenyl ethanol and tartaric acid. We have also *D*- and *L*-forms of some amino acids such as alanine and phenylalanine; however, we have faced with solubility problems when using them. We couldn't use water as our solvent to prevent competition for hydrogen bonding with solvents since the chiral

recognition was thought to be driven by hydrogen bonding interactions. Among coumarin-derivatives, only the compound **12** showed some selectivity towards (*S*)-α-methyl benzyl amine, but the results were not reproducible. The other sensors in this series (compounds **8**, **9**, **11**, **13** and **14**) did not show any selectivity towards any of the given enantiopure compounds. New coumarin derivatives (compounds **15-18**) were synthesized to investigate the presence of helical chirality expected for these compounds. Theoretical calculations were implemented in Gaussian 09, and helical chirality was not observed in optimized geometries. These achiral coumarin sensors were tested in differentiation of biologically important metal cations (sodium and potassium). Hopefully, compound **16** was able to differentiate sodium cation in the presence of potassium cation. To clarify this differentiation mechanism, experimental data were processed with Stern-Völmer and Benesi-Hildebrand curves and theoretical calculations were performed to support all these results. Moreover, compounds **19** and **20** were synthesized to contribute to the explanation of the mechanism of selectivity. All these studies revealed a structure for the complex formed between sodium cation and compound **16**. Although the selectivity towards sodium is promising, there are better reports in the literature. However, this part of our study is important in terms of easy and practical synthetic protocols of the sensors.

To perform chiral recognition studies with compounds **11-14**, another approach was adapted which is complexation with metal cations such as Zn^{2+}. However, the first trials for the characterization of the complex in UV-Vis and fluorescence spectroscopies revealed that our fluorescence sensors did not complex with Zn^{2+} cation. For this purpose, a new sensor (compound **21**) was synthesized. It was able to complex with Zn^{2+}, and this sensor-Zn^{2+} complex was found to be responsive to all carboxylic and α-hydroxycarboxylic acid derivatives which is characterized by change in the fluorescence signal intensity. However, it couldn't differentiate the enantiomers. The same fluorescence studies were performed in the absence of Zn^{2+}, and compound **21** was found to be responsive towards above-mentioned chiral compounds even in the absence of Zn^{2+}. To understand the mechanism in details,

theoretical calculations were performed for geometry optimization. The results of the theoretical calculations showed that compound **21** has a twisted structure and consists of a six-membered pseudoaromatic ring triggered by hydrogen bonding interaction between imine nitrogen and hydroxyl group on benzene unit. The results of theoretical studies were supported by ^{1}H NMR and HPLC experiments. In ^{1}H NMR study, Hünig's base (dipea) was added to investigate the changes in intensities of acidic protons which was thought to give indications of pseudoaromaticity. In HPLC studies, the presence of enantiomers were proved. Atropisomers were tried to be separated by applying two different strategies.

In the last part of this study, TCNQ was functionalized through using different chiral amines (compounds **22-26**). The photophysical properties of these chiral DADQs were in well-aggreement with those reported for achiral derivatives in the literature. To increase their low quantum yields, they were encapsulated in SDS micelles. When encapsulated in hydrophobic core of micelle, the intensities of fluorescence emission bands increased dramatically as expected. In this micellar microenvironment, fluorescence titration studies were performed using enantiopure 2-butanol, 1-phenylethanol and α-methylbenzyl amine. The mechanism of micelle formation and dye encapsulation cannot be clarified. Many different time and preparation conditions were applied during micelle preparation, dye addition, and addition of chiral impurities. Some selectivities were observed for each of the enantiopure compounds; however, the results cannot be reproduced. Organic solvents with different polarities and viscosities were screened. DCM and ACN gave promising results with compounds **24** and **25**. Fluorescence titration experiments revealed that the compound **24** was able to differentiate enantiopure (*S*)- α-methylbenzyl amine. The experimental data were further processed with theoretical curves such as Stern-Völmer and Benesi-Hildebrand. Theoretical calculations were implemented in Gaussian 09 to explain the origin of selectivity and to propose structure for complex formed between compound **25** and chiral amines used in this study.

As a result, eigtheen different fluorescence sensors were synthesized and fully characterized. Their activities in chiral recognition through fluorescence

spectroscopy were investigated. Having very mild synthetic protocols, these new fluorescence sensors are superior to the already-reported sensors in the literature. This contributes to the genuineness of our studies reported in this thesis.

As a future work, coumarin can be functionalized by using chiral naphthyl amines and they can be tested in chiral recognition studies by exciting naphthyl units. Moreover, new enantiopure compounds can be utilized to increase the substrate scope of each study. New techniques such as circular dichroism or cyclic voltammetry can be adapted for chiral recognition studies.

CHAPTER 6

EXPERIMENTAL

6.1 General Information

All the materials and solvents were purchased from Sigma Aldrich and used without any further purification. For structural elucidation, Bruker AVANCE III 400 MHz Solution NMR spectrometer has been used. ^{1}H NMR data were recorded in $CDCl_3$ with TMS as internal standard and spectrum data were assigned as chemical shift (δ, ppm), multiplicity as an s (singlet), bs (broad singlet), d (doublet), dd (doublet of doublet), t (triplet), m (multiplet), coupling constants (*J*) in Hz (Hertz) and integration. ^{13}C NMR spectra were recorded at 100 MHz, and chemical shifts were reported relative to the solvent peak (77.0 ppm for $CDCl_3$). Sweep width for ^{1}H NMR spectra and ^{13}C NMR spectra are 20.5575 and 238.9564, respectively. The probe temperature is 23-24°C. For the compounds having full NMR analysis, the number of scans for ^{1}H NMR is 8, while it is 1024 for ^{13}C NMR unless otherwise noted. All reactions were monitored by TLC (Merck Silica Gel 60 F254), visualized by UV light. All IR spectra were taken using Thermo Fischer Scientific Nicola iS10 FTIR spectrometer and only major peaks are reported in reciprocal centimeter (cm^{-1}). Mass spectra were recorded Waters Synapt G1 High Resolution Mass Spectrometer. All spectroscopic measurements were done at ambient temperature.

For chiral recognition studies with chiral coumarin derivatives, fluorescence spectra were recorded using Varian Cary Eclipse Fluorescence spectrophotometer and UV spectra were measured using Cary 100 Bio UV-Vis spectrophotometer. Melting poins were measured using Stuart SMP11 analogue melting point measurement apparatus.

For cation recognition studies, fluorescence spectra were recorded using Varian Cary Eclipse Fluorescence spectrophotometer and UV spectra were measured using UV2450 UV-Vis spectrometer. Melting points were measured using Scinco DSC N-650 Differential Scanning Calorimeter.

For chiral recognition studies with Schiff base, fluorescence spectra were recorded using Varian Cary Eclipse Fluorescence spectrophotometer and UV spectra were measured using Agilent Carry 60 UV-Vis spectrophotometer.

For chiral recognition studies with TCNQ derivatives, fluorescence spectra were recorded using and Perkin Elmer LS55 spectrofluorometer and UV-Vis spectra were recorded using UV2450 UV-Vis spectrometer. Melting poins were measured using Stuart SMP11 analogue melting point measurement apparatus.

All optical rotations were measured using Krüss Optironic automatic digital polarimeter P3001RS.

6.2 Synthesis of 2,4-dihydroxybenzaldehyde[95,142]

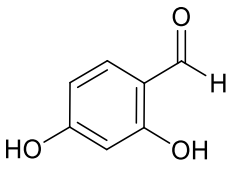

1

Resorcinol (1.4 g, 12.8 mmol) was dissolved in acetonitrile (15 ml), and cooled to 0 ºC, then DMF (1 ml) and $POCl_3$ (1.4 ml) were added to reaction mixture. The mixture was stirred at 0 ºC until white solids were formed. The salt residues were hydrolyzed by adding water and heating to 50 °C for 0.5 h. The product was obtained as a white solid in 34% yield. ^{1}H NMR (400 MHz, DMSO-d_6) δ 10.94 (bs, OH, 1H), 10.70 (bs, OH, 1H), 9.91 (s, 1H), 7.52 (d, *J* = 8.8 Hz, 1H), 6.39 (dd, *J* = 8.8, 2.4 Hz, 1H), 6.31 (d, *J* = 2.4 Hz, 1H). ^{13}C NMR (100 MHz, DMSO-d_6) δ 191.03, 165.41, 163.21, 132.95, 115.44, 108.91, 102.32.

6.3 Synthesis of 7-hydroxy-2*H*-chromene-3-carboxylic acid[93]

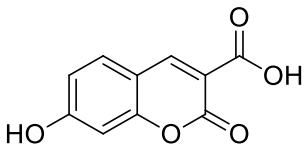

2

2,4-dihydroxybenzaldehyde (0.23 g, 1.7 mmol) was dissolved in EtOH (5 ml). Diethyl malonate (0.5 ml) was added to this solution. Then, glacial acetic acid (3 drops) and piperidine (0.1 ml) were added. The reaction mixture was refluxed for 3 hours. At the end of 3 hours, EtOH was removed under vacuum. Then, KOH solution (10%, 12.5 ml) was added to the crude mixture, and the mixture was refluxed for 1 hour. Then, the reaction mixture was brought to room temperature, and diluted with H_2O (20 ml). The mixture was acidified with HCl until pH becomes 3. The white solids that form at pH 3 were filtered, and recrystallized from MeOH. The product was obtained as a white solid in 46 % yield. ^{1}H NMR (400 MHz, DMSO-d_6) δ 11.13 (bs, OH, 1H), 8.68 (s, 1H), 7.74 (d, *J* = 8.8 Hz, 1H), 6.85 (dd, *J* = 8.8, 2.4 Hz, 1H), 6.75 (d, *J* = 2.8 Hz, 1H).

6.4 Synthesis of 7-hydroxy-2*H*-chromene-3-carbonyl chloride

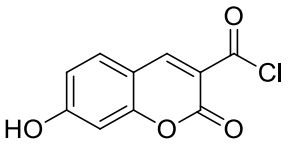

3

DMF (3-4 drops) was added to a round bottomed flask containing 7-hydroxy-2*H*-chromene-3-carboxylic acid (0.16 g, 0.78 mmol) and thionyl chloride (5 ml). The reaction mixture was refluxed 2 hours. Then, excess thionyl chloride was removed by rotary evaporator. The product was used for the next step without further purification.

6.5 Synthesis of (*S*)-7-hydroxy-N-(1-phenylethyl)-2*H*-chromene-3-carboxamide

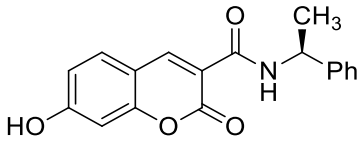

4

7-hydroxy-2*H*-chromene-3-carbonyl chloride (0.24 g, 0.78 mmol) was dissolved in toluene (6.5 ml), then (*S*)-α-methylbenzylamine (0.5 ml, 3.9 mmol) was added dropwise. The reaction mixture was stirred 3 hours at room temperature. At the end of 3 hours, toluene was removed by rotary evaporator. The crude product was dissolved in DCM (10 ml), and then extracted by dilute HCl (0.1M, 10 ml). Combined organic layers were dried over $MgSO_4$, filtered and concentrated. The product was purified by gradient elution in column chromatography (10:1, 8:1, 6:1, 5:1, 3:1, 1:1 Hexane: EtOAc) followed by recrystallization from Et_2O. The product was obtained as a light yellow solid in 30% yield. ^{1}H NMR (400 MHz, DMSO-d_6) δ 8.96 (d, *J* = 7.6 Hz, 1H), 8.76 (s, 1H), 7.80 (d, *J* = 8.8 Hz, 1H), 7.31 (m, 5H), 6.88 (dd, *J* = 8.8, 2.4 Hz, 2H), 6.82 (d, *J* = 2.1 Hz, 1H), 5.13 (p, *J* = 14.4 Hz, 1H), 1.48 (d, *J* = 6.8, 3H).^{13}C NMR (100 MHz, DMSO-d_6) δ 163.72, 161.25, 160.82, 156.29, 148.03, 143.83, 132.00, 128.50, 127.04, 125.97, 114.40, 113.71, 111.14, 101.84, 48.49, 22.60. IR (neat, cm^{-1}) 2880, 1714, 1622.

6.6 Synthesis of 2*H*-chromene-3-carboxylic acid[93]

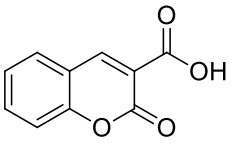

6

Salicylaldehyde (2.2 g, 18 mmol) was dissolved in EtOH (50 ml). Diethyl malonate (5.5 ml) was added to this solution. Then, glacial acetic acid (1.0 ml) and piperidine

(1.0 ml) were added. The reaction mixture was refluxed 3 hours. At the end of 3 hours, EtOH was removed under vacuum. Then KOH solution (10%, 125 ml) was added to crude mixture, and the mixture was refluxed 1 hour. Then the reaction mixture was brought to room temperature, and diluted with H_2O (200 ml). The mixture was acidified with HCl until pH becomes 3. The white solids that form at pH 3 were filtered, and recrystallized from MeOH. The product was obtained as a white solid in 73 % yield. ^{1}H NMR (400 MHz, $CDCl_3$) δ 12.26 (bs, OH, 1H), 8.96 (s, 1H), 7.79 (m, 2H), 7.49 (d, *J* = 7.4 Hz, 2H). ^{13}C NMR (100 MHz, $CDCl_3$) δ 164.26, 162.61, 154.74, 151.69, 135.96, 130.68, 126.44, 118.63, 117.39, 116.47.

6.7 Synthesis of 2*H*-chromene-3-carbonyl chloride

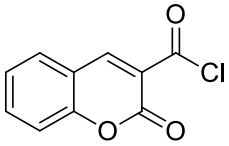

7

DMF (3-4 drops) was added to a round bottomed flask containing 2*H*-chromene-3-carboxylic acid (2.58 g, 13 mmol) and thionyl chloride (20 ml). The reaction mixture was refluxed 2 hours. Then, excess thionyl chloride was removed by rotary evaporator. The product was used for the next step without further purification.

6.8 Synthesis of (*S*) -N-(1-phenylethyl)-2*H*-chromene-3-carboxamide

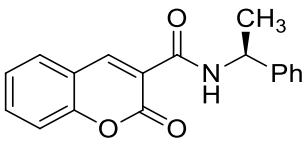

8

2*H*-chromene-3-carbonyl chloride (2.7 g, 13 mmol) was dissolved in toluene (108 ml), then (*S*)-α-methylbenzylamine (5 ml, 39 mmol) was added dropwise. The reaction mixture was stirred 3 hours at room temperature. At the end of 3 hours,

toluene was removed by rotary evaporator. The crude product was dissolved in DCM (75 ml), and then extracted by dilute HCl (0.1M, 75 ml). Combined organic layers were dried over $MgSO_4$, filtered and concentrated. The product was purified by gradient elution in column chromatography (10:1, 8:1, 6:1, 5:1, 3:1, 1:1 Hexane: EtOAc) followed by recrystallization from Et_2O. The product was obtained as a white solid in 46 % yield (R_f=0.41, Hexanes:EtOAc= 2:1). ^{1}H NMR (400 MHz, DMSO-d_6) δ 9.01 (d, *J* = 7.6 Hz, 1H), 8.83 (s, 1H), 7.98 (dd, *J* = 8.0, 0.8 Hz, 1H), 7.76 (t, *J* = 7.8 Hz 1H), 7.53 (d, *J* = 8.4 Hz, 1H), 7.40 (m, 5H), 7.27 (t, *J* = 6.8 Hz, 1H), 5.15 (p, *J* = 7.2 Hz, 1H), 1.49 (d, *J* = 6.8, 3H). ^{13}C NMR (100 MHz, DMSO-d_6) δ 160.53, 160.40, 153.85, 147.31, 143.68, 134.07, 130.22, 128.48, 127.00, 125.99, 125.15, 119.25, 118.46, 116.16, 48.76, 22.25. IR (neat, cm^{-1}) 3310, 1715, 1680. HRMS-EI (m/z): calcd for $C_{18}H_{16}NO_3Na$ $[M+H]^+$: 316.0950; found: 316.0956. mp: 123-124°C. $[\alpha]_D^{25} = -2.7°$ (*c*, 0.3, CH_2Cl_2).

6.9 Synthesis of (*R*) -N-(1-phenylethyl)-2*H*-chromene-3-carboxamide

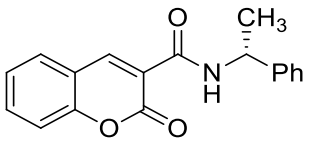

9

2*H*-chromene-3-carbonyl chloride (2.7 g, 13 mmol) was dissolved in toluene (108 ml), then (*R*)-α-methylbenzylamine (5 ml, 39 mmol) was added dropwise. The reaction mixture was stirred 3 hours at room temperature. At the end of 3 hours, toluene was removed by rotary evaporator. The crude product was dissolved in DCM (75 ml), and then extracted by dilute HCl (0.1M, 75 ml). Combined organic layers were dried over $MgSO_4$, filtered and concentrated. The product was purified by gradient elution in column chromatography (10:1, 8:1, 6:1, 5:1, 3:1, 1:1 Hexanes: EtOAc) followed by recrystallization from Et_2O. The product was obtained as a white solid in 24 % yield (R_f=0.41, Hexanes:EtOAc= 2:1). ^{1}H NMR (400 MHz, DMSO-d_6) δ 9.02 (d, *J* = 7.6 Hz, 1H), 8.83 (s, 1H), 7.97 (dd, *J* = 8.0, 1.2 Hz, 1H),

7.75 (m, 1H), 7.52 (d, *J* = 8.4 Hz, 1H), 7.40 (m, 5H), 7.26 (t, *J* = 6.8 Hz, 1H), 5.14 (p, *J* = 7.2 Hz, 1H), 1.49 (d, *J* = 7.2, 3H). ^{13}C NMR (100 MHz, DMSO-d_6) δ 160.52, 160.38, 153.83, 147.30, 143.67, 134.13, 130.20, 128.47, 126.99, 125.98, 125.13, 119.23, 118.45, 116.14, 48.67, 22.38. IR (neat, cm^{-1}) 3310, 1705, 1658. HRMS-EI (m/z): calcd for $C_{18}H_{16}NO_3$ $[M+H]^+$: 294.1130; found: 294.1115. mp: 122-123°C. $[\alpha]_D^{25} = +2.5°$ (*c*, 0.3, CH_2Cl_2).

6.10 Synthesis of 3-(*1H*-Benzotriazol-1-yl-carbonyl)-*2H*-chromen-2-one[96]

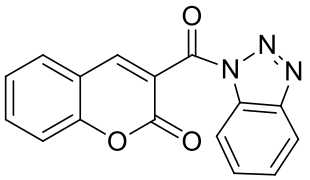

10

Thionyl chloride (0.89 g, 7.5 mmol) was added to a solution of benzotriazole (2.98 g, 25 mmol) in anhydrous THF (30 ml) at room temperature. After 20 minutes, *2H*-chromene-3-carboxylic acid, compound **6** (1.00 g, 5 mmol) was added and the reaction mixture was stirred for 4 hours at room temperature. After 4 hours, the white precipitate was filtered, and the filtrate was concentrated under vacuum. The crude product was dissolved in ethyl acetate (150 ml) and washed with Na_2CO_3 (3×50 ml) and brine (50 ml), dried over $MgSO_4$, filtered and concentrated. The product was obtained as a white solid in 34% yield. ^{1}H NMR (400 MHz, $CDCl_3$) δ 8.37 (s, 1H), 8.35 (s, 1H), 8.16 (d, *J* = 8.0 Hz, 1H), 7.71 (m, 3H), 7.57 (t, *J* = 7.8 Hz, 1H), 7.46 (m, 1H), 7.41 (m, 1H). ^{13}C NMR (100 MHz, $CDCl_3$) δ 182.16, 162.73, 157.76, 154.98, 147.18, 146.31, 134.67, 131.33, 131.03, 129.76, 126.96, 125.44, 120.57, 117.78, 117.32, 114.50.

6.11 Synthesis of (*S*)-2-(2-oxo-*2H*-chromene-3-carboxamido) propanoic acid[93]

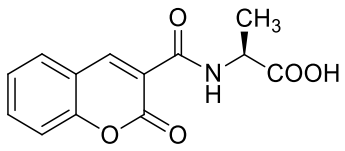

11

L-alanine (77 mg, 0.86 mmol) was dissolved in CH_3CN:H_2O (2:1, 13.5 ml) and Et_3N was added to this solution. Then, compound **10** (250 mg, 0.86 mmol) was added to the reaction mixture, and the resulting solution was stirred at 20ºC for 1 hour. After this time period, aqueous 4N HCl (1 ml) was then added and CH_3CN was removed under vacuum. The crude mixture was diluted with ethyl acetate (150 ml) and washed with 4N HCl (3×50 ml) and brine (50 ml), dried over $MgSO_4$, filtered and concentrated. The product was purified by recrystallization using ethyl acetate. The product was obtained as a white solid in 85% yield (R_f=0.21, EtOAc). ^{1}H NMR (400 MHz, DMSO-d_6) δ 9.11 (d, *J* = 6.8 Hz, 1H), 8.91 (s, 1H), 8.01 (dd, *J* = 7.8, 1.2 Hz, 1H), 7.77 (m, 1H), 7.53 (d, *J* = 8.4 Hz, 1H), 7.46 (t, *J* = 8.0 Hz, 1H), 4.48 (p, *J* = 7.2 Hz, 1H), 1.42 (d, *J* = 7.2 Hz, 3H). ^{13}C NMR (100 MHz, DMSO-d_6) δ 173.57, 160.57, 160.53, 154.00, 148.03, 134.33, 130.43, 125.22, 118.45, 118.27, 116.22, 48.20, 17.86. IR (neat, cm^{-1}) 3300, 1750, 1702, 1630. HRMS-EI (m/z): calcd for $C_{13}H_{12}NO_5$ $[M+H]^+$: 262.0715; found: 262.0715. mp: 203-204°C. $[\alpha]_D^{25} = +2.3°$ (*c*, 0.15, CH_2Cl_2).

6.12 Synthesis of (*R*)-2-(2-oxo-2*H*-chromene-3-carboxamido) propanoic acid

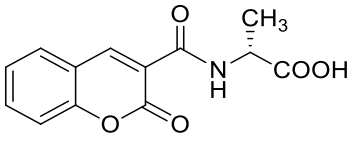

12

Adapting the same procedure as for compound **11**, the compound **12** was synthesized using *D*-alanine. The product was obtained as a white solid in 80% yield (R_f=0.21, EtOAc). ^{1}H NMR (DMSO-d_6) δ 13.03, (bs, 1H), 9.10 (d, *J* = 6.8 Hz, 1H), 8.91 (s, 1H), 8.01 (dd, *J* = 7.8, 1.2 Hz, 1H), 7.77 (ddd, *J* = 8.8, 7.4, 1.6 Hz, 1H), 7.53 (d, *J* = 8.4 Hz, 1H), 7.45 (td, *J* = 7.6, 0.8 Hz, 1H), 4.48 (p, *J* = 7.2 Hz, 1H), 1.42 (d, *J* = 7.2 Hz, 3H). ^{13}C NMR (100 MHz, DMSO-d_6) δ 173.51, 160.52, 153.97, 147.99, 134.29, 130.40, 125.18, 118.43, 118.28, 116.19, 48.30, 17.69. IR (neat, cm^{-1}) 3299, 1752, 1703, 1633. HRMS-EI (m/z): calcd for $C_{13}H_{12}NO_5$ $[M+H]^+$: 262.0715; found: 262.0703. mp: 204-205°C. $[\alpha]_D^{25} = -2.7°$ (*c*, 0.15, CH_2Cl_2).

6.13 Synthesis of (*S*)-2-(2-oxo-*2H*-chromene-3-carboxamido)-3-phenylpropanoic acid

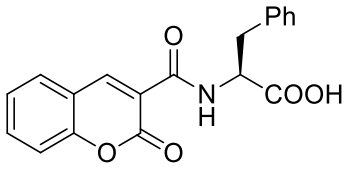

13

Adapting the same procedure as for compound **11**, the compound **13** was synthesized using *L*-phenylalanine. The product was obtained as a white solid in 89% yield (R_f=0.39, EtOAc). ^{1}H NMR (400 MHz, DMSO-d_6) δ 9.03 (d, *J* = 7.6 Hz, 1H), 8.91 (s, 1H), 8.00 (dd, *J* = 8.0, 1.4 Hz, 1H), 7.77 (m, 1H), 7.51 (d, *J* = 8.4 Hz, 1H), 7.45 (t, *J* = 7.6 Hz, 1H), 7.25 (m, 5H), 4.77 (m, 1H), 3.16 (ddd, *J* = 23.4, 13.8, 7.2 Hz, 2H). ^{13}C NMR (100 MHz, DMSO-d_6) δ 172.14, 160.65, 160.57, 154.06, 148.30, 136.64, 134.43, 130.49, 129.33, 128.36, 126.79, 125.31, 118.43, 117.91, 116.12, 53.70, 36.78. IR (neat, cm^{-1}) 3282, 1738, 1699, 1631. HRMS-EI (m/z): calcd for $C_{19}H_{16}NO_5$ $[M+H]^+$: 338.1028; found: 338.0983. mp:178°C. $[\alpha]_D^{25} = -6.5°$ (*c*, 0.3, CH_2Cl_2).

6.14 Synthesis of (*R*)-2-(2-oxo-*2H*-chromene-3-carboxamido)-3-phenylpropanoic acid

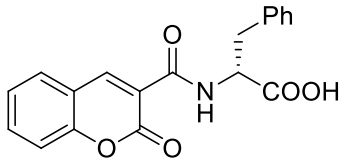

14

Adapting the same procedure as for compound **11**, the compound **14** was synthesized using D-phenylalanine. The product was obtained as a white solid in 85% yield (R_f=0.39, EtOAc). ^{1}H NMR (400 MHz, DMSO-d_6) δ 13.14(bs, 1H), 9.04 (d, *J* = 7.6 Hz, 1H), 8.90 (s, 1H), 7.98 (dd, *J* = 7.8, 1.4 Hz, 1H), 7.73 (m, 1H), 7.50 (d, *J* = 8.0 Hz, 1H), 7.40 (m, 1H), 7.25 (m, 5H), 4.77 (m, 1H), 3.16 (ddd, *J* = 23.6, 13.8, 6.8 Hz, 2H). ^{13}C NMR (100 MHz, DMSO-d_6) δ 172.08, 163.95, 160.61, 160.50, 153.94, 148.21, 136.61, 134.50, 130.41, 129.27, 128.30, 126.72, 125.18, 118.37, 117.89, 116.15, 53.67, 36.80. IR (neat, cm^{-1}) 3291, 1734, 1699, 1626. HRMS-EI (m/z): calcd for $C_{19}H_{16}NO_5$ $[M+H]^+$: 338.1028; found: 338.0982. mp:176°C. $[\alpha]_D^{25} = +6.2°$ (*c*, 0.3, CH_2Cl_2).

6.15 General procedure for synthesis of compounds 15-19[83]

Triethylene glycol (0.94 g, 6 mmol) and coumarin-3-acyl chloride (2.5 g, 12 mmol) were dissolved in 12.5 ml of pyridine. The mixture was stirred at 90°C for 29 h. After cooling to room temperature, the mixture was added into 95% ethanol to obtain white solids. The precipitates were filtered, dried and recrystallized from ethyl acetate. The product **17** was obtained in 20% yield as white crystals. Other derivatives were synthesized by adapting same procedure using ethylene glycol, diethylene glycol, tetraethylene glycol and 1,8- octanediol instead of triethylene glycol.

6.15.1 Synthesis of ethane-1,2-diyl bis(2-oxo-2*H*-chromene-3-carboxylate)

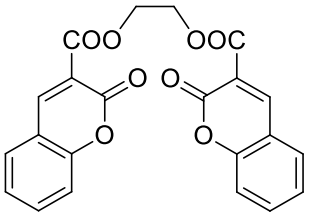

15

The product was obtained as white crystals in 26% yield. ^{1}H NMR (400 MHz, $CDCl_3$) δ 8.67 (s, 2H), 7.66 (m, 4H), 7.34 (d, *J* = 7.6 Hz, 4H), 4.69 (s, 4H). ^{13}C NMR (100 MHz, $CDCl_3$) δ 162.76, 156.63, 155.16, 149.31, 134.58, 129.86, 124.99, 117.93, 117.77, 116.77, 63.05. IR (neat, cm^{-1}): 2908, 1759, 1609, 1136. HRMS-EI (m/z): calcd for $C_{22}H_{14}O_8$ $[M+H]^+$: 407.0787; found: 407.0767. mp:217.7°C.

6.15.2 Synthesis of oxybis(ethane-2,1-diyl) bis(2-oxo-2*H*-chromene-3-carboxylate)

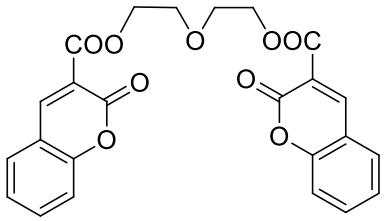

16

The product was obtained as white crystals in 10% yield. ^{1}H NMR (400 MHz, $CDCl_3$) δ 8.57 (s, 2H), 7.63 (m, 4H), 7.31 (dd, *J* = 12.5, 5.0 Hz, 4H), 4.53 (m, 4H), 3.91 (m, 4H). ^{13}C NMR (100 MHz, $CDCl_3$) δ 162.84, 156.54, 155.12, 148.92, 134.39, 129.69, 124.82, 117.85, 116.70, 68.92, 64.78. IR (neat, cm^{-1}): 2907, 1750, 1612, 1117. HRMS-EI (m/z): calcd for $C_{24}H_{19}O_9$ $[M+H]^+$: 451.1028; found: 451.1029. mp:165°C.

6.15.3 Synthesis of (ethane-1,2-diylbis(oxy))bis(ethane-2,1-diyl) bis(2-oxo-2*H*-chromene-3-carboxylate)

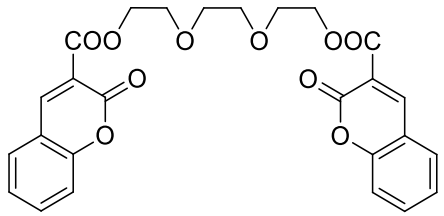

17

The product was obtained in 20% yield as white crystals. ^{1}H NMR (400 MHz, $CDCl_3$) δ 8.54 (s, 2H), 7.62 (m, 4H), 7.32 (m, 4H), 4.50 (dd, *J* = 10.5, 5.8 Hz, 4H), 3.85 (m, 4H), 3.73 (m, 4H). ^{13}C NMR (100 MHz, $CDCl_3$) δ 162.80, 156.48, 155.15, 148.74, 134.36, 129.56, 124.82, 117.94, 117.79, 116.71, 116.09, 70.67, 68.91, 64.84. IR (neat, cm-1): 2906, 1743, 1607, 1126. HRMS-EI (m/z): calcd for $C_{26}H_{23}O_{10}$ $[M+H]^+$: 495.1291; found: 495.1292. mp:130.1°C.

6.15.4 Synthesis of ((oxybis(ethane-2,1-diyl))bis(oxy))bis(ethane-2,1-diyl) bis(2-oxo-2*H*-chromene-3-carboxylate)

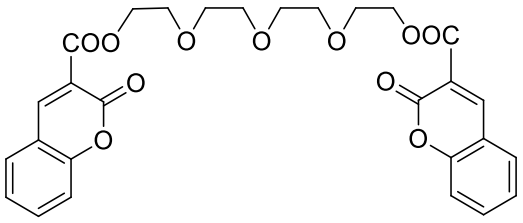

18

The product was obtained as white crystals a white solid in 5% yield. ^{1}H NMR (400 MHz, $CDCl_3$) δ 8.56 (s, 2H), 7.63 (m, 4H), 7.32 (m, 4H), 4.46 (m, 4H), 3.81 (m, 4H), 3.69 (m, 8H). ^{13}C NMR (100 MHz, $CDCl_3$) δ 162.79, 156.52, 156.13, 148.79, 134.40, 129.55, 124.83, 117.86, 117.77, 116.73, 70.61, 68.85, 64.82. IR (neat, cm^{-1}): 2907, 1764, 1608, 1117. HRMS-EI (m/z): calcd for $C_{28}H_{27}O_{11}$ $[M+H]^+$: 539.1553; found: 539.1549. mp:123.6°C

6.15.5 Synthesis of octane-1,8-diyl bis(2-oxo-2*H*-chromene-3-carboxylate)

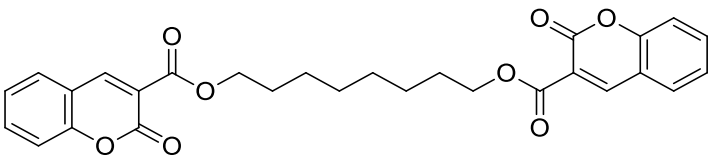

19

The product was obtained as green crystals in 10% yield. ^{1}H NMR (400 MHz, $CDCl_3$) δ 8.51 (s, 2H), 7.62 (m, 4H), 7.34 (m, 4H), 4.33 (t, *J*= 6.8 Hz, 4H), 1.76 (p, *J*= 6.8 Hz, 4H), 1.42 (m, 8H). ^{13}C NMR (100 MHz, $CDCl_3$) δ 163.12, 156.64, 155.11, 148.47, 134.27, 129.47, 124.78, 118.32, 117.83, 116.72, 65.97, 29.01, 28.48, 25.74. IR (neat, cm^{-1}): 2926, 2851, 1745, 1608, 1241, 1010. HRMS-EI (m/z): calcd for $C_{28}H_{27}O_8$ $[M+H]^+$**:** 491.1706; found: 491.1709. mp:135.8°C.

6.16 Synthesis of methyl ester of coumarin-3- carboxylic acid[143]

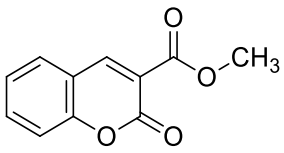

20

H_2SO_4 (0.3ml) was added dropwise to a solution of coumarin-3-carboxylic acid (1.06g, 5mmol) in 10 ml methanol. The resulting mixture was refluxed for 48h. After this time period, it was cooled down to room temperature. The reaction mixture was washed with saturated $NaHCO_3$ and the organic layer was dried over $MgSO_4$, filtered and concentrated under vacuum to afford methyl ester as a white solid in 98% yield. ^{1}H NMR (400 MHz, $CDCl_3$) δ 8.58 (s, 1H), 7.65 (ddd, *J* = 10.0, 8.2, 4.0 Hz, 2H), 7.34 (dd, *J* = 14.2, 7.6 Hz, 2H), 3.96 (s, 3H). ^{13}C NMR (100 MHz, $CDCl_3$) δ 163.82, 155.34, 149.26, 134.62, 129.71, 125.04, 117.98, 116.92, 53.03.

6.17 Synthesis of Sodium 4-(2-hydroxybenzylideneamino)-3-hydroxynaphthalene-1-sulfonate[120]

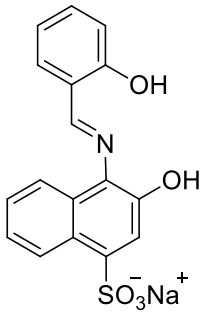

21

NaOH (0.1 g, 2.5 mmol) was added into solution of 1-amino-2-hydroxy-4-naphthalenesulfonic acid (0.6 g, 5 mmol) in 50 ml ethanol. The mixture was stirred 10 minutes. After the solution becomes clear, salicylaldehyde (0.3 g, 2.5 mmol) was added into the solution. The reaction mixture was stirred overnight at room temperature. Then, the precipitate is filtered, and washed with cold ethanol. After drying the precipitate, the desired product was obtained in 65% yield. ^{1}H NMR (400 MHz, DMSO-d_6) δ 13.52 (s, 1H), 10.10 (s, 1H), 9.11 (s, 1H), 8.77 (d, *J* = 8.4 Hz, 1H), 7.88 (d, *J* = 6.4 Hz, 2H), 7.67 (dd, *J* = 7.6, 1.2 Hz, 1H), 7.45 (m, 2H), 7.35 (m, 1H), 7.01 (m, 2H). ^{13}C NMR (100 MHz, DMSO-d_6) δ 168.16, 160.51, 143.10, 142.78, 133.09, 132.32, 128.30, 127.82, 126.23, 124.05, 122.93, 121.34, 119.59, 119.13, 117.97, 116.65.

6.18 Synthesis of 2-(4-(bis(((*S*)-1-phenylethyl)amino)methylene)cyclohexa-2,5-dien-1-ylidene)malononitrile

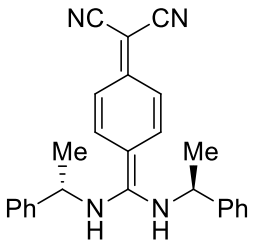

22

To a solution of 7,7,8,8-tetracyanoquinodimethane (0.600 g, 2.94 mmol) in CH_3CN (40 ml), was added (*S*)-(-)-α-methylbenzyl amine (0.94 ml). The reaction mixture was refluxed overnight. Then, solvent was removed by rotary evaporator. Crude mixture was recrystallized from MeOH:Et_2O to obtain compound **22** as a light yellow solid in 60% yield (R_f=0.25, EtOAc). ^{1}H NMR (400 MHz, DMSO-d_6) δ 9.82 (d, *J* = 6.0 Hz, 1H), 8.87 (d, *J* = 8.4 Hz, 1H), 7.40 (d, *J* = 4.0 Hz, 5H), 7.13 (m, 5H), 6.82 (d, *J* = 8.4 Hz, 4H), 5.31 (m, 1H), 4.74 (m, 1H), 1.57 (d, *J* = 6.8 Hz, 6H). ^{13}C NMR (100 MHz, DMSO-d_6) δ 163.25, 147.70, 142.04, 141.54, 128.93, 128.72, 128.35, 127.68, 127.16, 126.04, 125.34, 123.76, 117.32, 114.60, 54.94, 51.27, 22.18, 21.96. IR (neat, cm^{-1}): 3221, 2168, 2114, 1590. HRMS-EI (m/z): calcd for $C_{26}H_{24}N_4$ $[M+H]^+$**:** 393.2079; found 393.2083. mp:198°C. $[\alpha]_D^{25} = -24.1$ ° (*c*, 0.55, CH_2Cl_2).

6.19 Synthesis of 2-(4-(bis(((*R*)-1-phenylethyl)amino)methylene)cyclohexa-2,5-dien-1-ylidene)malononitrile

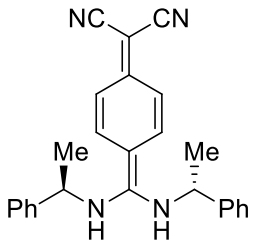

23

The compound **23** was obtained in 52% yield as a light yellow solid (R_f =0.25, EtOAc). ^{1}H NMR (400 MHz, DMSO-d_6) δ 9.81 (d, *J* = 7.2 Hz, 1H), 8.86 (d, *J* = 8.4 Hz, 1H), 7.40 (d, *J* = 4.0 Hz, 5H), 7.13 (m, 5H), 6.81 (d, *J* = 8.4 Hz, 4H), 5.30 (m, 1H), 4.74 (m, 1H), 1.56 (d, *J* = 6.4 Hz, 6H). ^{13}C NMR (100 MHz, DMSO-d_6) δ 163.25, 147.72, 142.03, 141.53, 128.92, 128.71, 128.35, 127.68, 127.15, 126.04, 125.34, 123.74, 117.31, 114.57, 54.91, 51.29, 22.15, 21.93. HRMS-EI (m/z): calcd for $C_{26}H_{24}N_4$ $[M+H]^+$**:** 393.2079; found 393.2074. IR (neat, cm^{-1}): 3210, 2181, 2121, 1600. mp=198°C. $[\alpha]_D^{25} = +24.3$ ° (*c*, 0.55, CH_2Cl_2).

6.20 2-(4-(bis(((*R*)-1-(naphthalen-1-yl)ethyl)amino)methylene)cyclohexa-2,5-dien-1-ylidene)malononitrile

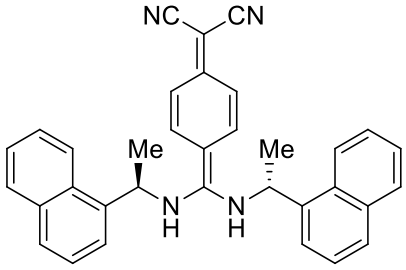

24

The compound **24** was obtained in 84% yield as a light yellow solid (R_f =0.36, EtOAc). ^{1}H NMR (400 MHz, DMSO-d_6) δ 9.86 (d, *J* = 7.2 Hz, 1H), 9.17 (d, *J* = 8.0 Hz, 1H), 7.86 (m, 5H), 7.28 (m, 2H), 7.14 (m, 4H), 6.74 (d, *J* = 8.4 Hz, 4H), 6.0 (m, 1H), 5.6 (m, 1H), 1.75 (s, 6H). ^{13}C NMR (100 MHz, DMSO-d_6) δ 141.98, 133.29, 130.12, 128.65, 126.00, 125.51, 125.49, 123.08, 122.09, 117.23, 45.92, 24.33. IR (neat, cm^{-1}): 3211, 2178, 2129, 1595. HRMS-EI (m/z): calcd for $C_{34}H_{29}N_4$ $[M+H]^+$**:** 493.2392; found 493.2384. mp:182°C. $[\alpha]_D^{25} = -20.5°$ (*c*, 0.20, CH_2Cl_2).

6.21 2-(4-(bis(((*S*)-1-(naphthalen-2-yl)ethyl)amino)methylene)cyclohexa-2,5-dien-1-ylidene)malononitrile

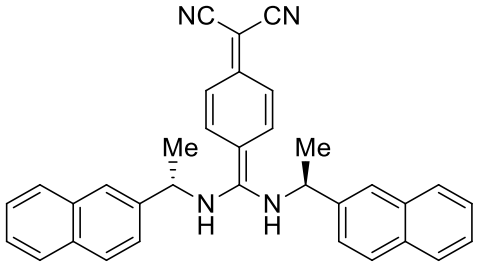

25

The compound **25** was obtained in 82% yield as a light yellow solid (R_f =0.21, EtOAc). ^{1}H NMR (400 MHz, DMSO-d_6) δ 9.96 (d, *J* = 5.2 Hz, 1H), 9.06 (d, *J* = 8.4 Hz, 1H), 7.92 (m, 3H), 7.85 (d, *J* = 8.0 Hz, 1H), 7.63 (d, *J* = 8.4 Hz, 1H), 7.54 (m, 3H), 7.37 (t, *J* = 8.0 Hz, 2H), 7.24 (t, *J* = 8.0 Hz, 3H), 7.09 (s, 1H), 6.97 (t, *J* = 6.8 Hz, 2H), 6.84 (d, *J* = 7.6 Hz, 2H), 5.51 (m, 1H), 4.90 (m, 1H), 1.67 (t, *J* = 6.0 Hz, 6H). ^{13}C NMR (100 MHz, DMSO-d_6) δ 163.34, 147.73, 139.44, 139.01, 136.13, 128.95, 128.62, 128.33, 127.86, 127.54, 127.33, 127.23, 126.44, 126.22, 126.01, 125.84, 123.71, 123.22, 117.40, 114.55, 55.92, 55.02, 51.49, 22.10, 21.97. IR (neat, cm^{-1}): 3209, 2176, 2131, 1592. HRMS-EI (m/z): calcd for $C_{34}H_{29}N_4$ $[M+H]^+$**:** 493.2392; found 493.2397. mp: decomposed above 227°C. $[\alpha]_D^{25} = +22.0°$ (*c*, 0.20, CH_2Cl_2).

6.22 2-(4-(bis(((*R*)-1-cyclohexylethyl)amino)methylene)cyclohexa-2,5-dien-1-ylidene)malononitrile

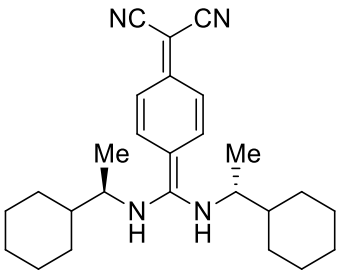

26

The compound **26** was obtained in 35% yield as a light yellow solid (R_f =0.32, EtOAc). ^{1}H NMR (400 MHz, DMSO-d_6) δ 9.06 (s, 1H), 8.23 (d, *J* = 8.0 Hz, 1H), 7.13 (d, *J* = 8.4 Hz, 2H), 6.84 (d, *J* = 8.4 Hz, 2H), 3.76 (m, 1H), 3.28 (m, 1H), 1.66 (m, 12H), 1.26 (d, *J* = 6.4 Hz, 6H), 1.11 (m, 8H). ^{13}C NMR (100 MHz, DMSO-d_6) δ 163.34, 147.45, 129.00, 123.99, 117.76, 115.63, 56.61, 52.19, 43.16, 41.55, 31.48, 29.27, 29.25, 28.95, 28.91, 28.81, 28.45, 28.41, 25.76, 25.58, 25.43, 25.14, 18.08, 17.14. IR (neat, cm^{-1}): 3211, 2173, 2129, 1590. HRMS-EI (m/z): calcd for $C_{26}H_{37}N_4$ $[M+H]^+$**:** 405.3018; found 405.3018. mp: decomposed above 183°C. $[\alpha]_D^{25} = -5.5°$ (*c*, 0.20, CH_2Cl_2).

REFERENCES

(1) Newton, I. *Opticks: A Treatise of the Reflections, Refractions, Inflections & Colors of Light*, Fourth Ed.; London, 1730.

(2) Turro, Nicholas J., Ramamurthy, V., Scaiano, J. C. *Principles of Molecular Photochemistry An Introduction*; First Ed.; University Science Books, 2008.

(3) Al-Azzawi, A. *Light and Optics: Principles and Practices*; First Ed.; CRC Press, 2006.

(4) Wayne, R. P. *Photochemistry*; American Elsevier Publishing Company: New York, 1970.

(5) Huygens, C. *Treatise on Light*; Fourth Ed.; University of Chicago Press, 1960.

(6) Maxwell, J. C. *A Treatise on Electricity and Magnetism*, First Ed.; Oxford: Clarendon Press: London, 1892.

(7) Pais, A. Einstein and the Quantum Theory. *Rev. Mod. Phys.* **1979**, *51* (4), 863–913.

(8) Waldman, G. *Introduction to Light: The Physics of Light, Vision and Color*, Revised Ed.; Dover Publications, 2003.

(9) Wardle, B. *Principles and Applications of Photochemistry*; John Wiley & Sons, 2009.

(10) Gupta, V. P.; Turro, Nicholas J., Ramamurthy, V., Scaiano, J. C. *Interaction of Radiation and Matter and Electronic Spectra*; Stiefel, J., Ed.; Elsevier, 2009. https://doi.org/10.1016/B978-0-12-803478-1.00009-1.

(11) Born, M.; Oppenheimer, R. Zur Quantentheorie Der Molekeln. *Ann. Phys.* **1927**, *389* (20), 457–484. https://doi.org/10.1002/andp.19273892002.

(12) Anslyn, E.V., Dougherty, D. A. *Modern Physical Organic Chemistry*; Murdzek, J., Ed.; University Science Books, 2006.

(13) Hill, W. T. I.; Lee, C. H. *Light-Matter Interaction: Atoms and Molecules in External Fields and Nonlinear Optics*; Wiley VCH, 2006.

(14) Geddes, C. D.; Lakowicz, J. R. *Reviews in Fluorescence 2006*, Third Ed.; Springer Science and Bussiness Media, 2007.

(15) Nano, A. (2015), Towards Optical Memories : Switchable Optical Systems for Electron and Energy Transfer Processes, California Institute of Technology, Doctor of Philosophy.

(16) Kasha, M. Characterization of Electronic Transitions in Complex Molecules. *Discuss. Faraday Soc.* **1950**, *9*, 14. https://doi.org/10.1039/df9500900014.

(17) Perrin, F. La Fluorescence Des Solutions. *Ann. Phys. (Paris).* **1929**, *10* (12), 169–275. https://doi.org/10.1051/anphys/192910120169.

(18) Jabłoński, A. Über Das Entstehen Der Breiten Absorptions- Und Fluoreszenzbanden in Farbstofflösungen. *Zeitschrift für Phys.* **1932**, *73* (7–8), 460–469. https://doi.org/10.1007/BF01349853.

(19) Jablonski, A. Efficiency of Anti-Stokes Fluorescence in Dyes. *Nature* **1933**, *131* (3319), 839–840. https://doi.org/10.1038/131839b0.

(20) Herzberg, L.; Herzberg, G. FINE STRUCTURE OF THE INFRARED ATMOSPHERIC OXYGEN BANDS. *Astrophys. J.* **1947**, *105* (3), 353–359.

(21) Lakowicz, J. R. *Principles of Fluorescence Spectroscopy*, Third Edit.; Lakowicz, J. R., Ed.; Springer US: Boston, MA, 2006. https://doi.org/10.1007/978-0-387-46312-4.

(22) Douglas, Skoog A., Holler, James F., Crouch, S. R. *Principles of Instrumental Analysis*, 6th Edition; Cengage Learning, 2006.

(23) Nijegorodov, N. I.; Downey, W. S. The Influence of Planarity and Rigidity on the Absorption and Fluorescence Parameters and Intersystem Crossing Rate Constant in Aromatic Molecules. *J. Phys. Chem.* **1994**, *98* (22), 5639–5643. https://doi.org/10.1021/j100073a011.

(24) Vavilov, S. I. XXIX. The Dependence of the Intensity of the Fluorescence of

Dyes upon the Wave-Length of the Exciting Light. *London, Edinburgh, Dublin Philos. Mag. J. Sci.* **1922**, *43* (254), 307–320. https://doi.org/10.1080/14786442208565217.

(25) Vavilov, S. I. Die Fluoreszenzausbeute von Farbstofflösungen. *Zeitschrift für Phys.* **1924**, *22* (1), 266–272. https://doi.org/10.1007/BF01328130.

(26) Vavilov, S. I. Die Fluoreszenzausbeute von Farbstofflösungen Als Funktion Der Wellenlange Des Anregenden Lichtes. II. *Zeitschrift für Phys.* **1927**, *42* (4), 311–318. https://doi.org/10.1007/BF01397622.

(27) Wu, D.; Sedgwick, A. C.; Gunnlaugsson, T.; Akkaya, E. U.; Yoon, J.; James, T. D. Fluorescent Chemosensors: The Past, Present and Future. *Chem. Soc. Rev.* **2017**, *46* (23), 7105–7123. https://doi.org/10.1039/C7CS00240H.

(28) Galas, L.; Gallavardin, T.; Bénard, M.; Lehner, A.; Schapman, D.; Lebon, A.; Komuro, H.; Lerouge, P.; Leleu, S.; Franck, X. "Probe, Sample, and Instrument (PSI)": The Hat-Trick for Fluorescence Live Cell Imaging. *Chemosensors* **2018**, *6* (3), 40. https://doi.org/10.3390/chemosensors6030040.

(29) Wilson, G. M. RNA Folding and RNA-Protein Binding Analyzed by Fluorescence Anisotropy and Resonance Energy Transfer. In *Reviews in Fluorescence 2005*; Springer US: Boston, MA; pp 223–243. https://doi.org/10.1007/0-387-23690-2_10.

(30) Chattopadhyay, A.; Raghuraman, H. Application of Fluorescence Spectroscopy to Membrane Protein Structure and Dynamics. *Curr. Sci.* **2004**, *87* (2), 175–180.

(31) Lundblad, J. R.; Laurance, M.; Goodman, R. H. Fluorescence Polarization Analysis of Protein-DNA and Protein-Protein Interactions. *Mol. Endocrinol.* **1996**, *10* (6), 607–612. https://doi.org/10.1210/mend.10.6.8776720.

(32) Rudin, M.; Weissleder, R. Molecular Imaging in Drug Discovery and Development. *Nat. Rev. Drug Discov.* **2003**, *2*, 123–131.

(33) Jameson, D. M.; Ross, J. A. Fluorescence Polarization/Anisotropy in Diagnostics and Imaging. *Chem. Rev.* **2010**, *110* (5), 2685–2708. https://doi.org/10.1021/cr900267p.

(34) Dramićanin, T.; Dramićanin, M. Using Fluorescence Spectroscopy to Diagnose Breast Cancer. In *Applications of Molecular Spectroscopy to Current Research in the Chemical and Biological Sciences*; InTech, 2016. https://doi.org/10.5772/63534.

(35) Leung, D.; Kang, S. O.; Anslyn, E. V. Rapid Determination of Enantiomeric Excess: A Focus on Optical Approaches. *Chem. Soc. Rev.* **2012**, *41* (1), 448–479. https://doi.org/10.1039/C1CS15135E.

(36) Pu, L. Fluorescence of Organic Molecules in Chiral Recognition. *Chem. Rev.* **2004**, *104* (3), 1687–1716. https://doi.org/10.1021/cr030052h.

(37) Herrera, B. T.; Pilicer, S. L.; Anslyn, E. V.; Joyce, L. A.; Wolf, C. Optical Analysis of Reaction Yield and Enantiomeric Excess: A New Paradigm Ready for Prime Time. *J. Am. Chem. Soc.* **2018**, *140* (33), 10385–10401. https://doi.org/10.1021/jacs.8b06607.

(38) Kolanowski, J. L.; Liu, F.; New, E. J. Fluorescent Probes for the Simultaneous Detection of Multiple Analytes in Biology. *Chem. Soc. Rev.* **2018**, *47* (1), 195–208. https://doi.org/10.1039/C7CS00528H.

(39) Sigel, Astrid; Sigel, Helmut; Sigel, R. K. O. *The Alkali Metal Ions: Their Role for Life*, First Edit.; Springer, 2016.

(40) Perez, V.; Chang, E. T. Sodium-to-Potassium Ratio and Blood Pressure, Hypertension, and Related Factors. *Adv. Nutr.* **2014**, *5* (6), 712–741. https://doi.org/10.3945/an.114.006783.

(41) Yoon, J.; Czarnik, A. W. Fluorescent Chemosensors of Carbohydrates. A Means of Chemically Communicating the Binding of Polyols in Water Based on Chelation-Enhanced Quenching. *J. Am. Chem. Soc.* **1992**, *114* (14), 5874–5875. https://doi.org/10.1021/ja00040a067.

(42) Zhao, J.; Fyles, T. M.; James, T. D. Chiral Binol–Bisboronic Acid as Fluorescence Sensor for Sugar Acids. *Angew. Chemie Int. Ed.* **2004**, *43* (26), 3461–3464. https://doi.org/10.1002/anie.200454033.

(43) Zhao, J.; James, T. D. Enhanced Fluorescence and Chiral Discrimination for Tartaric Acid in a Dual Fluorophore Boronic Acid Receptor. *Chem. Commun.* **2005**, No. 14, 1889. https://doi.org/10.1039/b418279k.

(44) Gokel, G. W.; Leevy, W. M.; Weber, M. E. Crown Ethers: Sensors for Ions and Molecular Scaffolds for Materials and Biological Models. *Chem. Rev.* **2004**, *104* (5), 2723–2750. https://doi.org/10.1021/cr020080k.

(45) Finney, N. S.; McFarland, S. A. Fluorescent Chemosensors Based on Conformational Restriction of a Biaryl Fluorophore. *J. Am. Chem. Soc.* **2001**, *123*, 1260–1261. https://doi.org/10.1021/ja005701a.

(46) Seiji, Shinkai; Sandanayake, Samankumara; Nakashima, K. Specific Recognition of Disaccharides by Trans-3,3′-Stilbenediboronic Acid: Rigidification and Fluoresecence Enhancement of the Stilbene Skeleton upon Formation of a Sugar–Stilbene Macrocycle. *J. Chem. Soc. Chem. Commun.* **1994**, 1621–1622. https://doi.org/10.1039/C39940001621.

(47) McFarland, S. A.; Finney, N. S. Fluorescent Signaling Based on Control of Excited State Dynamics. Biarylacetylene Fluorescent Chemosensors. *J. Am. Chem. Soc.* **2002**, *124* (7), 1178–1179. https://doi.org/10.1021/ja017309i.

(48) Xu, X.; Xu, H.; Ji, H. New Fluorescent Probes for the Detection of Mixed Sodium and Potassium Metal Ions. **2001**, 2092–2093. https://doi.org/10.1039/b106632n.

(49) Cotton, F. A. *Chemical Applications of Group Theory*, Third Edit.; John Wiley & Sons: USA, 1990.

(50) Trost, B. M. Asymmetric Catalysis Special Feature Part I: Asymmetric Catalysis: An Enabling Science. *Proc. Natl. Acad. Sci.* **2004**, *101* (15), 5348–5355. https://doi.org/10.1073/pnas.0306715101.

(51) Campbell, D. B.; Wilson, K. Chirality and Its Importance in Drug Development. *Biochem. Soc. Trans.* **1991**, *19* (2), 472–475. https://doi.org/10.1042/bst0190472.

(52) Sarker, S. D.; Nahar, L. *Chemistry for Pharmacy Students*; Wiley, 2007. https://doi.org/10.1002/9781118687529.

(53) Bens, R. H. E. (1993), Acetals of 1-Aryl-2,2-Dimethyl-1,3-Propanediols Synthesis and Use as Chiral Auxiliary, University of Groningen, Doctor of Philosophy.

(54) Aitken, Alan R.; Kilenyi, N. S. Asymmetric Synthesis; Chapman & Hall: London, 1994; p 33.

(55) North, M. Principles and Applications of Stereochemistry; Stanley Thornes Publishers Ltd, 1998; pp 117–118.

(56) Cavazzini, A.; Pasti, L.; Massi, A.; Marchetti, N.; Dondi, F. Recent Applications in Chiral High Performance Liquid Chromatography: A Review. *Anal. Chim. Acta* **2011**, *706* (2), 205–222. https://doi.org/10.1016/j.aca.2011.08.038.

(57) Kotake, M.; Sakan, T.; Nakamura, N.; Senoh, S. RESOLUTION INTO OPTICAL ISOMERS OF SOME AMINO ACIDS BY PAPER CHROMATOGRAPHY. *J. Am. Chem. Soc.* **1951**, *73* (6), 2973–2974. https://doi.org/10.1021/ja01150a548.

(58) Wenzel, T. J.; Wilcox, J. D. Chiral Reagents for the Determination of Enantiomeric Excess and Absolute Configuration Using NMR Spectroscopy. *Chirality* **2003**, *15* (3), 256–270. https://doi.org/10.1002/chir.10190.

(59) Dale, J. A.; Dull, D. L.; Mosher, H. S. α-Methoxy-α-trifluoromethylphenylacetic Acid, a Versatile Reagent for the Determination of Enantiomeric Composition of Alcohols and Amines. *J. Org. Chem.* **1969**, *34* (9), 2543–2549. https://doi.org/10.1021/jo01261a013.

(60) Fales, H. M.; Wright, G. J. Detection of Chirality with the Chemical Ionization

Mass Spectrometer. “Meso” Ions in the Gas Phase. *J. Am. Chem. Soc.* **1977**, *99* (7), 2339–2340. https://doi.org/10.1021/ja00449a054.

(61) Awad, H.; El-Aneed, A. Enantioselectivity of Mass Spectrometry: Challenges and Promises. *Mass Spectrom. Rev.* **2013**, *32*, 466-483. https://doi.org/10.1002/mas.21379.

(62) Chen, X.; Kang, Y.; Zeng, S. Analysis of Stereoisomers of Chiral Drug by Mass Spectrometry. *Chirality* **2018**, *30* (5), 609–618. https://doi.org/10.1002/chir.22833.

(63) Han, D.-Q.; Yao, Z.-P. Chiral Mass Spectrometry: An Overview. *TrAC Trends Anal. Chem.* **2020**, *123*, 115763. https://doi.org/10.1016/j.trac.2019.115763.

(64) Tumambac, G. E.; Wolf, C. Enantioselective Analysis of an Asymmetric Reaction Using a Chiral Fluorosensor. *Org. Lett.* **2005**, *7* (18), 4045–4048. https://doi.org/10.1021/ol0516216.

(65) James, T. D.; Samankumara Sandanayake, K. R. A.; Shinkai, S. Chiral Discrimination of Monosaccharides Using a Fluorescent Molecular Sensor. *Nature* **1995**, *374* (6520), 345–347. https://doi.org/10.1038/374345a0.

(66) James, T. D.; Sandanayake, K. R. A. S.; Shinkai, S. Novel Photoinduced Electron-Transfer Sensor for Saccharides Based on the Interaction of Boronic Acid and Amine. *J. Chem. Soc. Chem. Commun.* **1994**, No. 4, 477. https://doi.org/10.1039/c39940000477.

(67) James, T. D.; Sandanayake, K. R. A. S.; Shinkai, S. A Glucose-Selective Molecular Fluorescence Sensor. *Angew. Chemie Int. Ed. English* **1994**, *33* (21), 2207–2209. https://doi.org/10.1002/anie.199422071.

(68) Pu, L. 1,1‘-Binaphthyl Dimers, Oligomers, and Polymers: Molecular Recognition, Asymmetric Catalysis, and New Materials †. *Chem. Rev.* **1998**, *98* (7), 2405–2494. https://doi.org/10.1021/cr970463w.

(69) Li, Z.-B.; Lin, J.; Sabat, M.; Hyacinth, M.; Pu, L. Enantioselective Fluorescent

Recognition of Chiral Acids by Cyclohexane-1,2-Diamine-Based Bisbinaphthyl Molecules. *J. Org. Chem.* **2007**, *72* (13), 4905–4916. https://doi.org/10.1021/jo0704715.

(70) Wen, K.; Yu, S.; Huang, Z.; Chen, L.; Xiao, M.; Yu, X.; Pu, L. Rational Design of a Fluorescent Sensor to Simultaneously Determine Both the Enantiomeric Composition and the Concentration of Chiral Functional Amines. *J. Am. Chem. Soc.* **2015**, *137* (13), 4517–4524. https://doi.org/10.1021/jacs.5b01049.

(71) Lin, J.; Hu, Q.-S.; Xu, M.-H.; Pu, L. A Practical Enantioselective Fluorescent Sensor for Mandelic Acid. *J. Am. Chem. Soc.* **2002**, *124* (10), 2088–2089. https://doi.org/10.1021/ja011971x.

(72) Li, Z.-B.; Lin, J.; Pu, L. A Cyclohexyl-1,2-Diamine-Derived Bis(Binaphthyl) Macrocycle: Enhanced Sensitivity and Enantioselectivity in the Fluorescent Recognition of Mandelic Acid. *Angew. Chemie Int. Ed.* **2005**, *44* (11), 1690–1693. https://doi.org/10.1002/anie.200462471.

(73) Mei, X.; Wolf, C. A Highly Congested N,N′-Dioxide Fluorosensor for Enantioselective Recognition of Chiral Hydrogen Bond Donors. *Chem. Commun.* **2004**, No. 18, 2078–2079. https://doi.org/10.1039/B407718K.

(74) Tumambac, G. E.; Wolf, C. Enantioselective Analysis of an Asymmetric Reaction Using a Chiral Fluorosensor †. *Org. Lett.* **2005**, *7* (18), 4045–4048. https://doi.org/10.1021/ol0516216.

(75) Wolf, C.; Liu, S.; Reinhardt, B. C. An Enantioselective Fluorescence Sensing Assay for Quantitative Analysis of Chiral Carboxylic Acids and Amino Acid Derivatives. *Chem. Commun.* **2006**, No. 40, 4242. https://doi.org/10.1039/b609880k.

(76) Ghosn, M. W.; Wolf, C. Chiral Amplification with a Stereodynamic Triaryl Probe: Assignment of the Absolute Configuration and Enantiomeric Excess of Amino Alcohols. *J. Am. Chem. Soc.* **2009**, *131* (45), 16360–16361. https://doi.org/10.1021/ja907741v.

(77) Mei, X.; Wolf, C. Determination of Enantiomeric Excess and Concentration of Chiral Compounds Using a 1,8-Diheteroarylnaphthalene-Derived Fluorosensor. *Tetrahedron Lett.* **2006**, *47* (45), 7901–7904. https://doi.org/10.1016/j.tetlet.2006.09.012.

(78) Ghosn, M. W.; Wolf, C. Enantioselective Recognition of Amines with an Atropisomeric 1,8-Bisphenolnaphthalene. *Tetrahedron* **2011**, *67* (36), 6799–6803. https://doi.org/10.1016/j.tet.2011.07.001.

(79) Mei, X.; Martin, R. M.; Wolf, C. Synthesis of a Sterically Crowded Atropisomeric 1,8-Diacridylnaphthalene for Dual-Mode Enantioselective Fluorosensing. *J. Org. Chem.* **2006**, *71* (7), 2854–2861. https://doi.org/10.1021/jo0600353.

(80) Pugh, V. J.; Hu, Q.-S.; Pu, L. The First Dendrimer-Based Enantioselective Fluorescent Sensor for the Recognition of Chiral Amino Alcohols. *Angew. Chemie Int. Ed.* **2000**, *112* (20), 3784–3787. https://doi.org/10.1002/1521-3757(20001016)112:20<3784::AID-ANGE3784>3.0.CO;2-%23.

(81) Bentley, K. W.; Wolf, C. Stereodynamic Chemosensor with Selective Circular Dichroism and Fluorescence Readout for in Situ Determination of Absolute Configuration, Enantiomeric Excess, and Concentration of Chiral Compounds. *J. Am. Chem. Soc.* **2013**, *135* (33), 12200–12203. https://doi.org/10.1021/ja406259p.

(82) Bentley, K. W.; Nam, Y. G.; Murphy, J. M.; Wolf, C. Chirality Sensing of Amines, Diamines, Amino Acids, Amino Alcohols, and α-Hydroxy Acids with a Single Probe. *J. Am. Chem. Soc.* **2013**, *135* (48), 18052–18055. https://doi.org/10.1021/ja410428b.

(83) Zhang, H.; Yu, T.; Zhao, Y.; Fan, D.; Qian, L.; Yang, C.; Zhang, K. Syntheses, Characterization and Fluorescent Properties of Two Triethylene-Glycol Dicoumarin-3-Carboxylates. *Spectrochim. Acta Part A Mol. Biomol. Spectrosc.* **2007**, *68* (3), 725–727. https://doi.org/10.1016/j.saa.2006.12.052.

(84) Lei, L.; Xue, Y.; Liu, Z.; Peng, S.; He, Y.; Zhang, Y.; Fang, R.; Wang, J.; Luo,

Z.; Yao, G.; Zhang, J.; Zhang, G.; Song, H.; Zhang, Y. Coumarin Derivatives from Ainsliaea Fragrans and Their Anticoagulant Activity. *Sci. Rep.* **2015**, *5* (1), 13544. https://doi.org/10.1038/srep13544.

(85) Dingels, C.; Frey, H. From Biocompatible to Biodegradable: Poly(Ethylene Glycol)s with Predetermined Breaking Points. In *Hierarchical Macromolecular Structures: 60 Years after the Staudinger Nobel Prize II*; Springer, 2013; pp 167–190. https://doi.org/10.1007/12_2013_235.

(86) Perkin, W. H. VI.—On the Artificial Production of Coumarin and Formation of Its Homologues. *J. Chem. Soc.* **1868**, *21*, 53–63. https://doi.org/10.1039/JS8682100053.

(87) Vekariya, R. H.; Patel, H. D. Recent Advances in the Synthesis of Coumarin Derivatives via Knoevenagel Condensation: A Review. *Synth. Commun.* **2014**, *44* (19), 2756–2788. https://doi.org/10.1080/00397911.2014.926374.

(88) Heravi, M. M.; Khaghaninejad, S.; Mostofi, M. Pechmann Reaction in the Synthesis of Coumarin Derivatives; 2014; pp 1–50. https://doi.org/10.1016/B978-0-12-800171-4.00001-9.

(89) Cao, D.; Liu, Z.; Verwilst, P.; Koo, S.; Jangjili, P.; Kim, J. S.; Lin, W. Coumarin-Based Small-Molecule Fluorescent Chemosensors. *Chem. Rev.* **2019**, *119* (18), 10403–10519. https://doi.org/10.1021/acs.chemrev.9b00145.

(90) Medina, F. G.; Marrero, J. G.; Macías-Alonso, M.; González, M. C.; Córdova-Guerrero, I.; Teissier García, A. G.; Osegueda-Robles, S. Coumarin Heterocyclic Derivatives: Chemical Synthesis and Biological Activity. *Nat. Prod. Rep.* **2015**, *32* (10), 1472–1507. https://doi.org/10.1039/C4NP00162A.

(91) Mantulin, W. W.; Song, P.-S. Excited States of Skin-Sensitizing Coumarins and Psoralens. Spectroscopic Studies. *J. Am. Chem. Soc.* **1973**, *95* (16), 5122–5129. https://doi.org/10.1021/ja00797a004.

(92) Donovalová, J.; Cigáň, M.; Stankovičová, H.; Gašpar, J.; Danko, M.; Gáplovský, A.; Hrdlovič, P. Spectral Properties of Substituted Coumarins in

Solution and Polymer Matrices. *Molecules* **2012**, *17* (3), 3259–3276. https://doi.org/10.3390/molecules17033259.

(93) Luan, X.; Cerqueira, N.; Oliveira, A.; Raposo, M.; Rodrigues, L.; Coelho, P.; Oliveira-Campos, A. Synthesis of Fluorescent 3-Benzoxazol-2-Yl-Coumarin. *Adv. Color Sci. Technol.* **2002**, *5* (1), 18–23.

(94) Zhang, X.; Yin, J.; Yoon, J. Recent Advances in Development of Chiral Fluorescent and Colorimetric Sensors. *Chem. Rev.* **2014**, *114* (9), 4918–4959. https://doi.org/10.1021/cr400568b.

(95) Jiang, Y.; Liu, G.; Wang, X.; Hu, J.; Zhang, G.; Liu, S. Cytosol-Specific Fluorogenic Reactions for Visualizing Intracellular Disintegration of Responsive Polymeric Nanocarriers and Triggered Drug Release. *Macromolecules* **2015**, *48* (3), 764–774. https://doi.org/10.1021/ma502389w.

(96) Katritzky, A.; Narindoshvili, T.; Angrish, P. Chiral N -(Coumarin-3-Ylcarbonyl)-α-Amino Acids: Fluorescent Markers for Amino Acids and Dipeptides. *Synthesis (Stuttg).* **2008**, *2008* (13), 2013–2022. https://doi.org/10.1055/s-2008-1067078.

(97) Hu, M.; Yuan, Y.-X.; Wang, W.; Li, D.-M.; Zhang, H.-C.; Wu, B.-X.; Liu, M.; Zheng, Y.-S. Chiral Recognition and Enantiomer Excess Determination Based on Emission Wavelength Change of AIEgen Rotor. *Nat. Commun.* **2020**, *11* (1), 161. https://doi.org/10.1038/s41467-019-13955-z.

(98) Hirano, T. Quantum Chemistry of Gauche-Oxygen Effect Observed in Polyethers. In *Contemporary Topics in Polymer Science*; Springer New York: Boston, MA, 1984; pp 545–555. https://doi.org/10.1007/978-1-4615-6743-1_37.

(99) Frisch, M. J.; Trucks, G. W.; Schlegel, H. B.; Scuseria, G. E.; Robb, M. A.; Cheeseman, J. R. Scalmani, G.; Barone, V.; Petersson, G. A.; Nakatsuji, H.; Li, X.; Caricato, M.; Marenich, A.; Bloino, J.; Janesko, B. G.; Gomperts, R.; Mennucci, B.; Hratchian, H. P.; Ortiz, J. V.; Izmaylov, A. F.; Sonnenberg, J. L.; Williams-Young R., D.; Ding, F.; Lipparini, F.; Egidi, F.; Goings, J.; Peng,

B.; Petrone, A.; Henderson, T.; Ranasinghe, D.; Zakrzewski, V. G.; Gao, J.; Rega, N.; Zheng, G.; Liang, W.; Hada, M.; Ehara, M.; Toyota, K.; Fukuda, R.; Hasegawa, J.; Ishida, M.; Nakajima, T.; Honda, Y.; Kitao, O.; Nakai, H.; Vreven, T.; Throssell, K.; Montgomery, Jr., J. A.; Peralta, J. E.; Ogliaro, F.; Bearpark, M.; Heyd, J. J.; Brothers, E.; Kudin, K. N.; Staroverov, V. N.; Keith, T.; Kobayashi, R.; Normand, J. J.; Raghavachari, K.; Rendell, A.; Burant, J. C.; Iyengar, S. S.; Tomasi, J.; Cossi, M.; Millam, J. M.; Klene, M.; Adamo, C.; Cammi, R.; Ochterski, J. W.; Martin, R. L.; Morokuma, K.; Farkas, O.; Foresman, J. B.; and Fox, D. J. Gaussian 09, Revision A02. Gaussian, Inc.: Wallingford CT 2016.

(100) Hamilton, G. R. C.; Sahoo, S. K.; Kamila, S.; Singh, N.; Kaur, N.; Hyland, B. W.; Callan, J. F. Optical Probes for the Detection of Protons, and Alkali and Alkaline Earth Metal Cations. *Chem. Soc. Rev.* **2015**, *44* (13), 4415–4432. https://doi.org/10.1039/C4CS00365A.

(101) Sahana, S.; Bharadwaj, P. K. Detection of Alkali and Alkaline Earth Metal Ions by Fluorescence Spectroscopy. *Inorganica Chim. Acta* **2014**, *417*, 109–141. https://doi.org/10.1016/j.ica.2014.03.004.

(102) Yin, J.; Hu, Y.; Yoon, J. Fluorescent Probes and Bioimaging: Alkali Metals, Alkaline Earth Metals and PH. *Chem. Soc. Rev.* **2015**, *44* (14), 4619–4644. https://doi.org/10.1039/C4CS00275J.

(103) Gunnlaugsson, T.; Leonard, J. P. Synthesis and Evaluation of Colorimetric Chemosensors for Monitoring Sodium and Potassium Ions in the Intracellular Concentration Range. *J. Chem. Soc. Perkin Trans. 2* **2002**, No. 12, 1980–1985. https://doi.org/10.1039/b207551m.

(104) He, H.; Mortellaro, M. A.; Leiner, M. J. P.; Young, S. T.; Fraatz, R. J.; Tusa, J. K. A Fluorescent Chemosensor for Sodium Based on Photoinduced Electron Transfer. *Anal. Chem.* **2003**, *75* (3), 549–555. https://doi.org/10.1021/ac0205107.

(105) Wang, K.; Guo, D.; Jiang, B.; Liu, Y. Highly Selective Fluorescent

Chemosensor for Na+ Based on Pyrene-Modified Calix[4]Arene Derivative. *Sci. China Ser. B Chem.* **2009**, *52* (4), 513–517. https://doi.org/10.1007/s11426-009-0011-5.

(106) Formica, M.; Fusi, V.; Giorgi, L.; Micheloni, M. New Fluorescent Chemosensors for Metal Ions in Solution. *Coord. Chem. Rev.* **2012**, *256* (1–2), 170–192. https://doi.org/10.1016/j.ccr.2011.09.010.

(107) M.D., S. H. The Electrical Properties of Cancer Cells http://www.royalrife.com/haltiwanger1.pdf (accessed Dec 23, 2016).

(108) CN, P. B. Some Basic Rules on how Cancer behaves http://www.brighterdayfoods.com/PDFDocs/q/Q9XEQCKXX2R49KJUSH9EGHRGCA9KBX34.PDF (accessed Dec 23, 2016).

(109) Iwahori, T.; Miura, K.; Ueshima, H. Time to Consider Use of the Sodium-to-Potassium Ratio for Practical Sodium Reduction and Potassium Increase. *Nutrients* **2017**, *9* (7), 1–11. https://doi.org/10.3390/nu9070700.

(110) Ozcelik, B.; Brown, K. D.; Blencowe, A.; Ladewig, K.; Stevens, G. W.; Scheerlinck, J.-P. Y.; Abberton, K.; Daniell, M.; Qiao, G. G. Biodegradable and Biocompatible Poly(Ethylene Glycol)-Based Hydrogel Films for the Regeneration of Corneal Endothelium. *Adv. Healthc. Mater.* **2014**, *3* (9), 1496–1507. https://doi.org/10.1002/adhm.201400045.

(111) Wulfsberg, G.; Parks, K. D.; Rutherford, R.; Jackson, D. J.; Jones, F. E.; Derrick, D.; Ilsley, W.; Strauss, S. H.; Miller, S. M.; Anderson, O. P.; Babushkina, T. A.; Gushchin, S. I.; Kravchenko, E. A.; Morgunov, V. G. Weakly Coordinating Anions: Crystallographic and NQR Studies of Halogen−Metal Bonding in Silver, Thallium, Sodium, and Potassium Halomethanesulfonates. *Inorg. Chem.* **2002**, *41* (8), 2032–2040. https://doi.org/10.1021/ic010715i.

(112) Díaz-Torres, R.; Alvarez, S. Coordinating Ability of Anions and Solvents towards Transition Metals and Lanthanides. *Dalt. Trans.* **2011**, *40* (40), 10742. https://doi.org/10.1039/c1dt11000d.

(113) Gao, G.; Cao, Y.; Liu, W.; Li, D.; Zhou, W.; Liu, J. Fluorescent Sensors for Sodium Ions. *Anal. Methods* **2017**, *9* (38), 5570–5579. https://doi.org/10.1039/C7AY01708A.

(114) Benesi, H. A.; Hildebrand, J. H. A Spectrophotometric Investigation of the Interaction of Iodine with Aromatic Hydrocarbons. *J. Am. Chem. Soc.* **1949**, *71* (8), 2703–2707. https://doi.org/10.1021/ja01176a030.

(115) Jurek, K.; Kabatc, J.; Kostrzewska, K.; Grabowska, M. New Fluorescence Probes for Biomolecules. *Molecules* **2015**, *20* (7), 13071–13079. https://doi.org/10.3390/molecules200713071.

(116) Zhang, L.; Xia, Y.; Li, M.; Li, D.; Hou, R. Synthesis, Photophysical and Electrochemical Properties of Symmetric Silicon-Linked Coumarin-Oxadiazole Derivatives. *Tetrahedron* **2016**, *72* (47), 7438–7442. https://doi.org/10.1016/j.tet.2016.09.033.

(117) Walkup, G. K.; Imperiali, B. Stereoselective Synthesis of Fluorescent α-Amino Acids Containing Oxine (8-Hydroxyquinoline) and Their Peptide Incorporation in Chemosensors for Divalent Zinc. *J. Org. Chem.* **1998**, *63* (19), 6727–6731. https://doi.org/10.1021/jo980563h.

(118) Bentley, K. W.; de los Santos, Z. A.; Weiss, M. J.; Wolf, C. Chirality Sensing With Stereodynamic Biphenolate Zinc Complexes. *Chirality* **2015**, *27* (10), 700–707. https://doi.org/10.1002/chir.22489.

(119) Maher, K. Schiff Bases Derived from 2-Hydroxynaphthalene-1-Carbaldehyde and Their Metal Complexes. *Asian J. Chem.* **2018**, *30* (6), 1171–1182. https://doi.org/10.14233/ajchem.2018.21286.

(120) Atahan, A.; Durmus, S. 1-Amino-2-Hydroxy-4-Naphthalenesulfonic Acid Based Schiff Bases or Naphtho[1,2-d]Oxazoles: Selective Synthesis and Photophysical Properties. *Spectrochim. Acta Part A Mol. Biomol. Spectrosc.* **2015**, *144*, 61–67. https://doi.org/10.1016/j.saa.2015.01.085.

(121) Jmol: an open-source Java viewer for chemical structures in 3D

http://www.jmol.org/.

(122) Schleyer, P. von R. Introduction: Aromaticity. *Chem. Rev.* **2001**, *101* (5), 1115–1118. https://doi.org/10.1021/cr0103221.

(123) Fallah-Bagher-Shaidaei, H.; Wannere, C. S.; Corminboeuf, C.; Puchta, R.; Schleyer, P. v. R. Which NICS Aromaticity Index for Planar π Rings Is Best? *Org. Lett.* **2006**, *8* (5), 863–866. https://doi.org/10.1021/ol0529546.

(124) Chen, Z.; Wannere, C. S.; Corminboeuf, C.; Putcha, R.; Schleyer, P. von R. Nucleus-Independent Chemical Shifts (NICS) as an Aromaticity Criterion. *Chem. Rev.* **2005**, *105* (10), 3842–3888. https://doi.org/10.1021/cr030088+.

(125) Craig, D. P. 698. CycloButadiene and Some Other Pseudoaromatic Compounds. *J. Chem. Soc.* **1951**, 3175. https://doi.org/10.1039/jr9510003175.

(126) Layer, R. W. The Chemistry of Imines. *Chem. Rev.* **1963**, *63* (5), 489–510. https://doi.org/10.1021/cr60225a003.

(127) Ma, G.; Deng, J.; Sibi, M. P. Fluxionally Chiral DMAP Catalysts: Kinetic Resolution of Axially Chiral Biaryl Compounds. *Angew. Chemie Int. Ed.* **2014**, *53* (44), 11818–11821. https://doi.org/10.1002/anie.201406684.

(128) Ma, G.; Deng, C.; Deng, J.; Sibi, M. P. Dynamic Kinetic Resolution of Biaryl Atropisomers by Chiral Dialkylaminopyridine Catalysts. *Org. Biomol. Chem.* **2018**, *16* (17), 3121–3126. https://doi.org/10.1039/C8OB00384J.

(129) Moustafa, G. A. I.; Kasama, K.; Higashio, K.; Akai, S. Base-Promoted Lipase-Catalyzed Kinetic Resolution of Atropisomeric 1,1′-Biaryl-2,2′-Diols. *RSC Adv.* **2019**, *9* (3), 1165–1175. https://doi.org/10.1039/C8RA09070J.

(130) Ma, L.; Hu, P.; Jiang, H.; Kloc, C.; Sun, H.; Soci, C.; Voityuk, A. A.; Michel-Beyerle, M. E.; Gurzadyan, G. G. Single Photon Triggered Dianion Formation in TCNQ and F4TCNQ Crystals. *Sci. Rep.* **2016**, *6* (1), 28510. https://doi.org/10.1038/srep28510.

(131) Rietsch, P.; Witte, F.; Sobottka, S.; Germer, G.; Becker, A.; Güttler, A.;

Sarkar, B.; Paulus, B.; Resch-Genger, U.; Eigler, S. Diaminodicyanoquinones: Fluorescent Dyes with High Dipole Moments and Electron-Acceptor Properties. *Angew. Chemie Int. Ed.* **2019**, *58* (24), 8235–8239. https://doi.org/10.1002/anie.201903204.

(132) Sudhakar, P.; Radhakrishnan, T. P. A Strongly Fluorescent Molecular Material Responsive to Physical/Chemical Stimuli and Their Coupled Impact. *Chem. – An Asian J.* **2019**, *14* (24), 4754–4759. https://doi.org/10.1002/asia.201901086.

(133) Srujana, P.; Sudhakar, P.; Radhakrishnan, T. P. Enhancement of Fluorescence Efficiency from Molecules to Materials and the Critical Role of Molecular Assembly. *J. Mater. Chem. C* **2018**, *6* (35), 9314–9329. https://doi.org/10.1039/C8TC03305F.

(134) Hertler, W. R.; Hartzler, H. D.; Acker, D. S.; Benson, R. E. Substituted Quinodimethans. III. Displacement Reactions of 7,7,8,8-Tetracyanoquinodimethan. *J. Am. Chem. Soc.* **1962**, *84* (17), 3387–3393. https://doi.org/10.1021/ja00876a030.

(135) Szablewski, M.; Fox, M. A.; Dias, F. B.; Namih, H.; Snedden, E. W.; King, S. M.; Dai, D.; Pålsson, L.-O. Ultrafast Dynamics and Computational Studies on Diaminodicyanoquinodimethanes (DADQs). *J. Phys. Chem. B* **2014**, *118* (24), 6815–6828. https://doi.org/10.1021/jp411358d.

(136) Srujana, P.; Gera, T.; Radhakrishnan, T. P. Fluorescence Enhancement in Crystals Tuned by a Molecular Torsion Angle: A Model to Analyze Structural Impact. *J. Mater. Chem. C* **2016**, *4* (27), 6510–6515. https://doi.org/10.1039/C6TC01610C.

(137) Bloor, D.; Kagawa, Y.; Szablewski, M.; Ravi, M.; Clark, S. J.; Cross, G. H.; Palsson, L.-O.; Beeby, A.; Parmer, C.; Rumbles, G. Matrix Dependence of Light Emission from TCNQ Adducts. *J. Mater. Chem.* **2001**, *11* (12), 3053–3062.

(138) Reichardt, C. Solvatochromic Dyes as Solvent Polarity Indicators. *Chem. Rev.*

1994, *94* (8), 2319–2358. https://doi.org/10.1021/cr00032a005.

(139) Tunuli, M. S.; Rauf, M. A.; Farhataziz. Dimroth's ET(30) as Parameters of Solvent Polarity: A Caveat. *J. Photochem.* **1984**, *24* (4), 411–413. https://doi.org/10.1016/0047-2670(84)80023-4.

(140) Shakerizadeh-Shirazi, F.; Hemmateenejad, B.; Mehranpour, A. M. Determination of the Empirical Solvent Polarity Parameter E T (30) by Multivariate Image Analysis. *Anal. Methods* **2013**, *5* (4), 891–896. https://doi.org/10.1039/C2AY26185E.

(141) Reichardt, C.; Harbusch-Görnert, E. Über Pyridinium-N-Phenolat-Betaine Und Ihre Verwendung Zur Charakterisierung Der Polarität von Lösungsmitteln, X. Erweiterung, Korrektur Und Neudefinition DerET-Lösungsmittelpolaritätsskala Mit Hilfe Eines Lipophilen Penta-Tert-Butyl-Substituierten Pyridi. *Liebigs Ann. der Chemie* **1983**, *1983* (5), 721–743. https://doi.org/10.1002/jlac.198319830502.

(142) Ramadas, S.; Krupadanam, G. L. D. Enantioselective Acylation of 2-Hydroxymethyl-2,3-Dihydrobenzofurans Catalysed by Lipase from Pseudomonas Cepacia (Amano PS) and Total Stereoselective Synthesis of (−)-(R)-MEM-Protected Arthrographol. *Tetrahedron: Asymmetry* **2000**, *11* (16), 3375–3393. https://doi.org/10.1016/S0957-4166(00)00302-5.

(143) Xi, G.-L.; Liu, Z.-Q. Coumarin-Fused Coumarin: Antioxidant Story from N , N -Dimethylamino and Hydroxyl Groups. *J. Agric. Food Chem.* **2015**, *63* (13), 3516–3523. https://doi.org/10.1021/acs.jafc.5b00399.

APPENDICES

A. Characterization data for chiral coumarin derivarives

8.1 NMR spectra

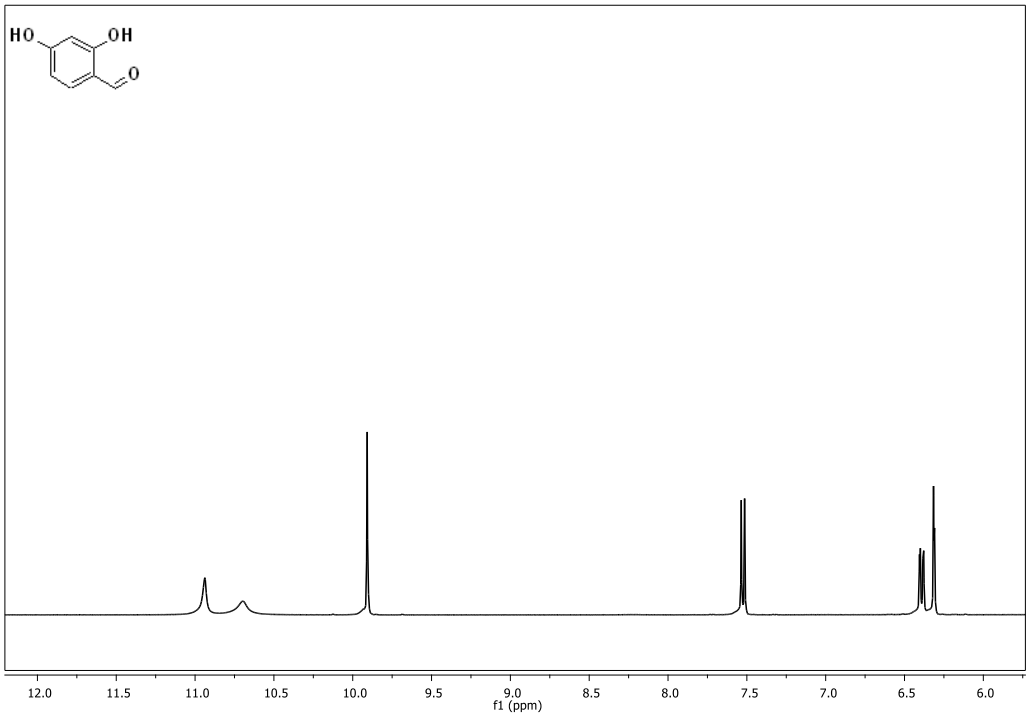

Figure A. 1 ^{1}H NMR spectrum of compound **1**

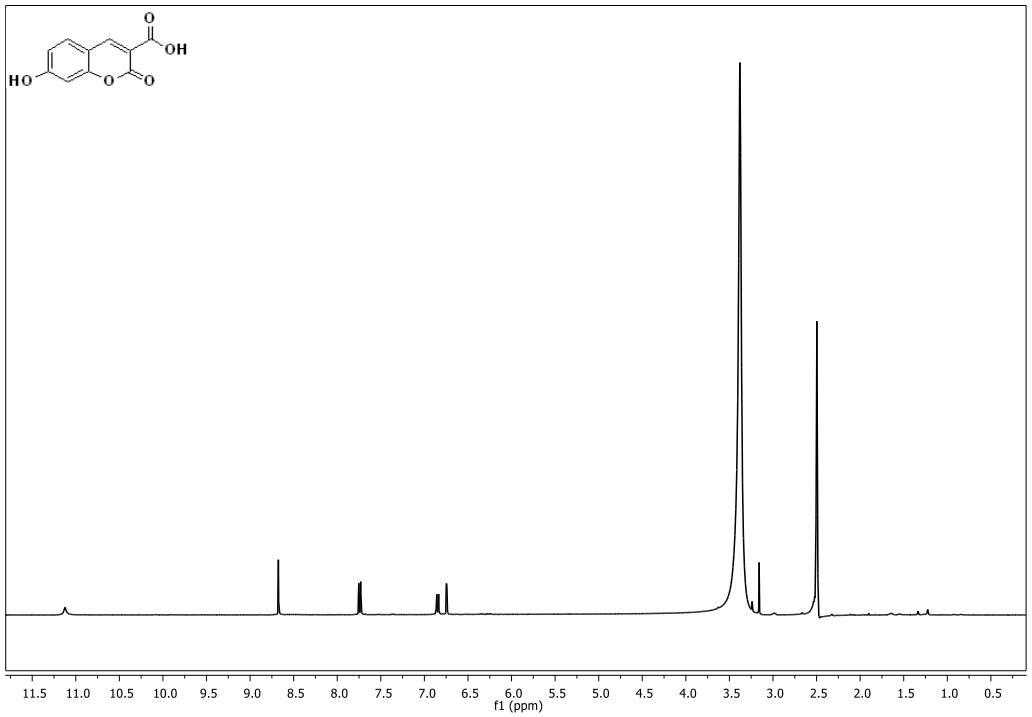

Figure A. 2 ^{1}H NMR spectrum of compound **2**

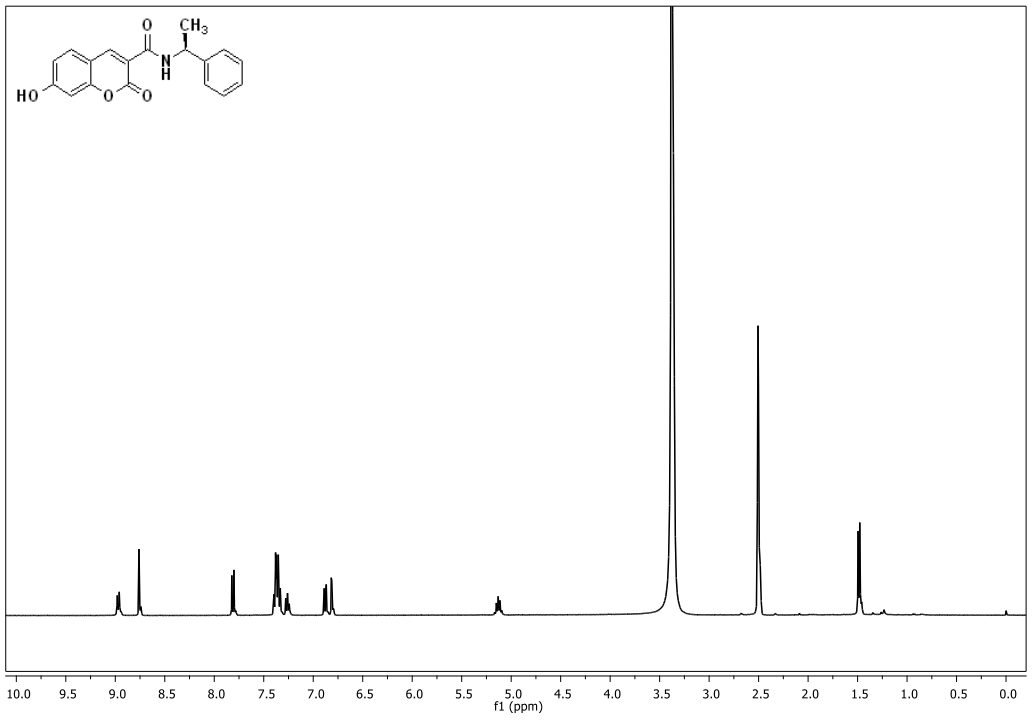

Figure A. 3 ^{1}H NMR spectrum of compound **4**

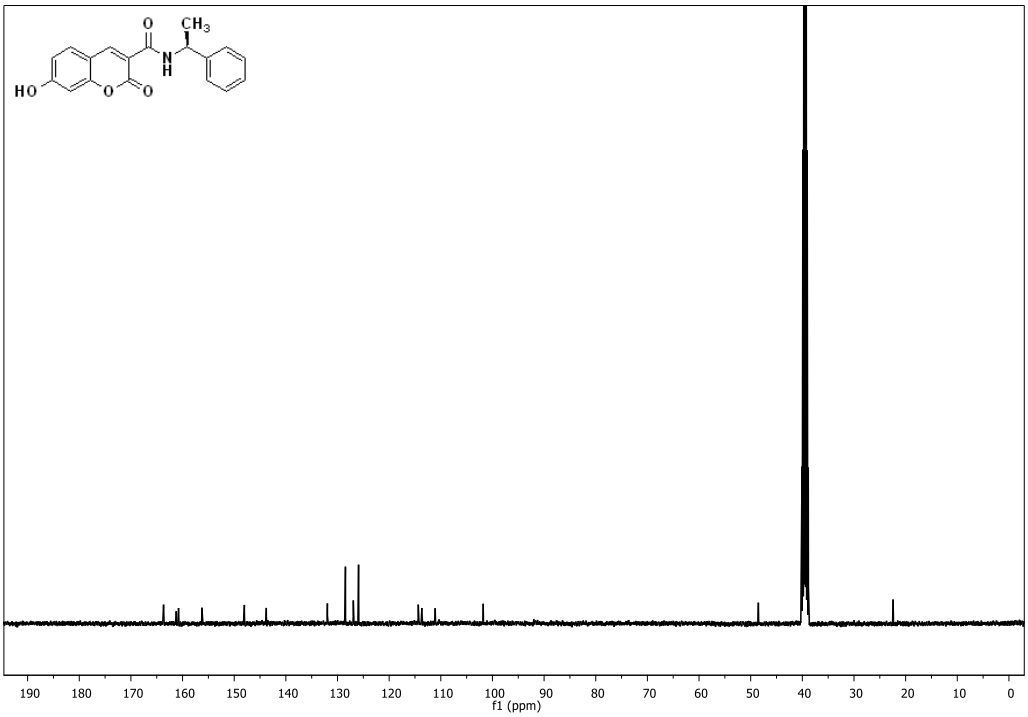

Figure A. 4 ^{13}C NMR spectrum of compound **4**

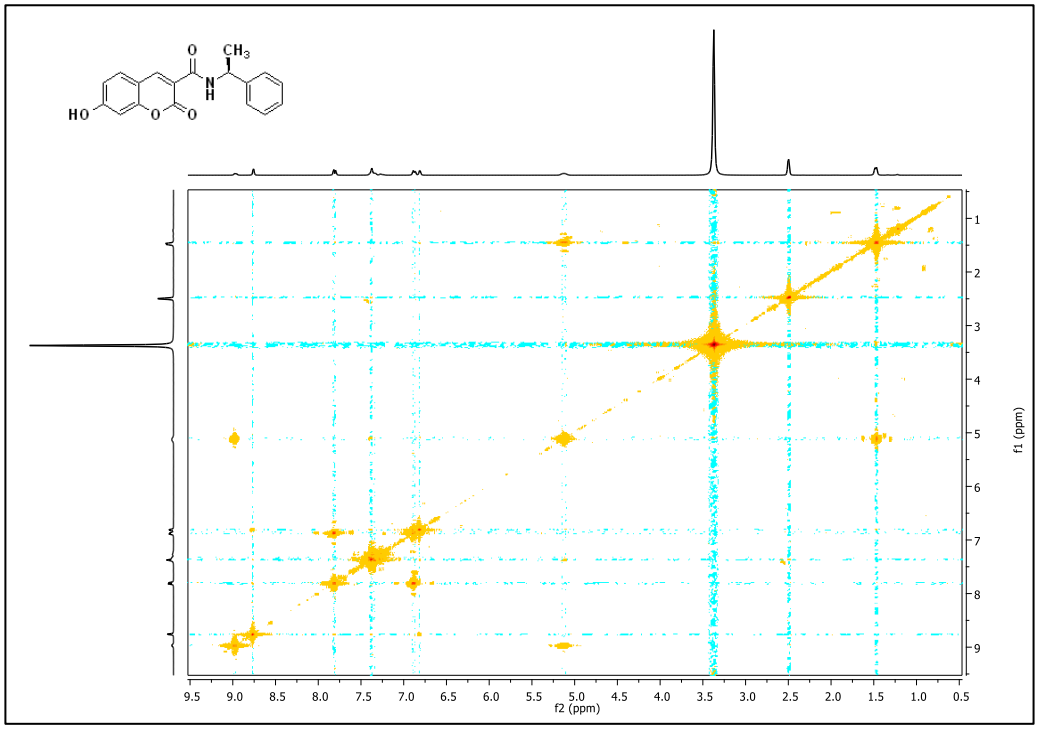

Figure A. 5 COSY spectrum of coompound **4**

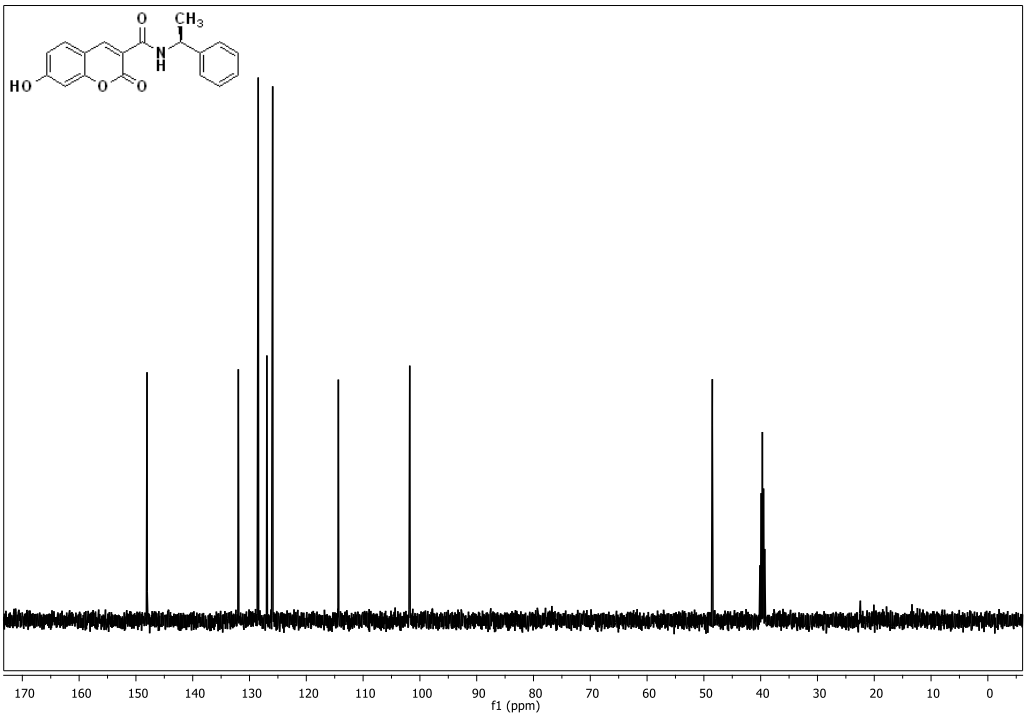

Figure A. 6 DEPT90 spectrum of compound **4**

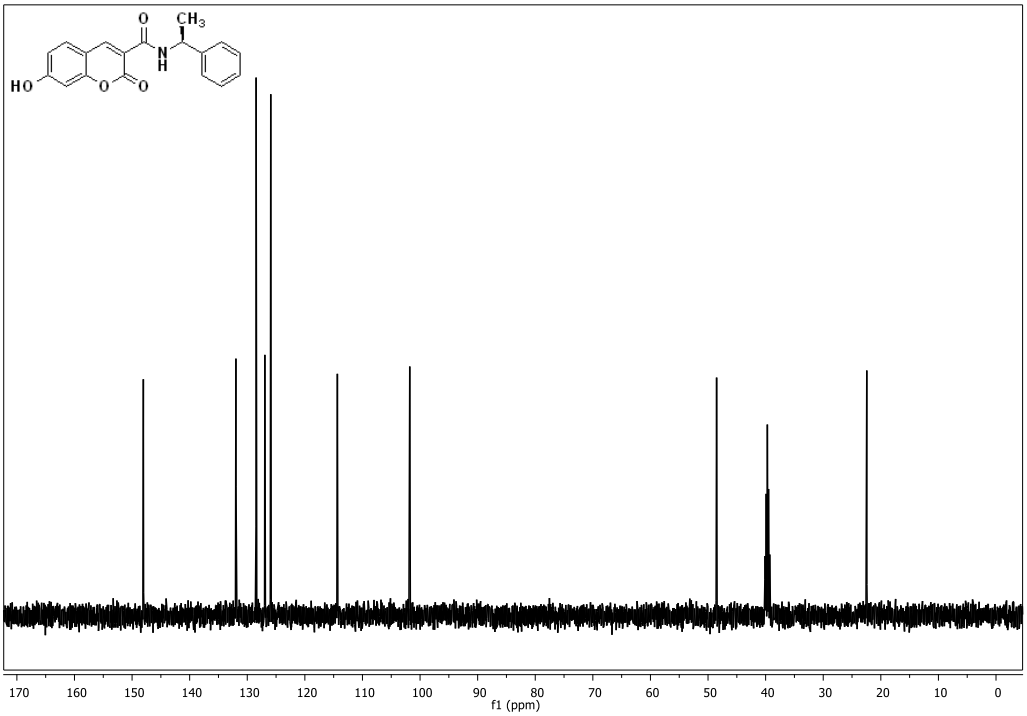

Figure A. 7 DEPT135 spectrum of compound **4**

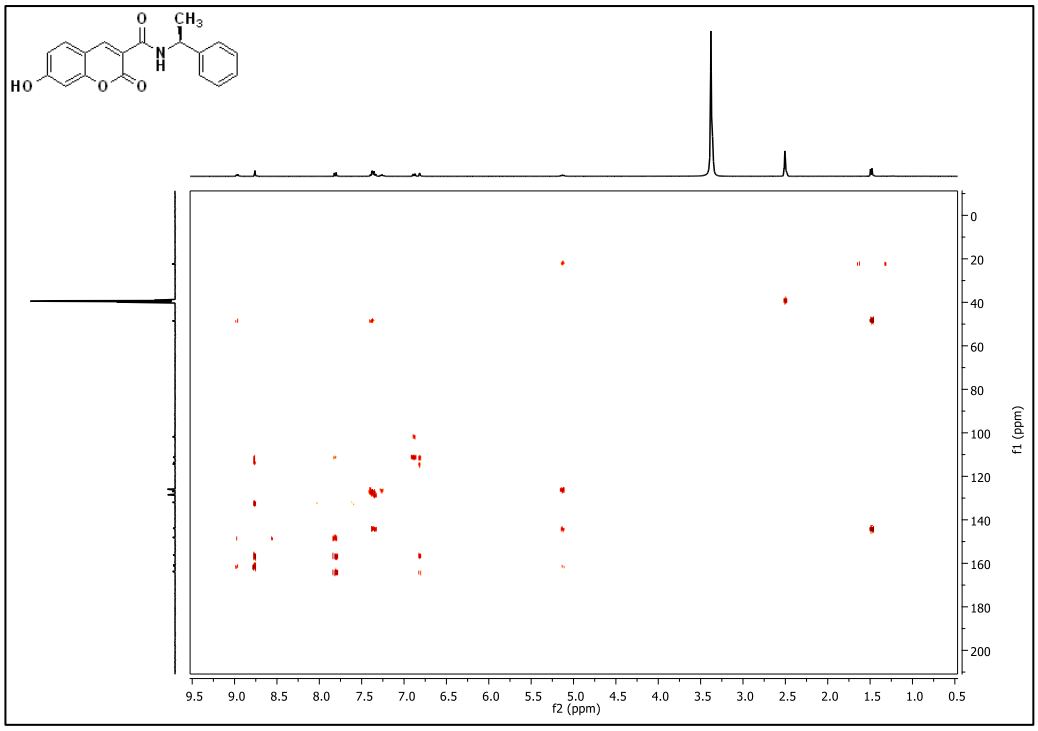

Figure A. 8 HMBC spectrum of compound **4**

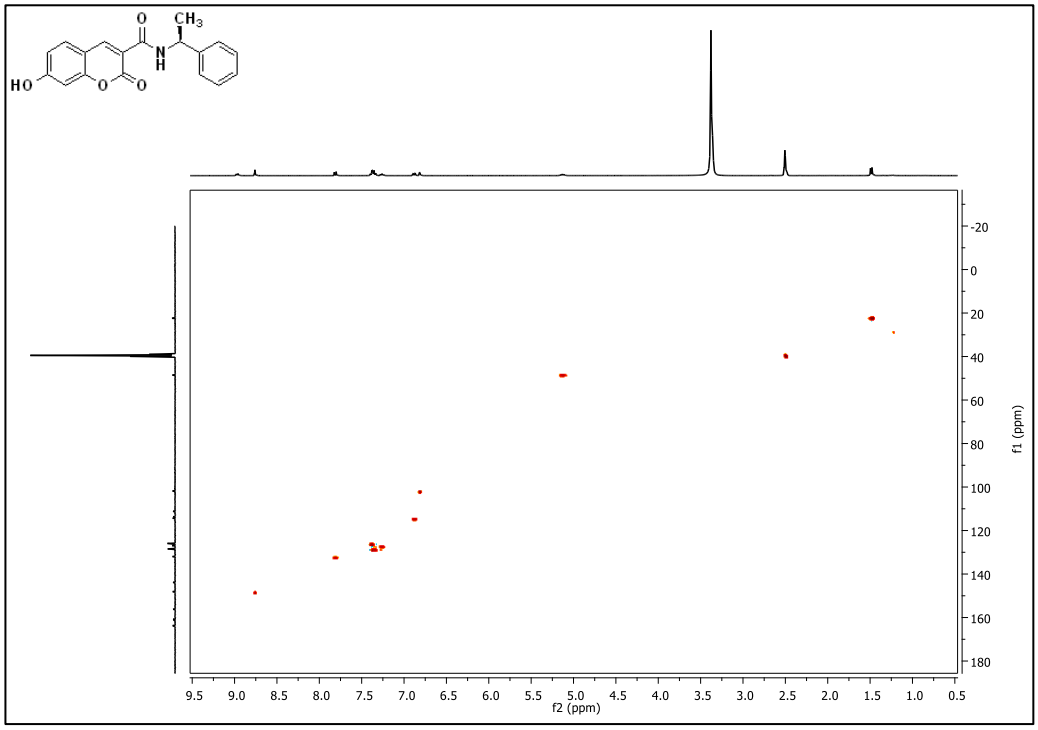

Figure A. 9 HSQC spectrum of compound **4**

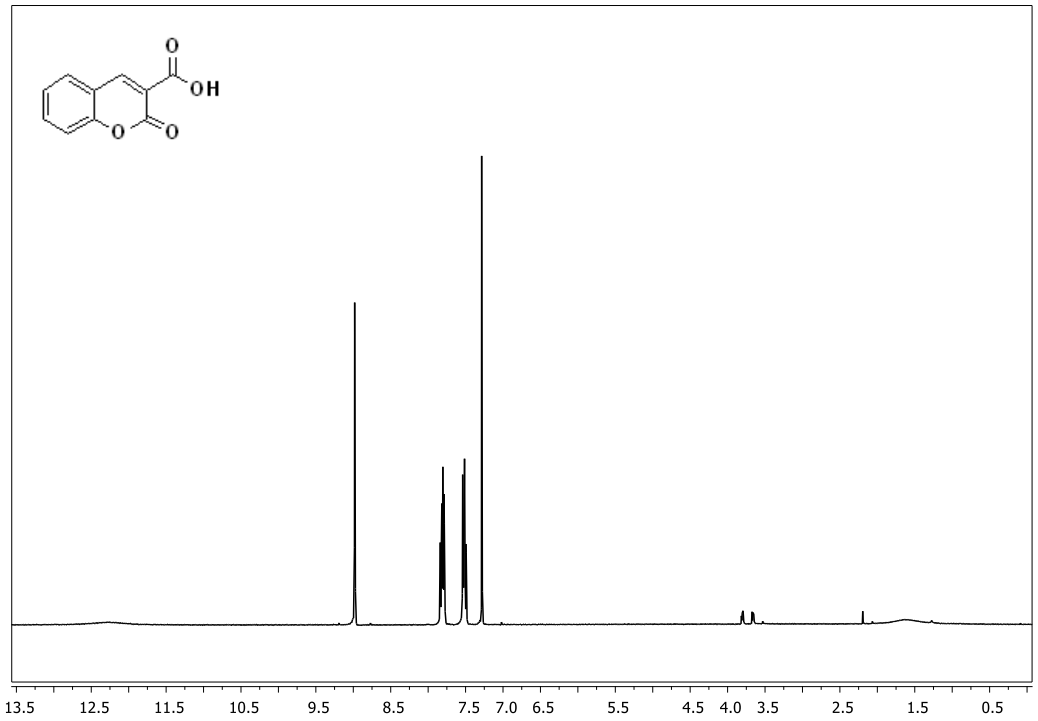

Figure A. 10 ^{1}H NMR spectrum of compound **6**

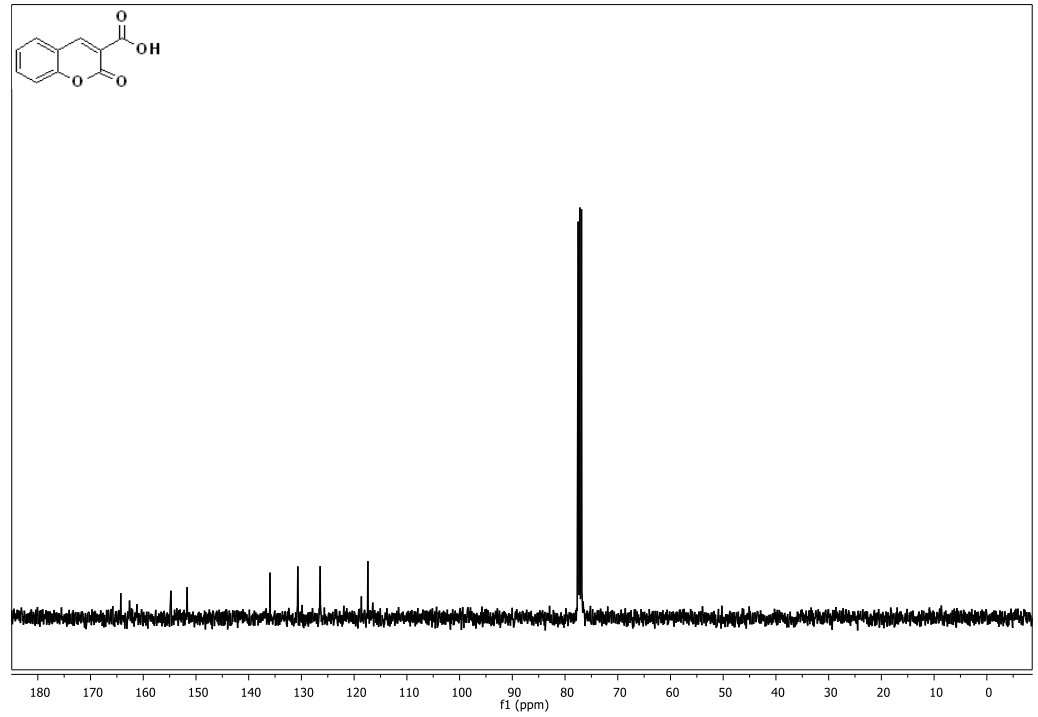

Figure A. 11 ^{13}C NMR spectrum of compound **6**

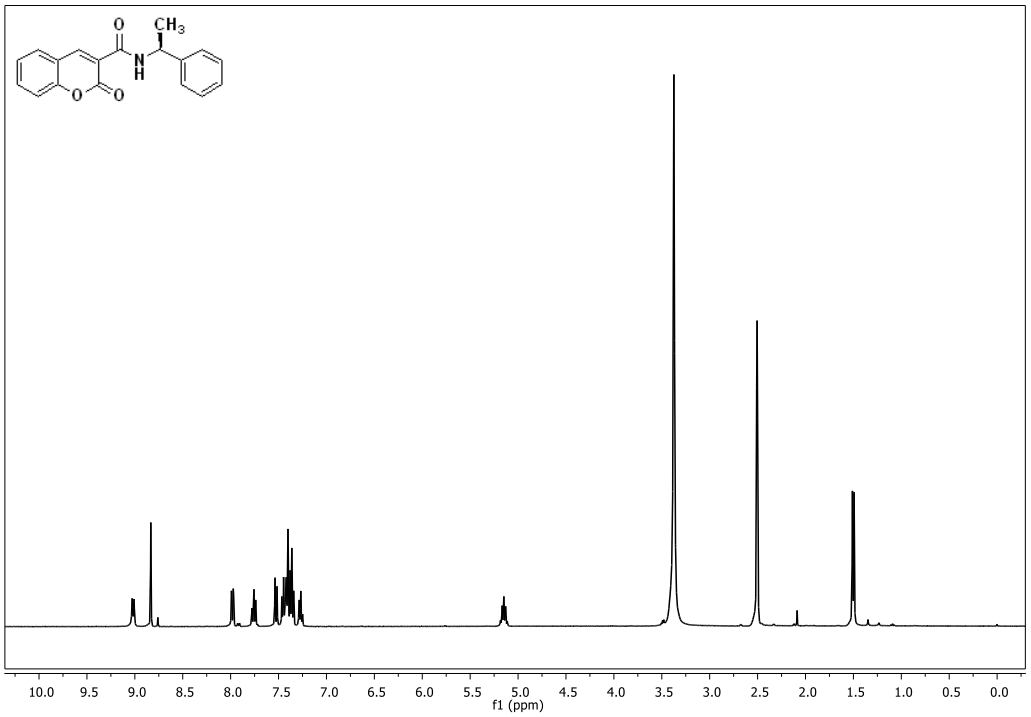

Figure A. 12 ^{1}H NMR spectrum of compound **8**

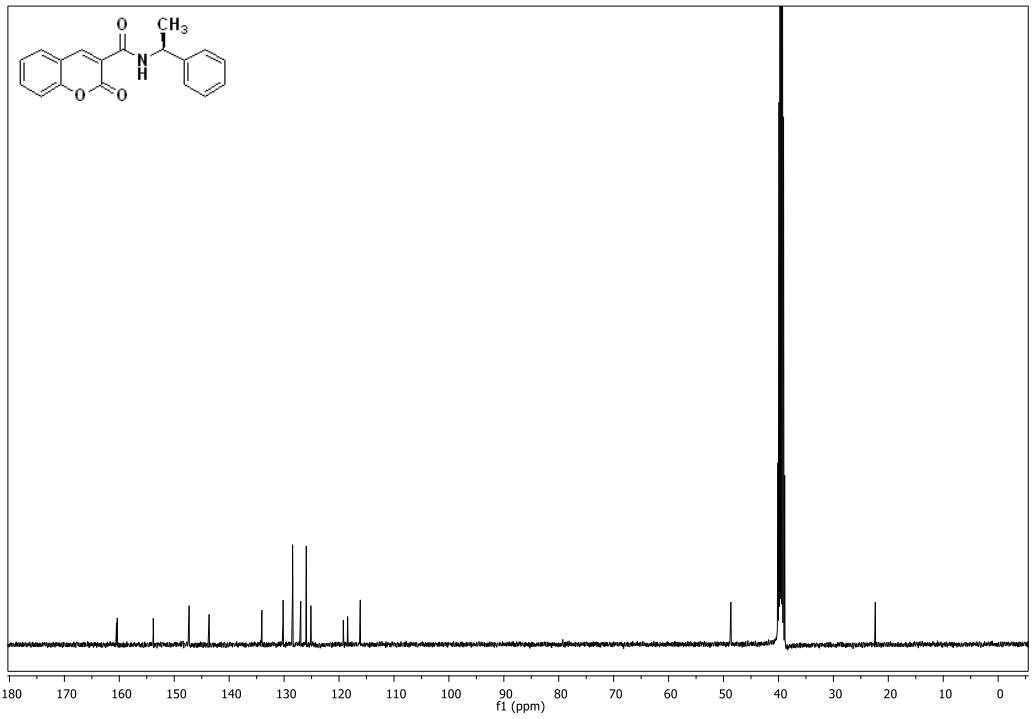

Figure A. 13 ^{13}C NMR spectrum of compound **8**

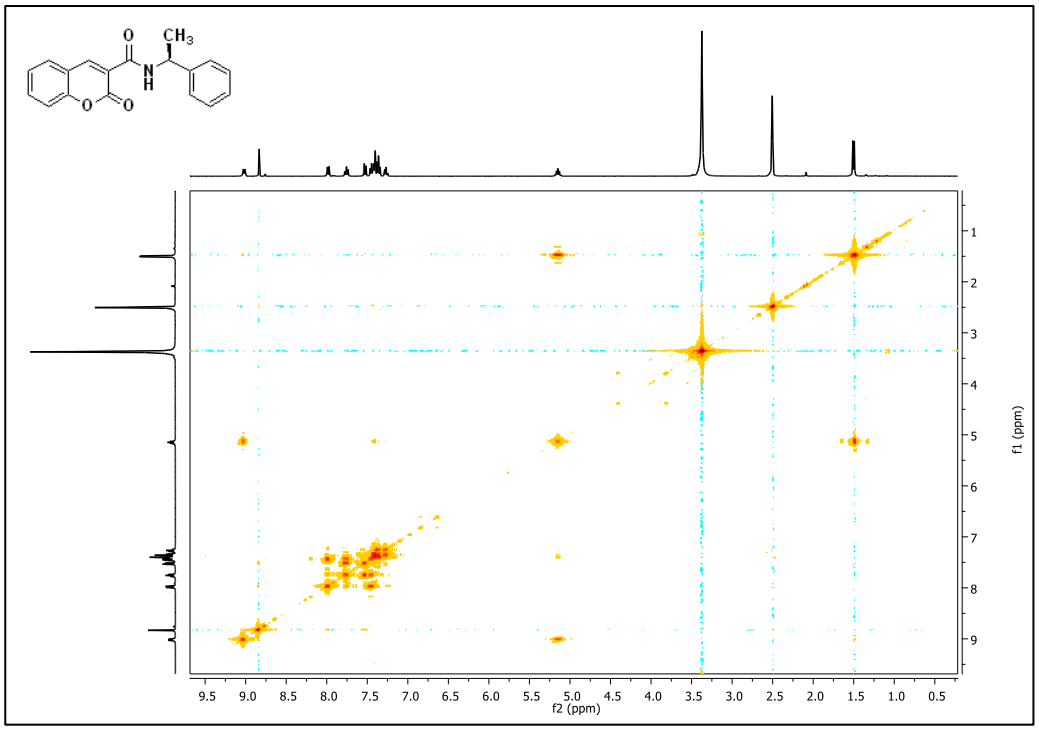

Figure A. 14 COSY spectrum of compound **8**

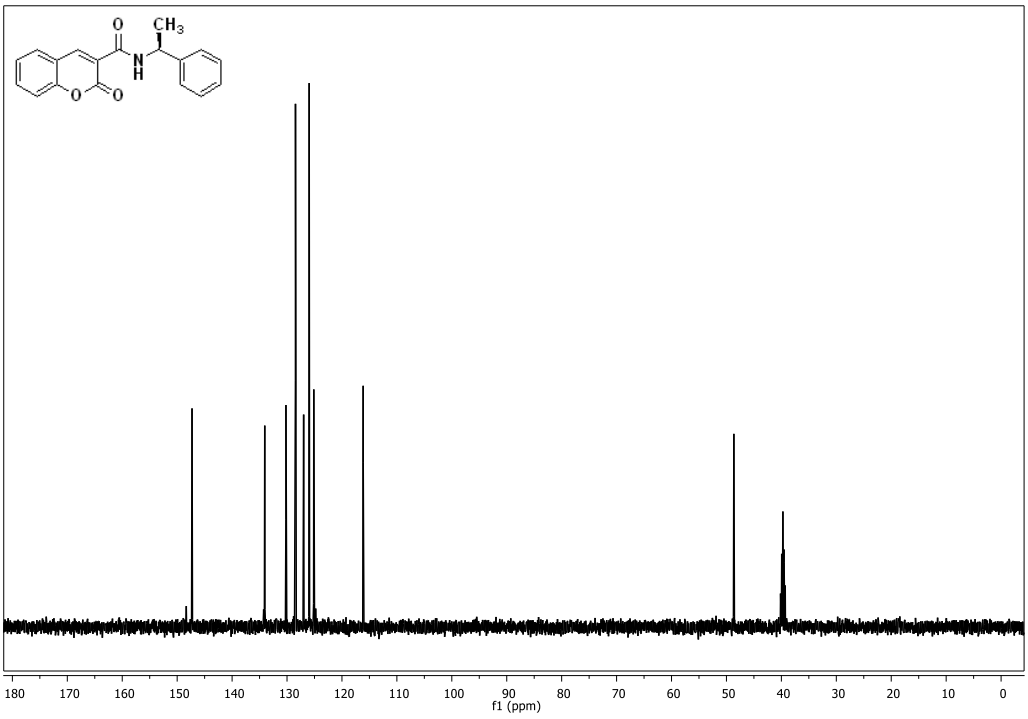

Figure A. 15 DEPT90 spectrum of compound **8**

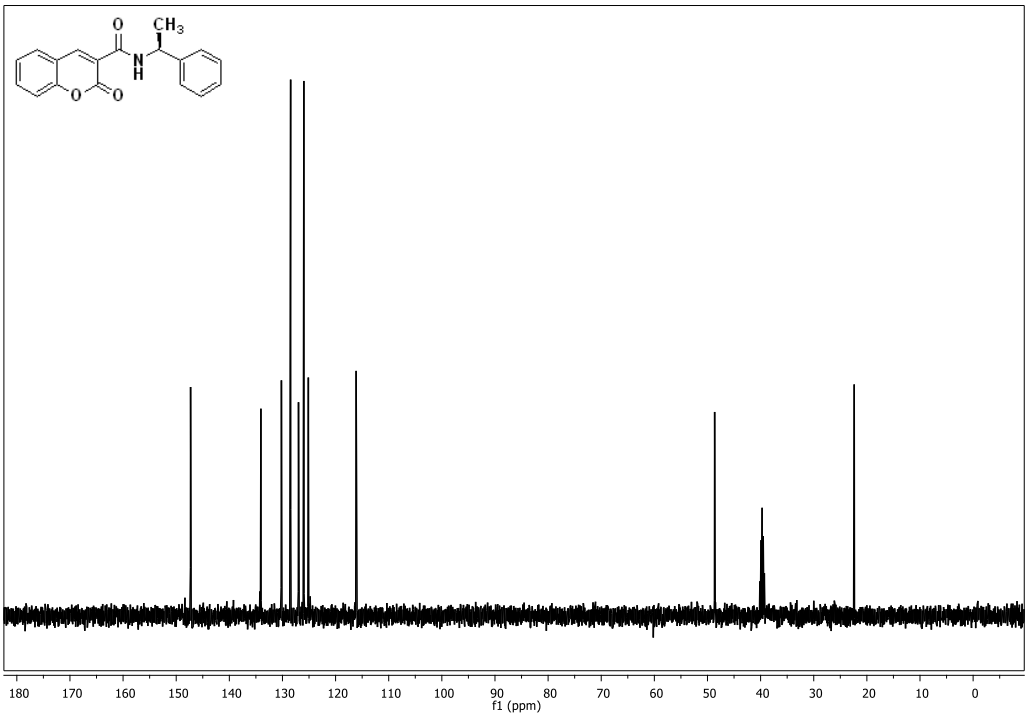

Figure A. 16 DEPT135 spectrum of compound **8**

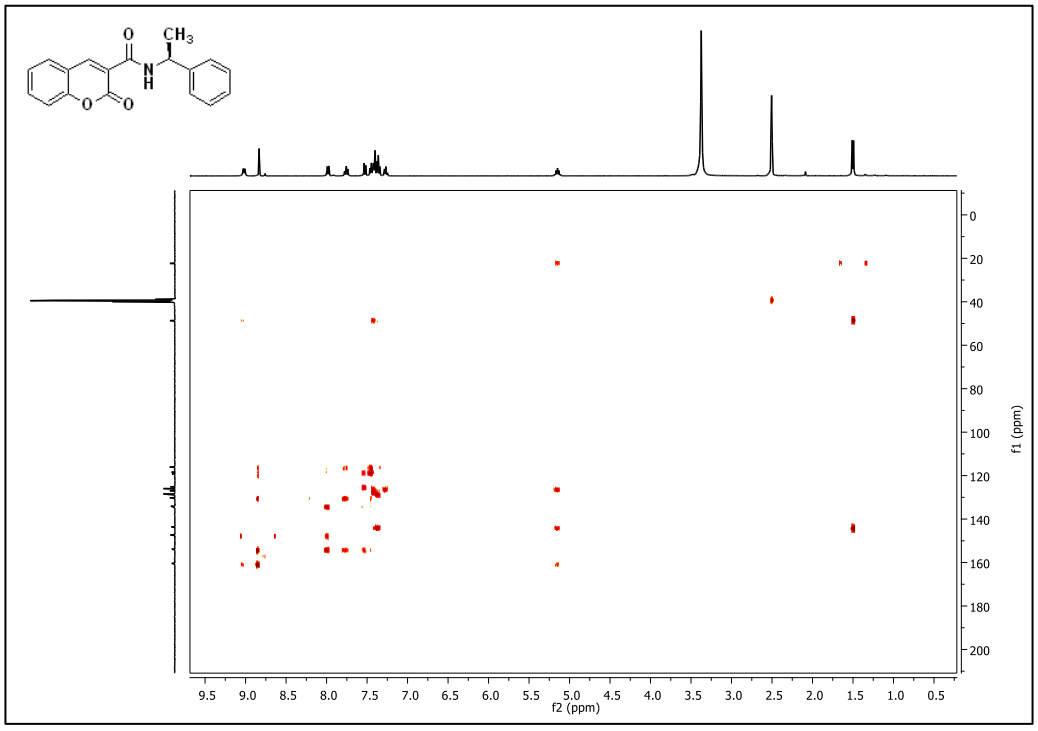

Figure A. 17 HMBC spectrum of compound **8**

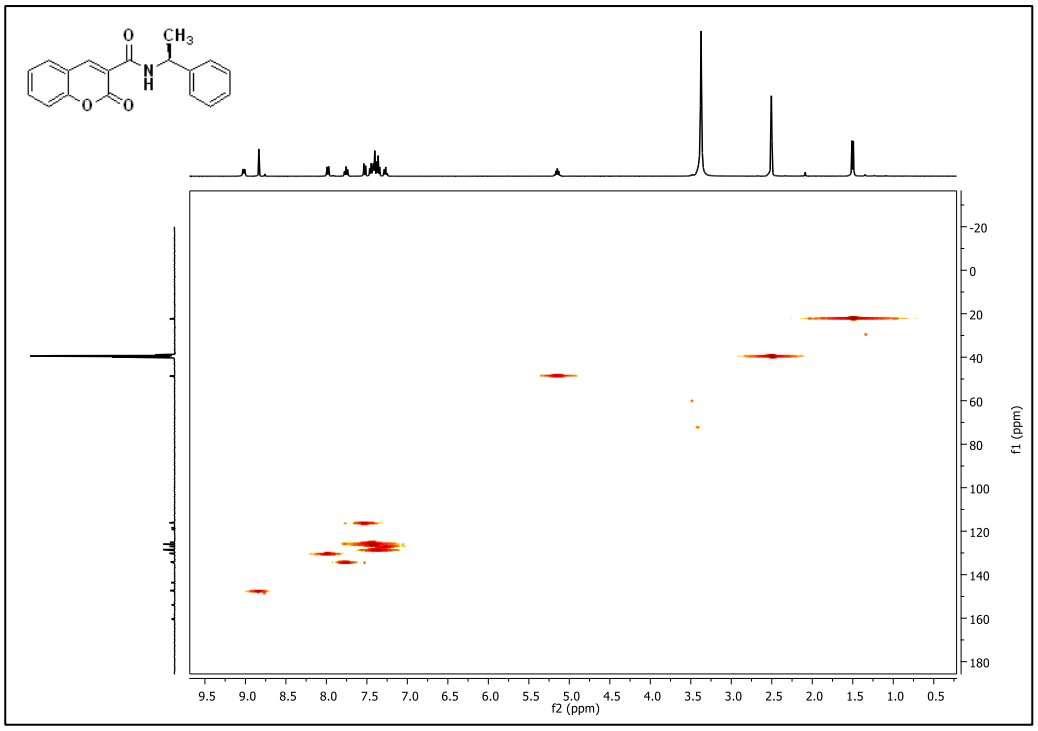

Figure A. 18 HSQC spectrum of compound **8**

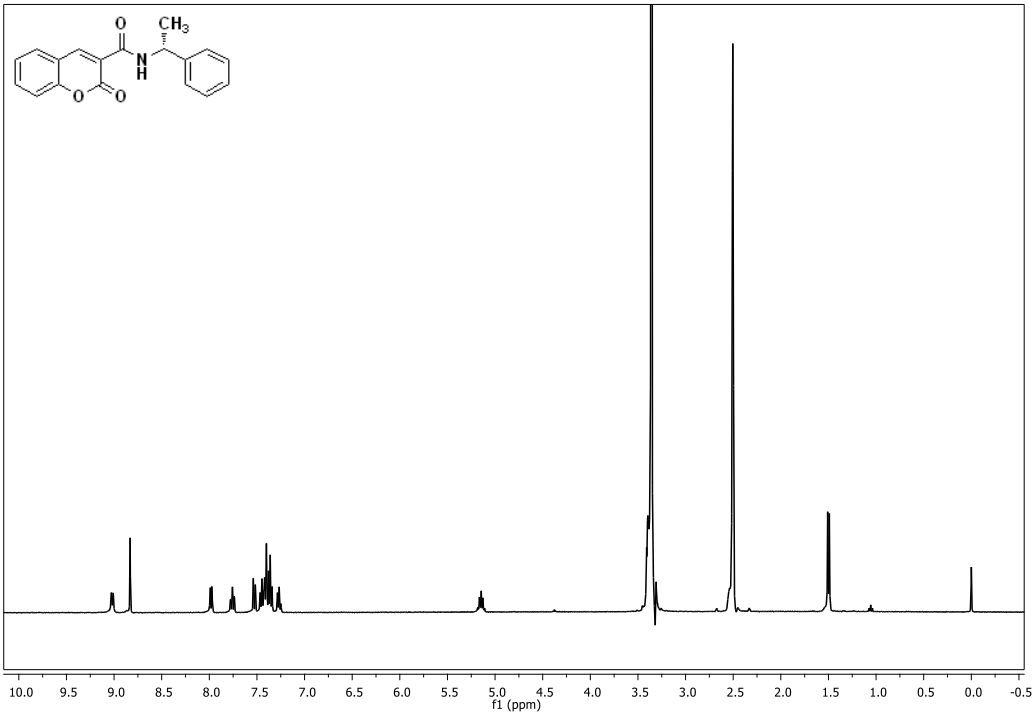

Figure A. 19 ^{1}H NMR spectrum of compound **9**

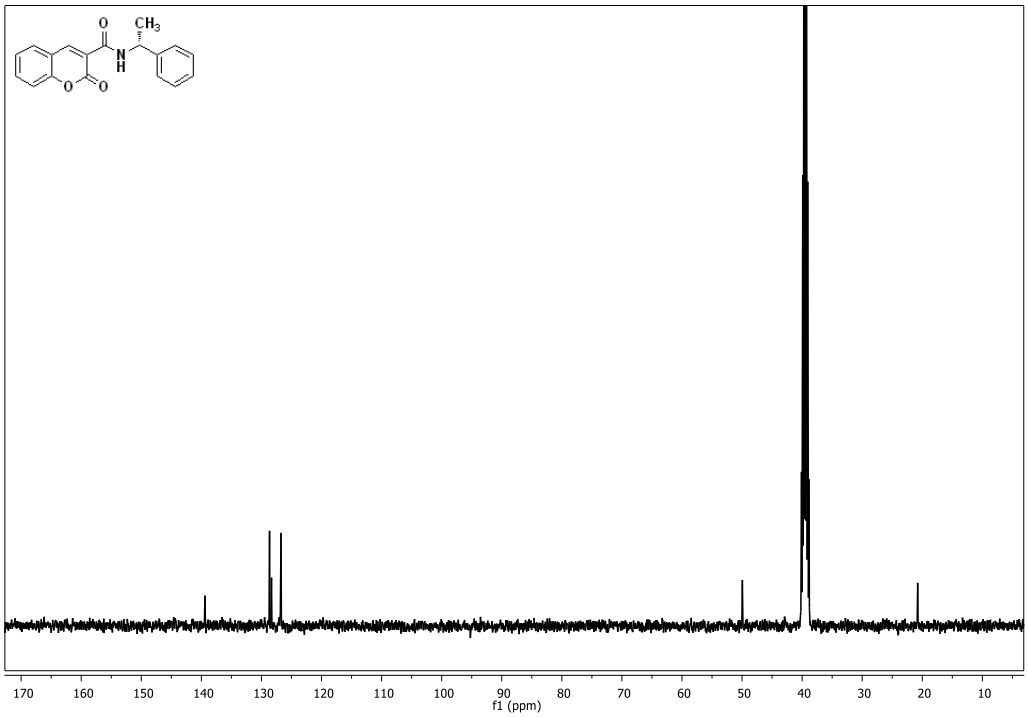

Figure A. 20 ^{13}C NMR spectrum of compound **9**

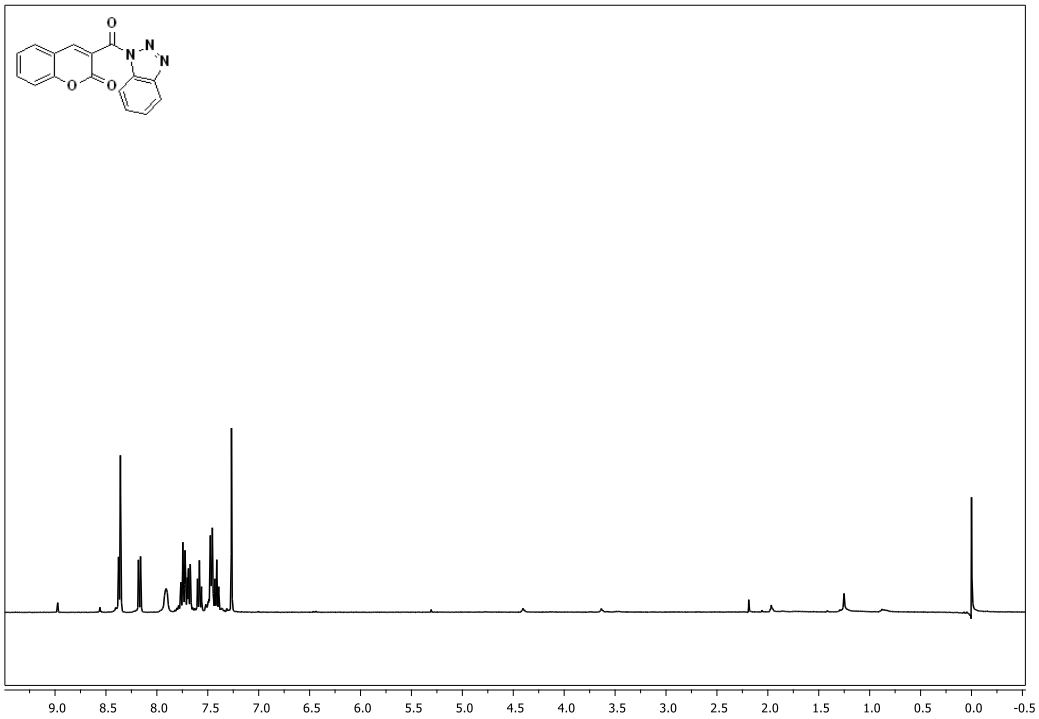

Figure A. 21^{1}H NMR spectrum of compound **10**

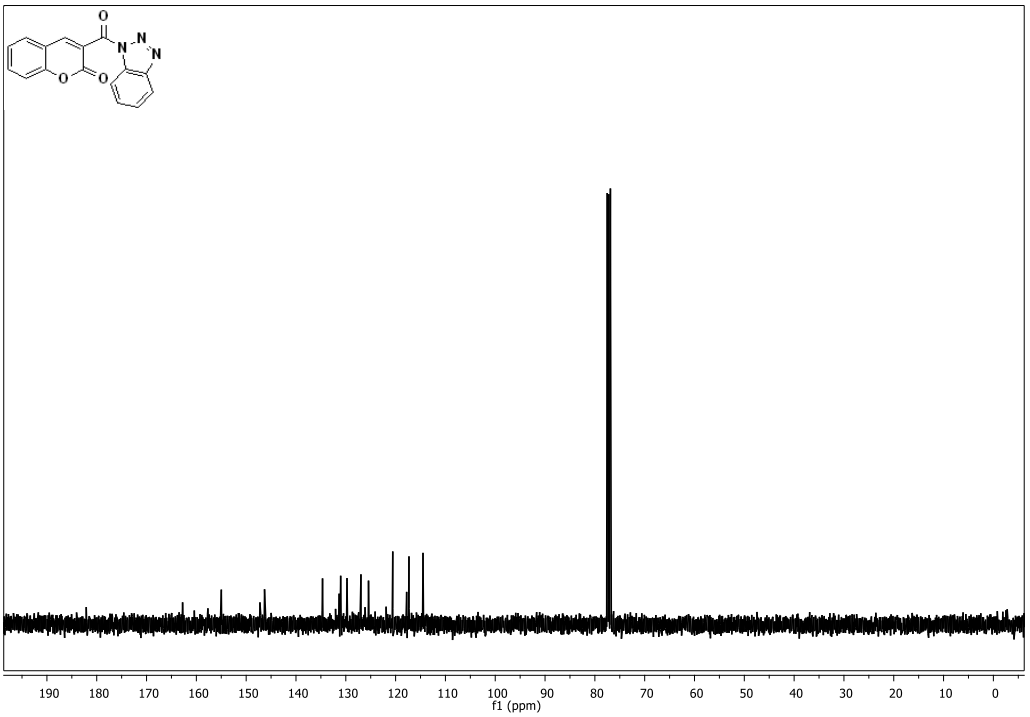

Figure A. 22 ^{13}C NMR spectrum of compound **10**

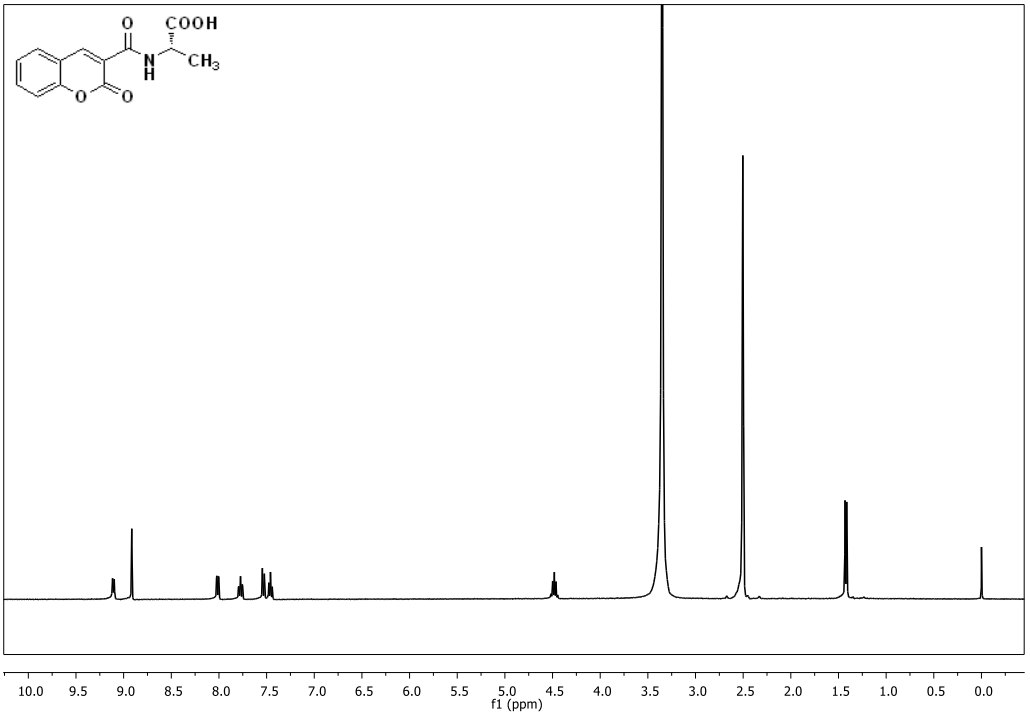

Figure A. 23 ^{1}H NMR spectrum of compound **11**

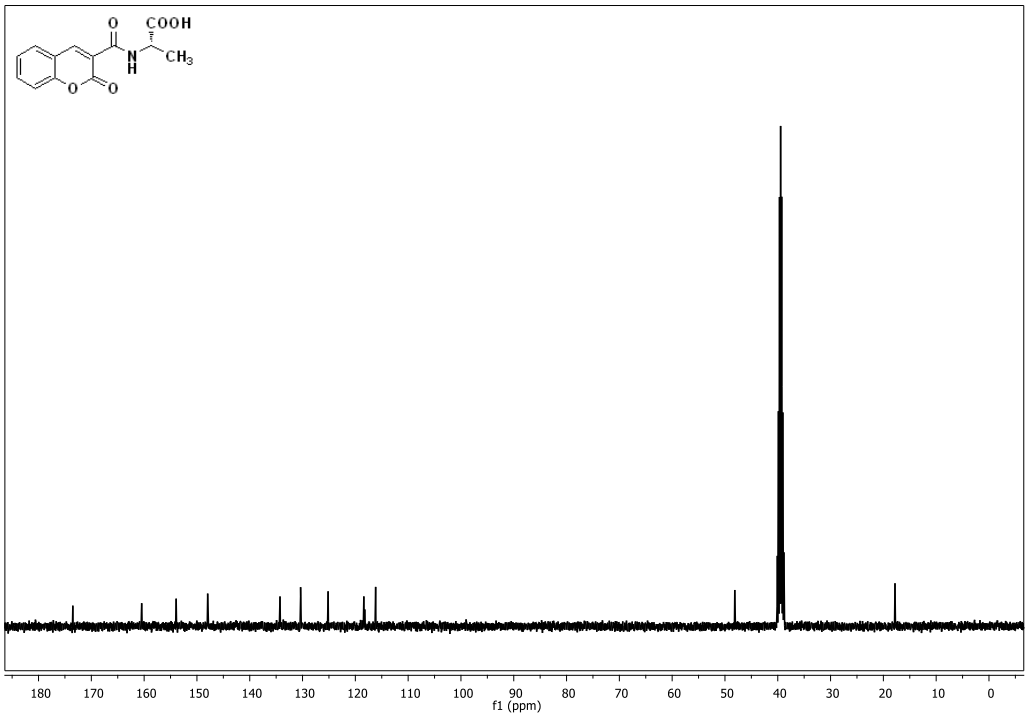

Figure A. 24 ^{13}C NMR spectrum of compound **11**

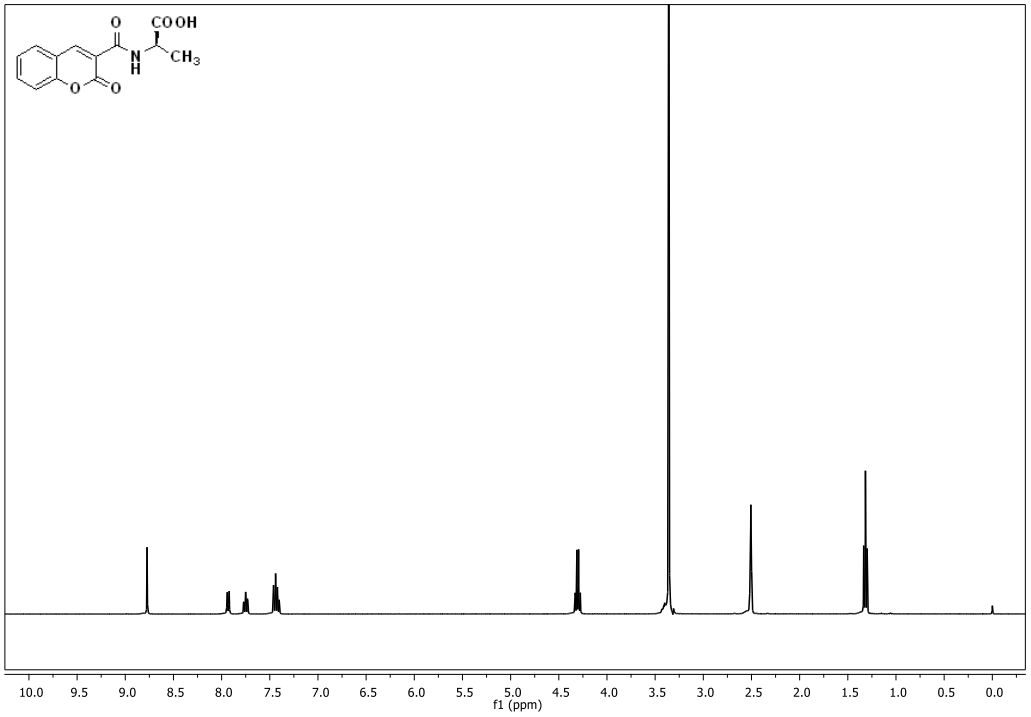

Figure A. 25 ^{1}H NMR spectrum of compound **12**

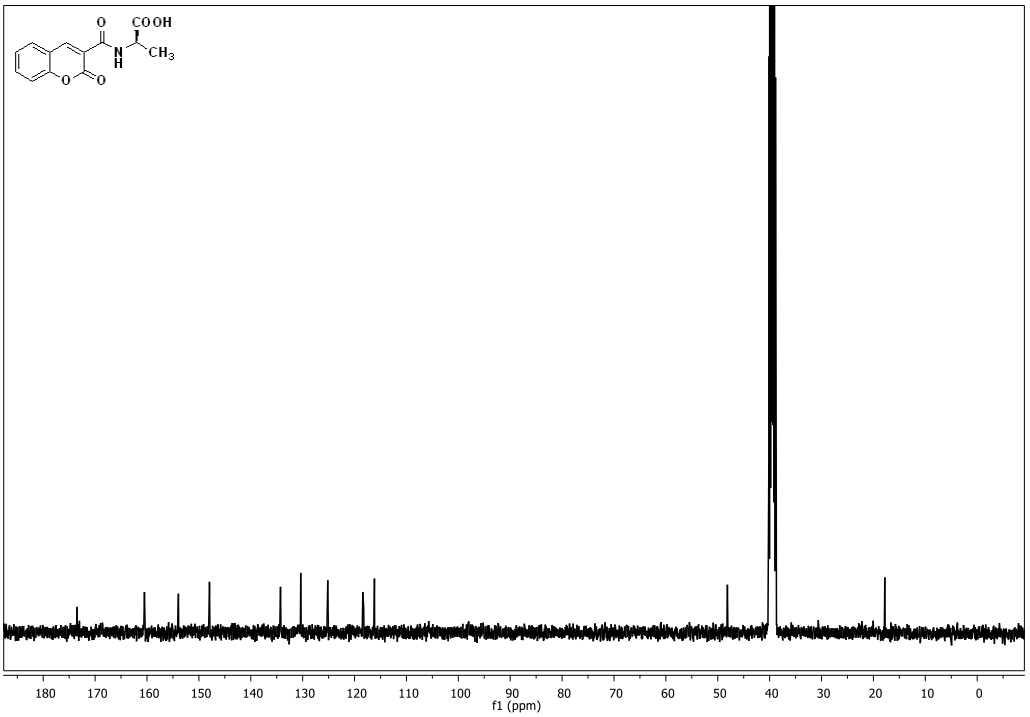

Figure A. 26 ^{13}C NMR spectrum of compound **12**

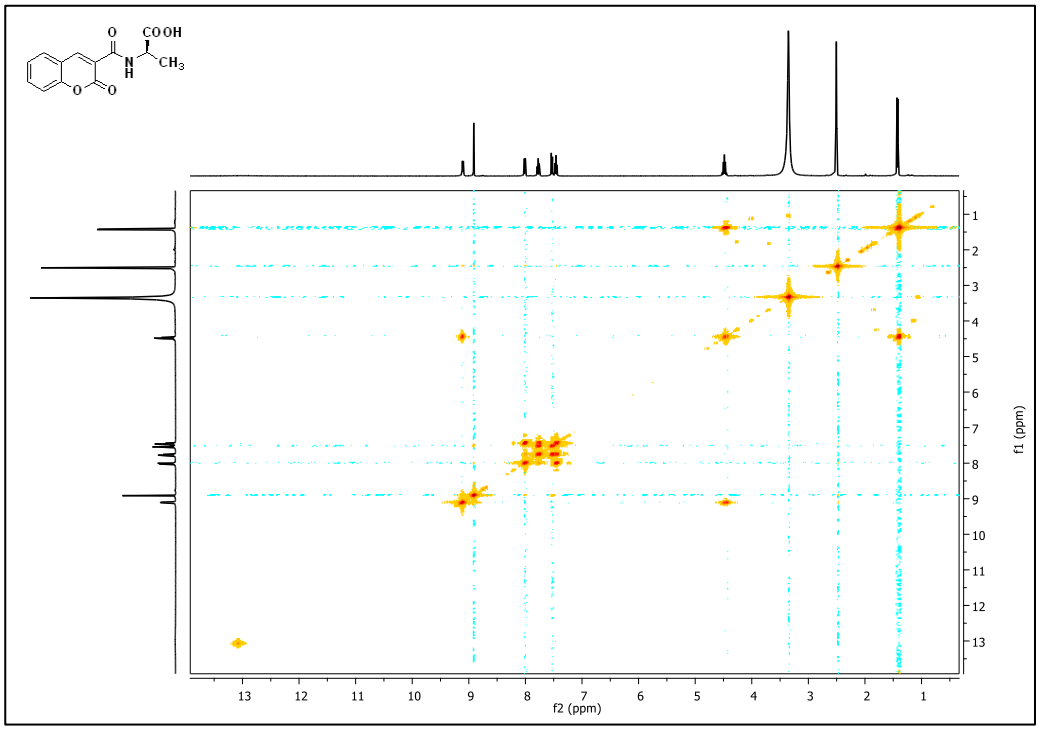

Figure A. 27 COSY spectrum of compound **12**

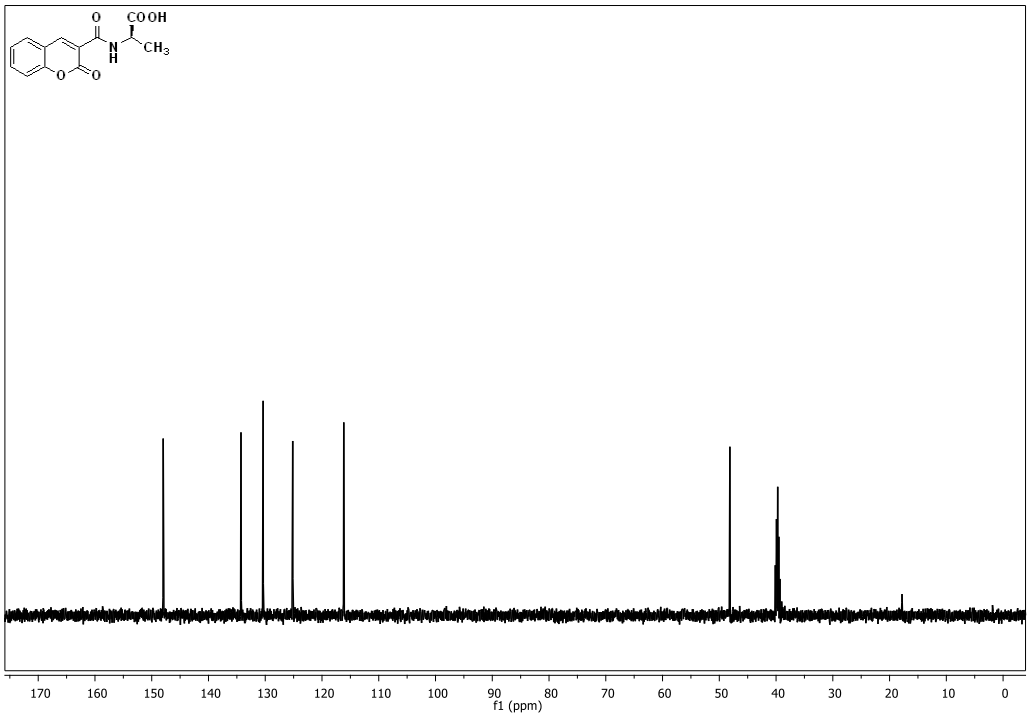

Figure A. 28 DEPT90 spectrum of compound **12**

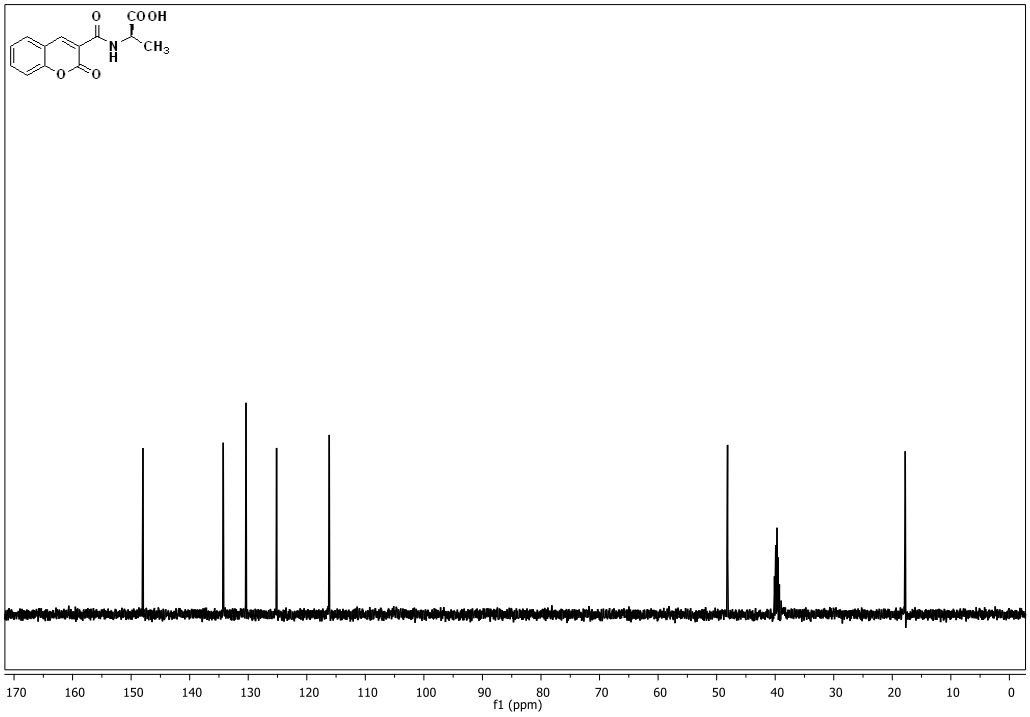

Figure A. 29 DEPT135 spectrum of compound **12**

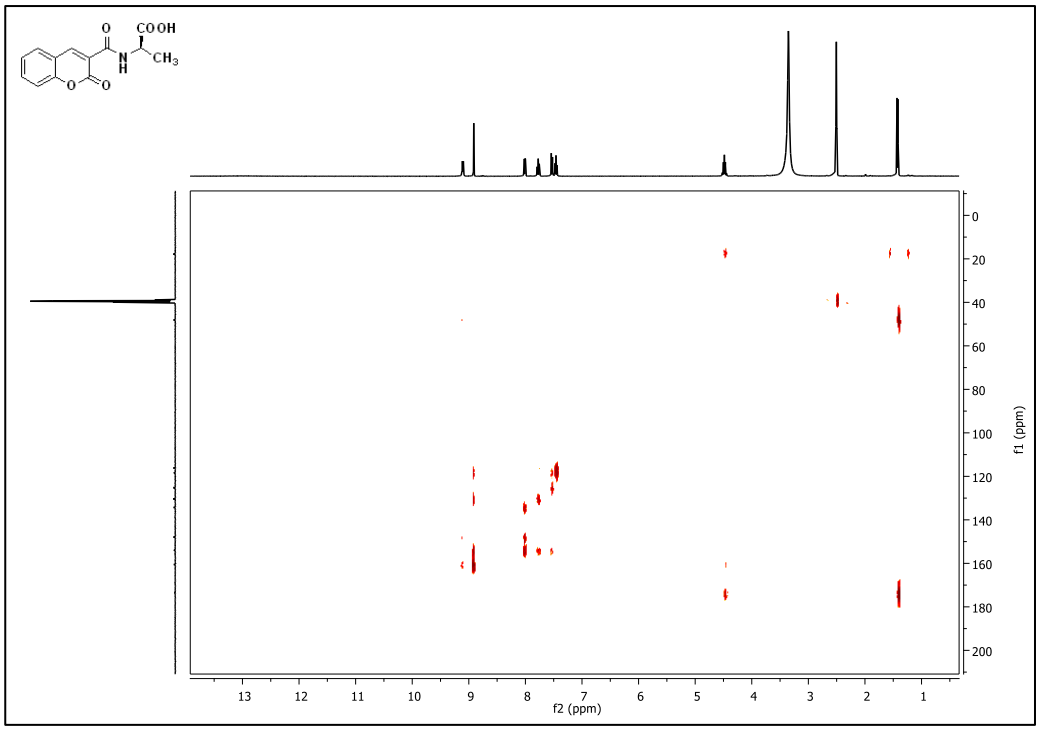

Figure A. 30 HMBC spectrum of compound **12**

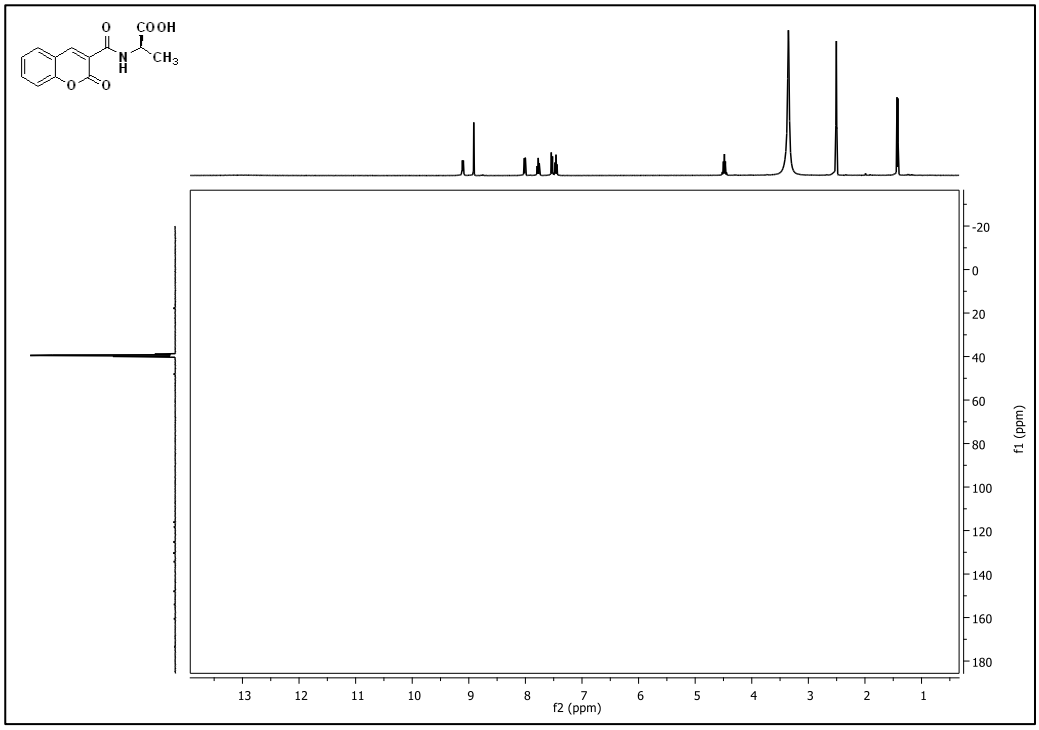

Figure A. 31 HSQC spectrum of compound **12**

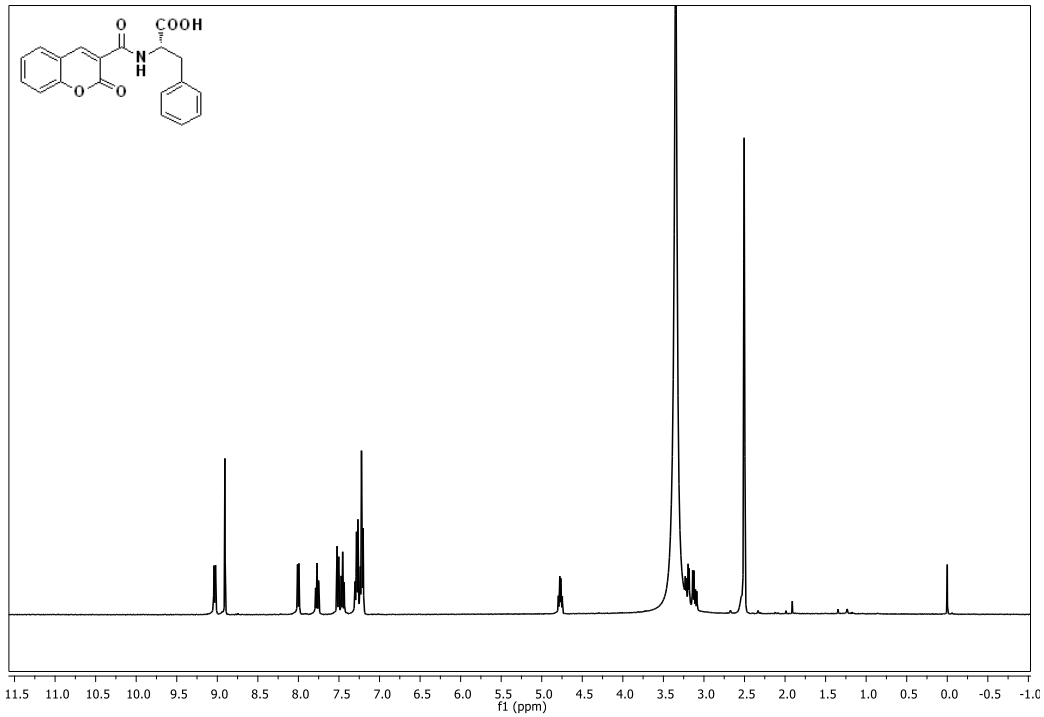

Figure A. 32 ^{1}H NMR spectrum of compound **13**

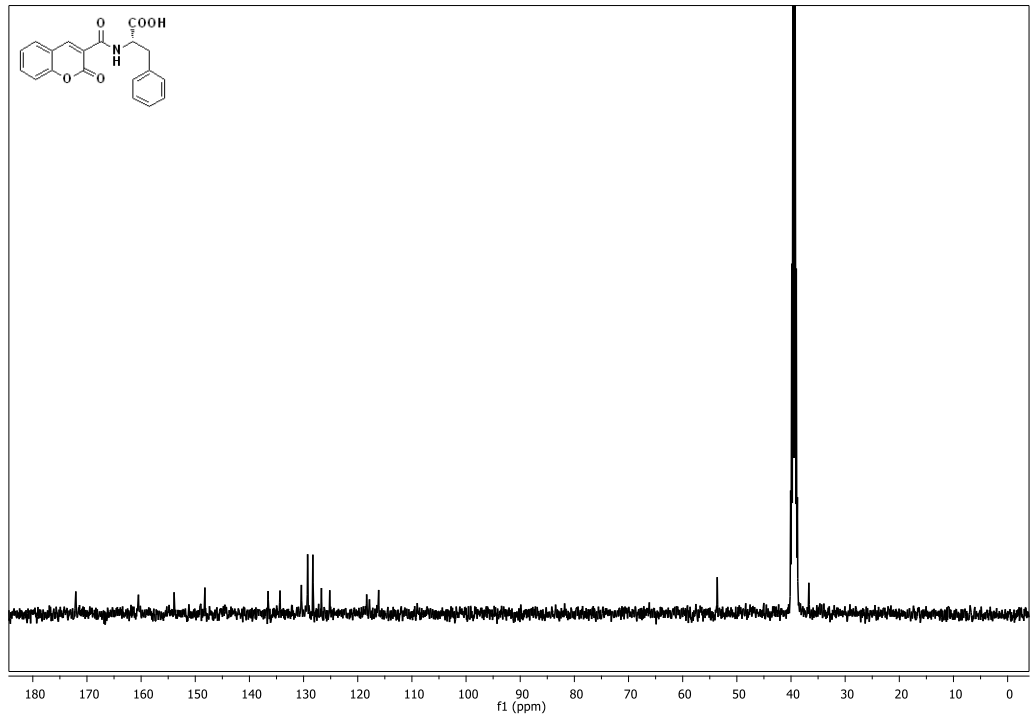

Figure A. 33 ^{13}C NMR spectrum of compound **13**

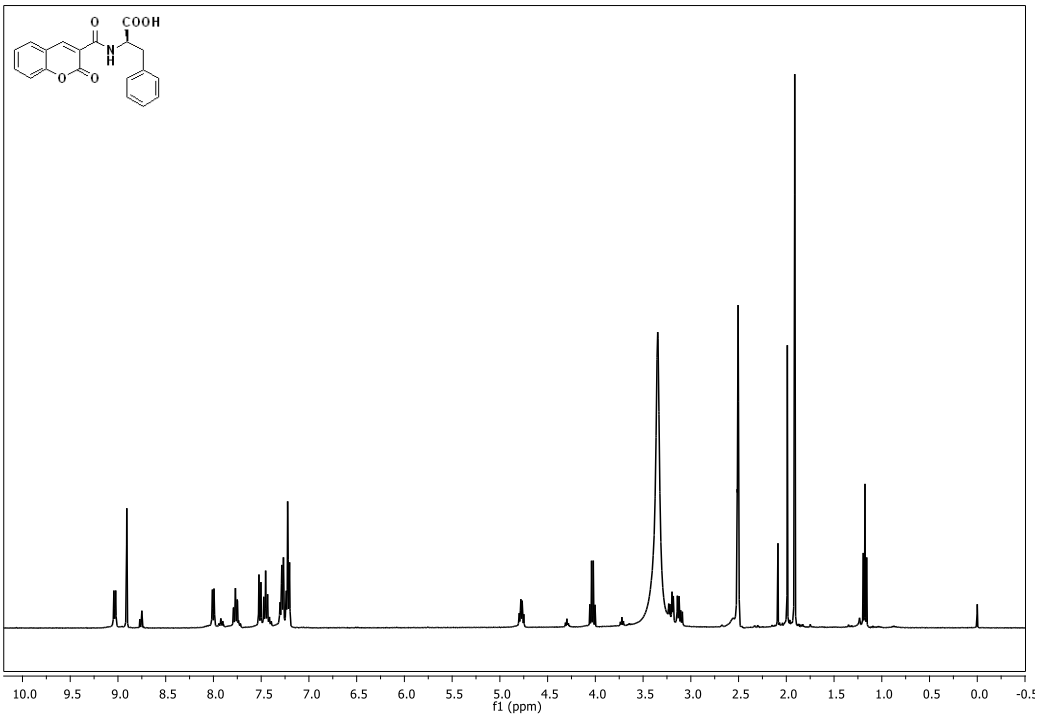

Figure A. 34 ^{1}H NMR spectrum of compound **14**

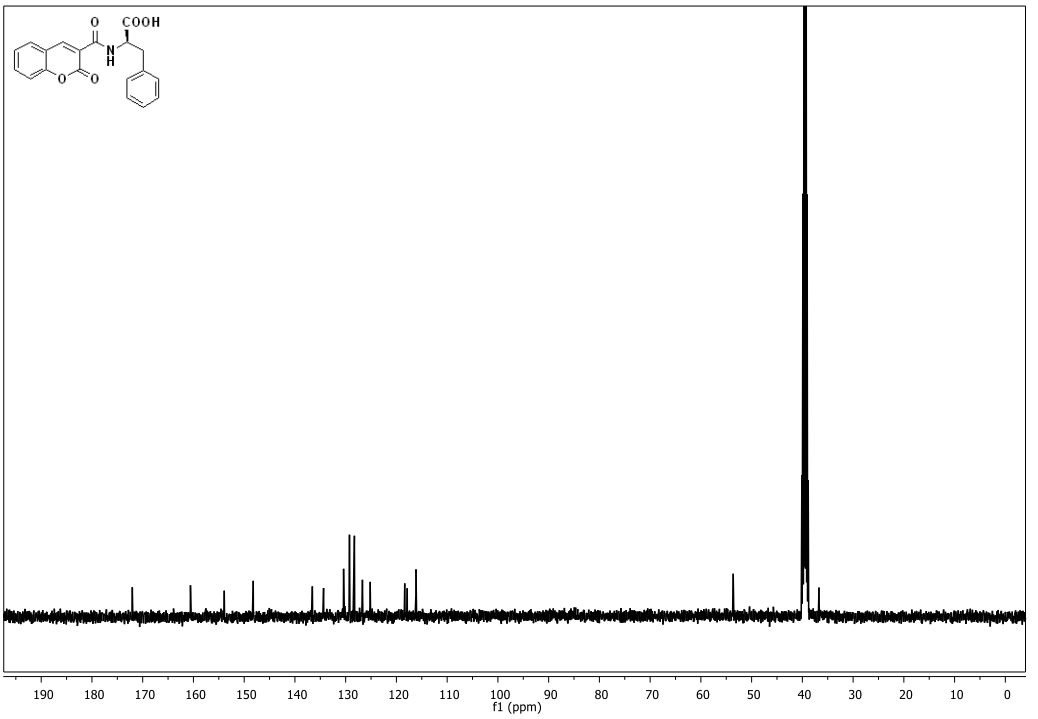

Figure A. 35 ^{13}C NMR spectrum of compound **15**

8.2 IR spectra of chiral coumarins

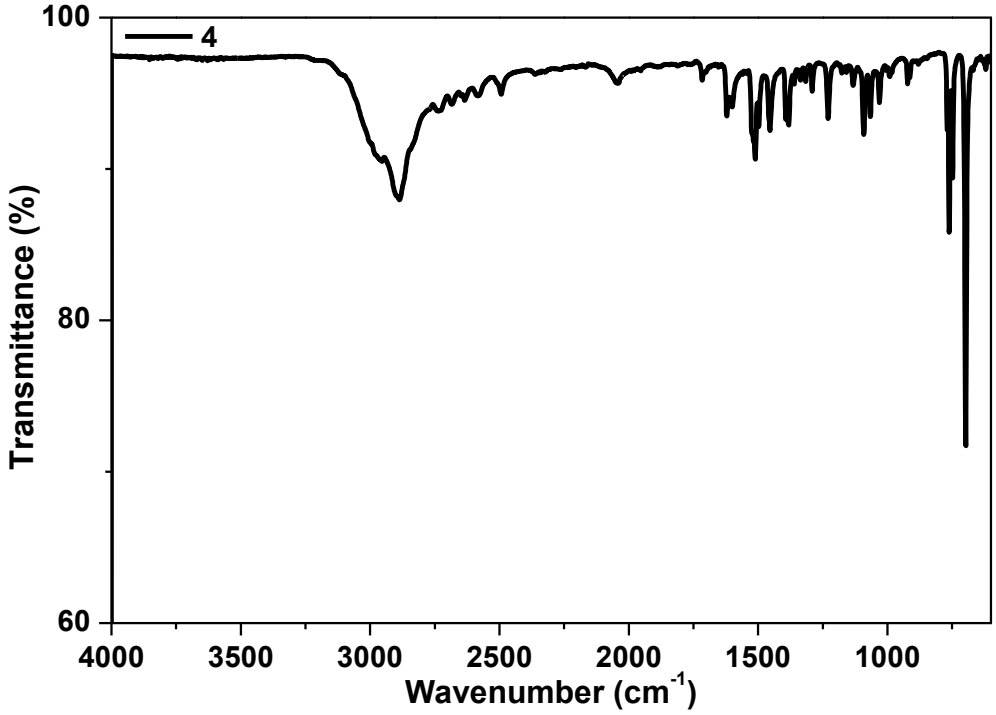

Figure A. 36 IR spectrum of compound **4**

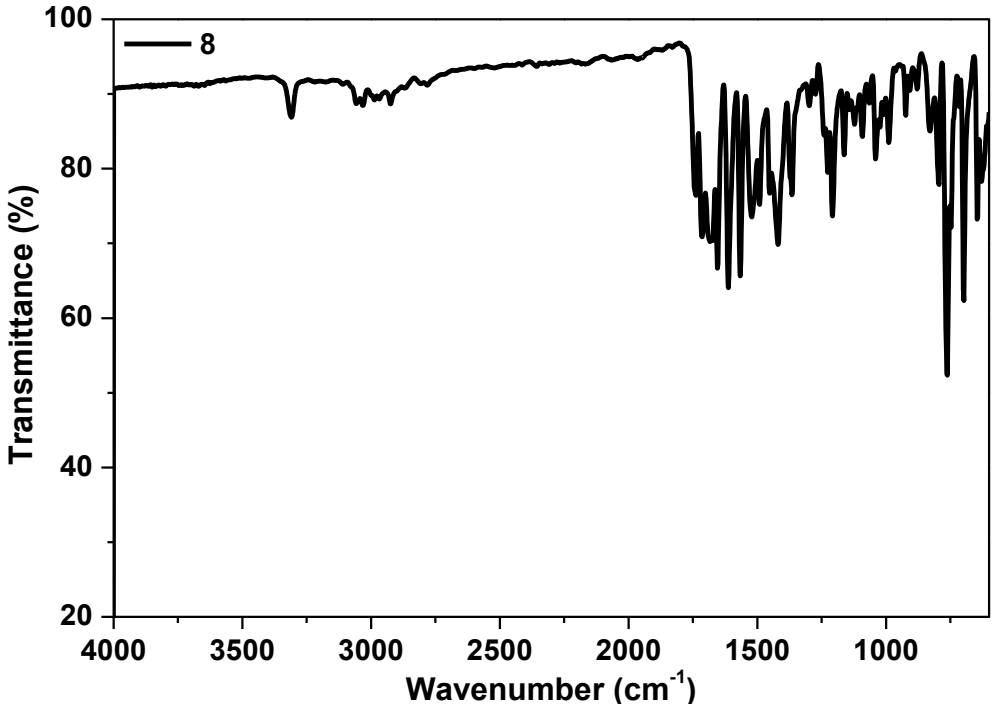

Figure A. 37 IR spectrum of compound **8**

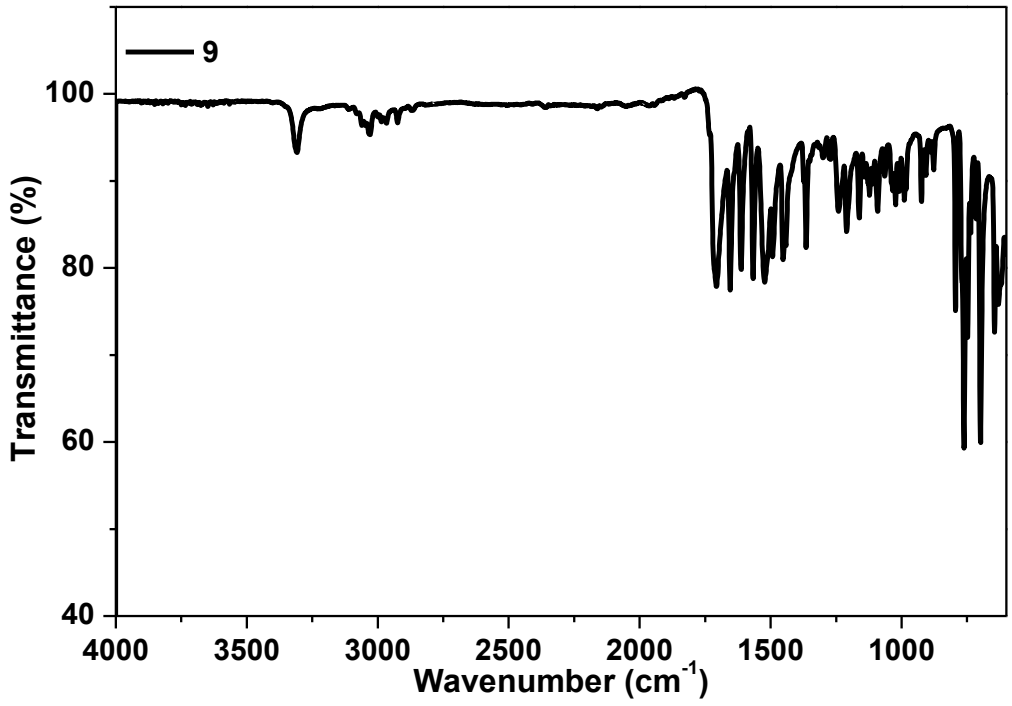

Figure A. 38 IR spectrum of compound **9**

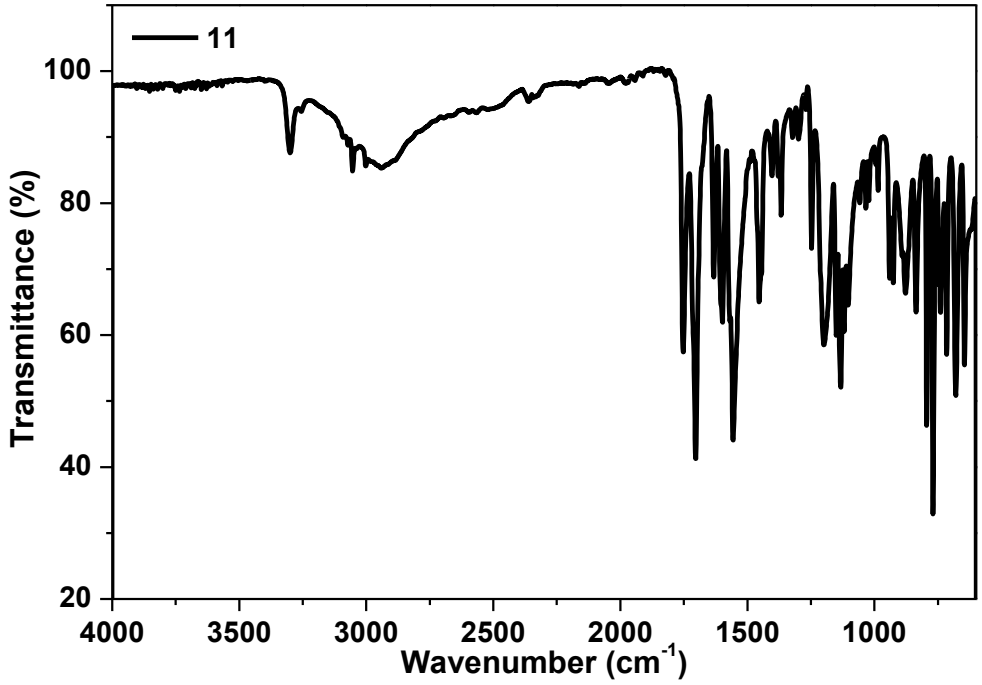

Figure A. 39 IR spectrum of compound **11**

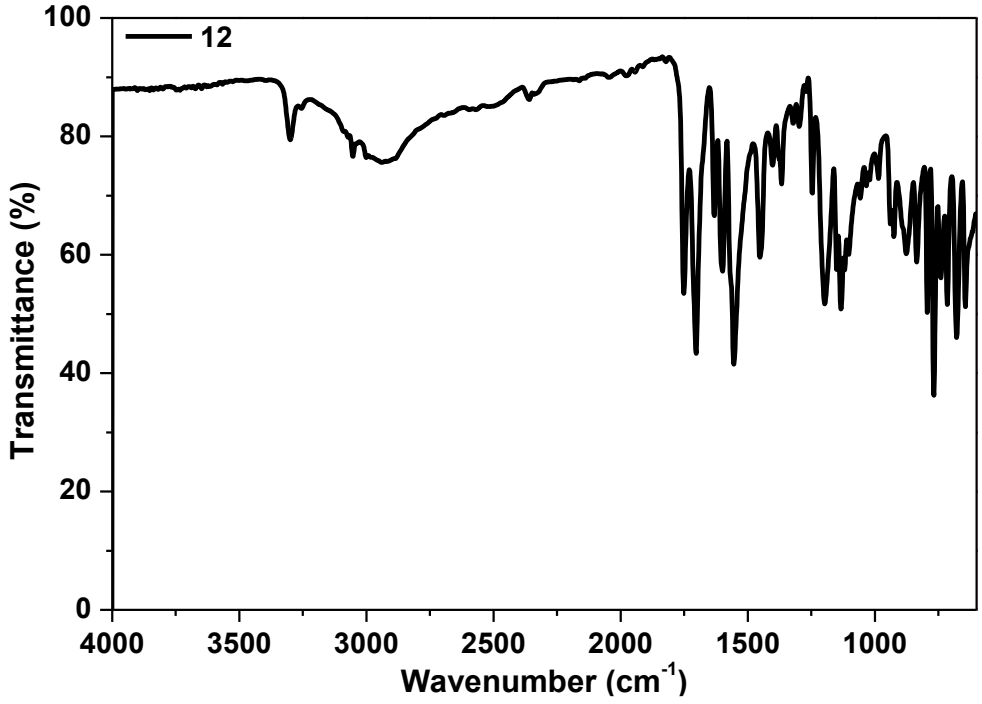

Figure A. 40 IR spectrum of compound **12**

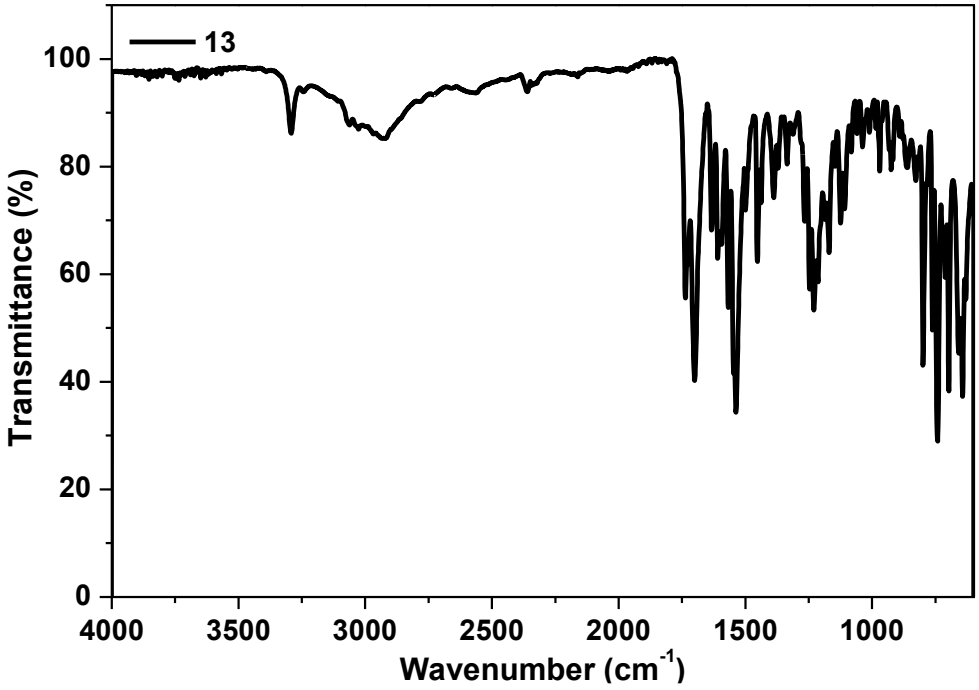

Figure A. 41 IR spectrum of compound **13**

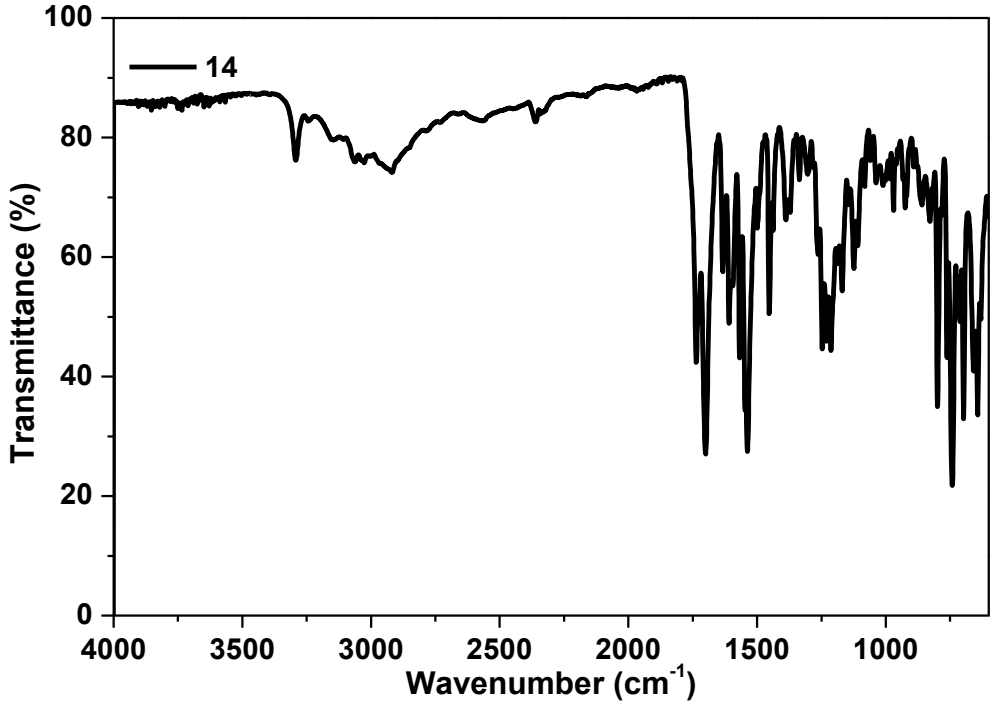

Figure A. 42 IR spectrum of compound **14**

8.3 HRMS spectra of chiral coumarins

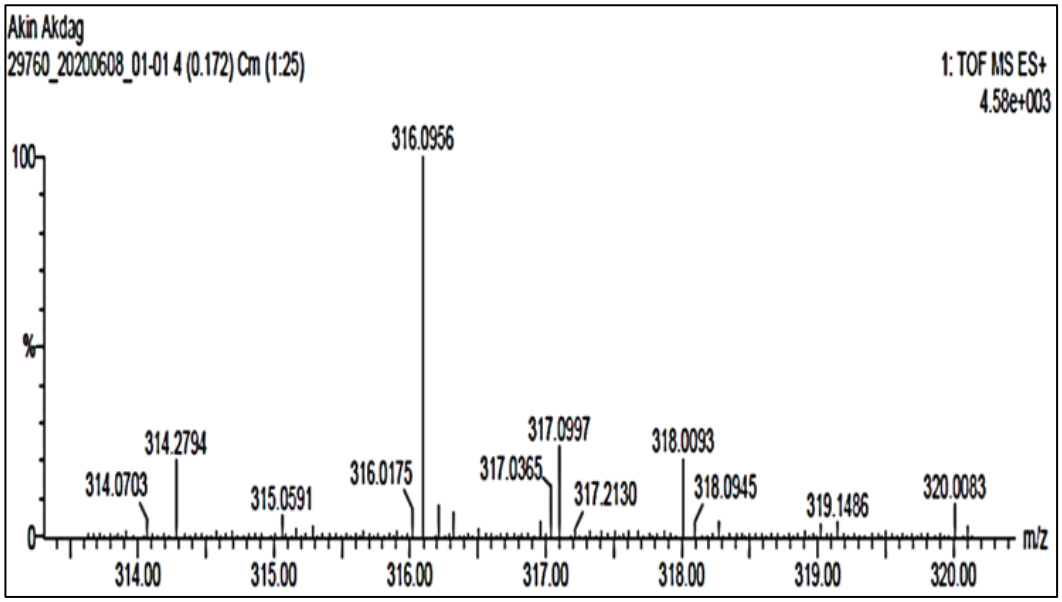

Figure A. 43 HRMS spectrum of compound **8**

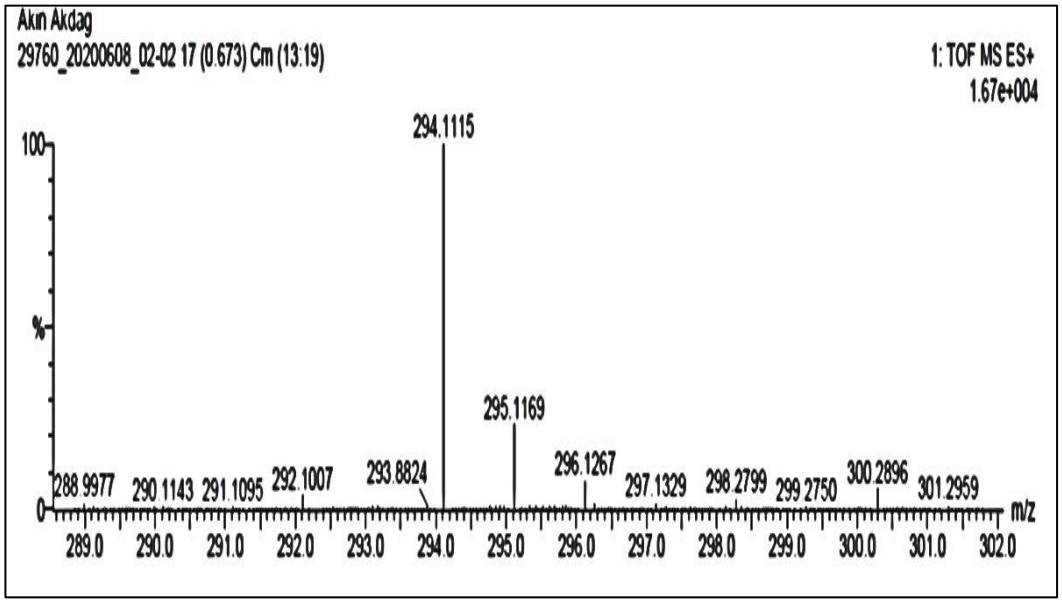

Figure A. 44 HRMS spectrum of compound **9**

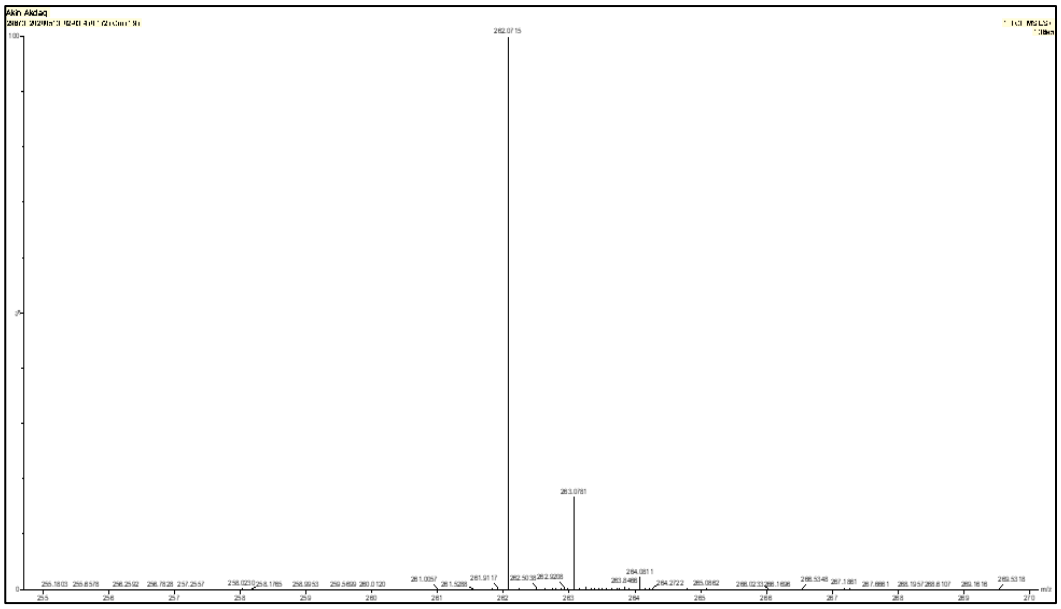

Figure A. 45 HRMS spectrum of compound **11**

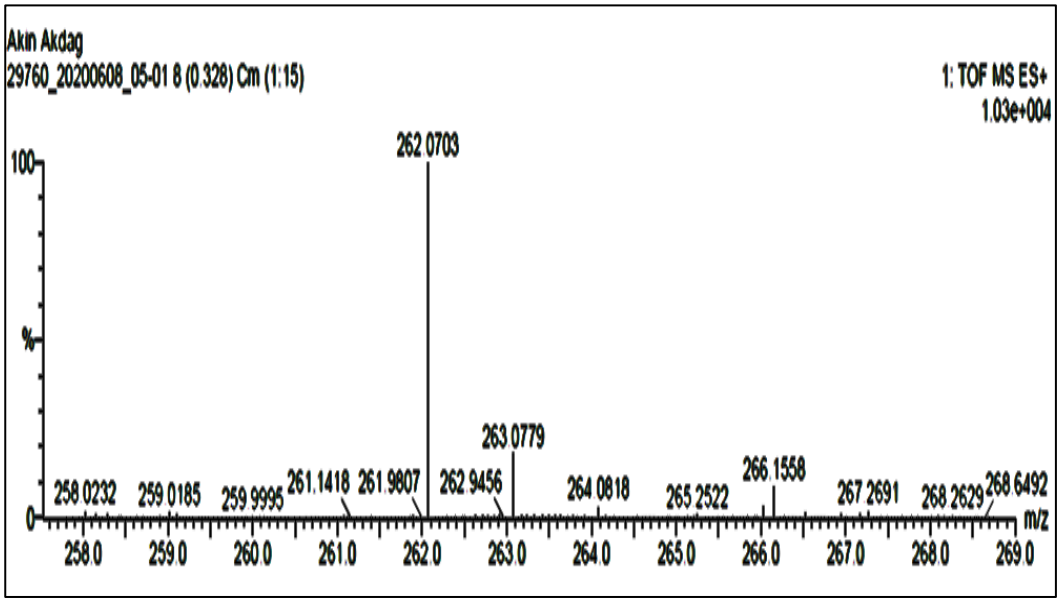

Figure A. 46 HRMS spectrum of compound **12**

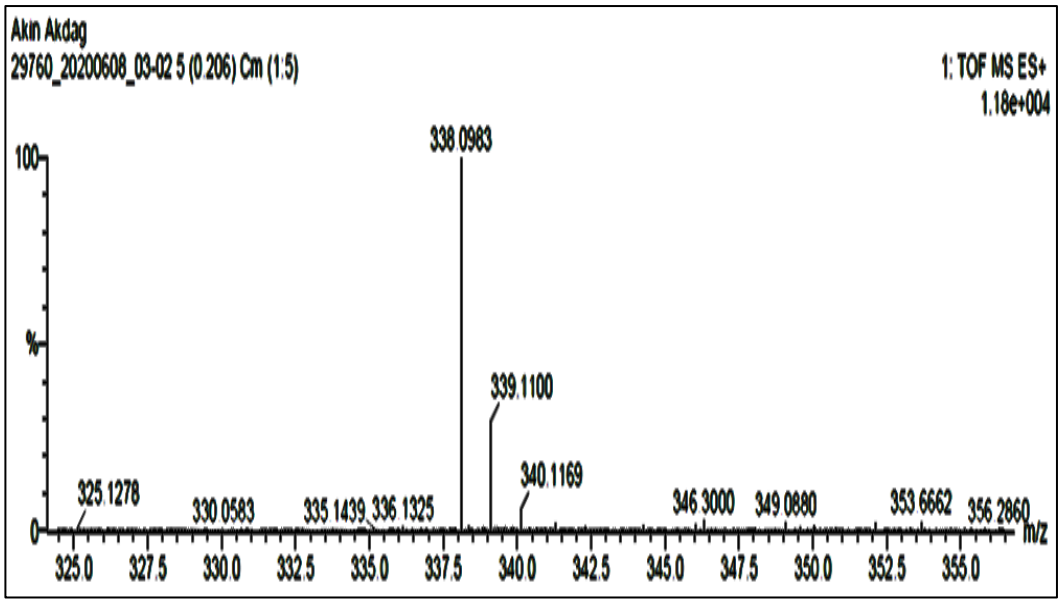

Figure A. 47 HRMS spectrum of compound **13**

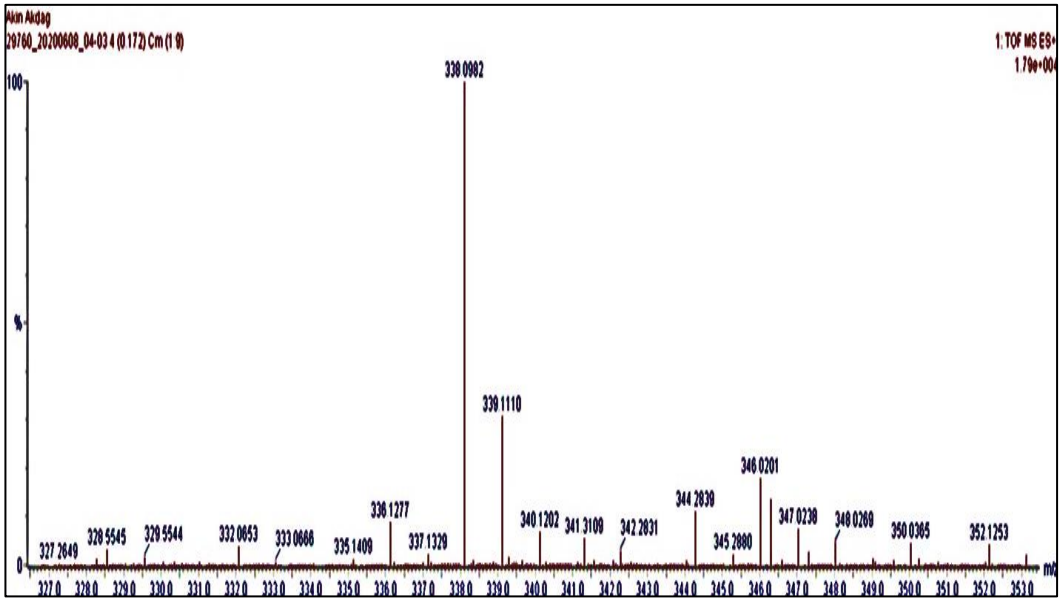

Figure A. 48 HRMS spectrum of compound **14**

B. Characterization data for coumarin dimers

8.4 NMR Spectra

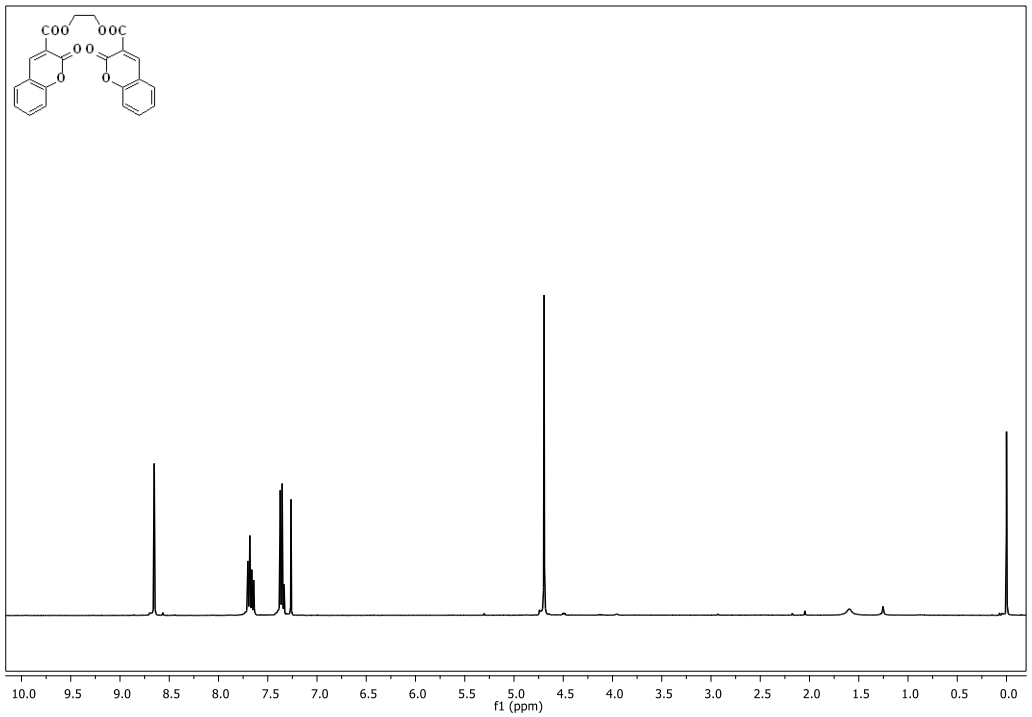

Figure B. 1 ^{1}H NMR spectrum of compound **15**

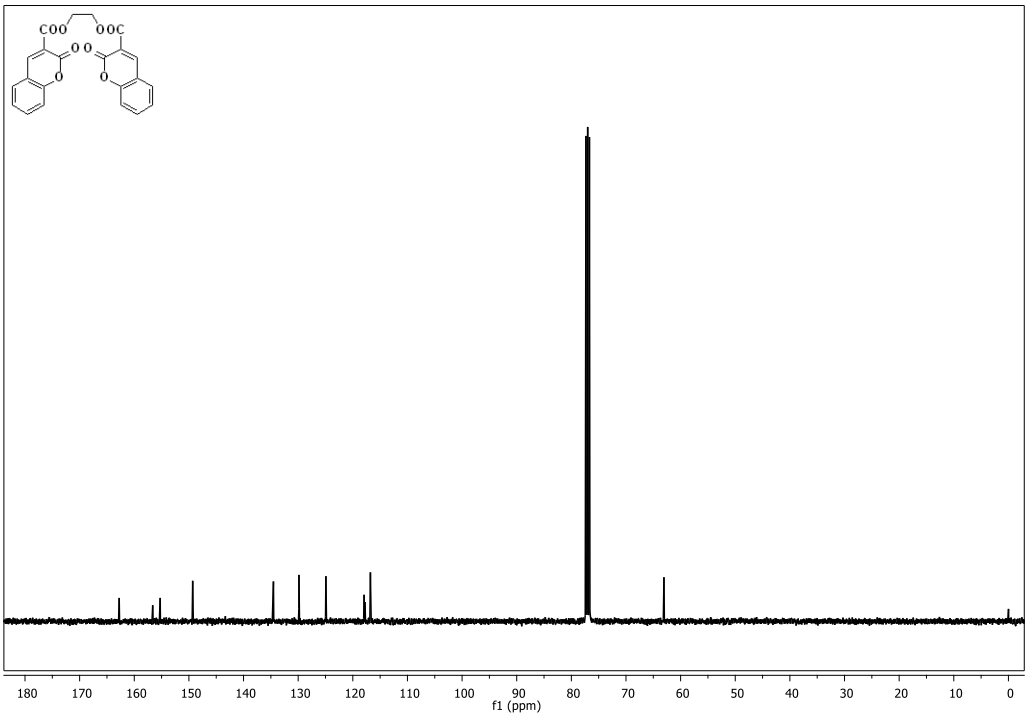

Figure B. 2 ^{13}C NMR spectrum of compound **15**

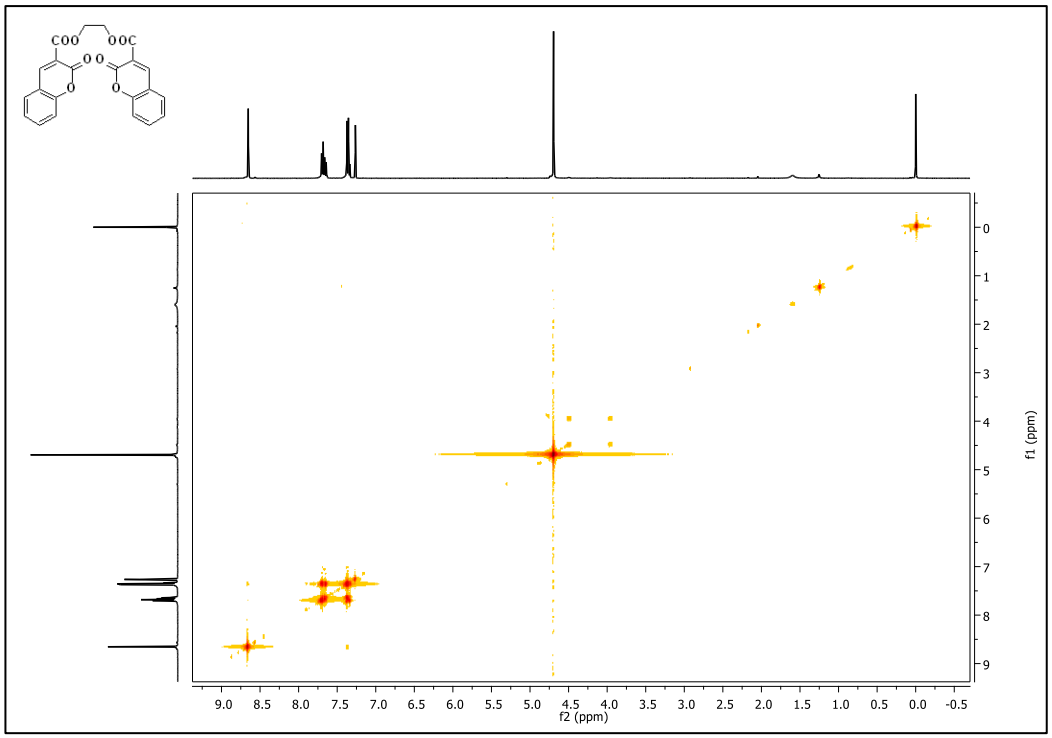

Figure B. 3 COSY spectrum of compound **15**

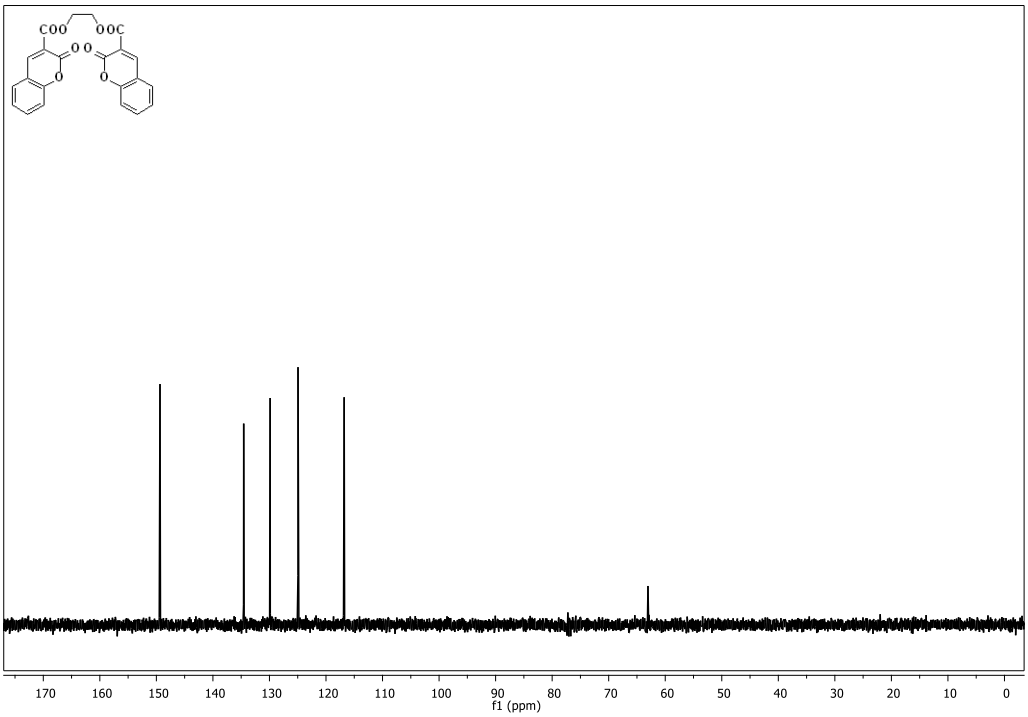

Figure B. 4 DEPT90 spectrum of compound **15**

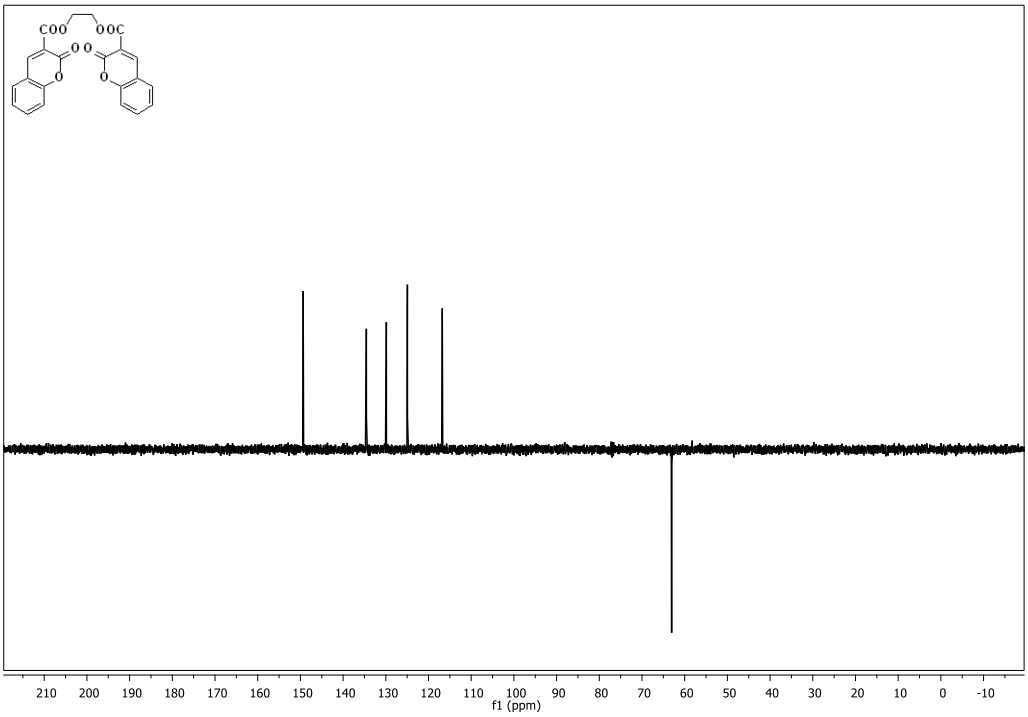

Figure B. 5 DEPT135 spectrum of compound **15**

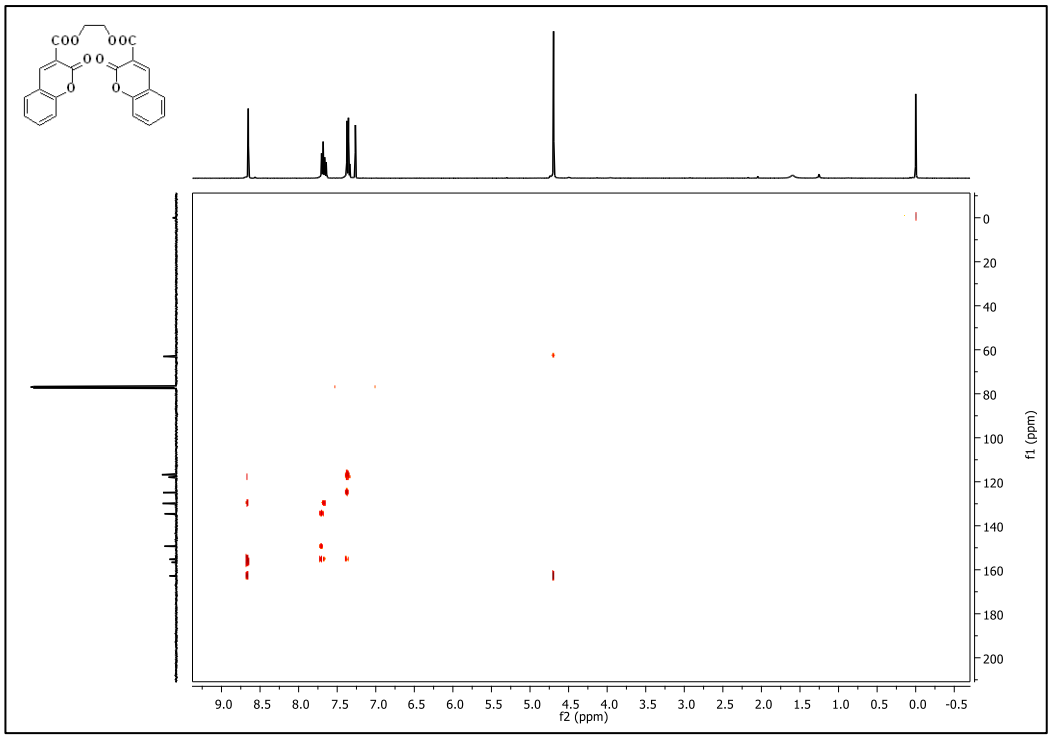

Figure B. 6 HMBC spectrum of compound **15**

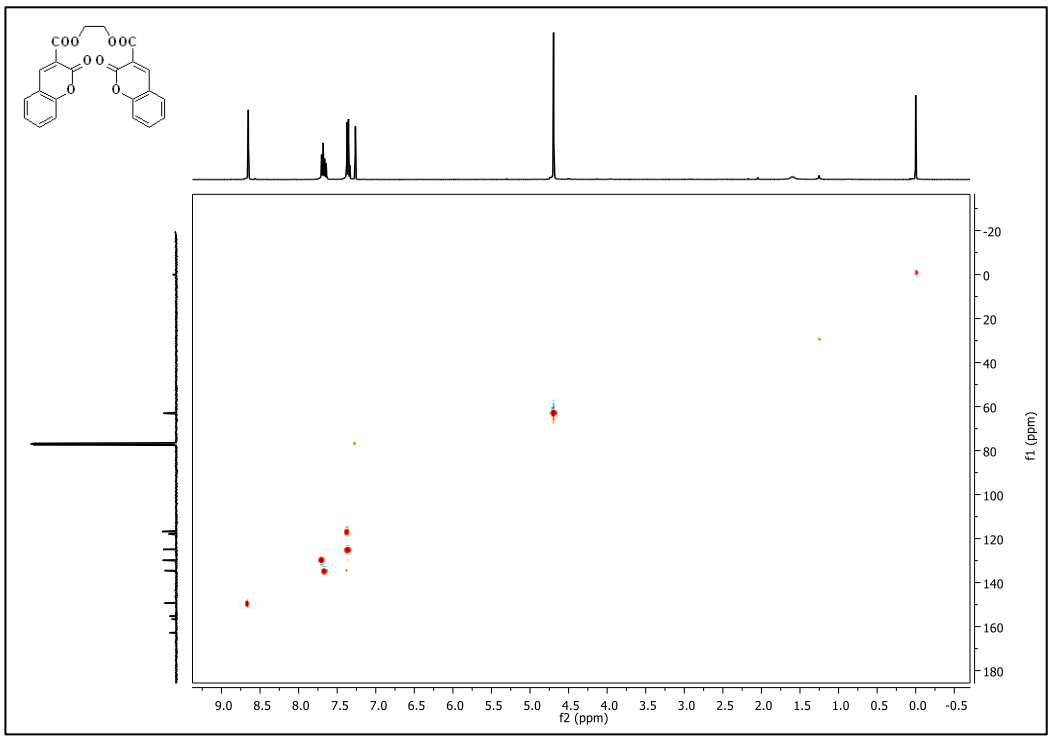

Figure B. 7 HSQC spectrum of compound **15**

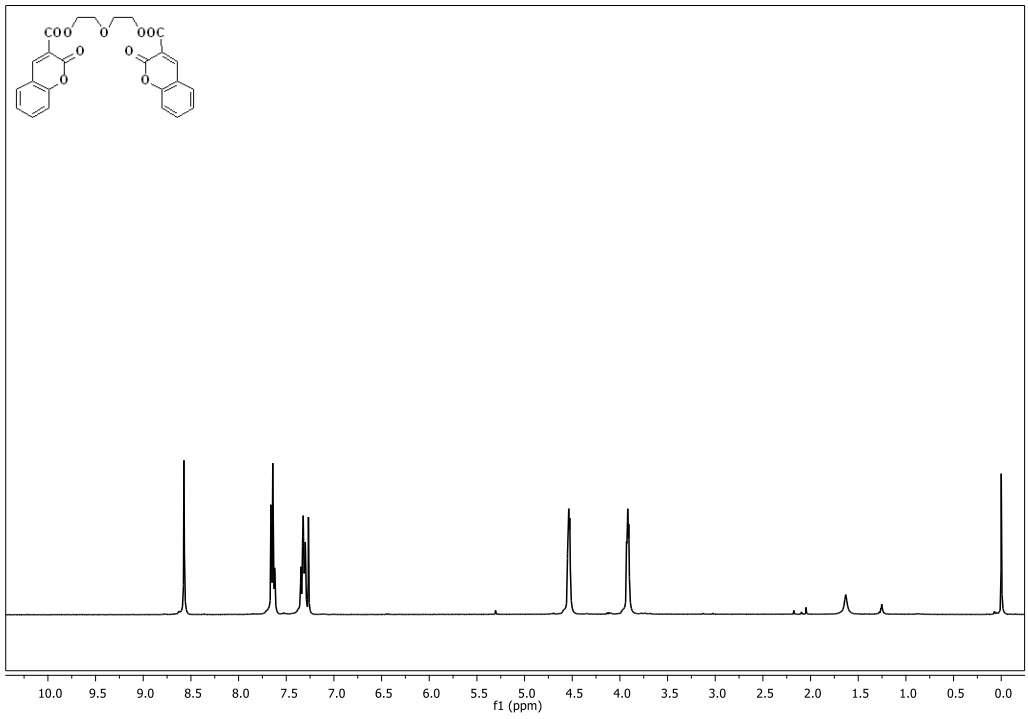

Figure B. 8 ^{1}H NMR spectrum of compound **16**

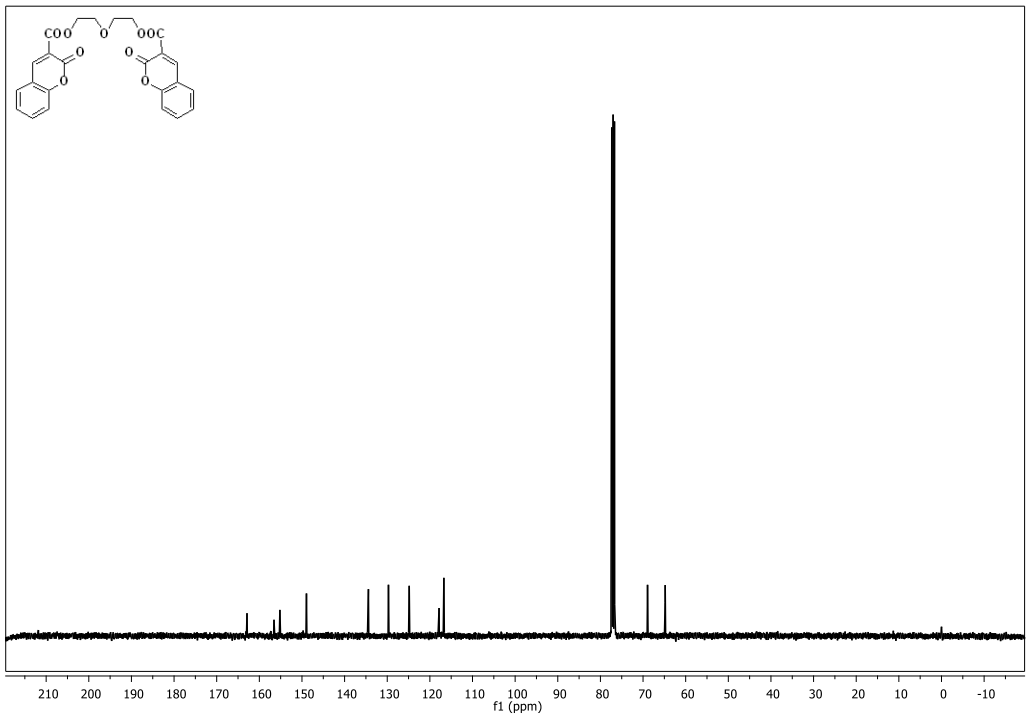

Figure B. 9 ^{13}C NMR spectrum of compound **16**

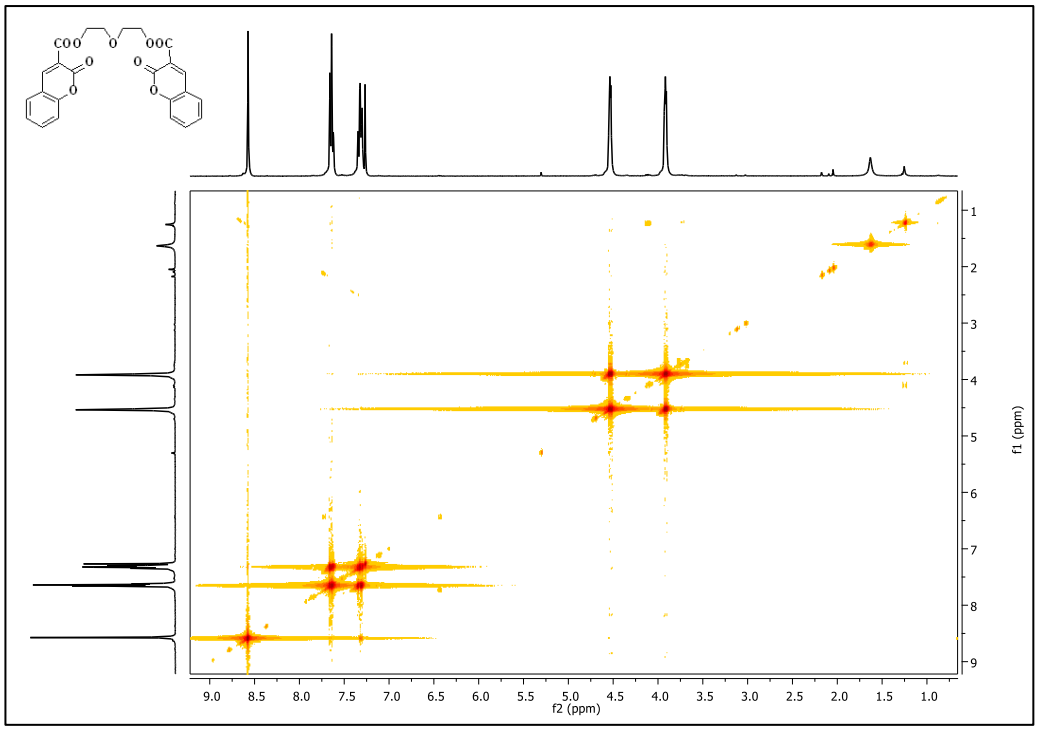

Figure B. 10 COSY spectrum of compound **16**

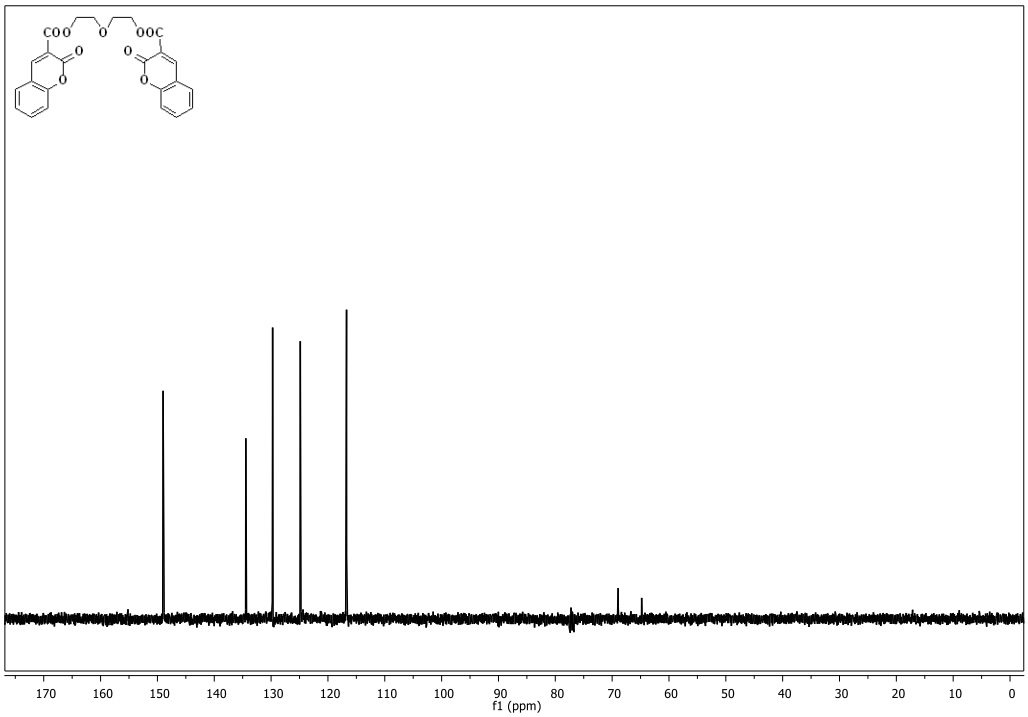

Figure B. 11 DEPT90 spectrum of compound **16**

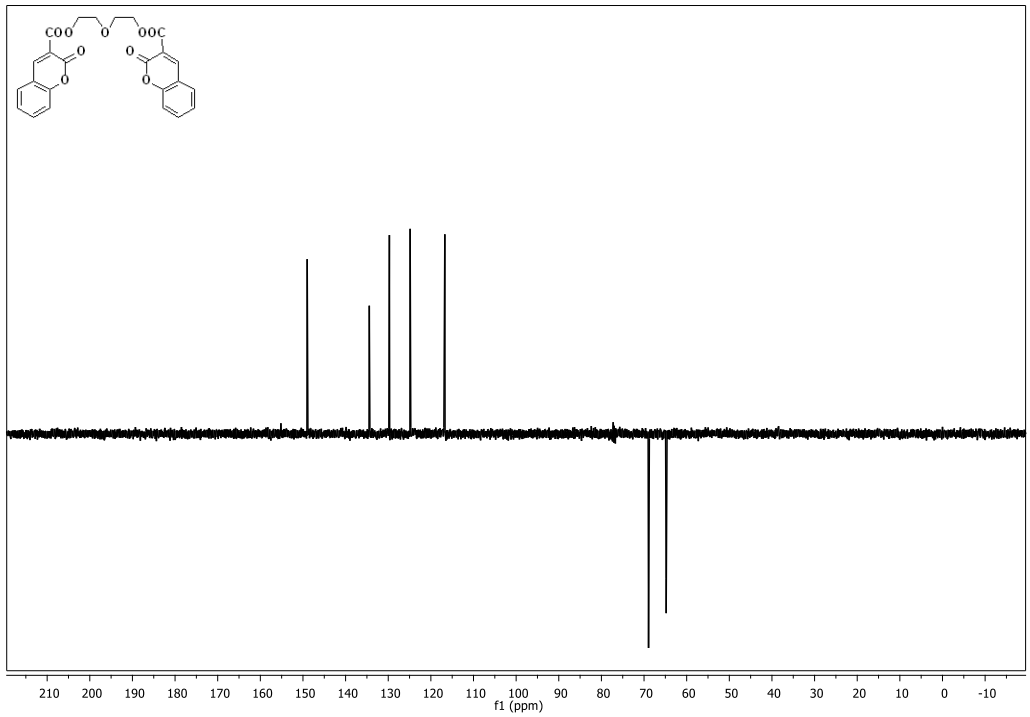

Figure B. 12 DEPT135 spectrum of compound **16**

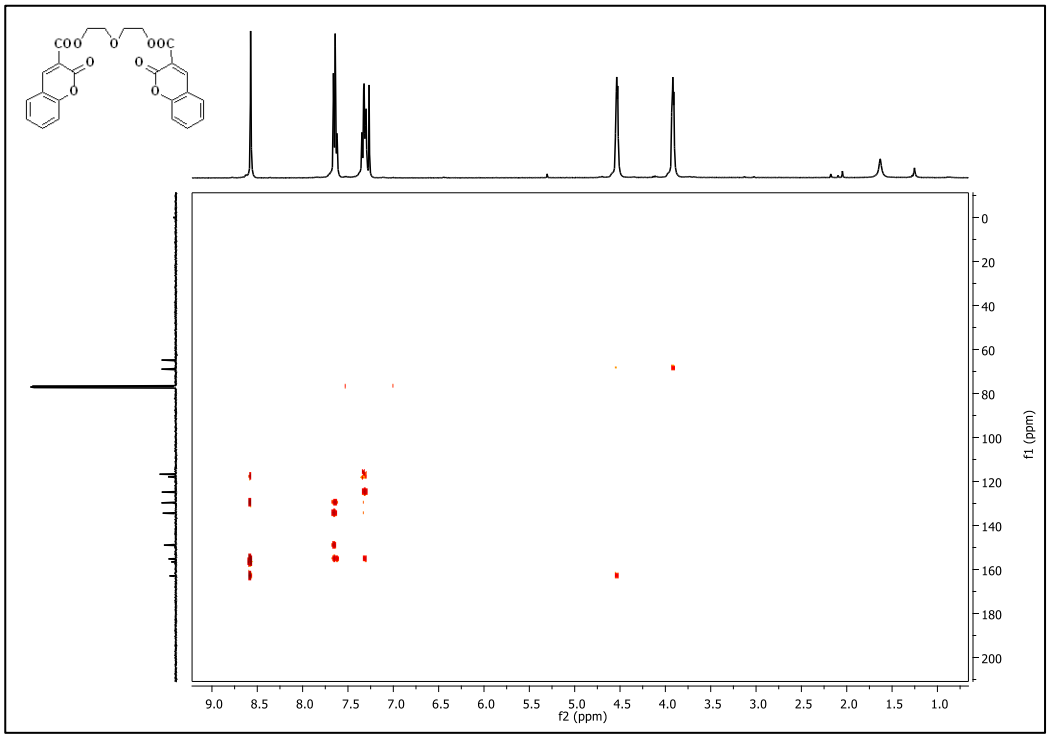

Figure B. 13 HMBC spectrum of compound **16**

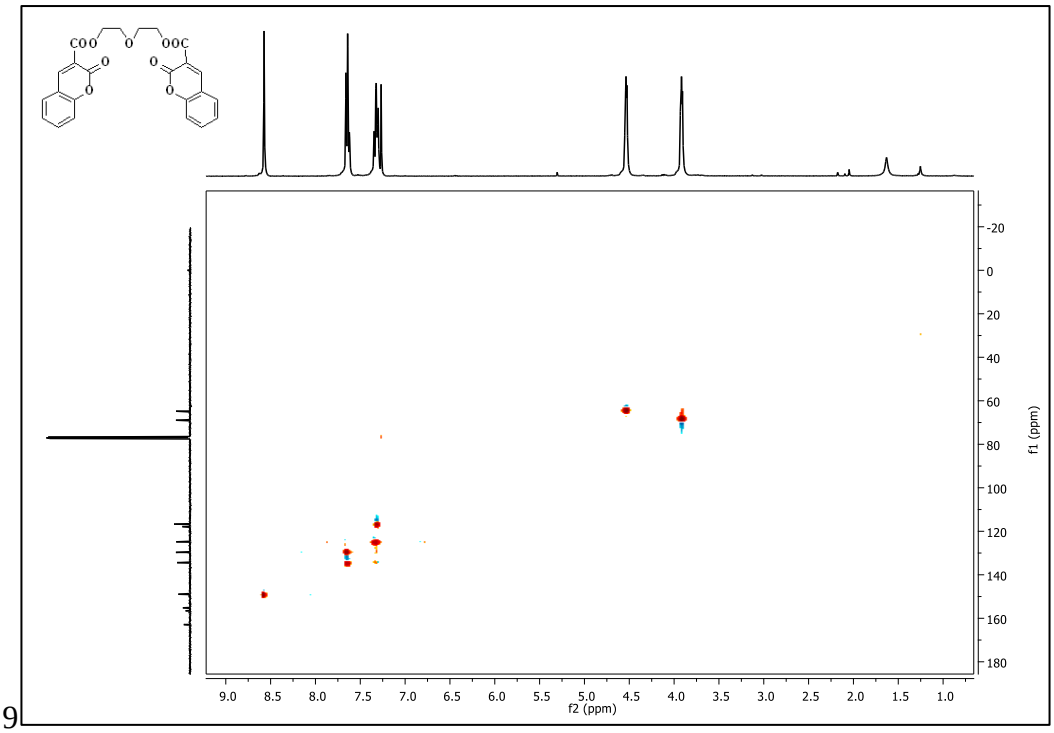

9

Figure B. 14 HSQC spectrum of compound **16**

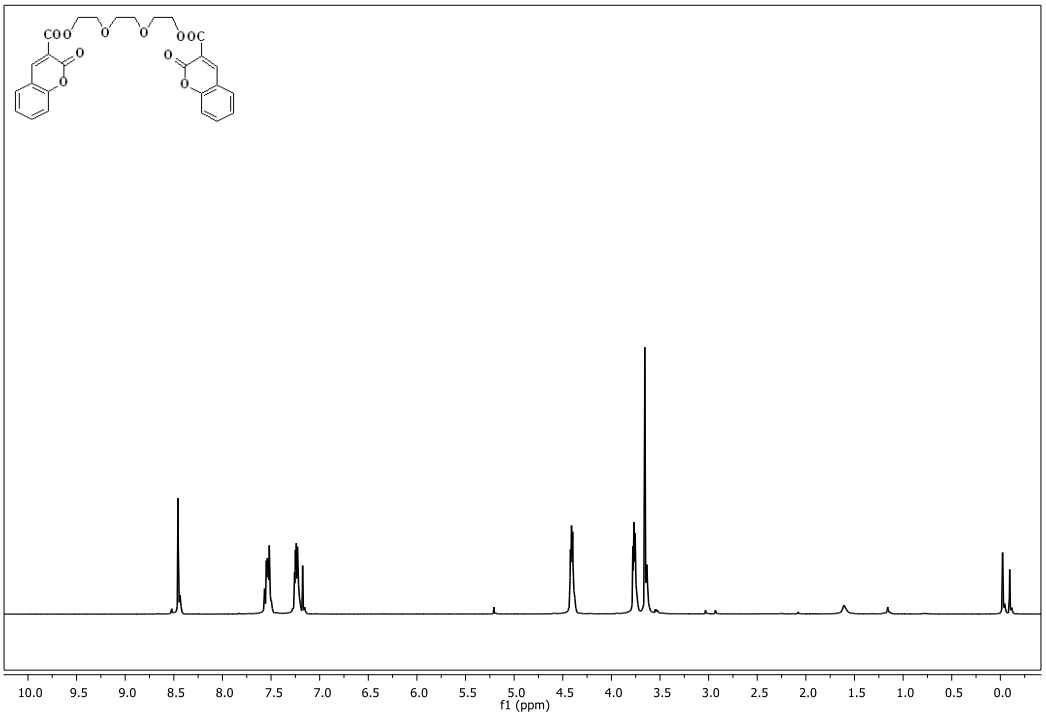

Figure B. 15 ^{1}H NMR spectrum of compound **17**

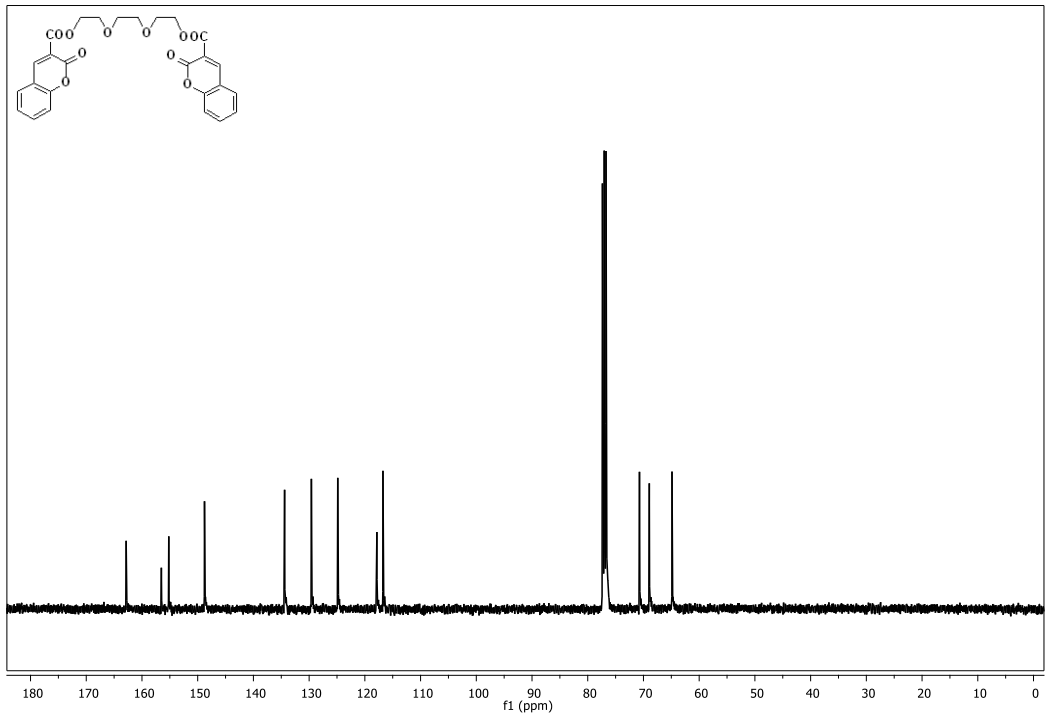

Figure B. 16 ^{13}C NMR spectrum of compound **17**

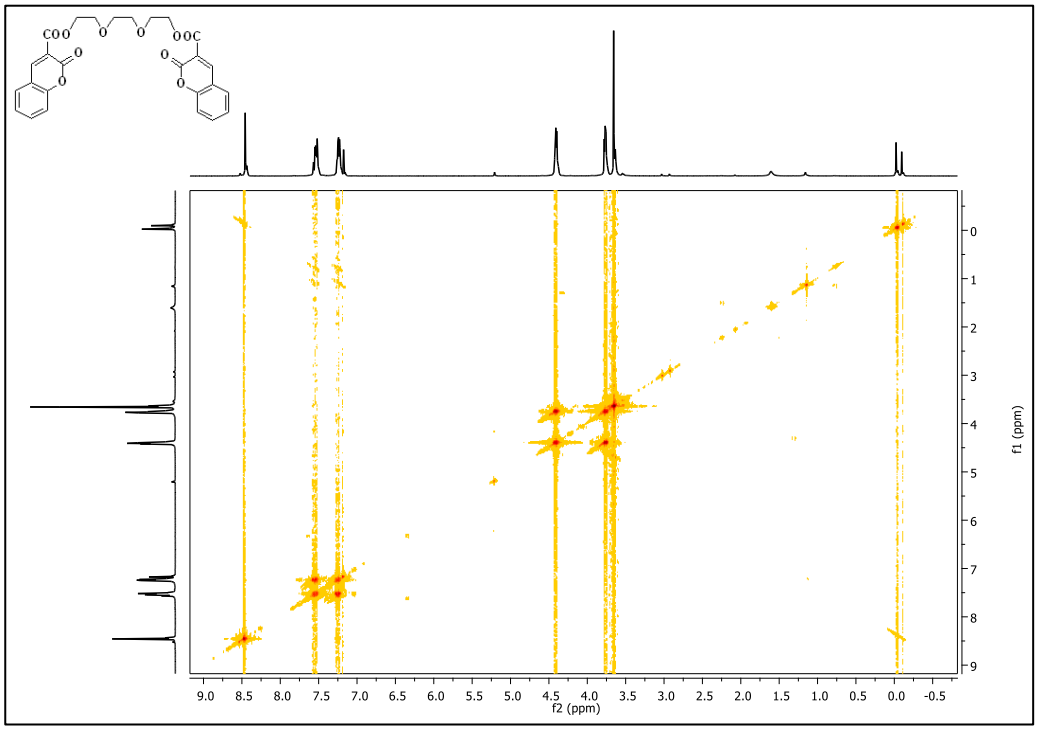

Figure B. 17 COSY spectrum of compound **17**

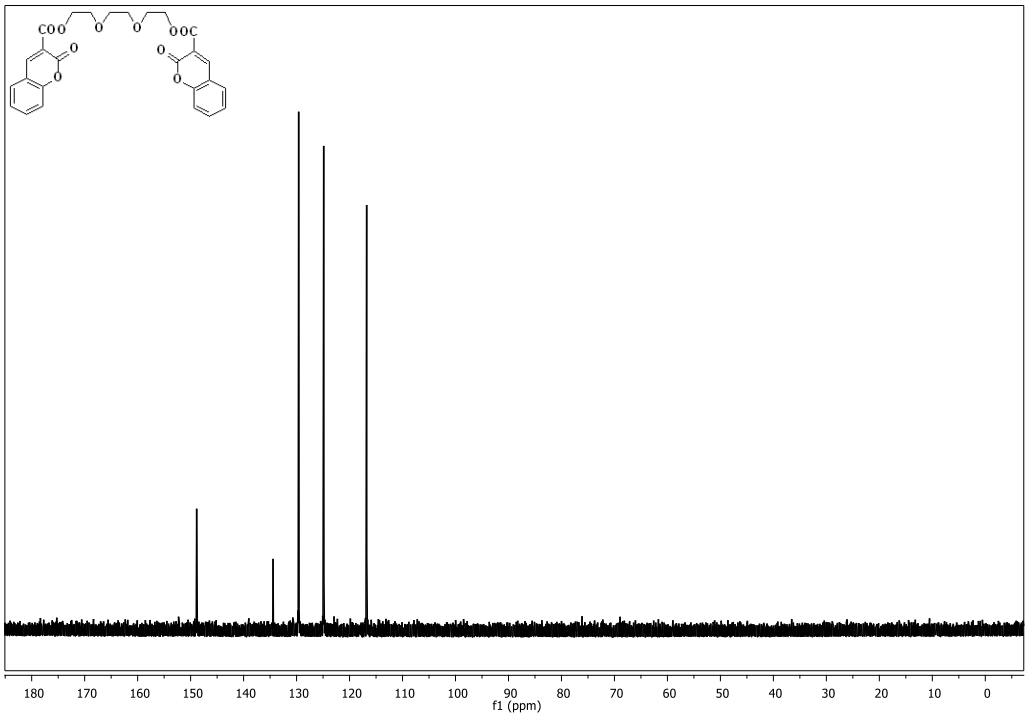

Figure B. 18 DEPT90 spectrum of compound **17**

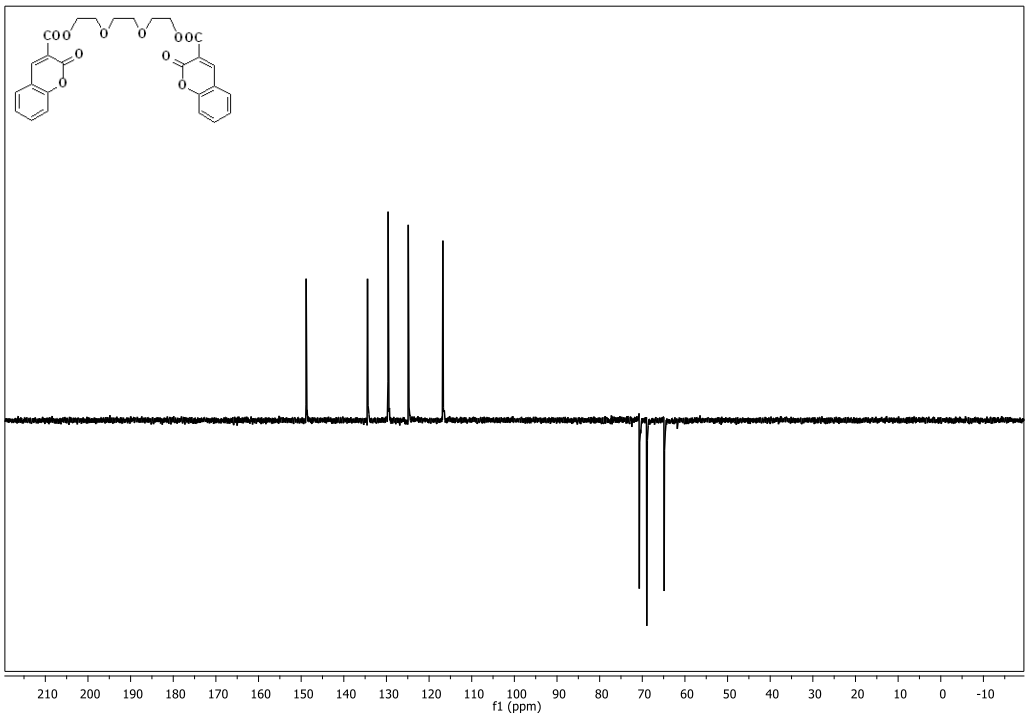

Figure B. 19 DEPT135 spectrum of compound **17**

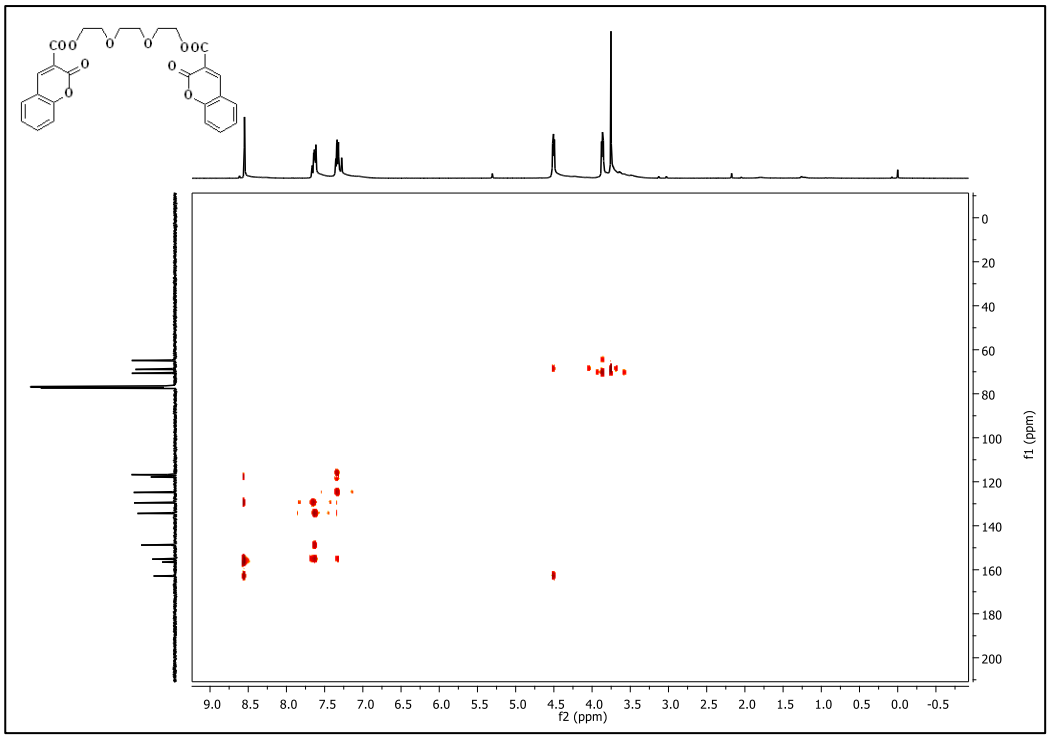

Figure B. 20 HMBC spectrum of compound **17**

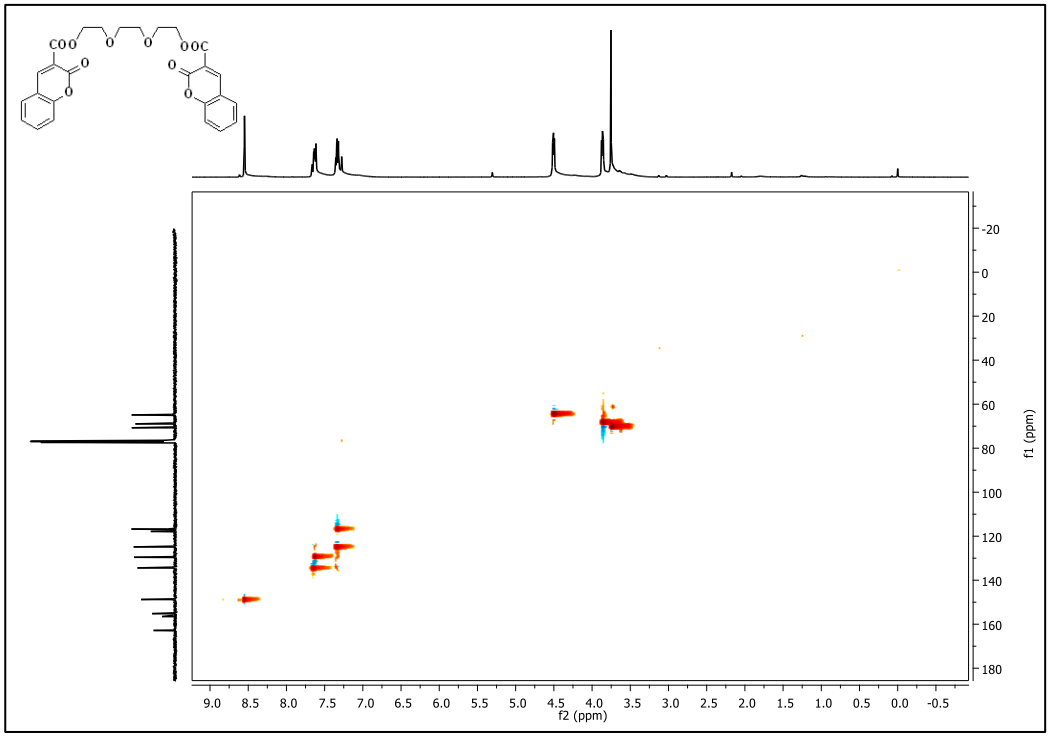

Figure B. 21 HSQC spectrum of compound **17**

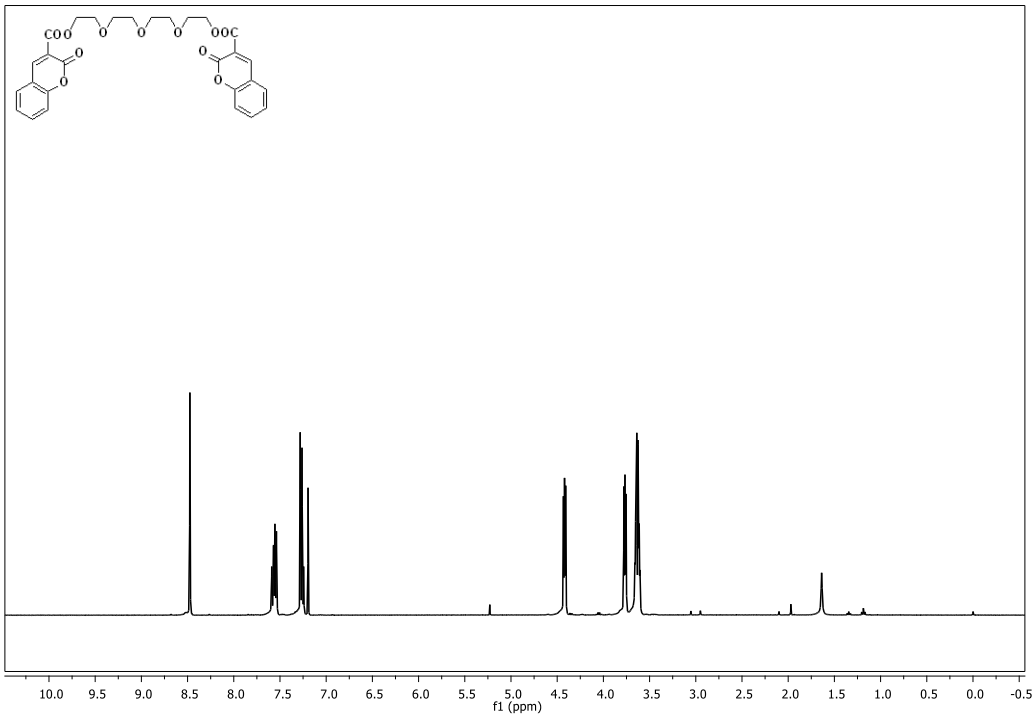

Figure B. 22 ^{1}H NMR spectrum of compound **18**

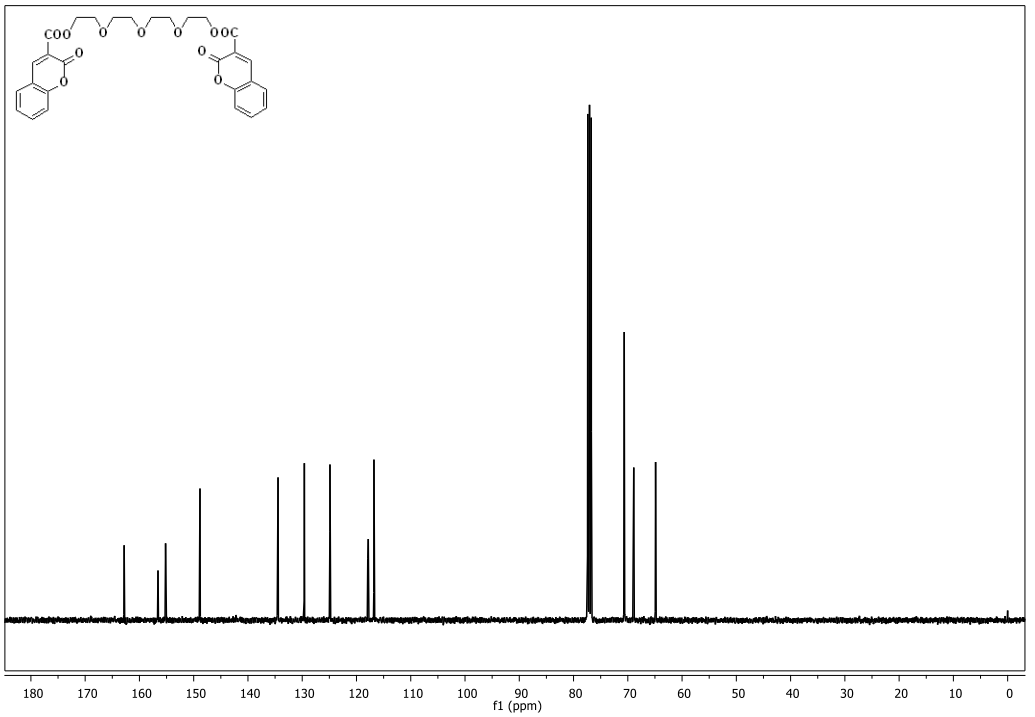

Figure B. 23 ^{13}C NMR spectrum of compound **18**

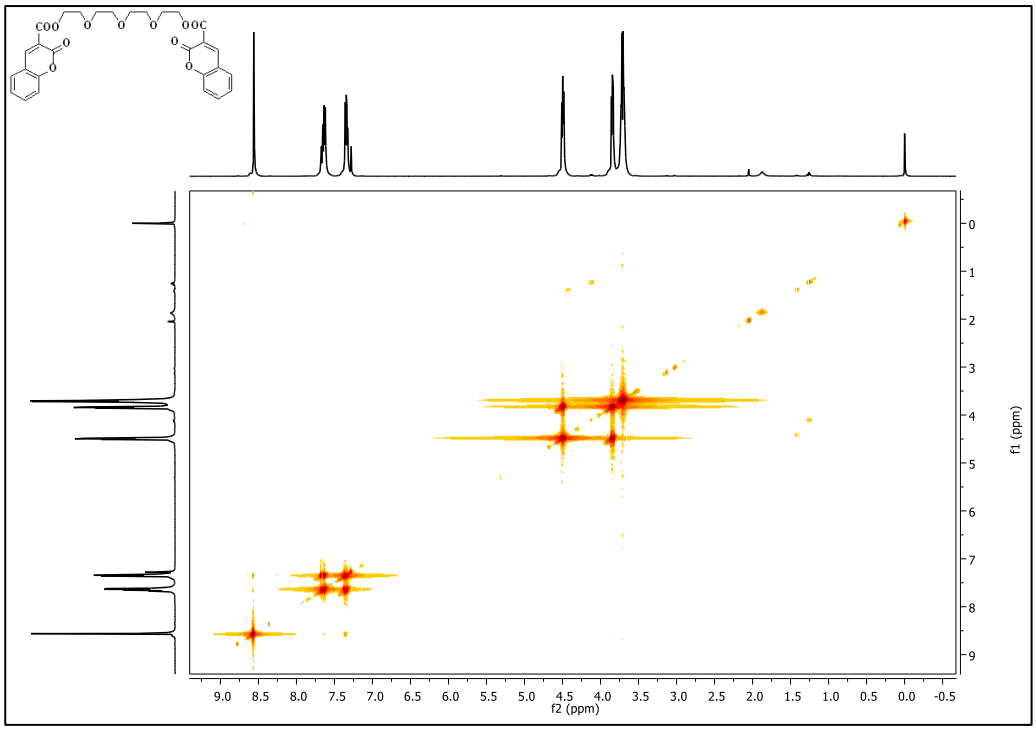

Figure B. 24 COSY spectrum of compound **18**

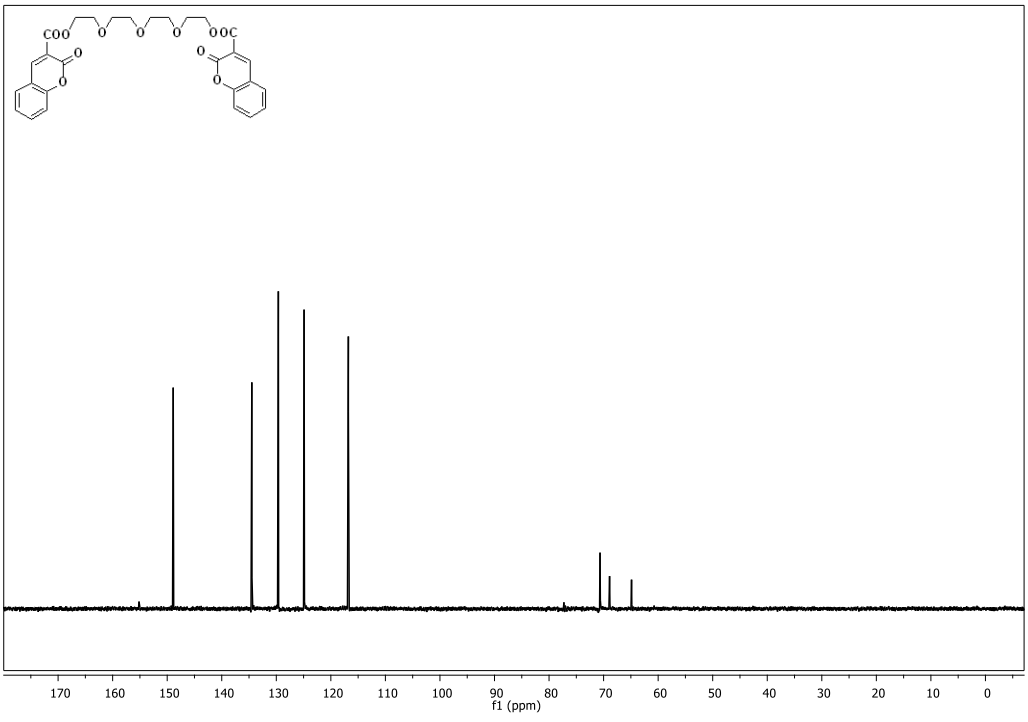

Figure B. 25 DEPT90 spectrum of compound **18**

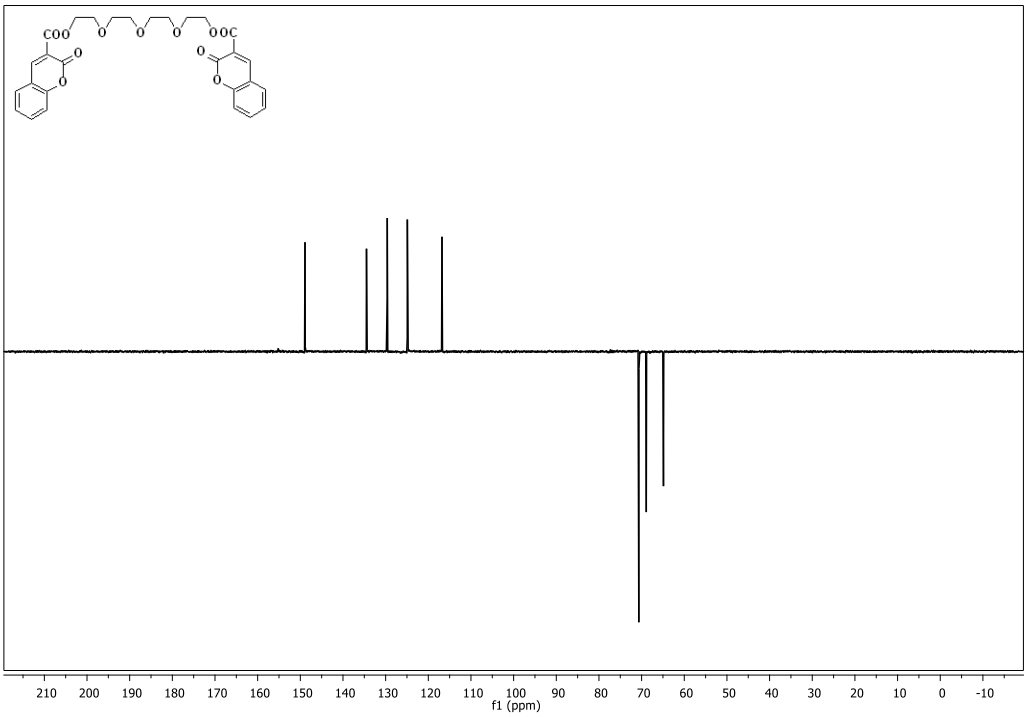

Figure B. 26 DEPT135 spectrum of compound **18**

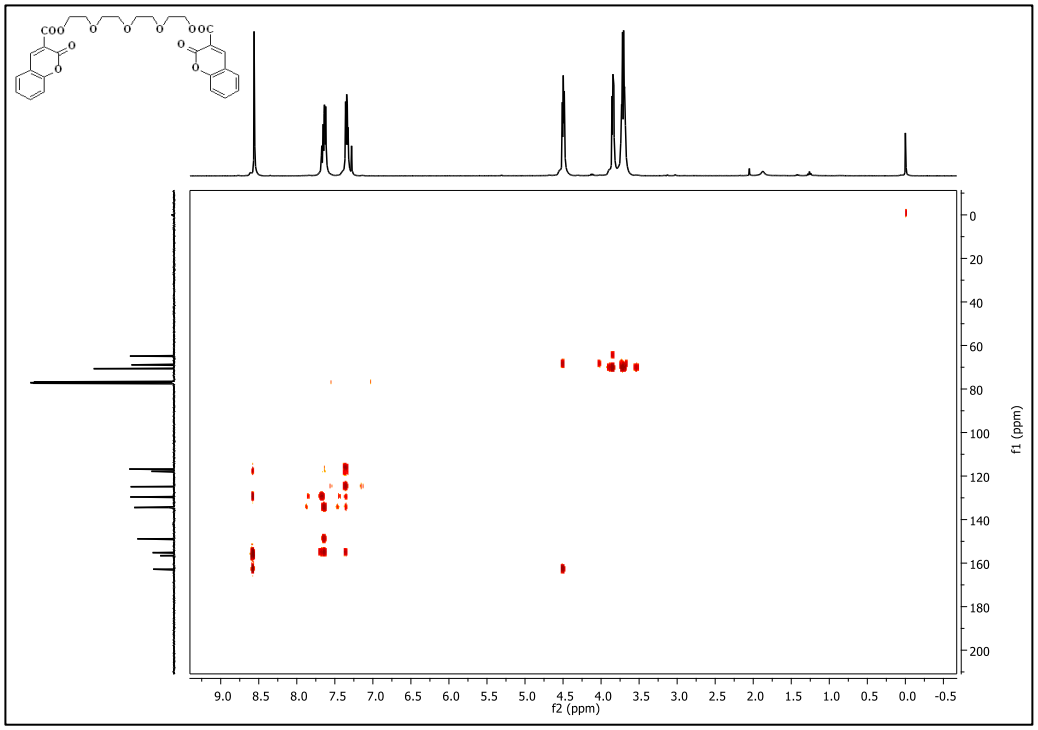

Figure B. 27 HMBC spectrum of compound **18**

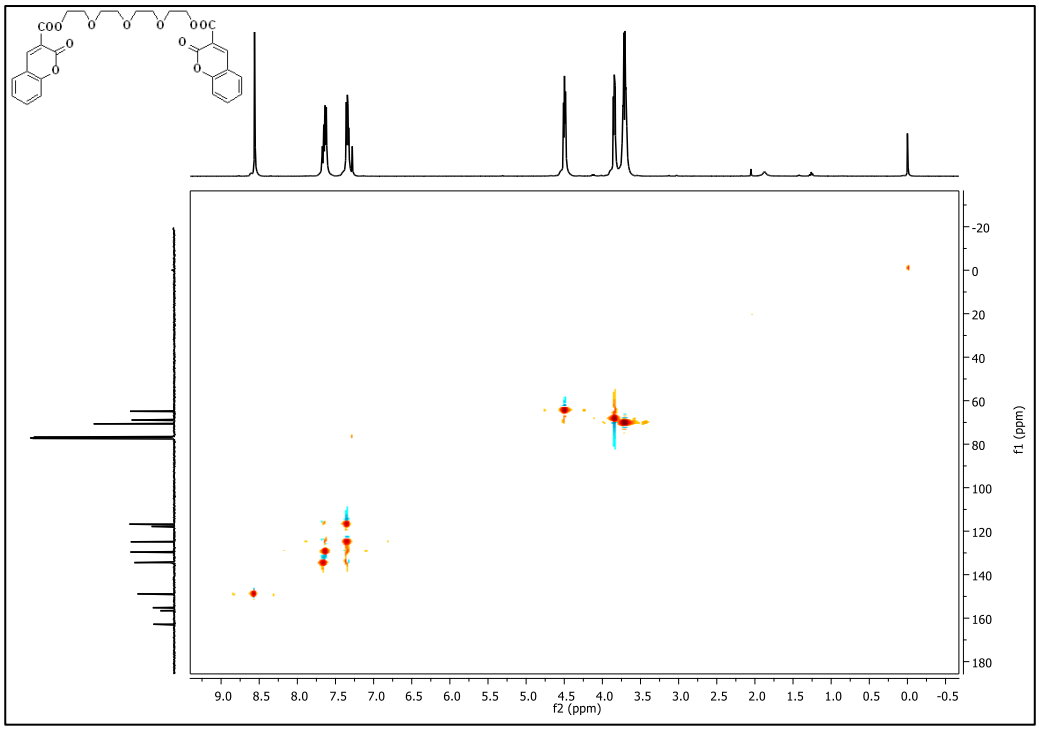

Figure B. 28 HSQC spectrum of compound **18**

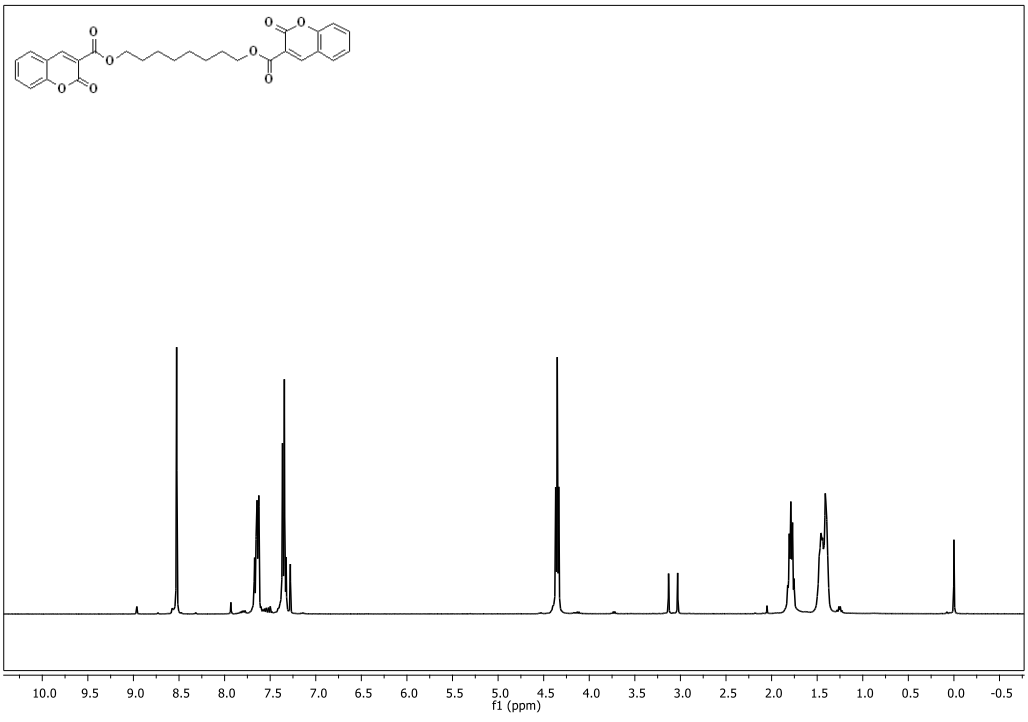

Figure B. 29 ^{1}H NMR spectrum of compound **19**

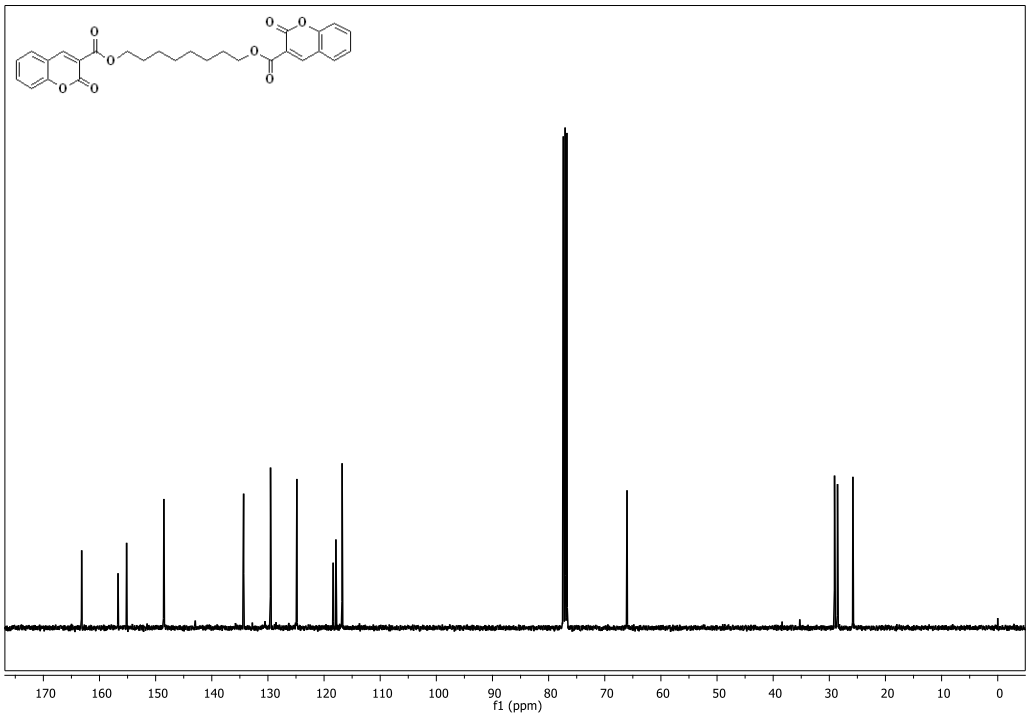

Figure B. 30 ^{13}C NMR spectrum of compound **19**

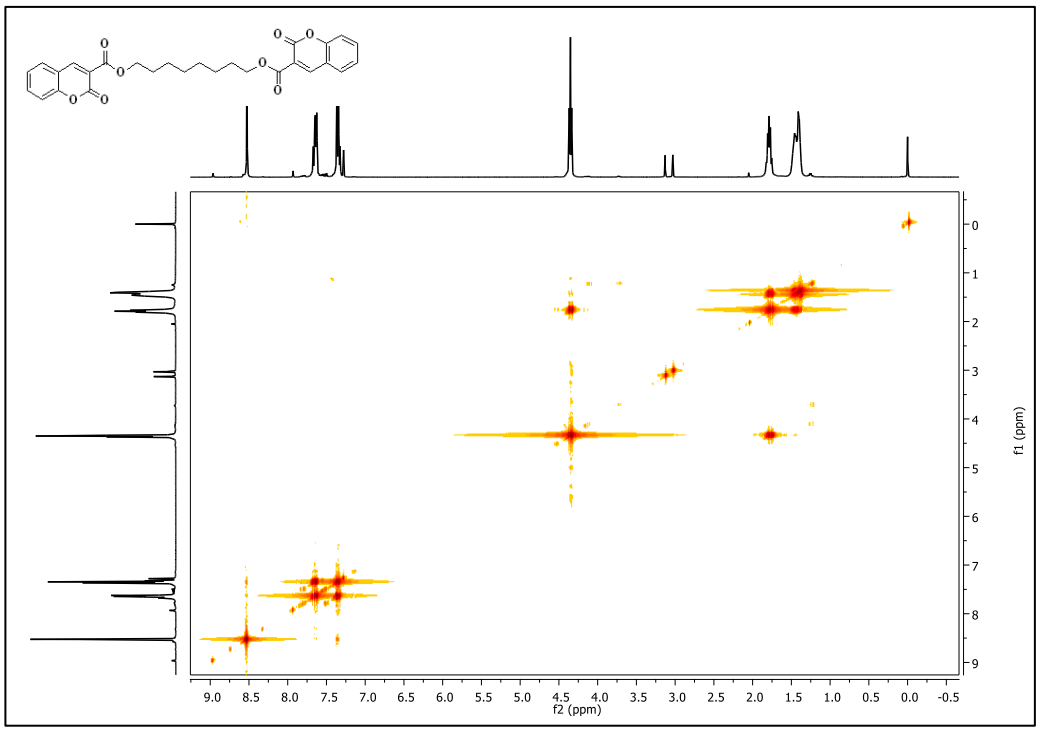

Figure B. 31 COSY spectrum of compound **19**

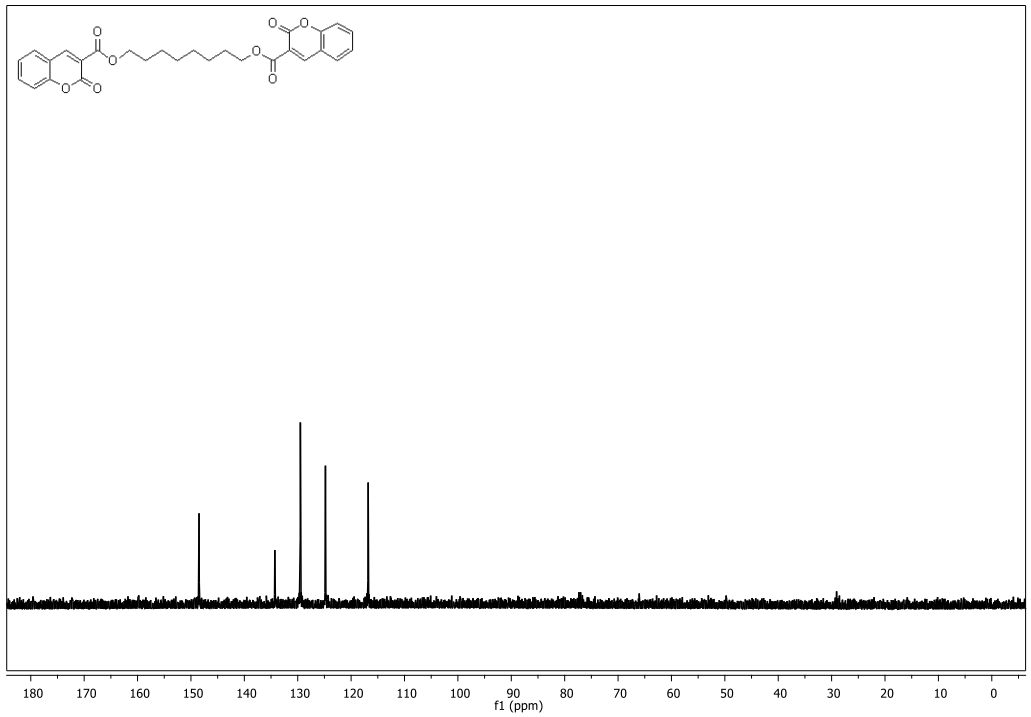

Figure B. 32 DEPT90 spectrum of compound **19**

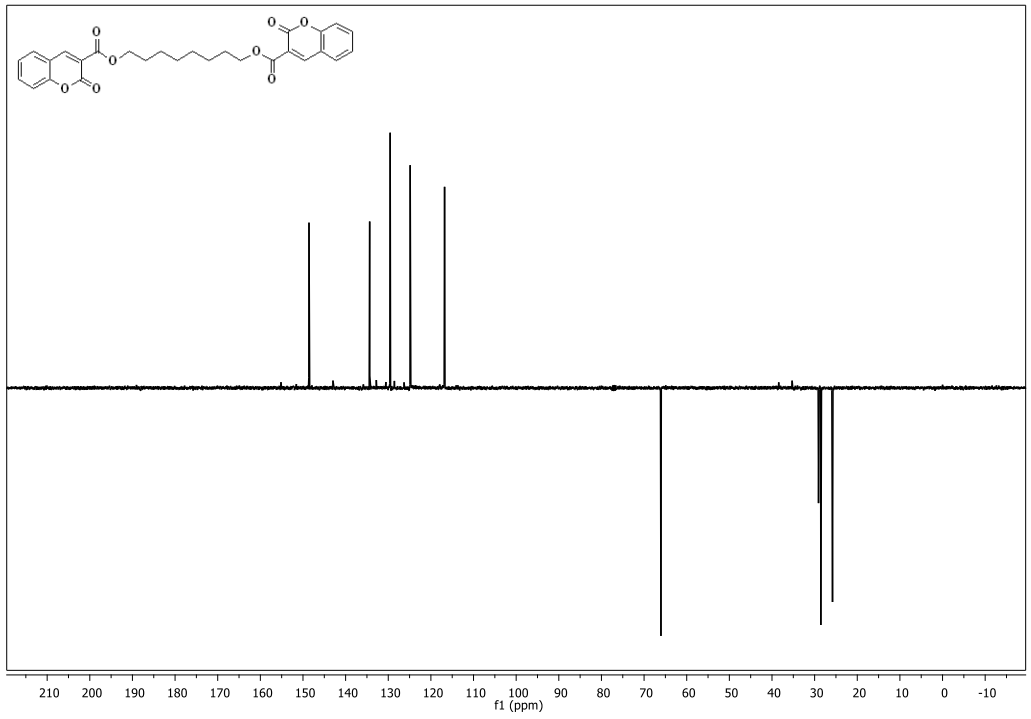

Figure B. 33 DEPT135 spectrum of compound **19**

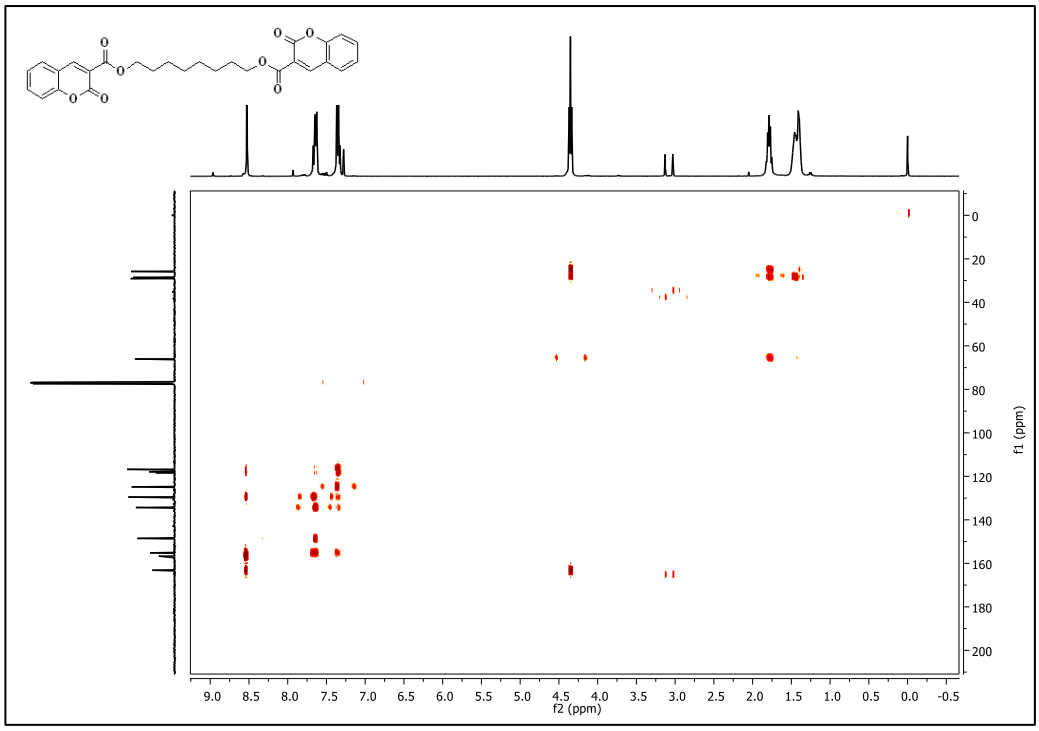

Figure B. 34 HMBC spectrum of compound **19**

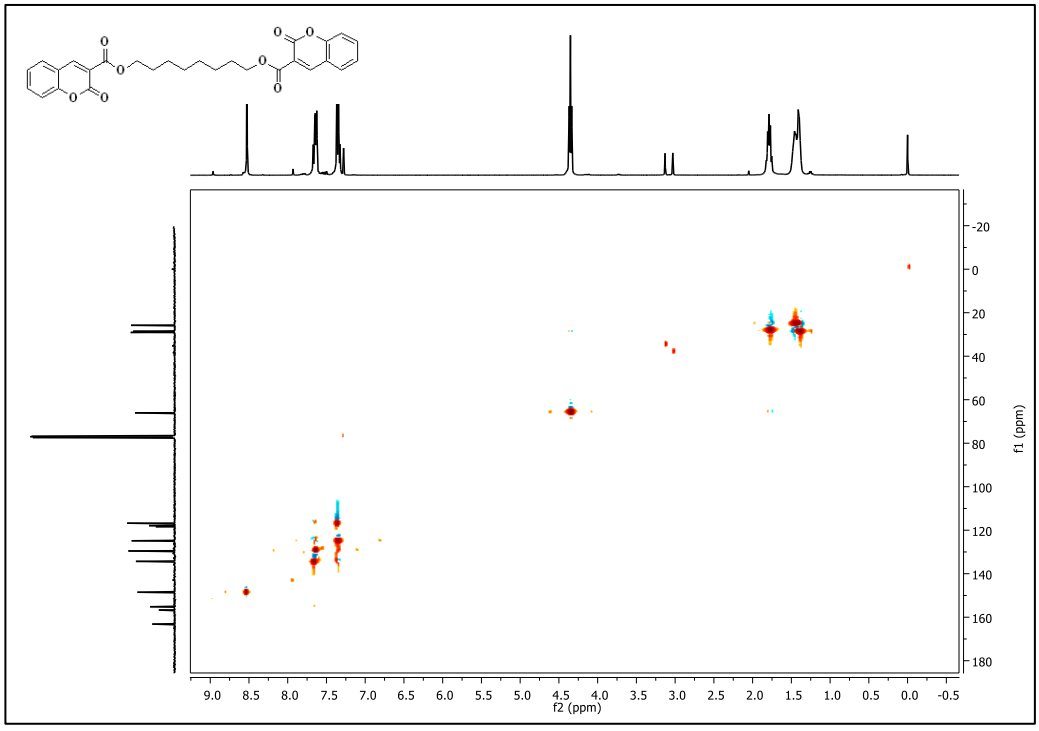

Figure B. 35 HSQC spectrum of compound **19**

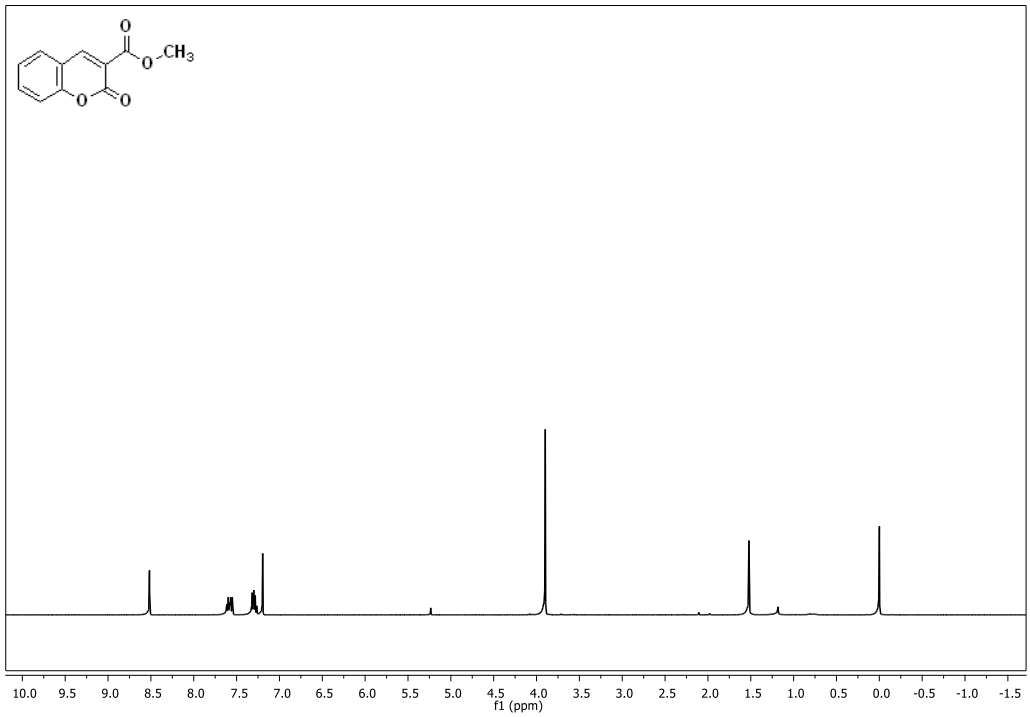

Figure B. 36 ^{1}H NMR spectrum of compound **20**

8.5 IR Spectra

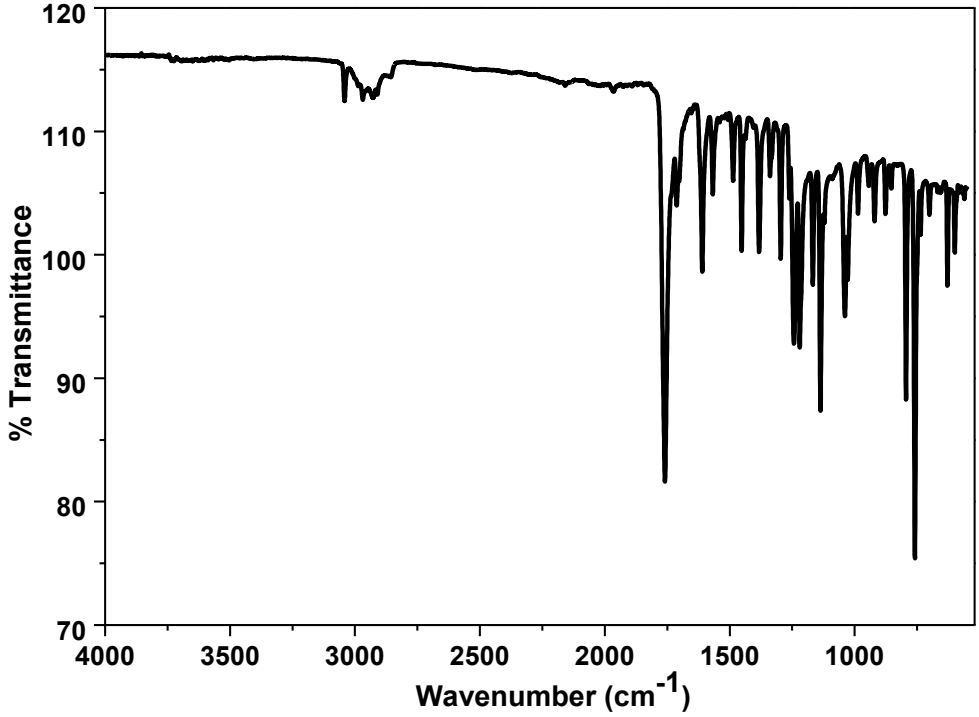

Figure B. 37 IR spectrum of compound **15**

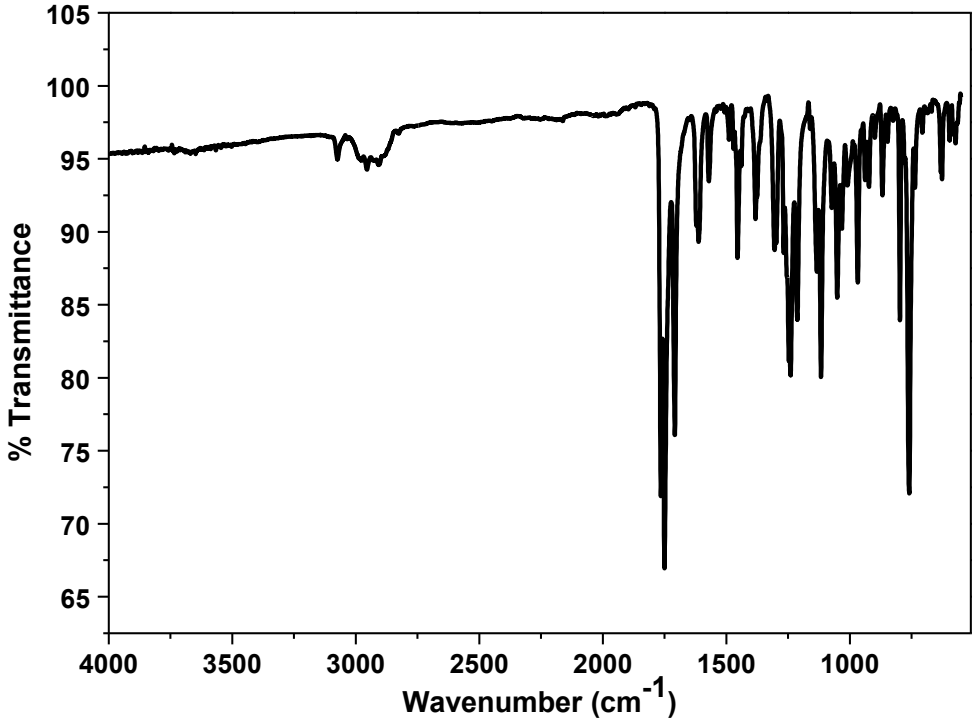

Figure B. 38 IR spectrum of compound **16**

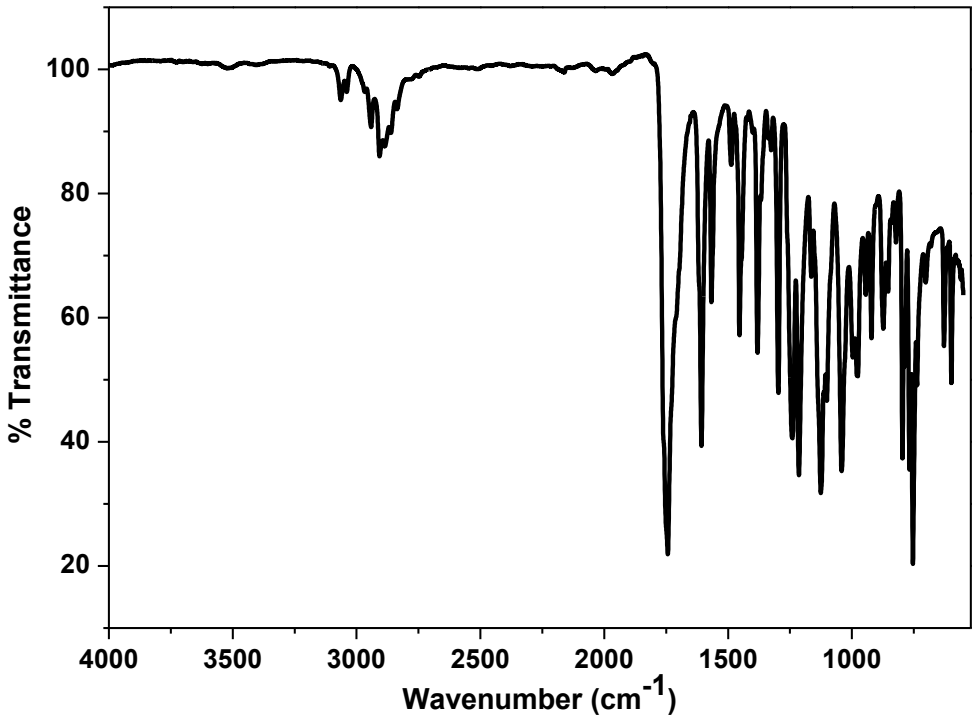

Figure B. 39 IR spectrum of compound **17**

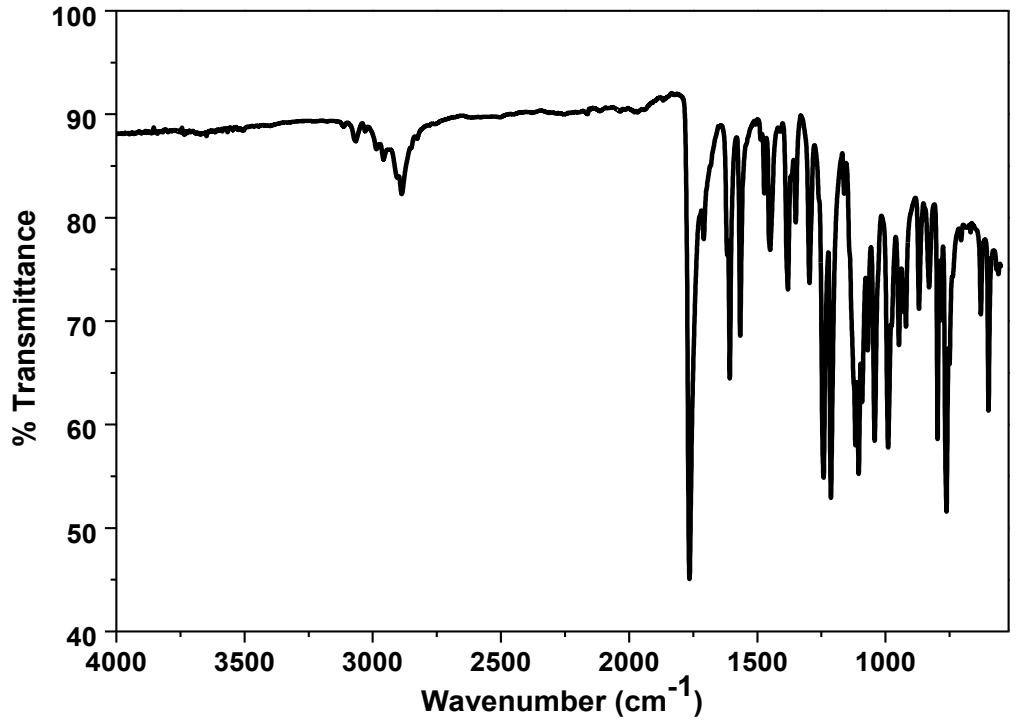

Figure B. 40 IR spectrum of compound **18**

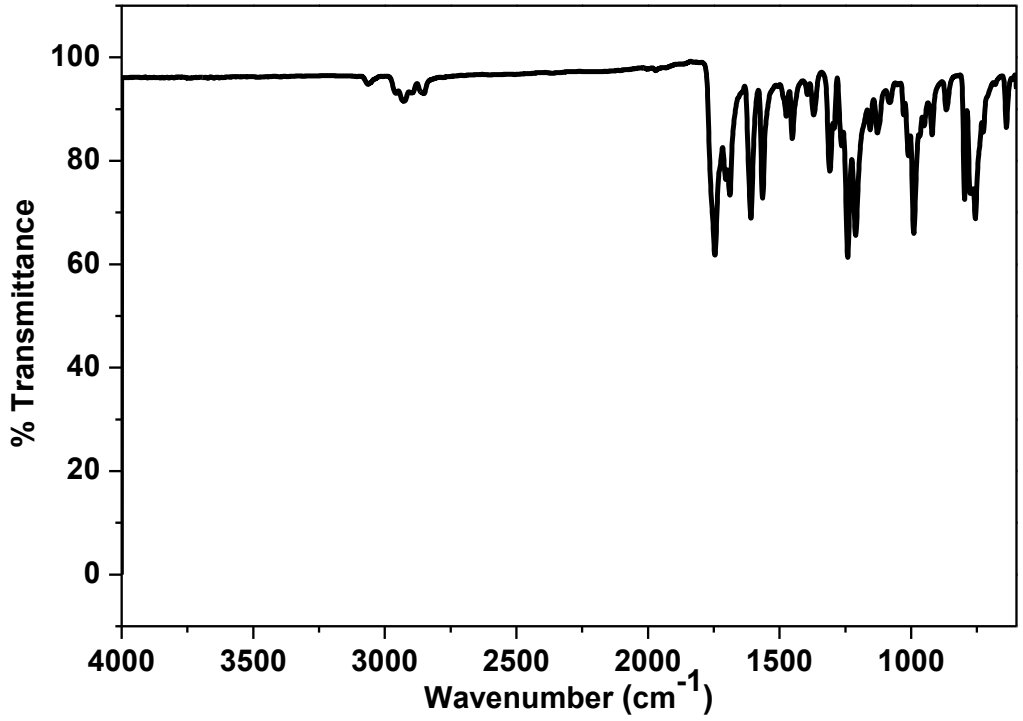

Figure B. 41 IR spectrum of compound **19**

8.6 Mass Spectra

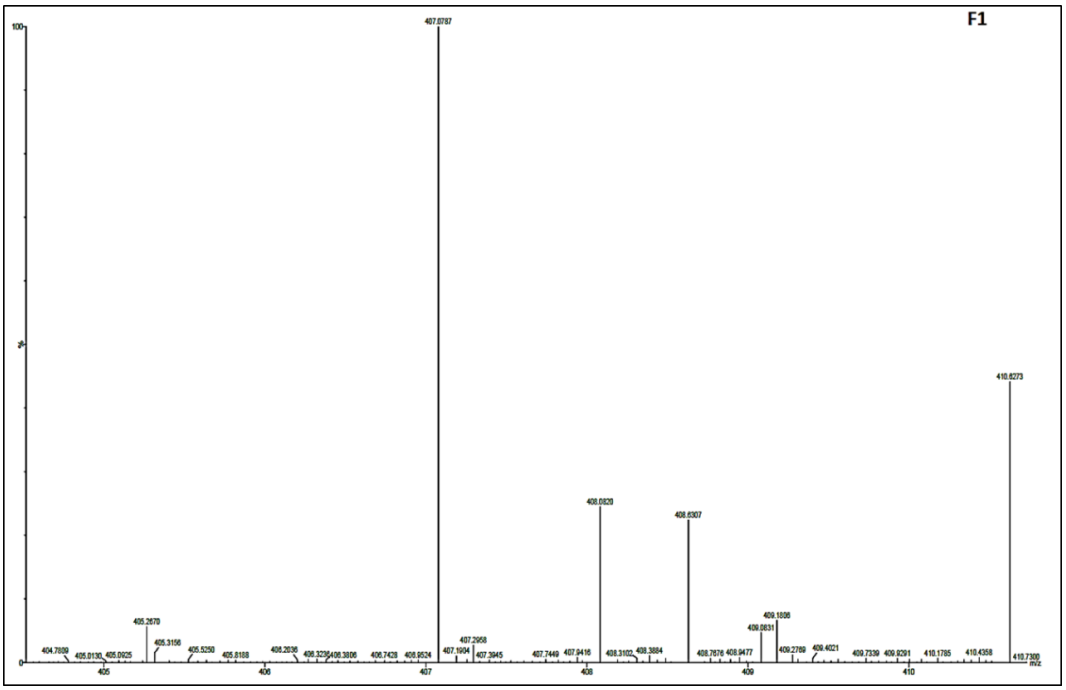

Figure B. 42 HRMS spectrum of compound **15**

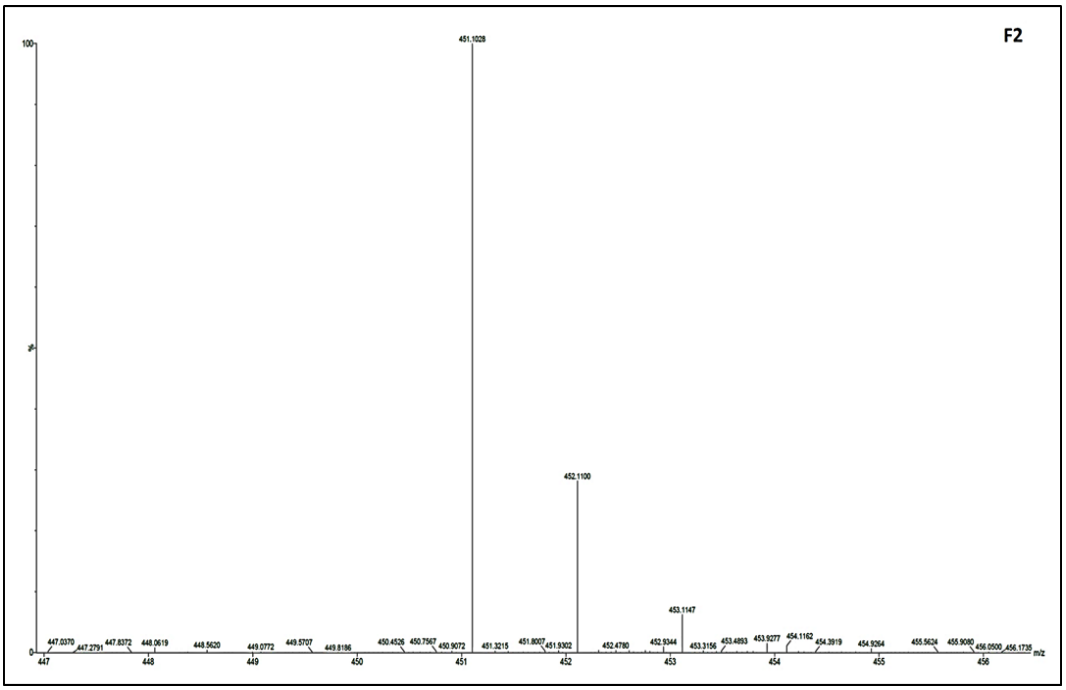

Figure B. 43 HRMS spectrum of compound **16**

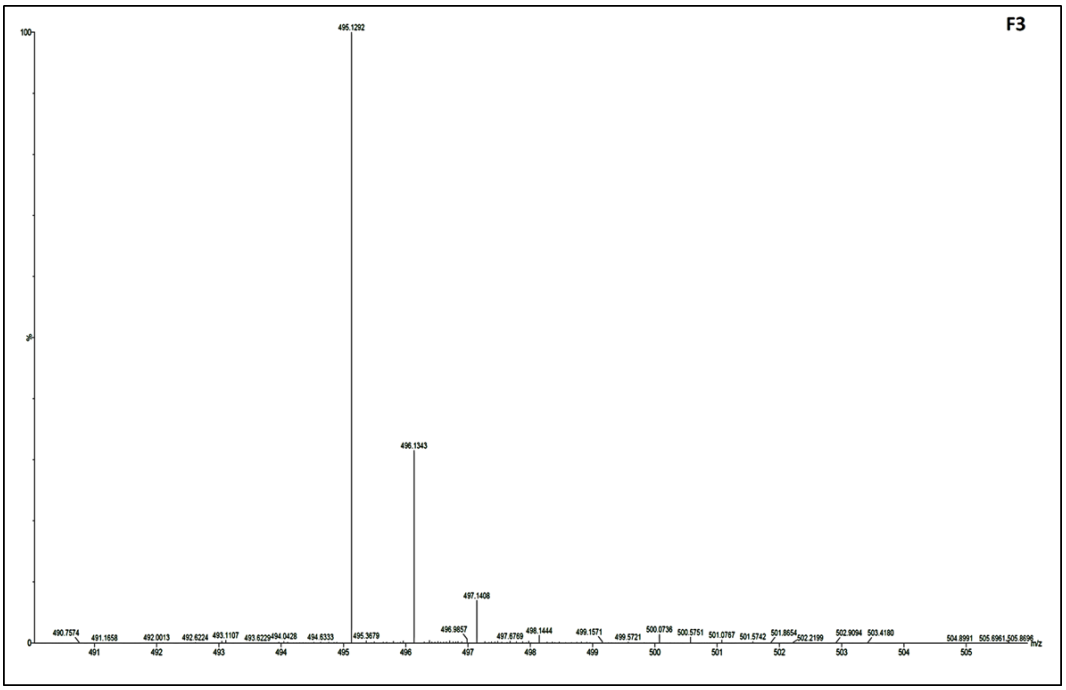

Figure B. 44 HRMS spectrum of compound **17**

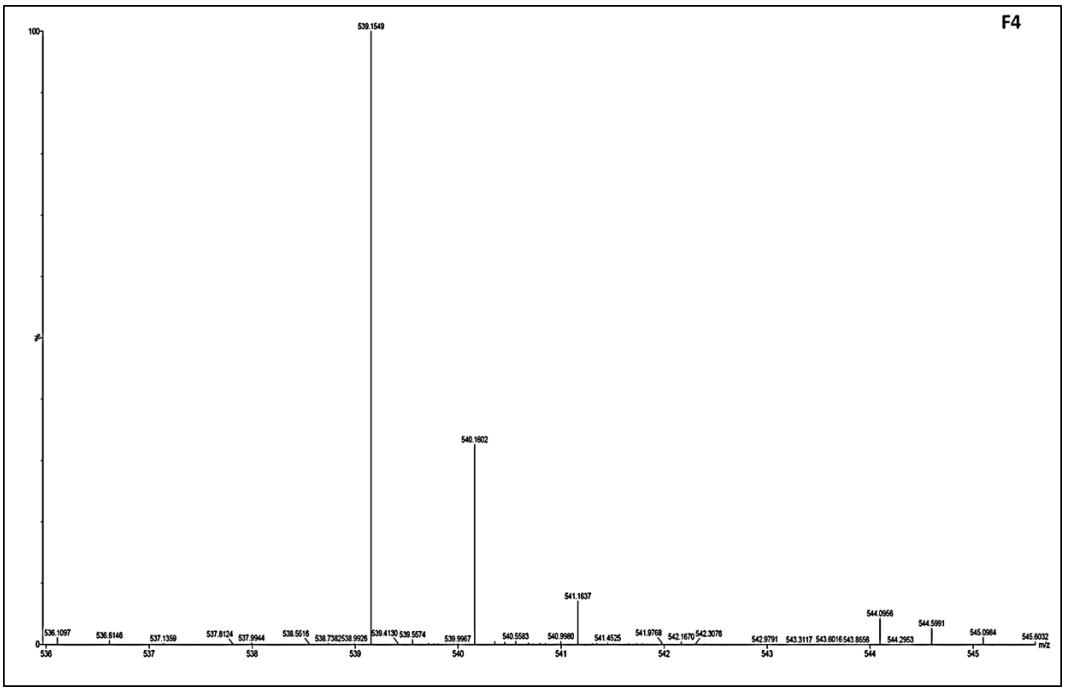

Figure B. 45 HRMS spectrum of compound **18**

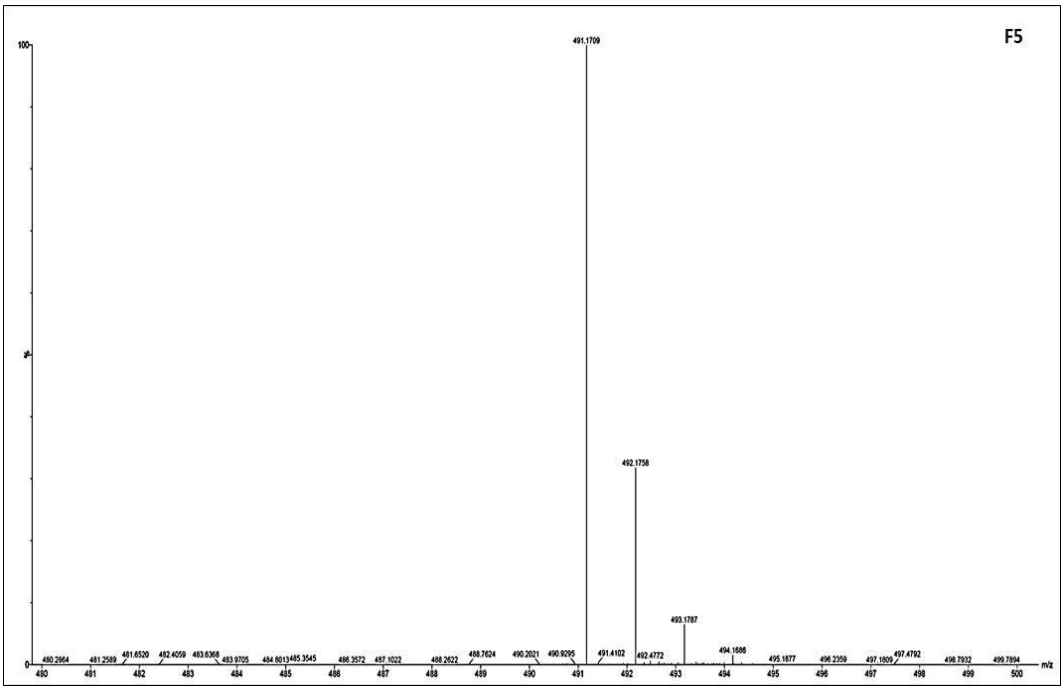

Figure B. 46 HRMS spectrum of compound **19**

8.7 DSC Thermograms

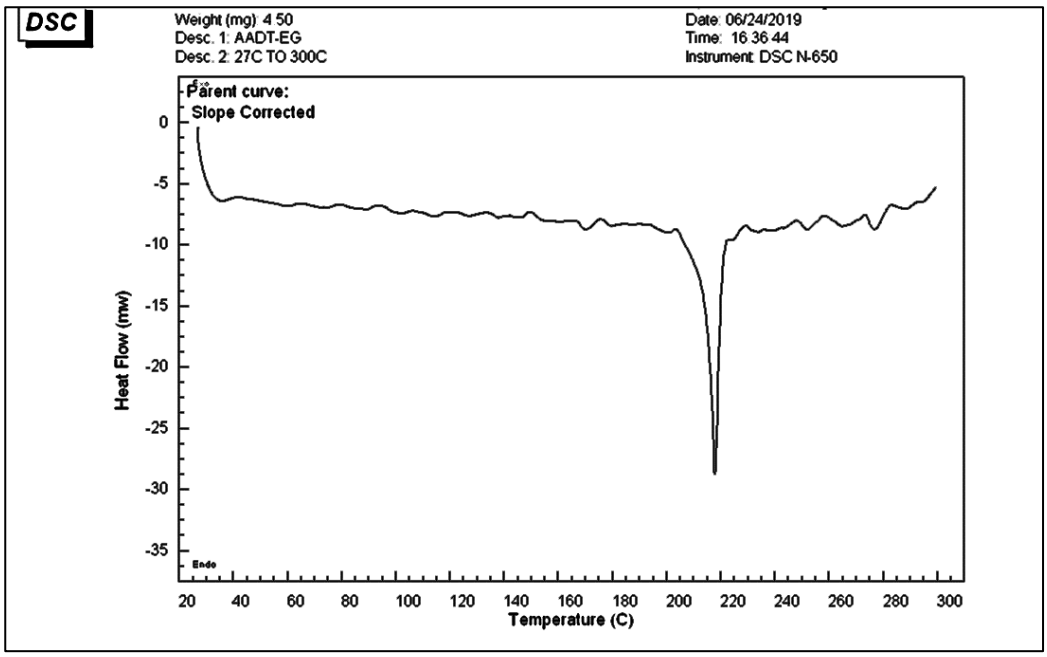

Figure B. 47 DSC thermogram of compound **15**

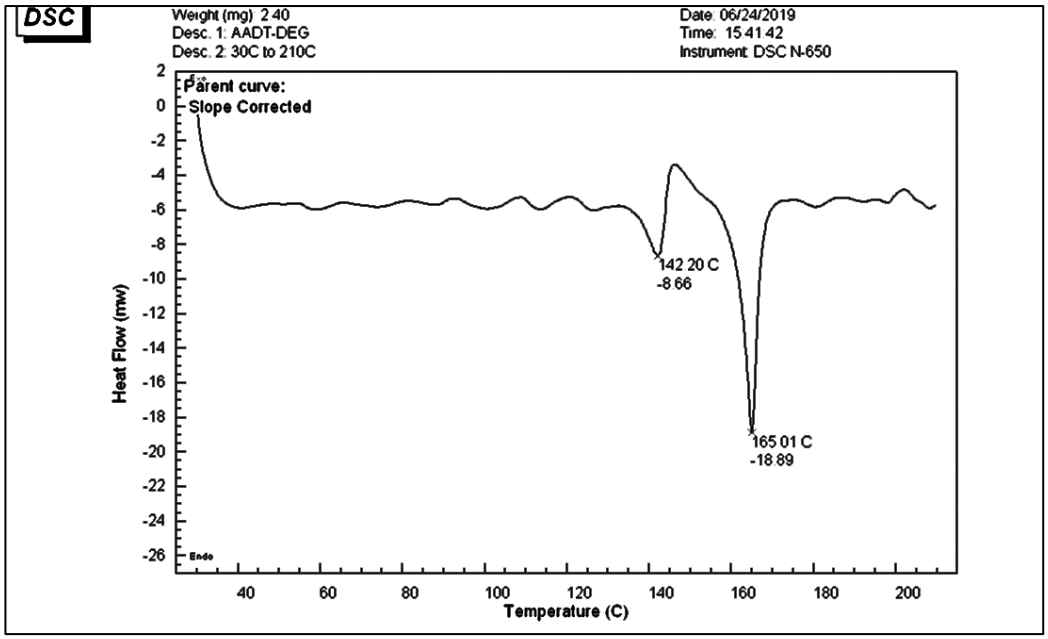

Figure B. 48 DSC thermogram of compound **16**

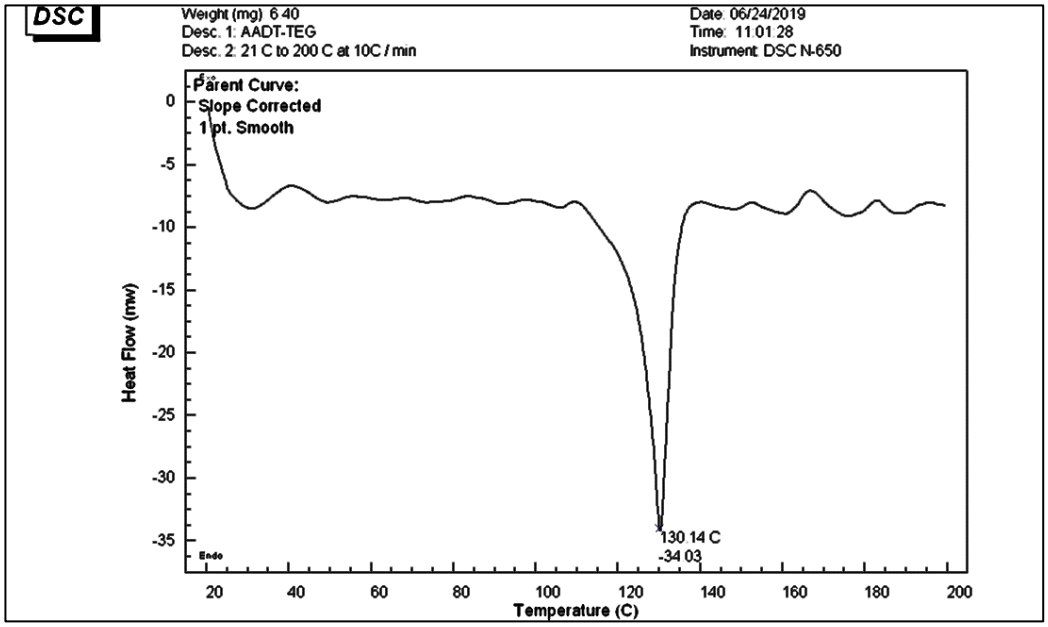

Figure B. 49 DSC thermogram of compound **17**

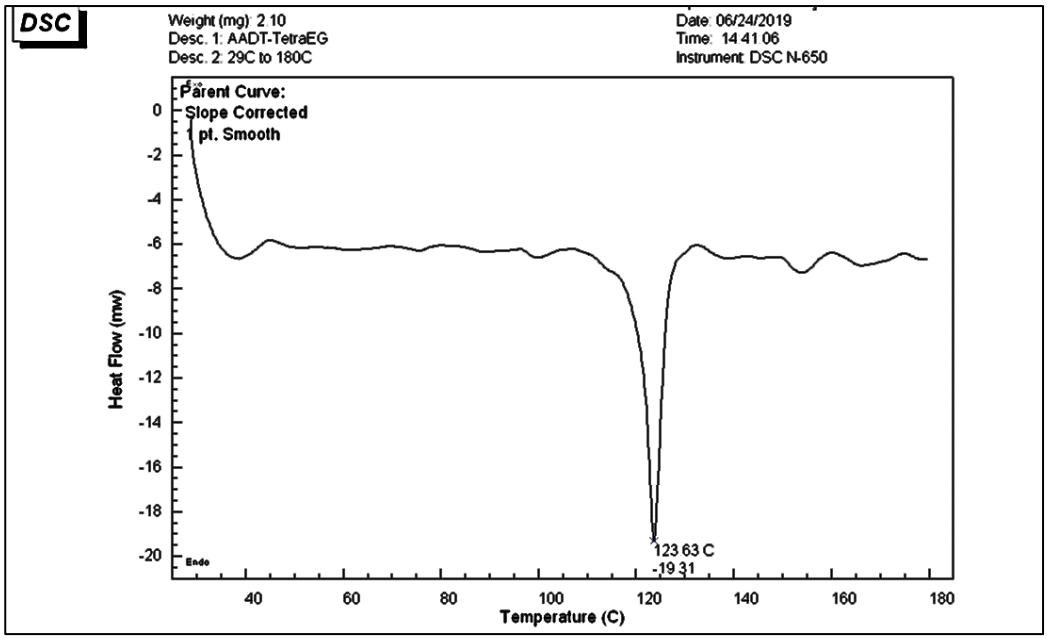

Figure B. 50 DSC thermogram of compound **18**

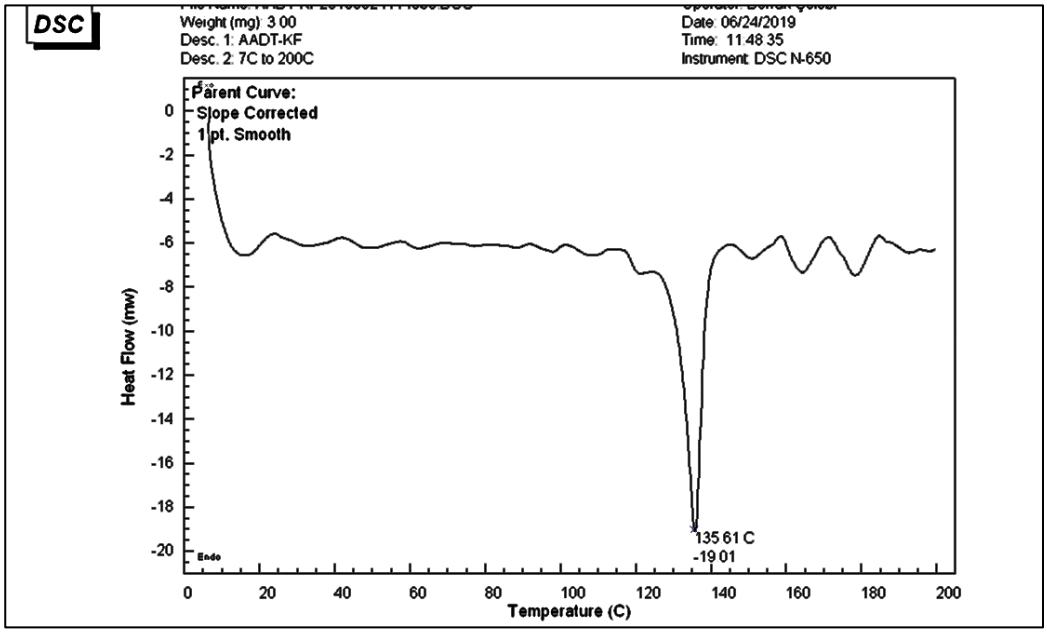

Figure B. 51 DSC thermogram of compound **19**

8.8 UV-Vis Spectra

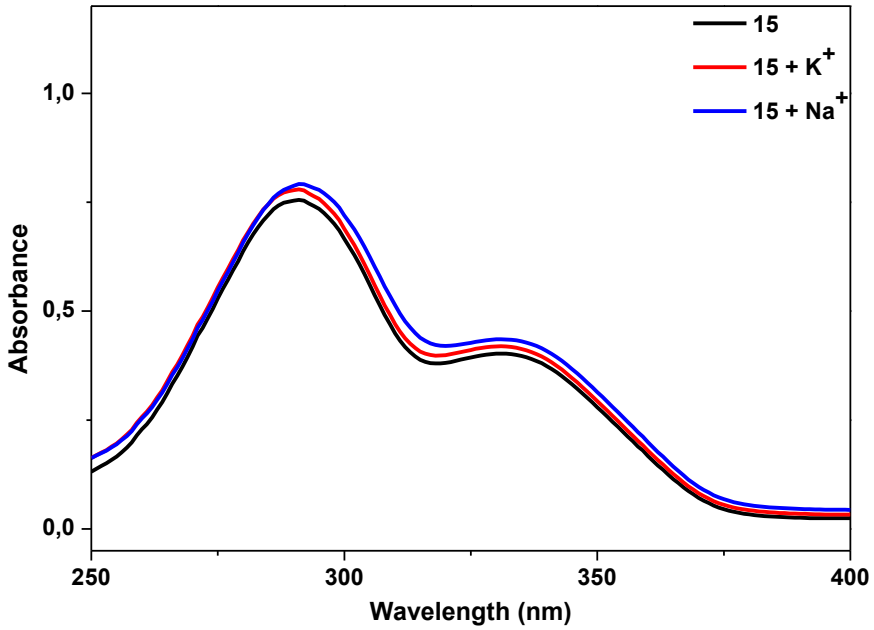

Figure B. 52 UV-Vis spectra of compound **15** in the presence of Na^+ and K^+ cations

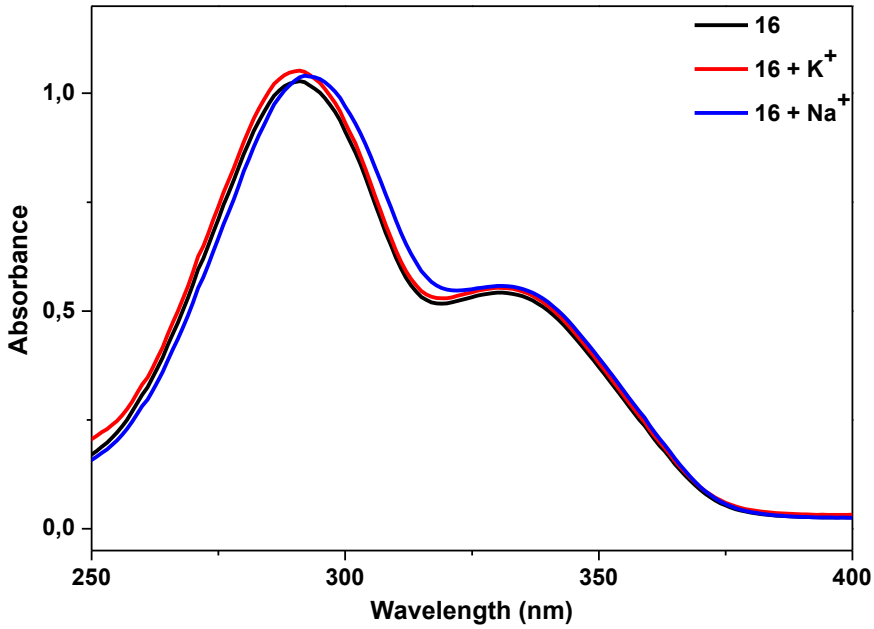

Figure B. 53 UV-Vis spectra of compound **16** in the presence of Na^+ and K^+ cations

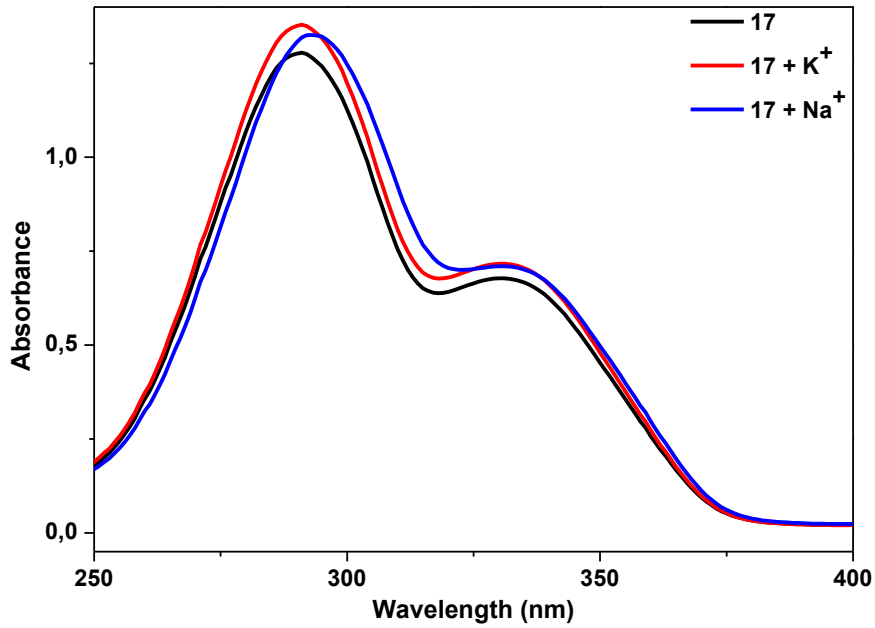

Figure B. 54 UV-Vis spectra of compound **17** in the presence of Na^+ and K^+ cations

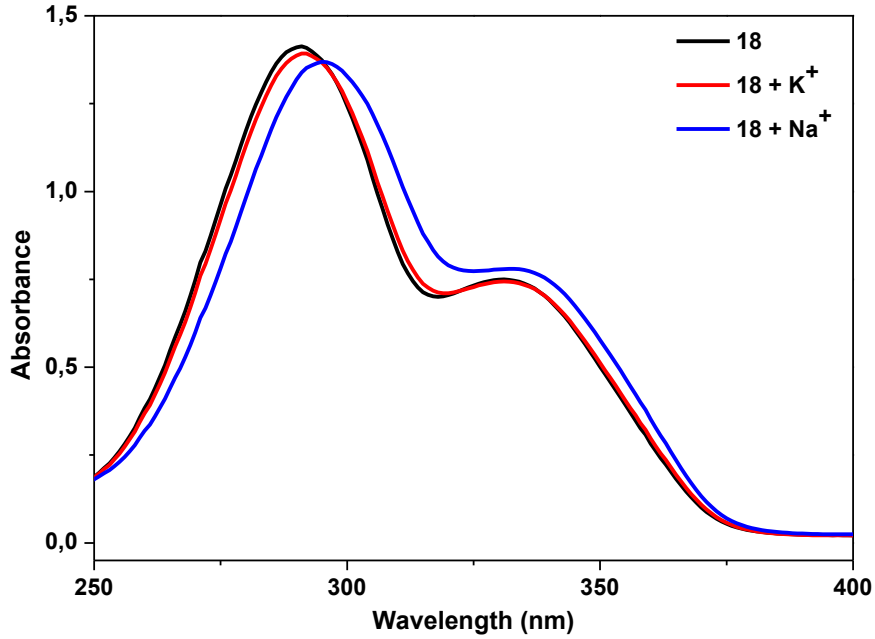

Figure B. 55 UV-Vis spectra of compound **18** in the presence of Na^+ and K^+ cations

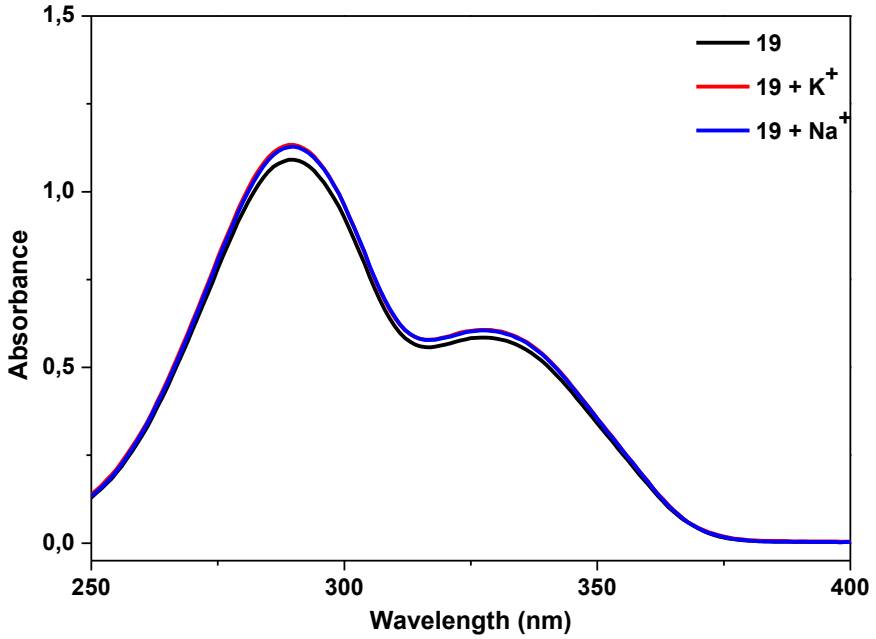

Figure B. 56 UV-Vis spectra of compound **19** in the presence of Na^+ and K^+ cations

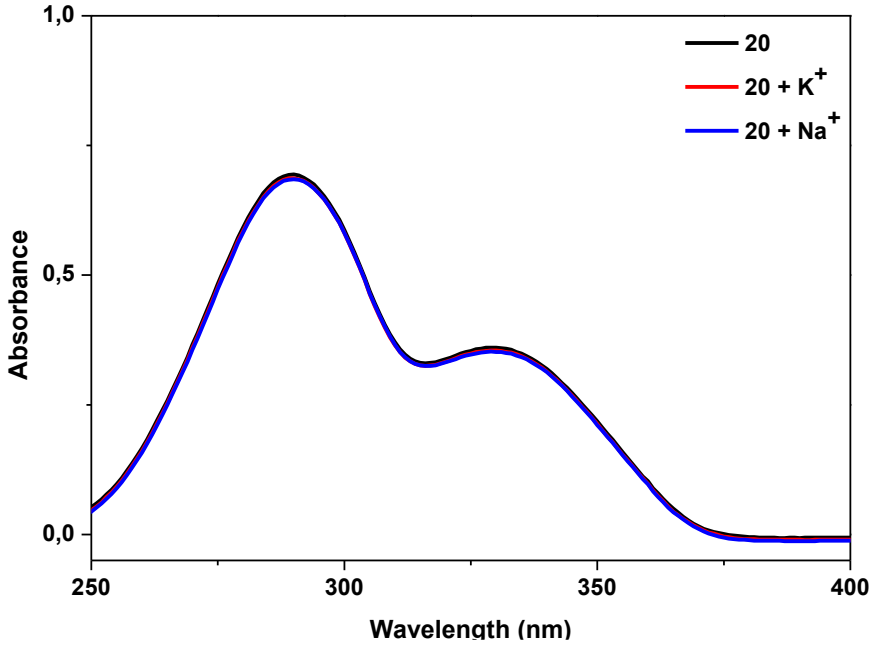

Figure B. 57 UV-Vis spectra of compound **20** in the presence of Na^+ and K^+ cations

8.9 XY Coordinates of Optimized Structures

8.9.1 Optimized structure of 16

6	-5.576438	-2.013087	-1.880316
6	-5.031584	-3.098076	-1.169658
6	-4.010397	-2.906107	-0.242436
6	-3.527762	-1.611151	-0.024960
6	-4.060528	-0.506840	-0.722930
6	-5.094886	-0.729810	-1.657249
6	-3.517637	0.787081	-0.416279
6	-2.534204	0.948957	0.514051
6	-1.939428	-0.222715	1.180051
8	-2.525267	-1.445089	0.872639
6	-2.049737	2.309594	0.910773
8	-2.165787	3.172865	-0.127049
6	-1.705921	4.517548	0.059587
6	-0.349732	4.707519	-0.591241
8	0.603649	3.967799	0.119438
6	1.916559	4.067319	-0.377920
6	2.865147	3.316965	0.537019
8	2.699797	1.896755	0.492813
6	3.381958	1.232916	-0.473773

6	3.197581	-0.244447	-0.343836
6	4.096720	-1.129717	-1.115013
8	3.876416	-2.500571	-0.928231
6	2.926858	-3.024598	-0.121728
6	2.056262	-2.188792	0.610613
6	2.233977	-0.770285	0.471799
6	1.074982	-2.779704	1.438368
6	0.981527	-4.162901	1.529397
6	1.862010	-4.977610	0.794536
6	2.833137	-4.418687	-0.032580
8	-0.993403	-0.234601	1.921624
8	4.982547	-0.819074	-1.856496
8	-1.662122	2.604621	2.008484
8	4.047627	1.793202	-1.308462
1	-3.572276	-3.735042	0.315644
1	0.224272	-4.618061	2.171481
1	1.786263	-6.065498	0.870206
1	3.524973	-5.032731	-0.611490
1	0.389831	-2.128066	1.985251
1	1.577506	-0.100636	1.032638
1	3.900126	3.571579	0.265847
1	2.666461	3.601377	1.579862

1	1.990567	3.675832	-1.411151
1	2.243211	5.129019	-0.407944
1	-0.395624	4.389956	-1.653966
1	-0.107406	5.792719	-0.584705
1	-1.646933	4.739169	1.134402
1	-2.448111	5.172207	-0.421215
1	-3.913722	1.665766	-0.930292
1	-5.509799	0.123615	-2.199625
1	-6.376212	-2.181451	-2.604392
1	-5.411564	-4.107249	-1.346262

8.9.2 Optimized structure of 16 + Na^+

6	5.061004	-3.471467	-0.034308
6	4.433804	-2.225473	0.035963
6	4.892519	-1.125464	-0.722654
6	6.011050	-1.303677	-1.570750
6	6.637100	-2.538154	-1.647456
6	6.159673	-3.617464	-0.877810
6	4.195651	0.111267	-0.568081
6	3.123326	0.231991	0.278671
6	2.649077	-0.938987	1.030173
8	3.359454	-2.095440	0.858315

6	2.438223	1.538057	0.492424
8	1.634562	1.759913	1.377358
8	1.690092	-0.987160	1.771330
8	2.831257	2.459097	-0.392812
6	2.368699	3.817787	-0.255420
6	1.184901	4.135169	-1.148967
8	0.000090	3.612208	-0.599295
6	-1.184607	4.134947	-1.149390
6	-2.368598	3.817814	-0.255991
8	-2.831155	2.459086	-0.393218
6	-2.438314	1.538190	0.492243
8	-1.634756	1.760158	1.377245
6	-3.123414	0.232100	0.278580
6	-4.195856	0.111356	-0.568005
6	-4.892700	-1.125412	-0.722507
6	-4.433756	-2.225455	0.035917
8	-3.359216	-2.095399	0.858051
6	-2.649033	-0.938878	1.030018
6	-6.011395	-1.303635	-1.570367
6	-6.637371	-2.538164	-1.647046
6	-6.159709	-3.617495	-0.877598
6	-5.060861	-3.471487	-0.034317

8	-1.690030	-0.986927	1.771157
11	0.000110	0.430046	2.279417
1	-4.679360	-4.297241	0.568068
1	7.500524	-2.676563	-2.300849
1	6.658415	-4.587446	-0.941169
1	4.679685	-4.297193	0.568235
1	6.371573	-0.456280	-2.158895
1	4.530996	0.986481	-1.128515
1	3.225396	4.437367	-0.555108
1	2.110747	4.013778	0.794307
1	1.367163	3.749748	-2.172874
1	1.122840	5.240632	-1.223809
1	-1.366660	3.749158	-2.173200
1	-1.122556	5.240384	-1.224652
1	-2.110816	4.013982	0.793745
1	-3.225241	4.437335	-0.555945
1	-4.531370	0.986562	-1.128345
1	-6.372120	-0.456225	-2.158367
1	-7.500923	-2.676571	-2.300266
1	-6.658389	-4.587512	-0.940929

8.9.3 Optimized structure of 16 + K^+

6	4.903761	-3.548147	0.057495
6	4.319072	-2.279138	0.067791
6	4.662644	-1.303571	-0.893699
6	5.617529	-1.631264	-1.884673
6	6.199885	-2.889471	-1.902487
6	5.840793	-3.843120	-0.929801
6	4.024446	-0.029543	-0.788489
6	3.112876	0.242931	0.198738
6	2.748479	-0.803038	1.168297
8	3.403394	-2.003269	1.031872
6	2.501695	1.597180	0.339521
8	1.856529	1.973473	1.295586
8	1.931435	-0.721599	2.056373
8	2.779769	2.373109	-0.718529
6	2.381619	3.755760	-0.706165
6	1.177224	4.016984	-1.587442
8	-0.001804	3.579423	-0.955202
6	-1.181231	4.017614	-1.586289
6	-2.385013	3.755792	-0.704342
8	-2.782788	2.373103	-0.716925
6	-2.502490	1.596494	0.340064

8	-1.856344	1.972579	1.295529
6	-3.112861	0.241896	0.199073
6	-4.025651	-0.030482	-0.787080
6	-4.662922	-1.304937	-0.892478
6	-4.317050	-2.281081	0.067619
8	-3.400314	-2.005296	1.030637
6	-2.746211	-0.804514	1.167223
6	-5.618958	-1.632561	-1.882385
6	-6.200224	-2.891249	-1.900528
6	-5.838816	-3.845505	-0.929270
6	-4.900618	-3.550630	0.056920
8	-1.928094	-0.723221	2.054308
19	0.000671	0.886324	2.914283
1	-4.610981	-4.278639	0.816156
1	6.937363	-3.142975	-2.666348
1	6.304256	-4.832353	-0.947120
1	4.615880	-4.275692	0.817841
1	5.888077	-0.879370	-2.630032
1	4.277503	0.752931	-1.506669
1	3.245217	4.311454	-1.099066
1	2.171510	4.069317	0.325273
1	1.315260	3.526867	-2.572809

1	1.135864	5.110789	-1.771393
1	-1.320028	3.528192	-2.571894
1	-1.139843	5.111542	-1.769473
1	-2.174421	4.069147	0.327065
1	-3.248977	4.311426	-1.096529
1	-4.280335	0.752414	-1.504222
1	-5.891230	-0.880182	-2.626626
1	-6.938604	-3.144712	-2.663531
1	-6.301409	-4.835142	-0.946861

C. Characterization and Fluorescence data for Schiff base

8.10 NMR spectra

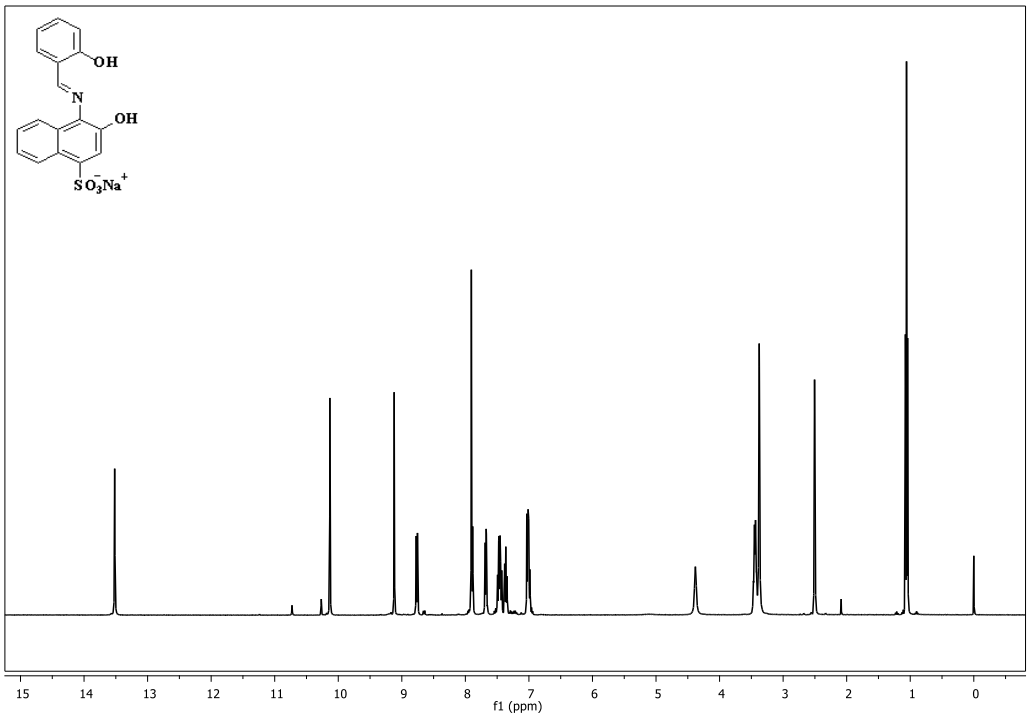

Figure C. 1 ^{1}H NMR spectrum of compound **21**

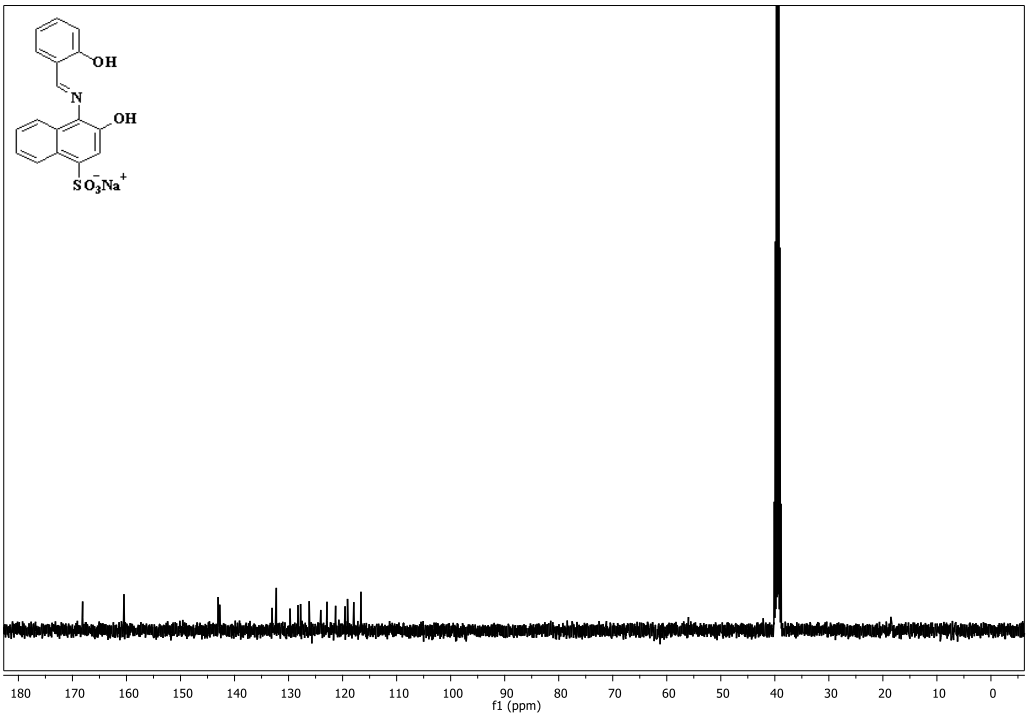

Figure C. 2 ^{13}C NMR spectrum of compound **21**

8.11 XY Coordinates of Optimized Structures

8.11.1 For 21-C1

C	4.543270	-1.132519	6.248142
C	3.449686	-0.256342	6.209107
C	3.338054	0.749267	7.196922
C	4.324448	0.845436	8.179926
C	5.391073	-0.029057	8.187636
C	5.511893	-1.029065	7.220610
C	2.454925	-0.413416	5.175554
N	1.447777	0.367156	5.053861

C	0.510594	0.167670	4.038244
C	0.828827	0.337668	2.661977
C	-0.176859	0.143150	1.665561
C	-1.483161	-0.184784	2.110723
C	-1.773058	-0.334253	3.441821
C	-0.782810	-0.142885	4.413075
C	2.126635	0.724353	2.246313
C	2.427820	0.872057	0.922403
C	1.446097	0.644621	-0.058890
C	0.175081	0.299374	0.302627
S	-2.741459	-0.545582	0.906359
O	-4.065603	-0.649558	1.840513
O	-1.038697	-0.286144	5.732816
O	2.328133	1.612178	7.238798
O	-2.945131	0.597509	0.046216
O	-2.509502	-1.854434	0.365786
H	-0.575175	0.162936	-0.470064
H	1.693978	0.760615	-1.110860
H	3.428812	1.176023	0.625561
H	2.884934	0.925706	2.997362
H	4.612328	-1.906786	5.484368
H	6.354635	-1.714144	7.237632

H	6.147810	0.064598	8.963537
H	4.218503	1.625130	8.929752
H	2.598367	-1.260194	4.483311
H	-2.778610	-0.610850	3.750857
H	-4.603310	0.145567	1.716357
H	-1.967992	-0.496803	5.869522
H	1.705194	1.415130	6.503091

8.11.2 For 21-C2

C	-6.945941	1.661035	2.430747
C	-6.228329	0.676581	1.708950
C	-4.814257	0.820681	1.566250
C	-4.195901	1.973161	2.110455
C	-4.922602	2.910585	2.787707
C	-6.308865	2.746856	2.960006
C	-6.834897	-0.457508	1.110851
C	-6.107766	-1.362718	0.383907
C	-4.722021	-1.215025	0.245638
C	-4.068388	-0.154881	0.845611
N	-2.691521	-0.053807	0.645896
C	-1.875499	-0.083759	1.631664
C	-0.445762	0.022296	1.467778

C	0.147470	0.109146	0.186620
C	1.536946	0.201291	0.088813
C	2.319102	0.207187	1.224676
C	1.747070	0.118365	2.495658
C	0.377962	0.024961	2.602292
O	-0.558320	0.102454	-0.939085
S	-8.600013	-0.637556	1.223383
O	-8.821788	-2.082520	0.515454
O	-3.975551	-2.105381	-0.445804
O	-8.992069	-0.802494	2.604738
O	-9.226388	0.346308	0.386917
H	-8.018603	1.560160	2.565455
H	-6.879785	3.494004	3.505234
H	-4.428446	3.792665	3.187984
H	-3.130577	2.123315	1.961962
H	-0.092906	-0.048741	3.582365
H	2.372818	0.121393	3.383553
H	3.399802	0.280590	1.124011
H	1.971572	0.266670	-0.905251
H	-2.241382	-0.203174	2.665453
H	-6.604778	-2.211244	-0.080476
H	-4.545399	-2.750393	-0.876916

H	-9.102567	-2.721233	1.186250
H	-1.514180	0.018599	-0.720082

8.11.3 For 21-C3

C	4.461275	-0.552278	-4.601932
C	4.759992	0.094175	-3.322759
C	5.961926	0.841762	-3.153300
C	6.870612	0.942916	-4.155728
C	6.601813	0.307126	-5.399880
C	5.456971	-0.392558	-5.623714
C	3.804519	0.090846	-2.319114
N	2.731610	-0.697440	-2.356651
C	1.478334	-0.431379	-1.758775
C	1.295442	-0.409576	-0.353583
C	0.014675	-0.080689	0.176292
C	-1.032853	0.167269	-0.757578
C	-0.836552	0.114514	-2.106465
C	0.434645	-0.195479	-2.629636
C	2.345869	-0.720740	0.539319
C	2.149191	-0.678177	1.892303
C	0.895031	-0.323865	2.416499
C	-0.150028	-0.042499	1.579624

S	-2.628313	0.653953	-0.126035
O	-2.534926	1.999506	0.362341
O	0.538825	-0.218232	-3.965099
O	3.394765	-1.182117	-4.810857
O	-3.523236	0.704073	-1.472085
O	-3.166933	-0.409497	0.689782
H	-1.119065	0.197743	2.006305
H	0.747090	-0.289250	3.492545
H	2.965059	-0.930203	2.565520
H	3.309895	-1.025391	0.139874
H	6.138561	1.325640	-2.192528
H	7.789415	1.506341	-4.021754
H	7.336029	0.392295	-6.199550
H	5.251460	-0.868360	-6.579377
H	3.891404	0.766753	-1.464732
H	-1.634134	0.331223	-2.809139
H	1.443936	-0.386597	-4.285564
H	2.743388	-1.306847	-3.186876
H	-4.086145	-0.082138	-1.520275

8.11.4 For 21-C4

C	0.167890	0.053153	0.188193
C	-0.439669	0.058160	1.465394
C	0.376115	0.128127	2.605312
C	1.747128	0.181702	2.503600
C	2.331417	0.167106	1.235063
C	1.558049	0.105991	0.094204
C	-1.869329	-0.011857	1.628020
N	-2.686129	-0.121798	0.640940
C	-4.072682	-0.165509	0.844430
C	-4.808143	0.811578	1.577193
C	-6.221559	0.664233	1.719337
C	-6.836077	-0.453310	1.088361
C	-6.124285	-1.341983	0.333777
C	-4.735981	-1.196187	0.205116
C	-4.194176	1.961277	2.128540
C	-4.921494	2.889515	2.820223
C	-6.303548	2.716144	3.002223
C	-6.938056	1.634722	2.458256
S	-8.600778	-0.643284	1.234173
O	-8.945644	-0.882438	2.617132
O	-4.086029	-2.117877	-0.526967

O	-0.534512	-0.001506	-0.942378
O	-9.247343	0.386721	0.472299
O	-8.853503	-2.037046	0.449338
H	-8.010520	1.530815	2.591363
H	-6.875068	3.452704	3.560846
H	-4.428652	3.771333	3.222846
H	-3.131859	2.127151	1.972878
H	-0.103003	0.136495	3.583815
H	2.366333	0.234108	3.394379
H	3.414168	0.207499	1.140042
H	2.000989	0.098083	-0.898155
H	-2.242991	0.021133	2.663661
H	-6.601183	-2.173989	-0.173100
H	-3.146371	-1.886506	-0.543318
H	-9.029490	-2.741202	1.089636
H	-1.490783	0.019766	-0.721104

8.11.5 For 21-C5

C	0.215189	-0.367249	0.202768
C	-0.405183	0.097614	1.379598
C	0.414694	0.527615	2.428221
C	1.792698	0.536522	2.333855

C	2.385785	0.091193	1.160665
C	1.603483	-0.359668	0.111032
C	-1.844090	0.153896	1.586211
N	-2.705244	-0.039936	0.669804
C	-4.079981	-0.037122	0.861181
C	-4.843049	0.851598	1.674979
C	-6.255957	0.663172	1.783299
C	-6.841791	-0.396397	1.034826
C	-6.111548	-1.179588	0.184614
C	-4.726237	-0.992491	0.085291
C	-4.266781	1.964537	2.331780
C	-5.022595	2.806715	3.099636
C	-6.399868	2.580324	3.256186
C	-7.002191	1.541121	2.603585
S	-8.601602	-0.643993	1.153133
O	-8.942795	-1.023702	2.505383
O	-4.034353	-1.783219	-0.743446
O	-0.543399	-0.831097	-0.811148
O	-9.277448	0.434402	0.489425
O	-8.822054	-1.961440	0.236131
H	-8.073390	1.401396	2.712084
H	-6.994603	3.245425	3.876869

H	-4.556458	3.663156	3.581466
H	-3.212379	2.180571	2.189141
H	-0.065658	0.872339	3.343181
H	2.400186	0.884557	3.164242
H	3.468306	0.087418	1.059233
H	2.074607	-0.719373	-0.804443
H	-2.142884	0.363266	2.627019
H	-6.573176	-1.953357	-0.419343
H	-3.109961	-1.470347	-0.718964
H	-8.929280	-2.736815	0.805193
H	0.031245	-1.124511	-1.527732

D. Characterization and Fluorescence data for chiral diaminodicyanoquinones

8.12 NMR spectra

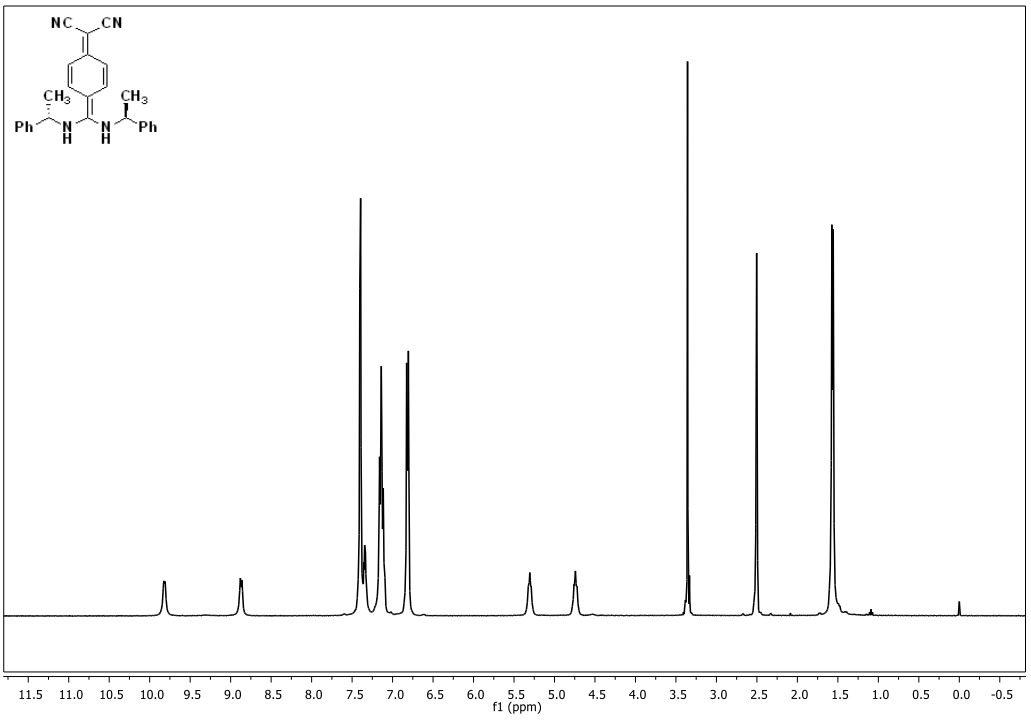

Figure D. 1 ^{1}H NMR spectrum of compound **22**

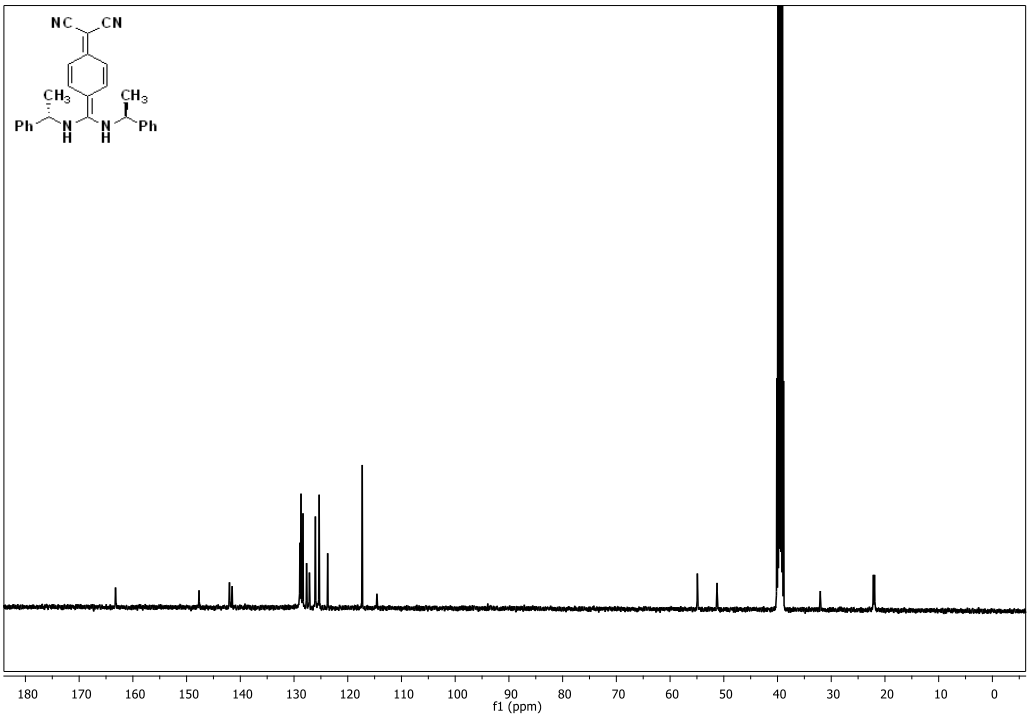

Figure D. 2 ^{13}C NMR spectrum of compound **22**

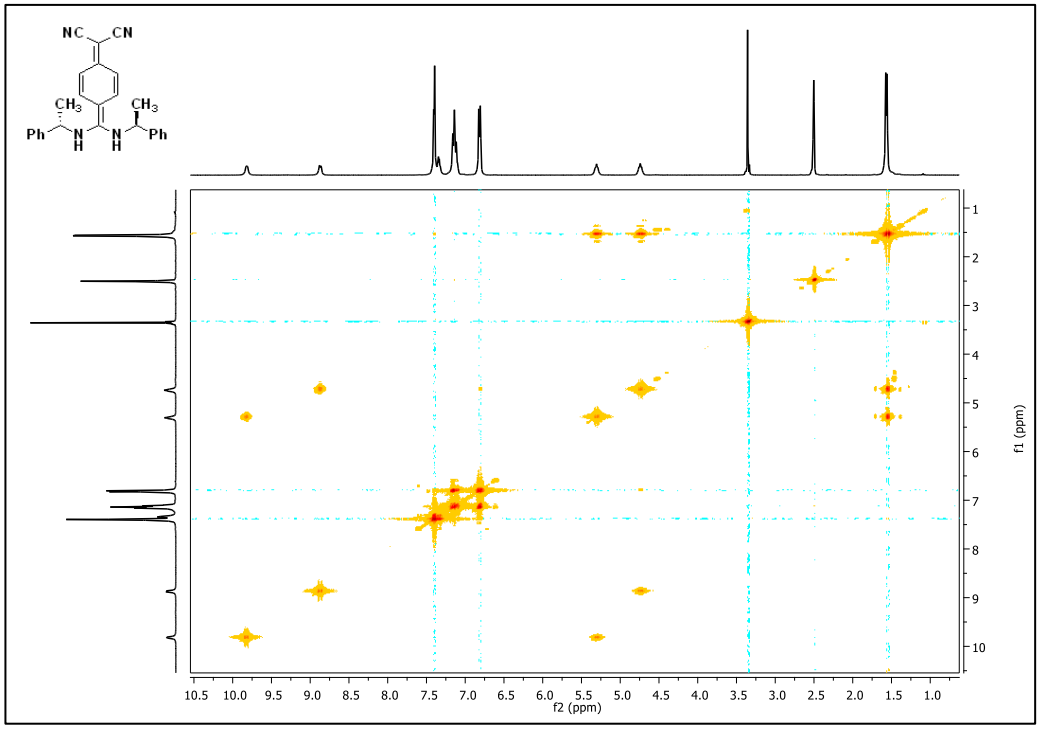

Figure D. 3 COSY spectrum of compound **22**

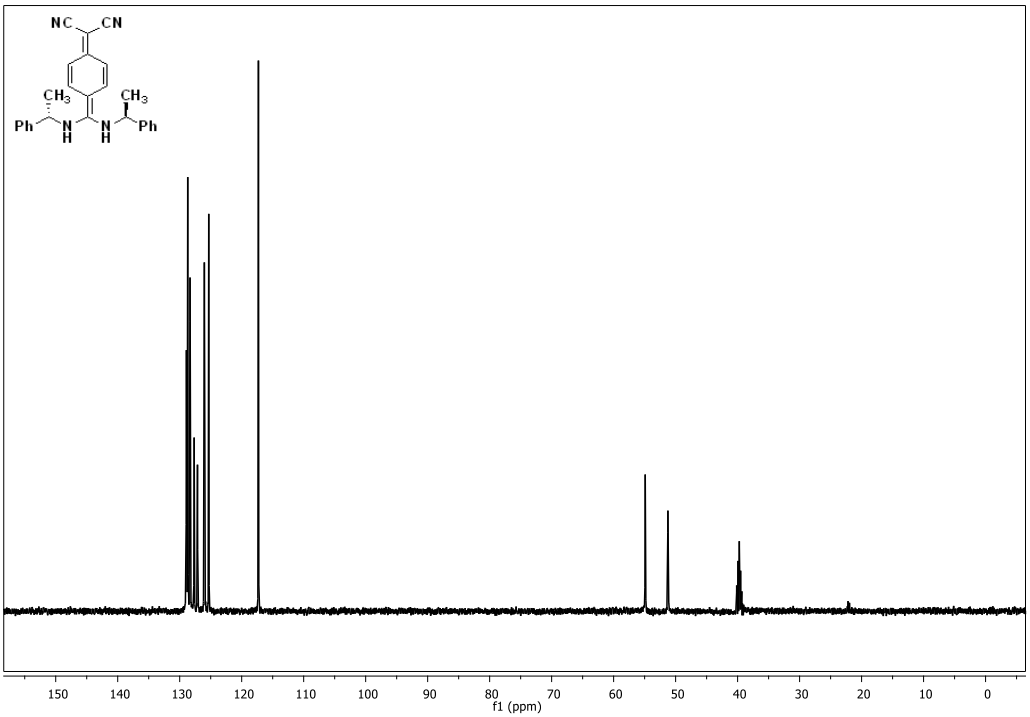

Figure D. 4 DEPT90 spectrum of compound **22**

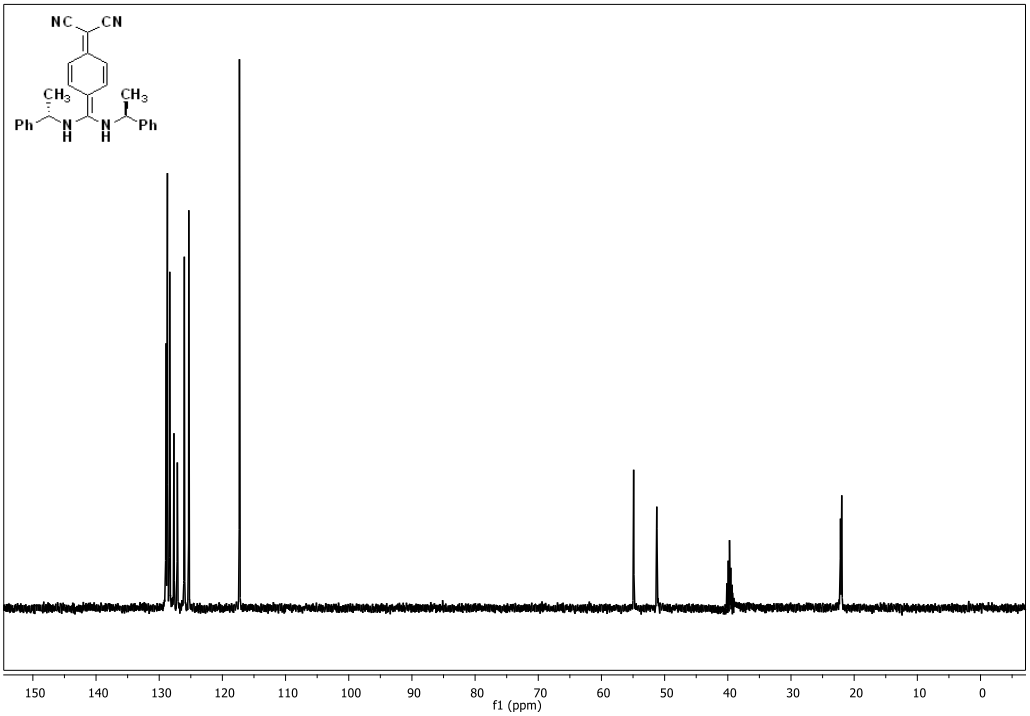

Figure D. 5 DEPT135 spectrum of compound **22**

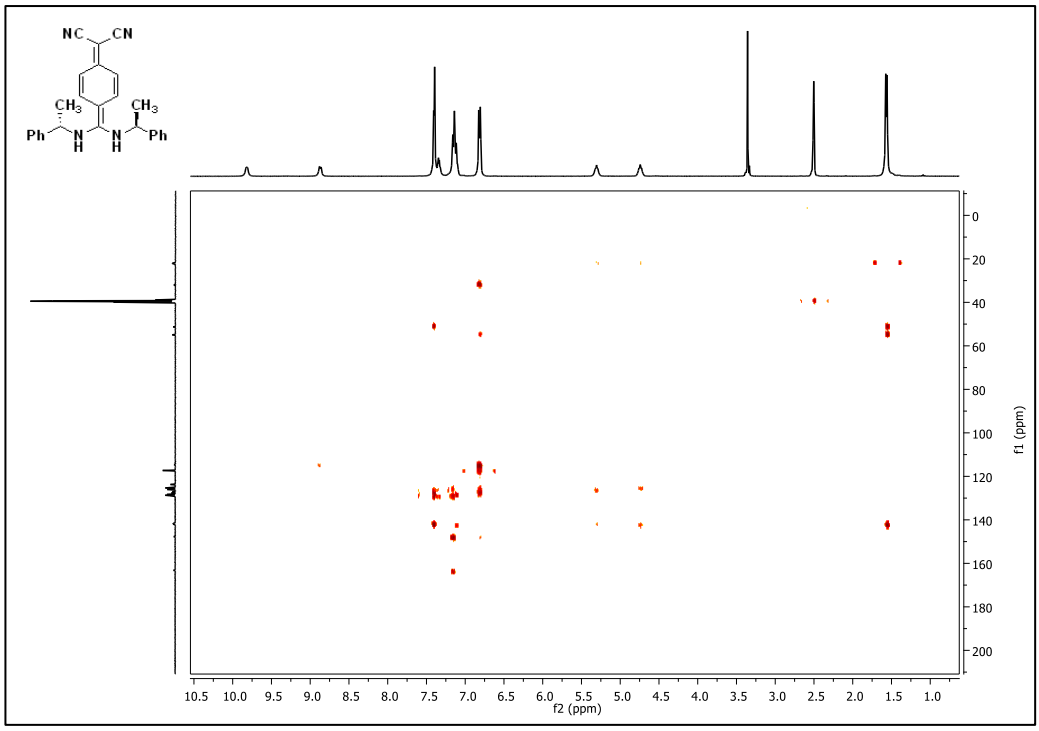

Figure D. 6 HMBC spectrum of compound **22**

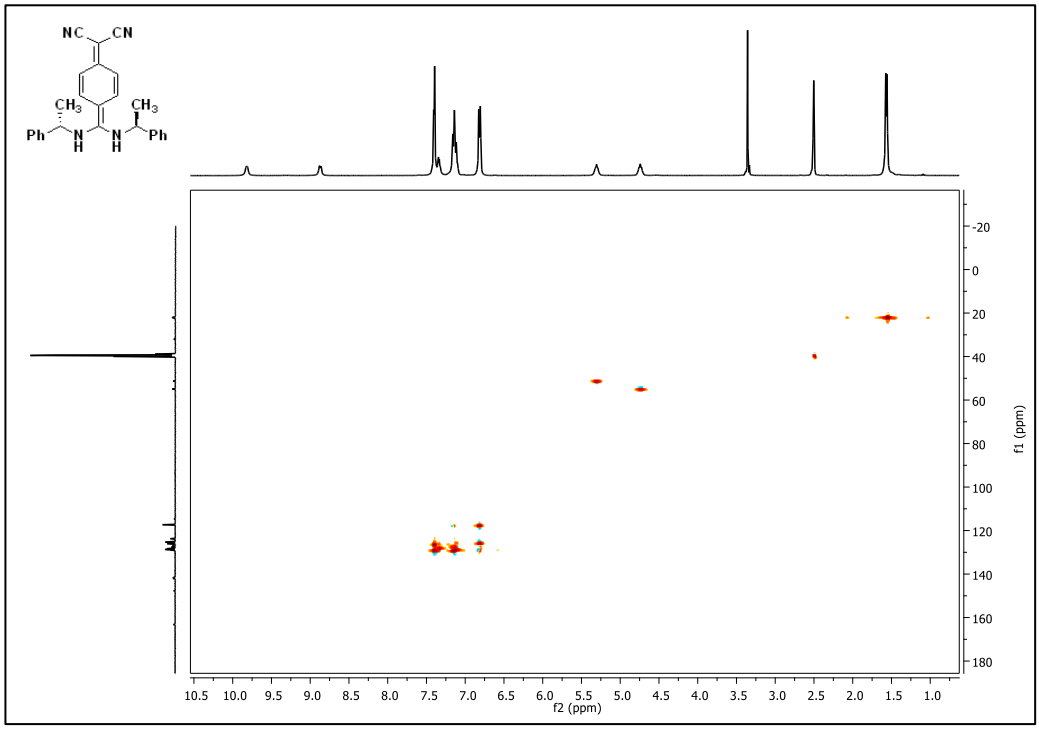

Figure D. 7 HSQC spectrum of compound **22**

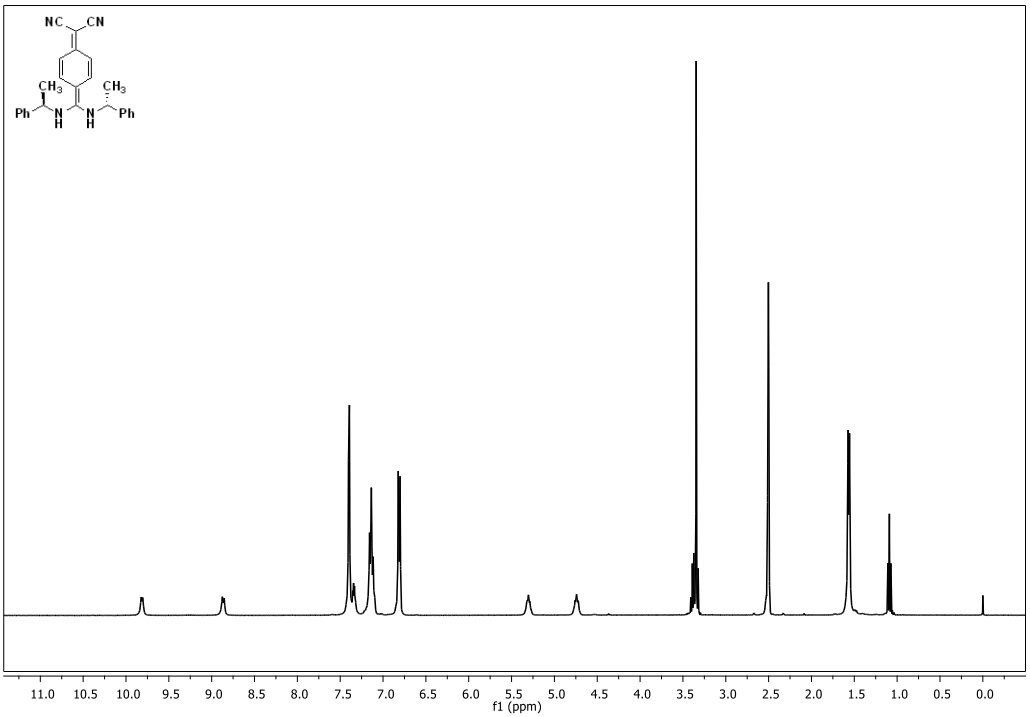

Figure D. 8 ^{1}H NMR spectrum of compound **23**

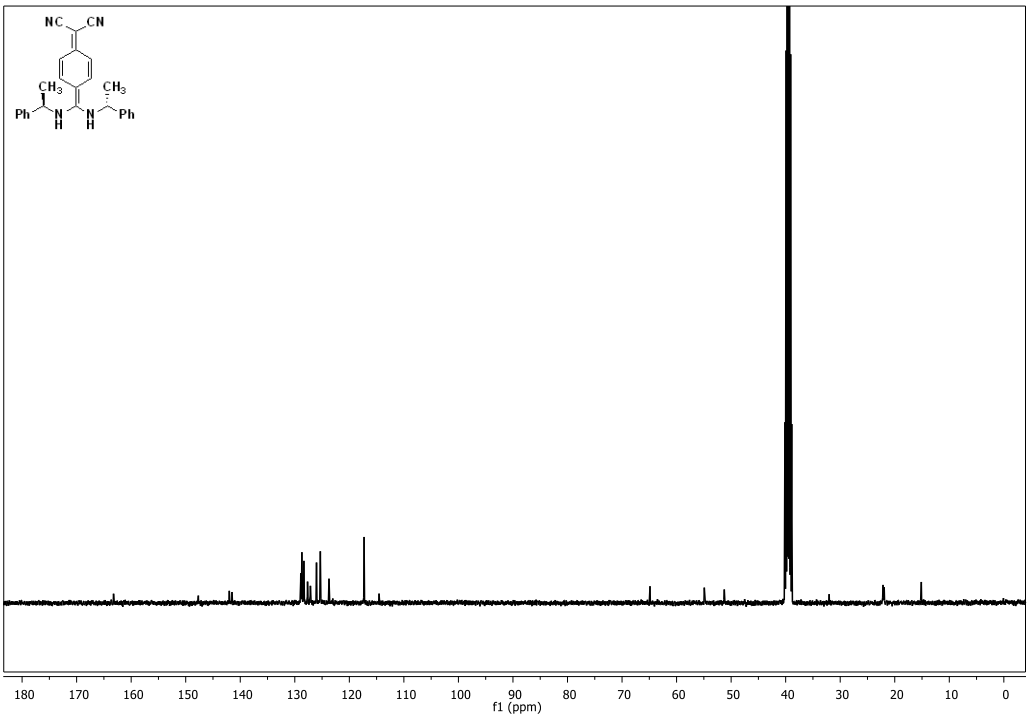

Figure D. 9 ^{13}C NMR spectrum of compound **23**

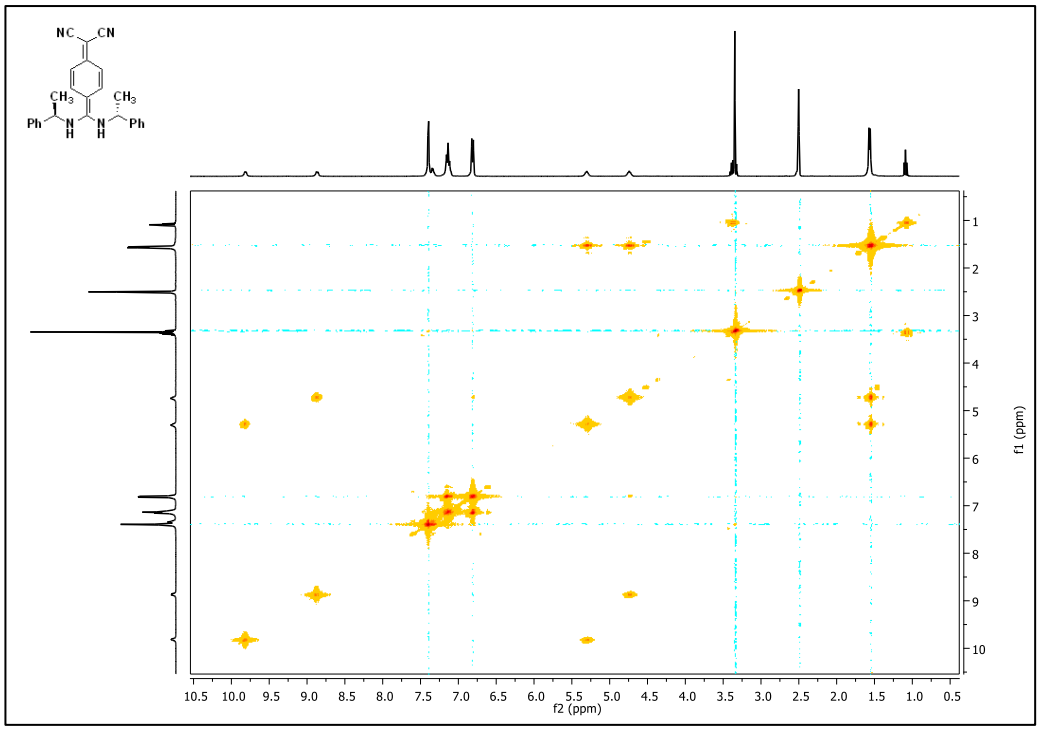

Figure D. 10 COSY spectrum of compound **23**

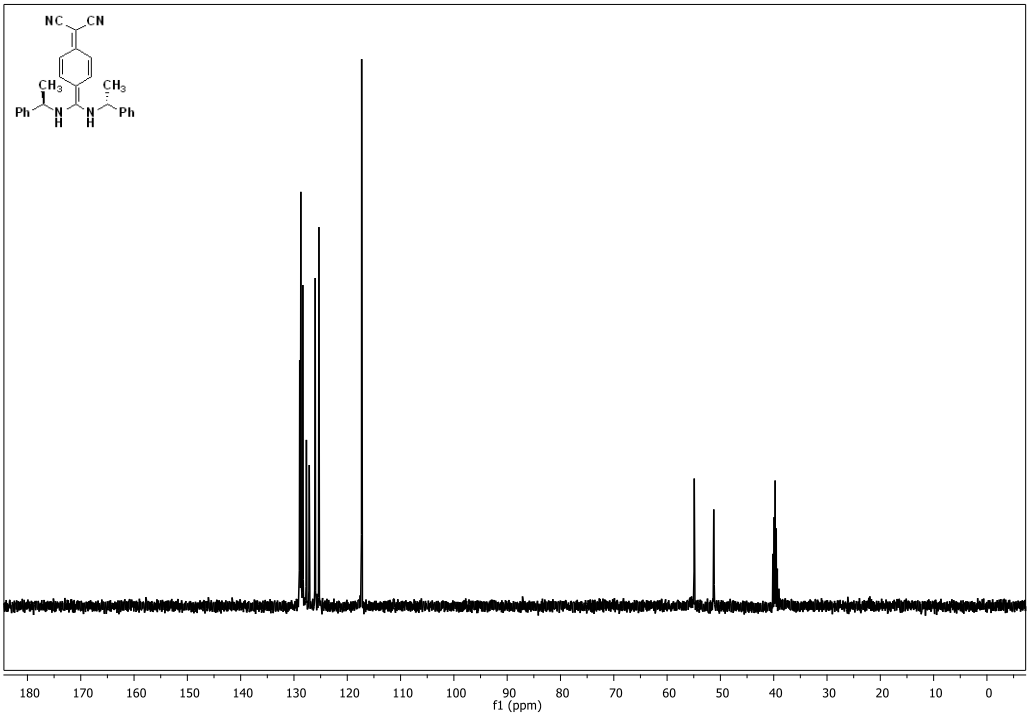

Figure D. 11 DEPT90 spectrum of compound **23**

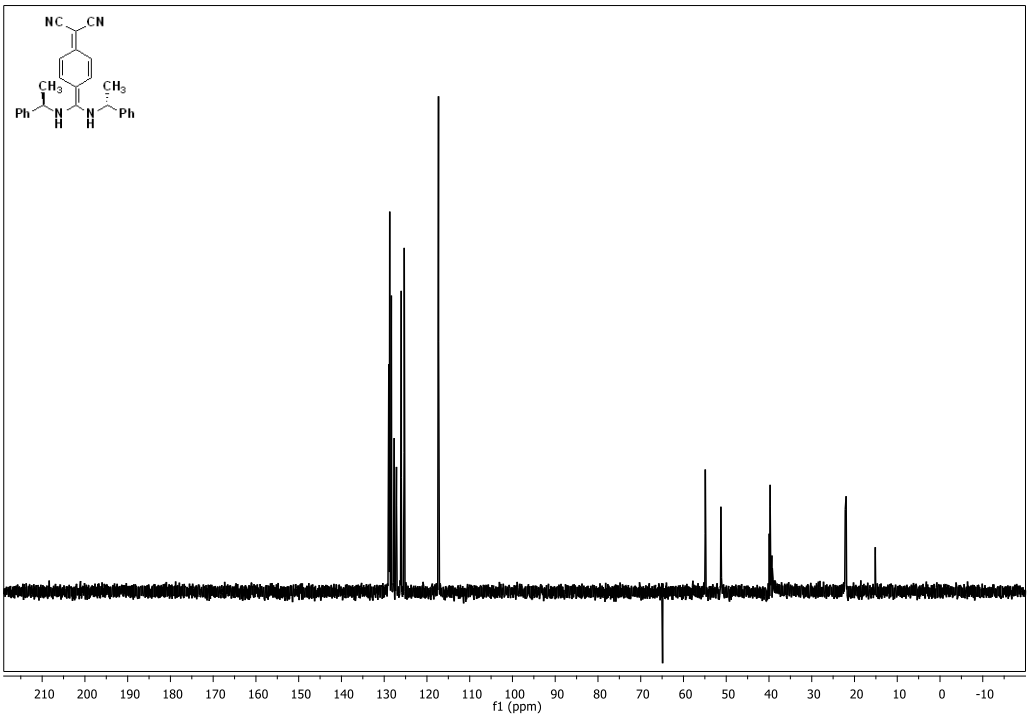

Figure D. 12 DEPT135 spectrum of compound **23**

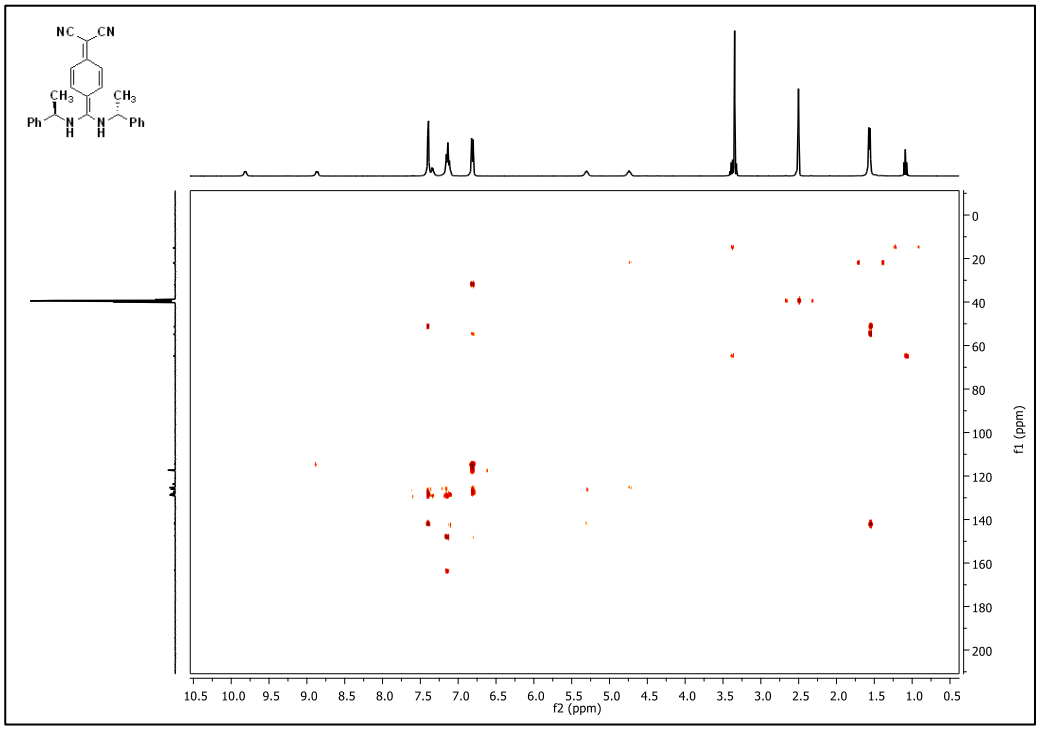

Figure D. 13 HMBC spectrum of compound **23**

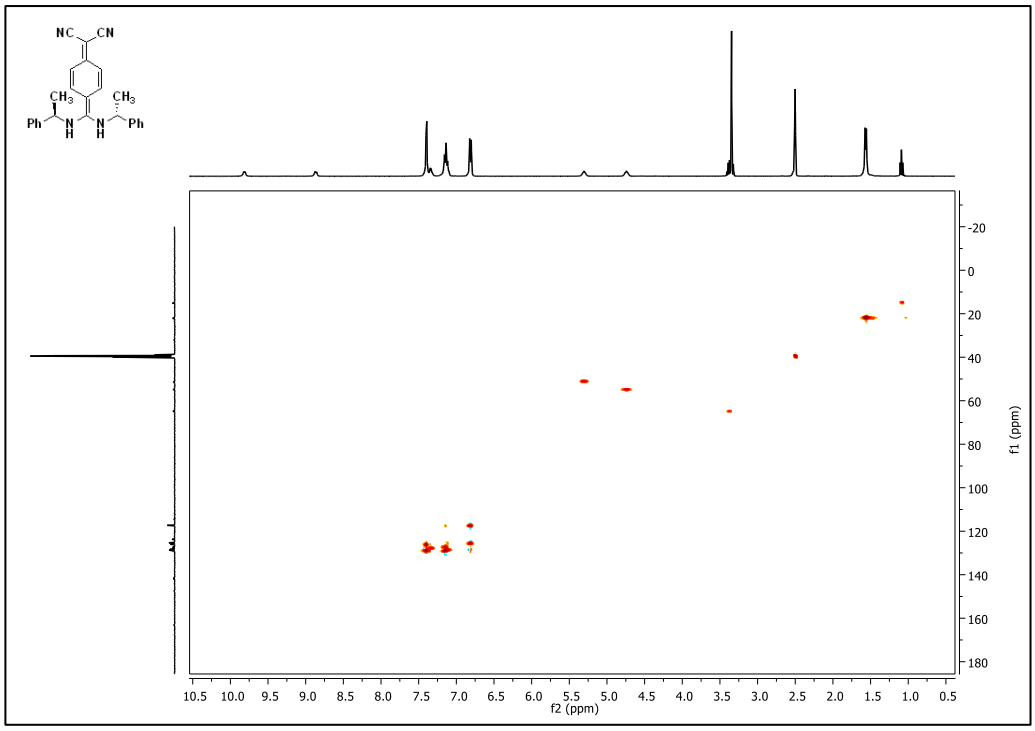

Figure D. 14 HSQC spectrum of compound **23**

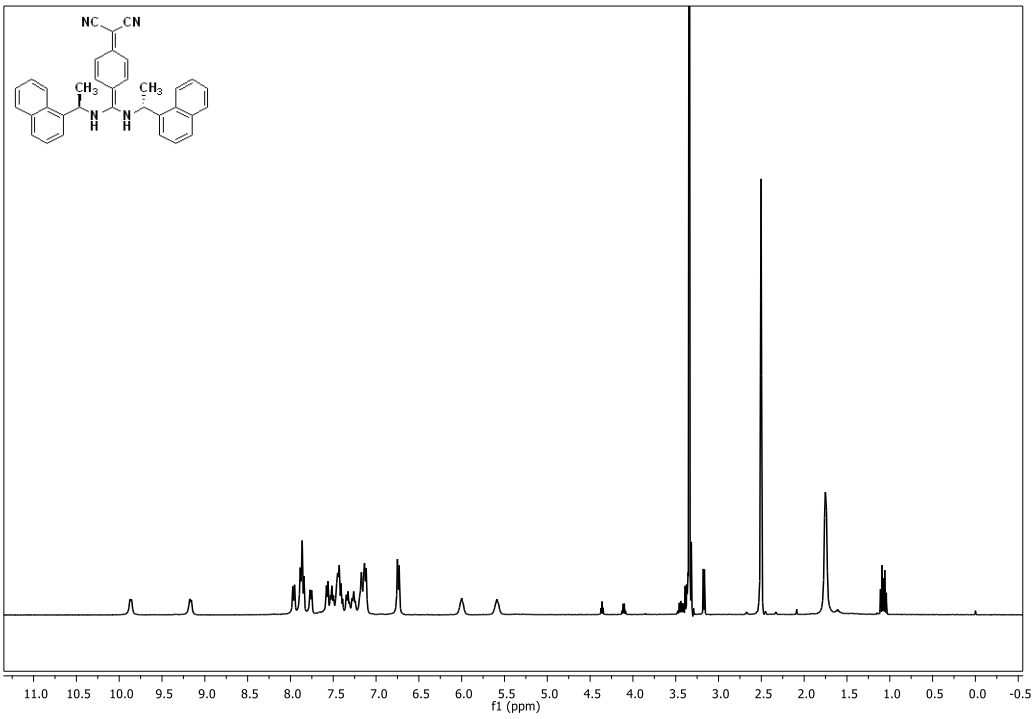

Figure D. 15 ^{1}H NMR spectrum of compound **24**

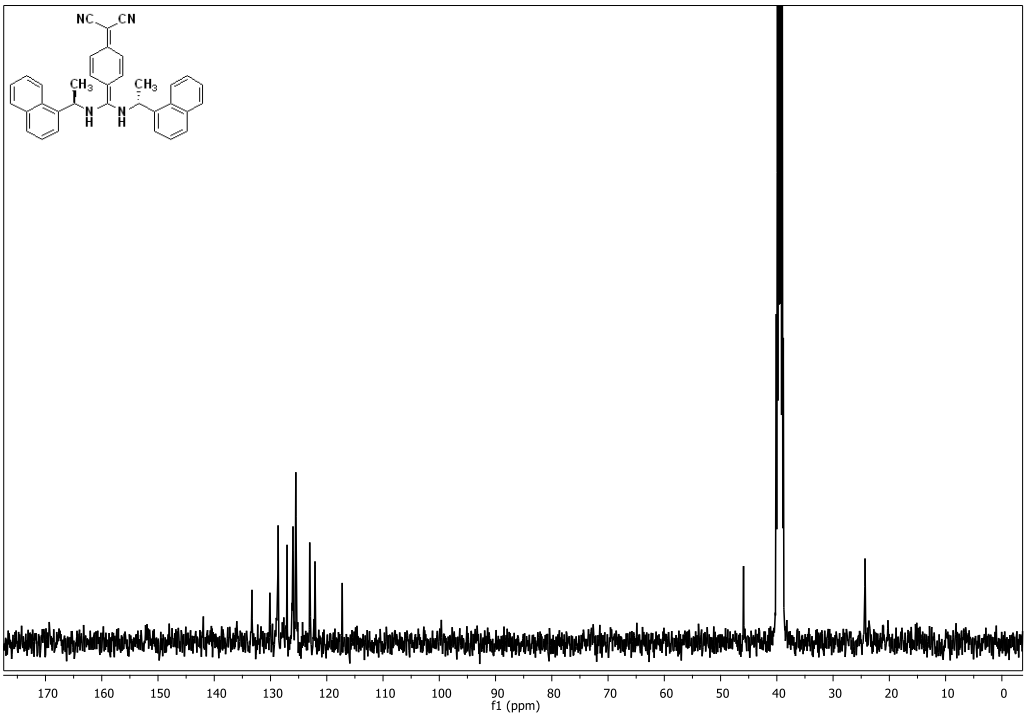

Figure D. 16 ^{13}C NMR spectrum of compound **24**

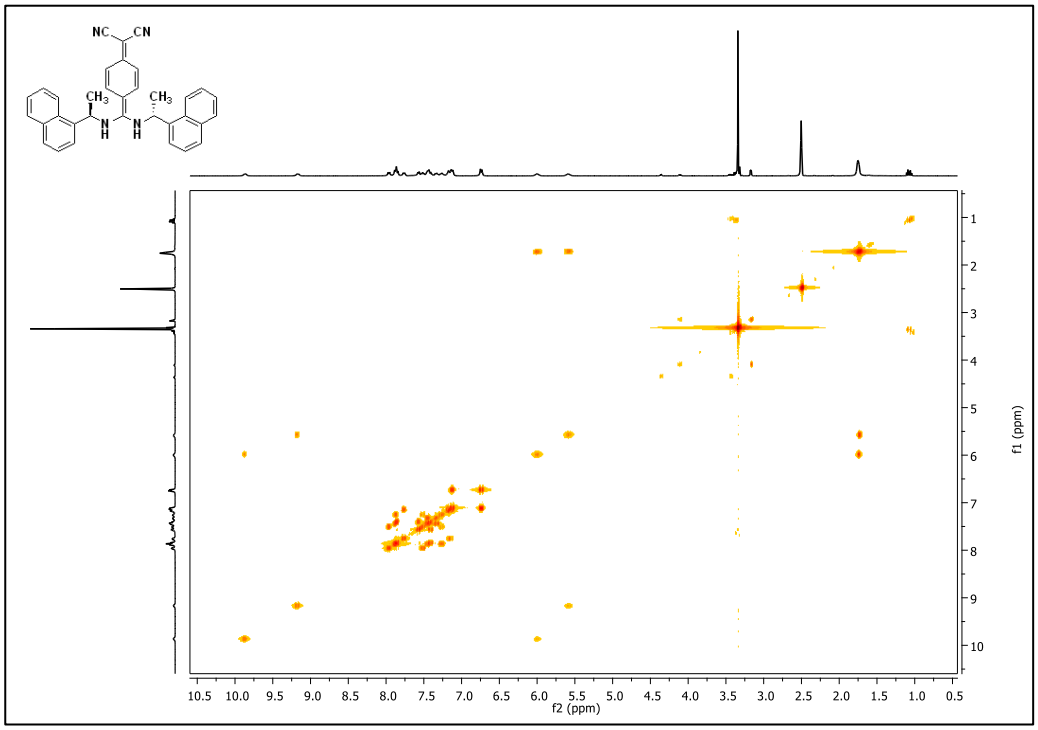

Figure D. 17 COSY spectrum of compound **24**

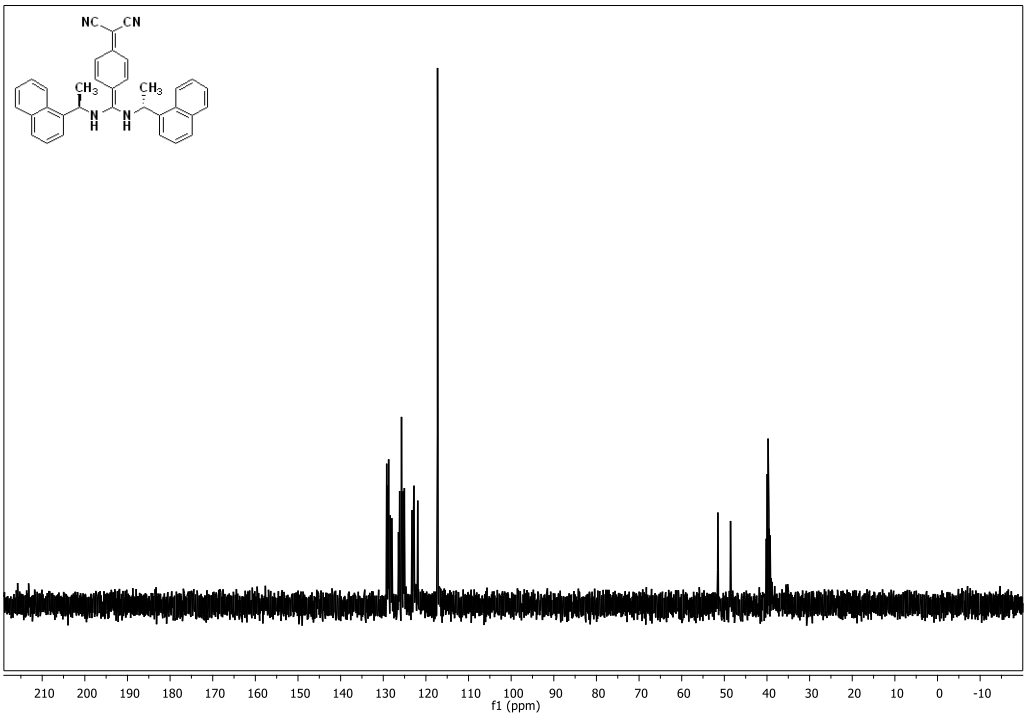

Figure D. 18 DEPT90 spectrum of compound **24**

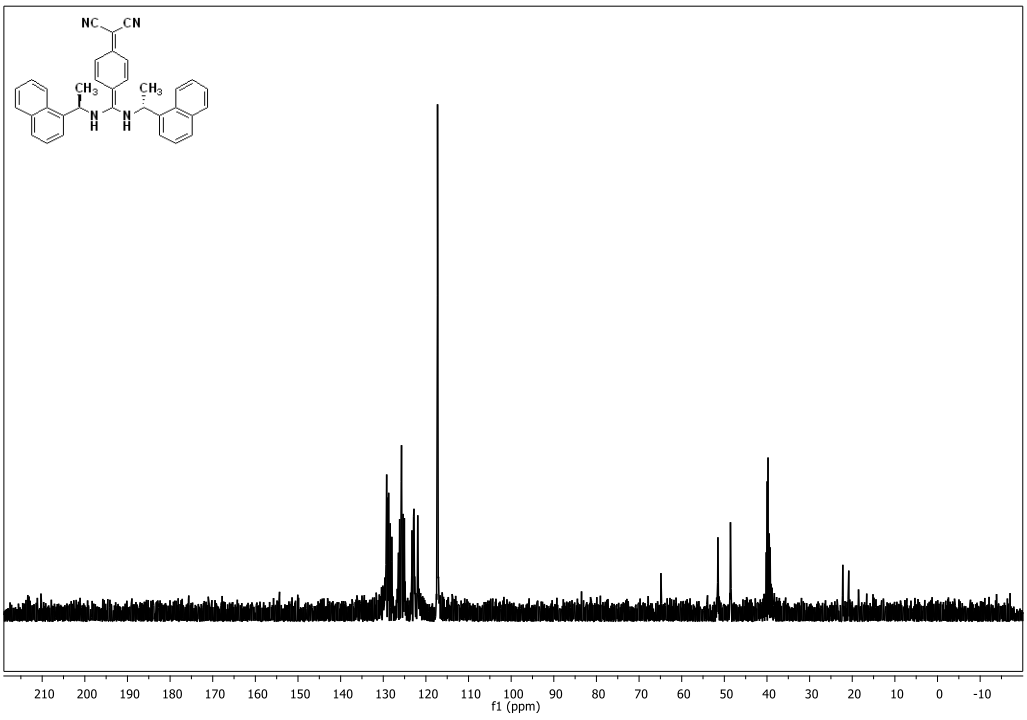

Figure D. 19 DEPT135 spectrum of compound **24**

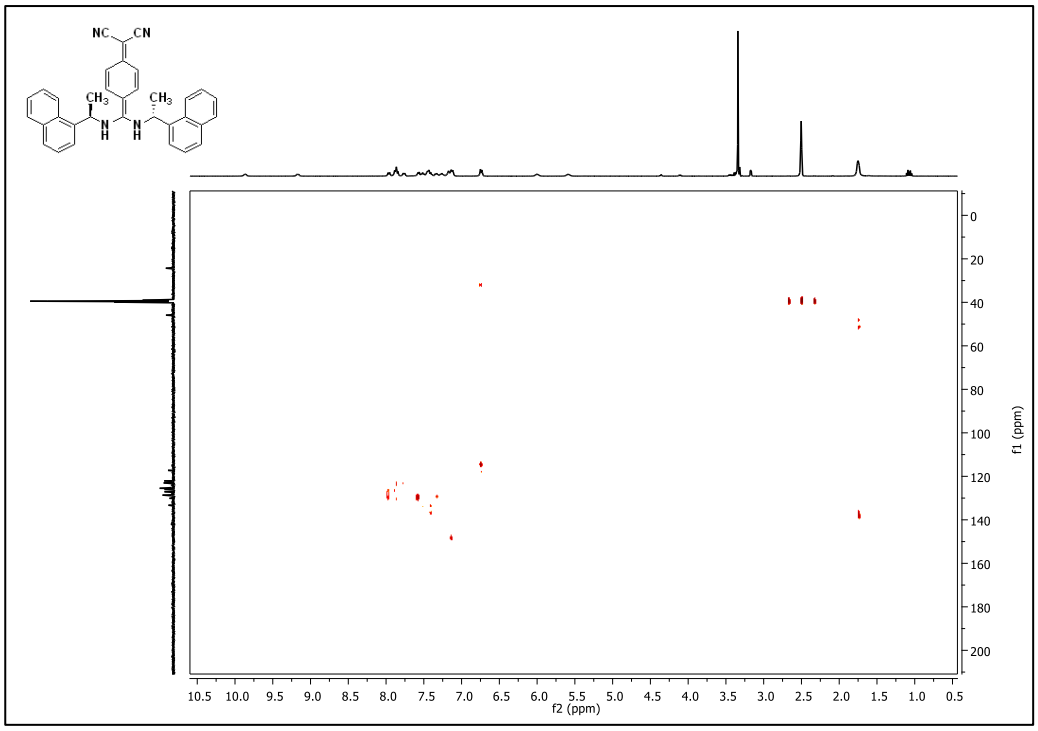

Figure D. 20 HMBC spectrum of compound **24**

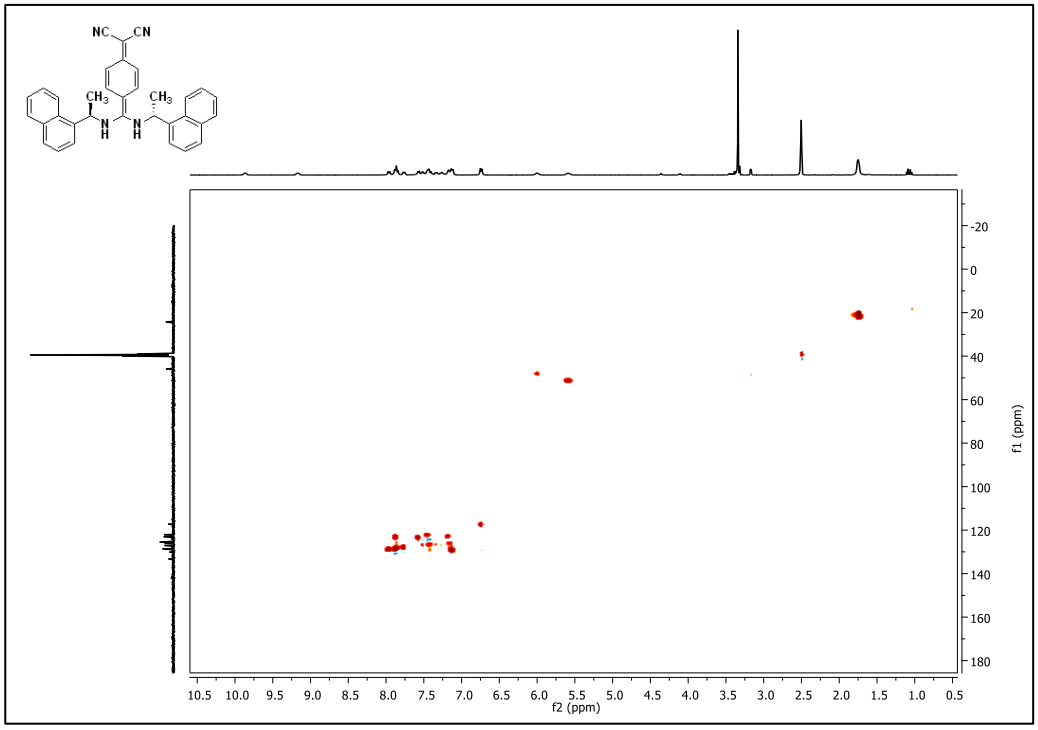

Figure D. 21 HSQC spectrum of compound **24**

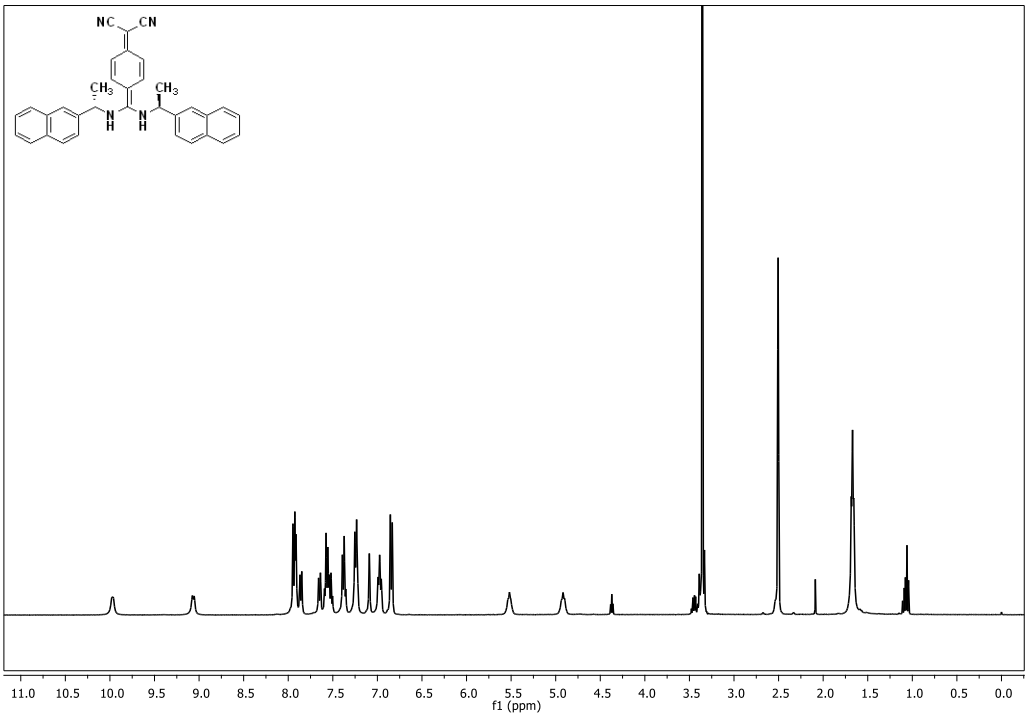

Figure D. 22 ^{1}H NMR spectrum of compound **25**

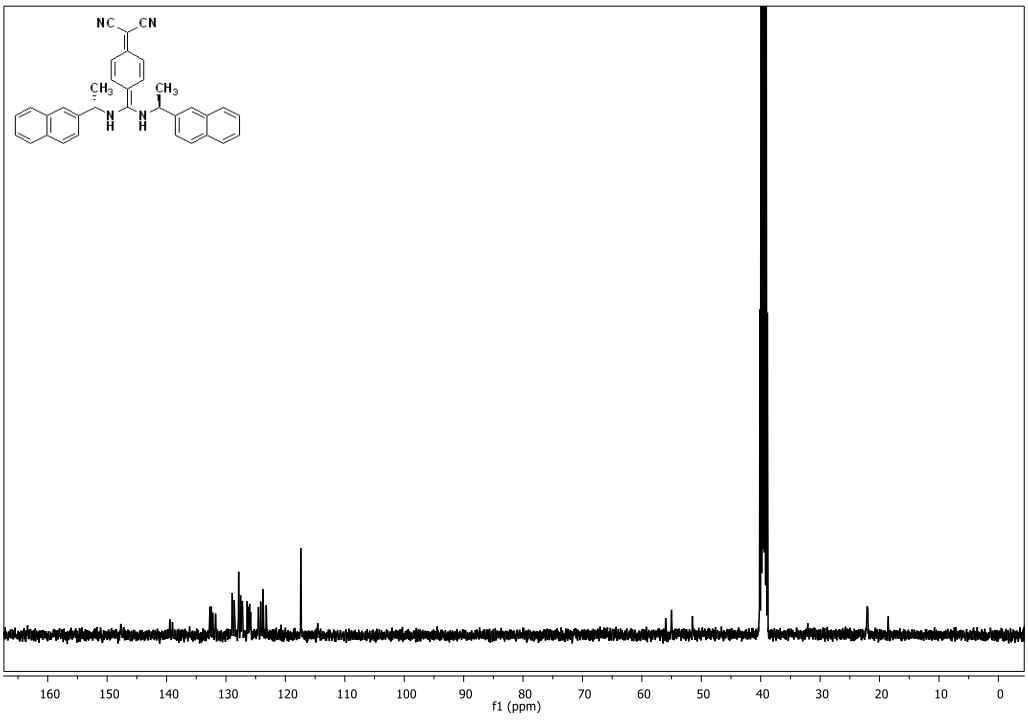

Figure D. 23 ^{13}C NMR spectrum of compound **25**

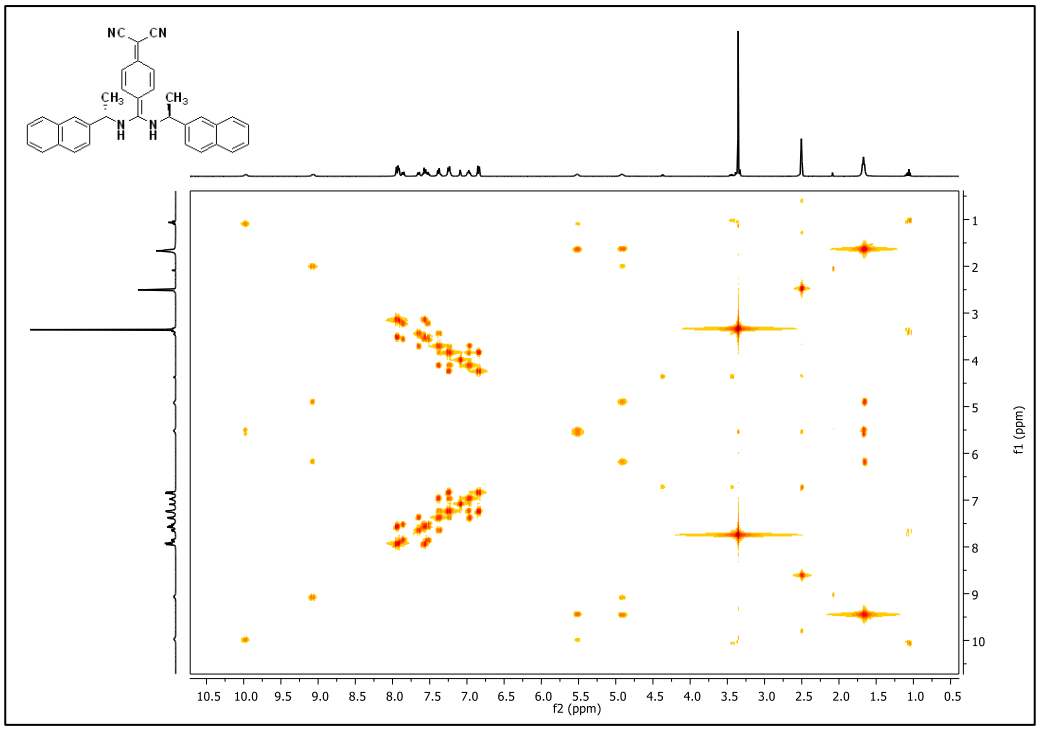

Figure D. 24 COSY spectrum of compound **25**

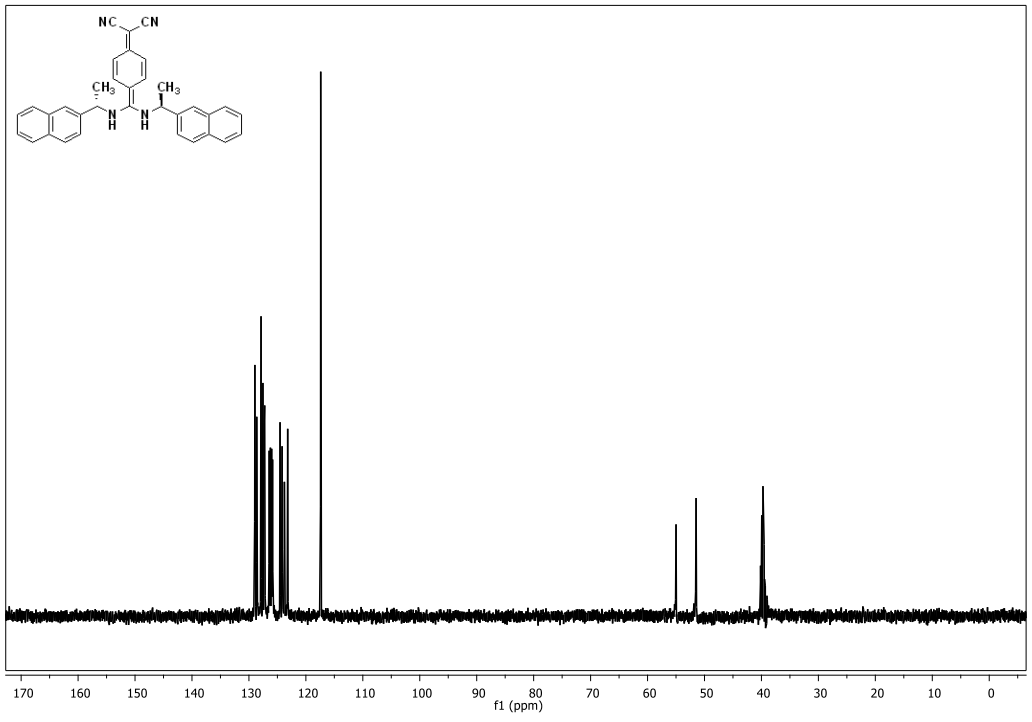

Figure D. 25 DEPT90 spectrum of compound **25**

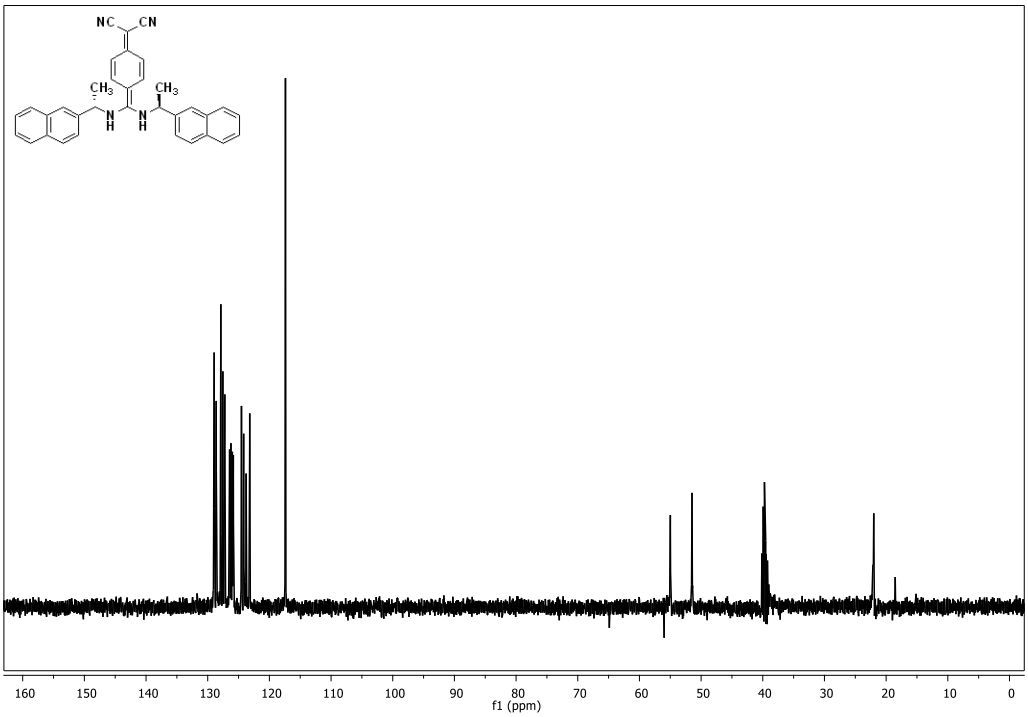

Figure D. 26 DEPT135 spectrum of compound **25**

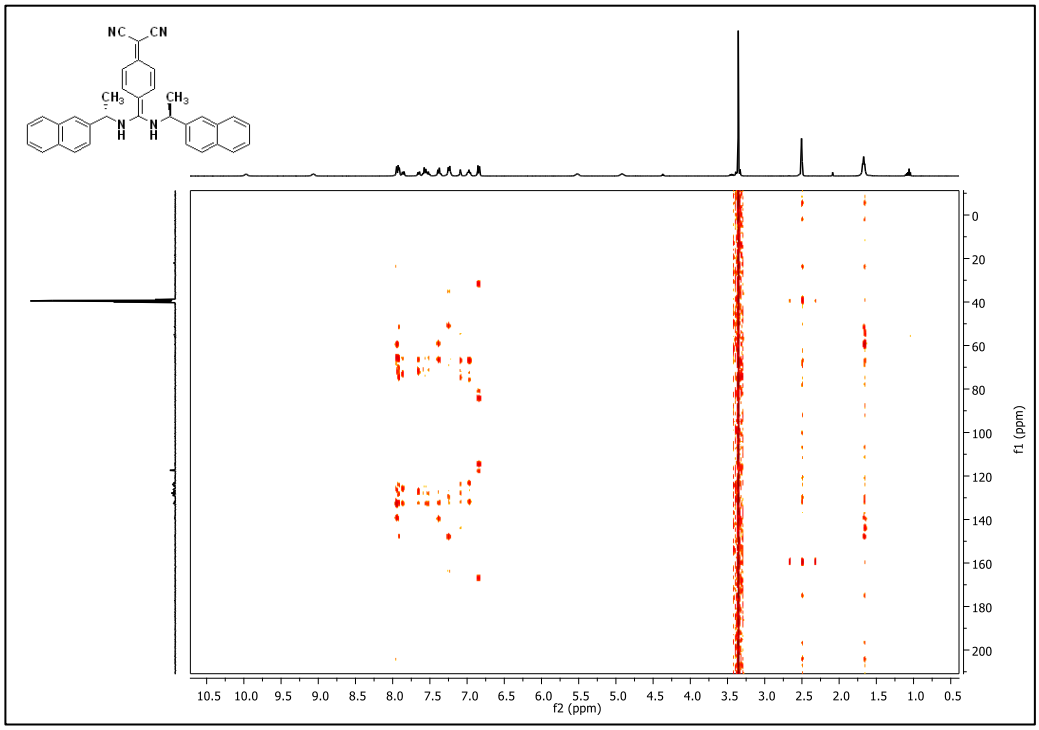

Figure D. 27 HMBC spectrum of compound **25**

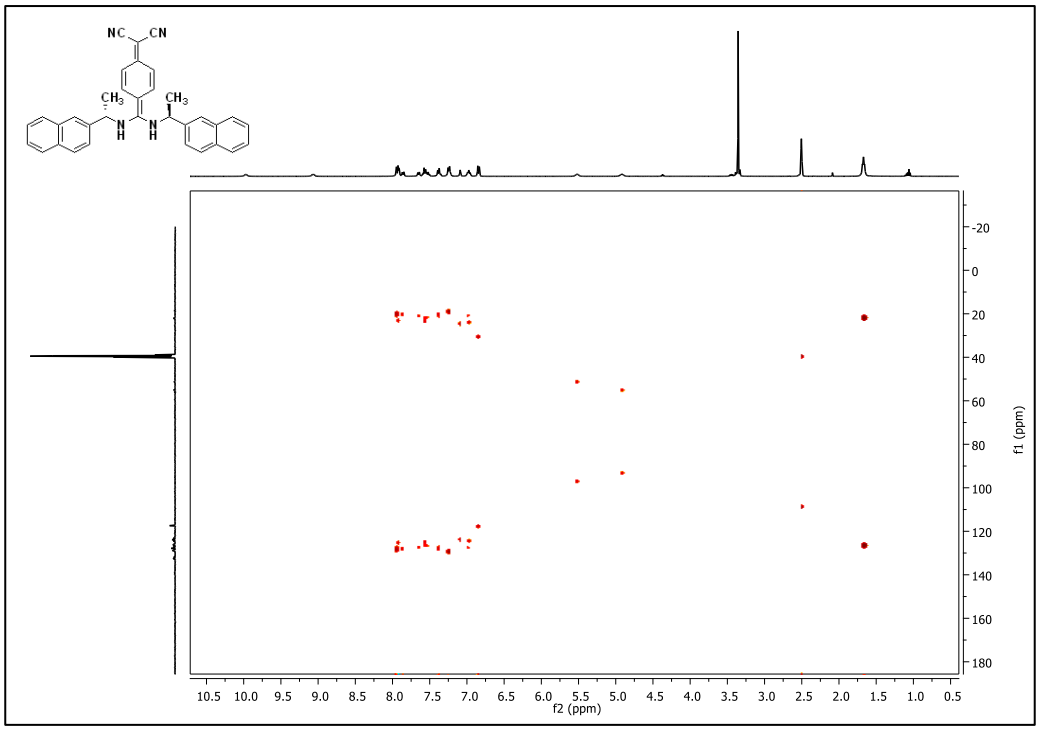

Figure D. 28 HSQC spectrum of compound **25**

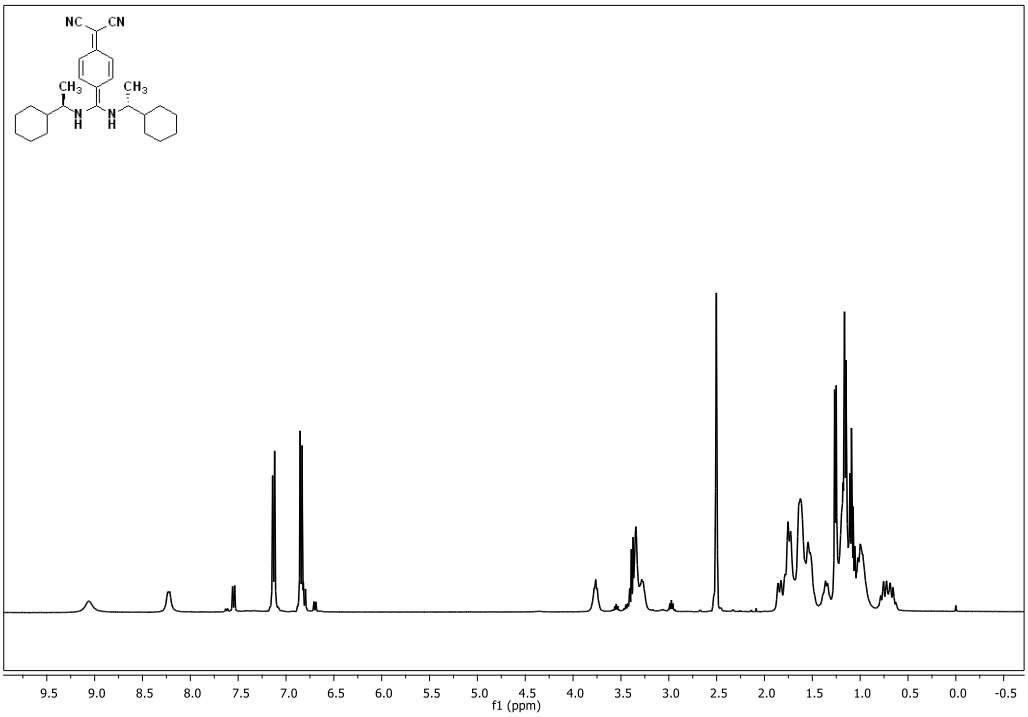

Figure D. 29 ^{1}H NMR spectrum of compound **26**

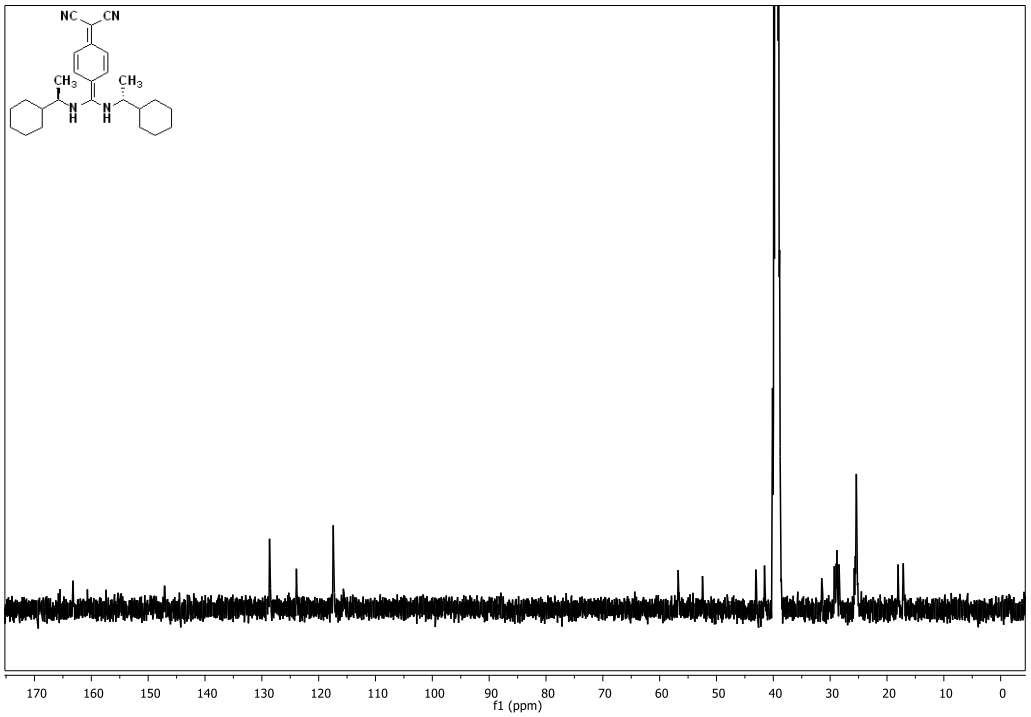

Figure D. 30 ^{13}C NMR spectrum of compound **26**

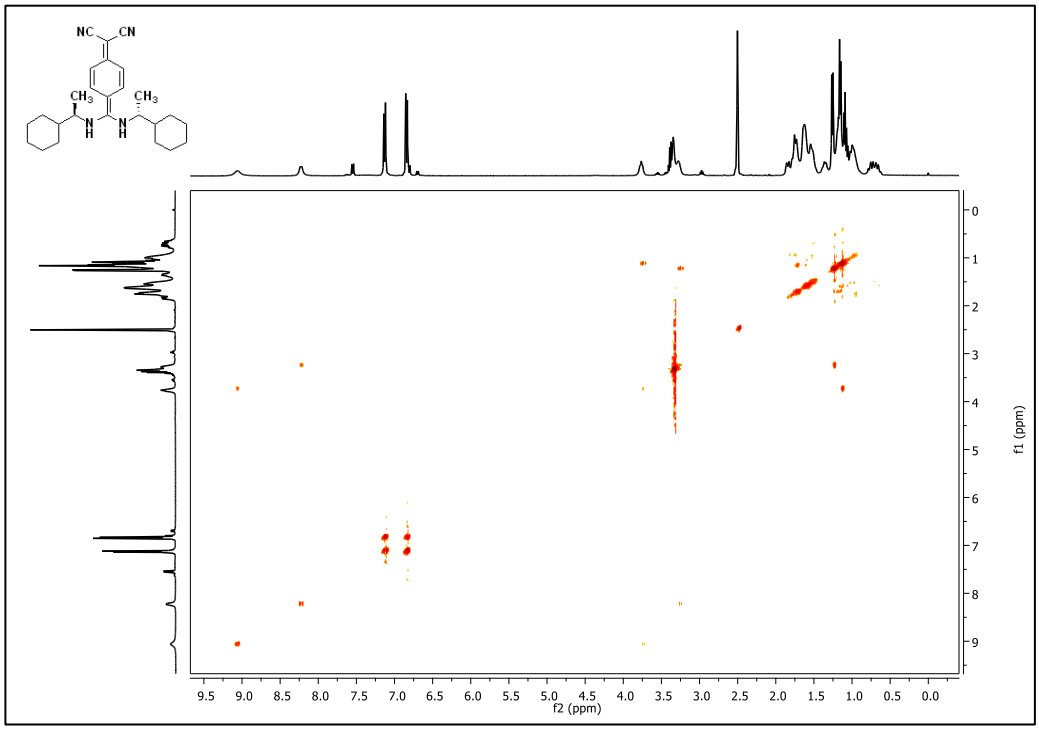

Figure D. 31 COSY spectrum of compound **26**

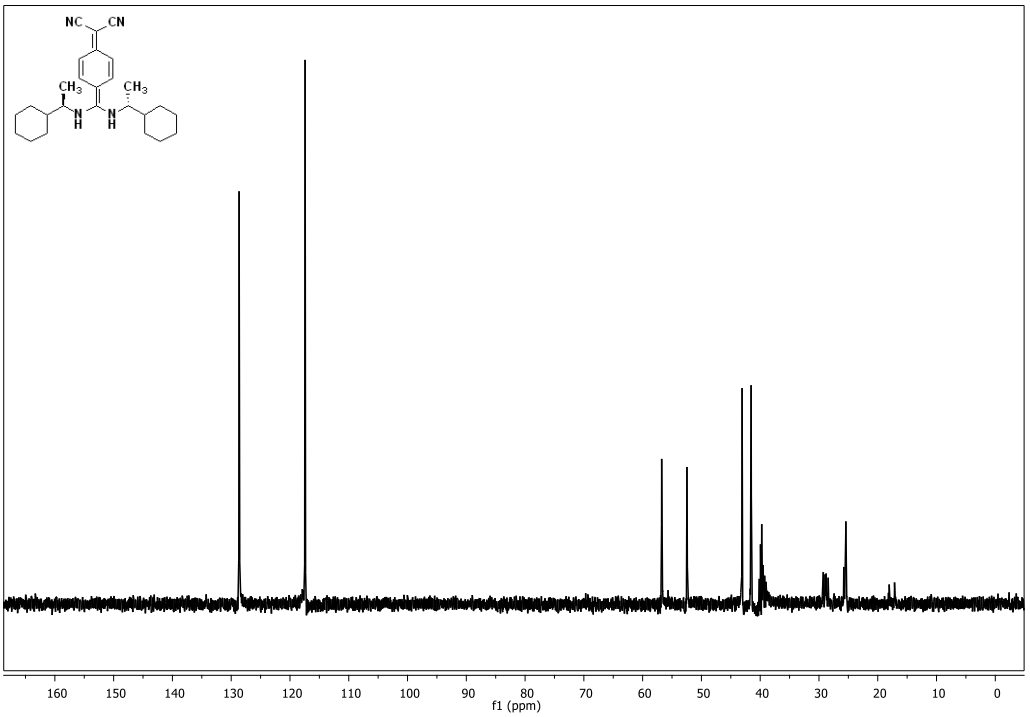

Figure D. 32 DEPT90 spectrum of compound **26**

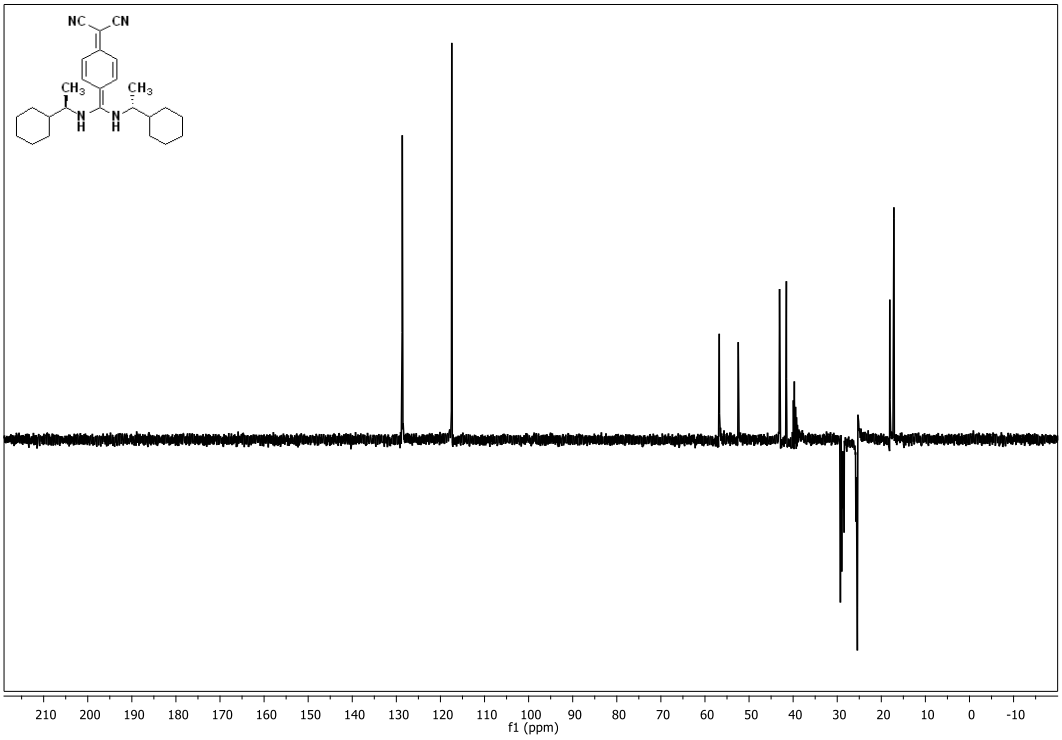

Figure D. 33 DEPT135 spectrum of compound **26**

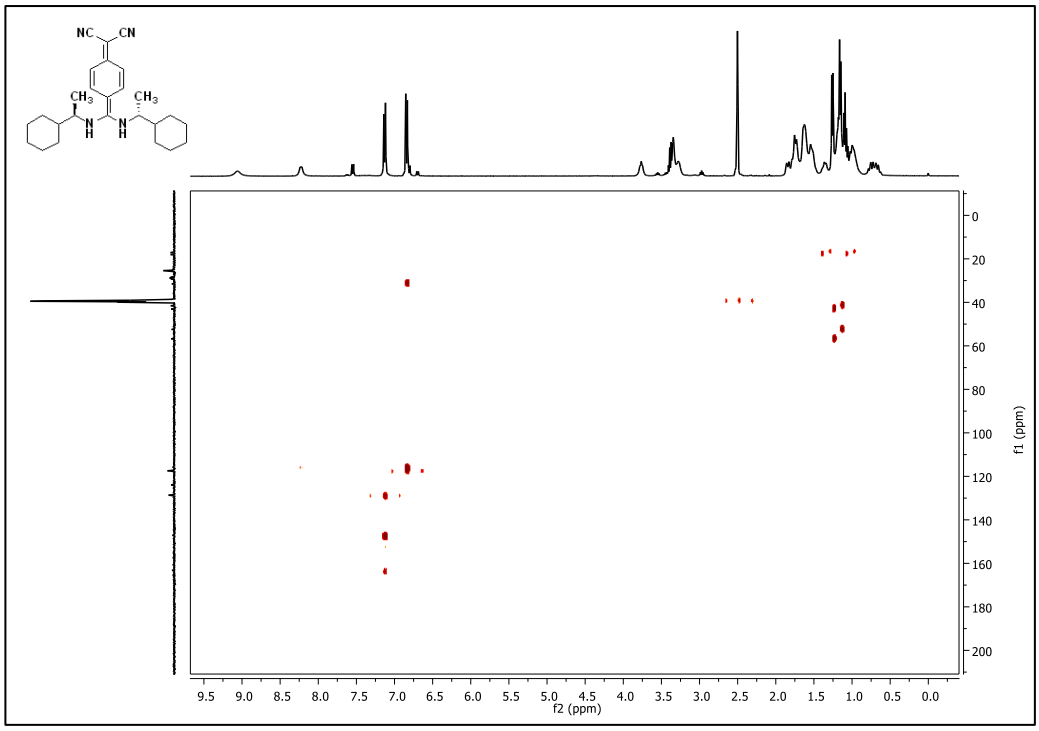

Figure D. 34 HMBC spectrum of compound **26**

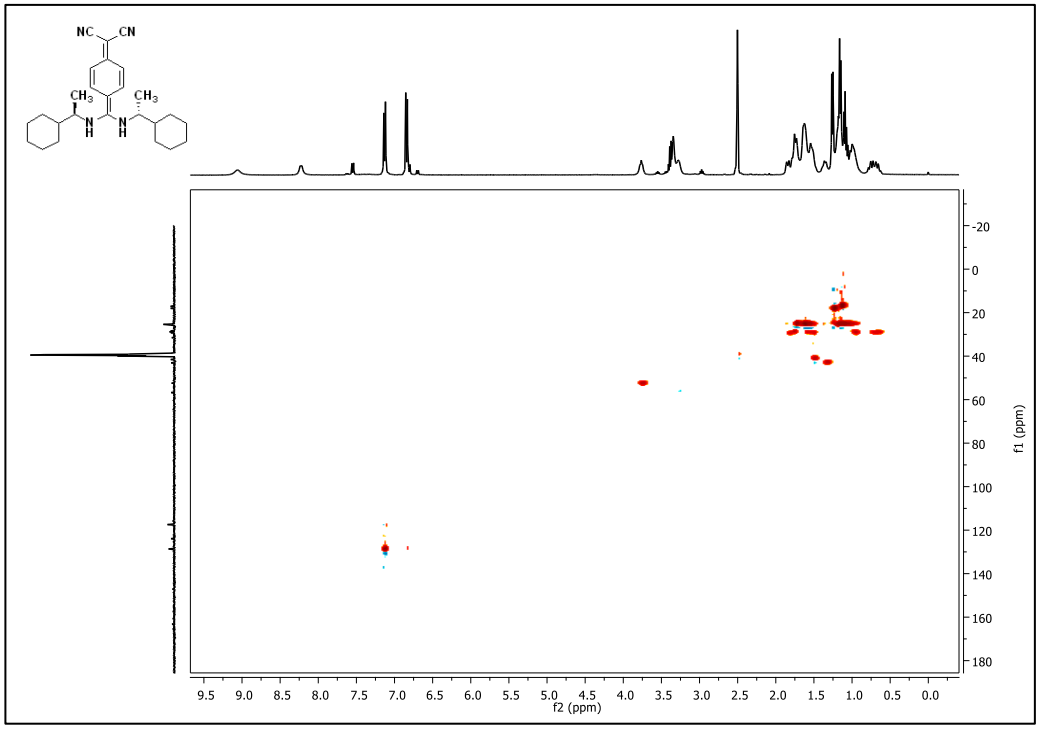

Figure D. 35 HSQC spectrum of compound **26**

8.13 IR spectra

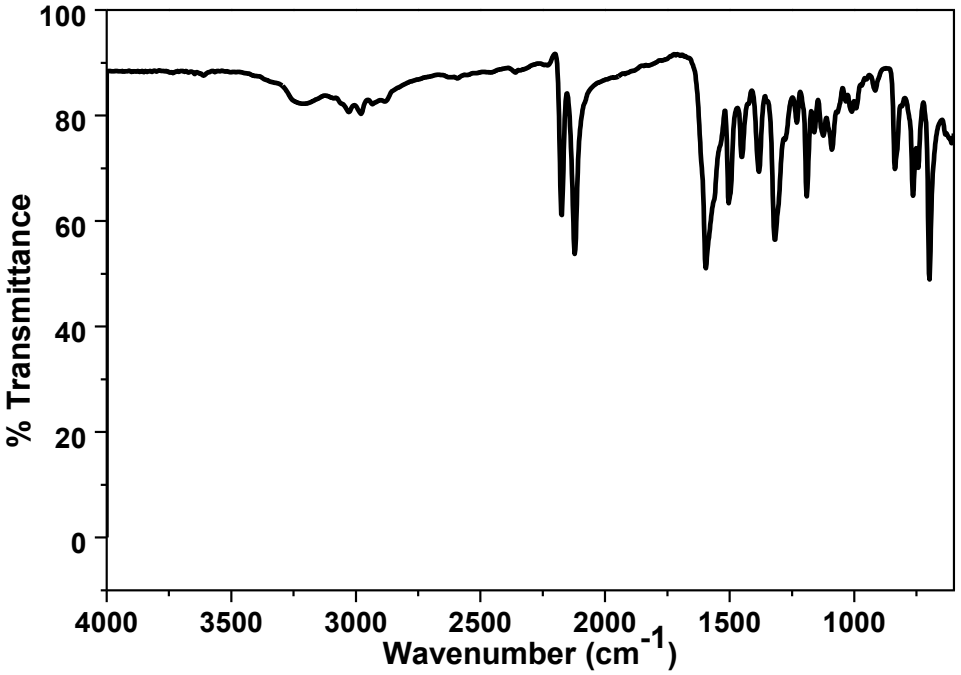

Figure D. 36 IR spectrum of compound **22**

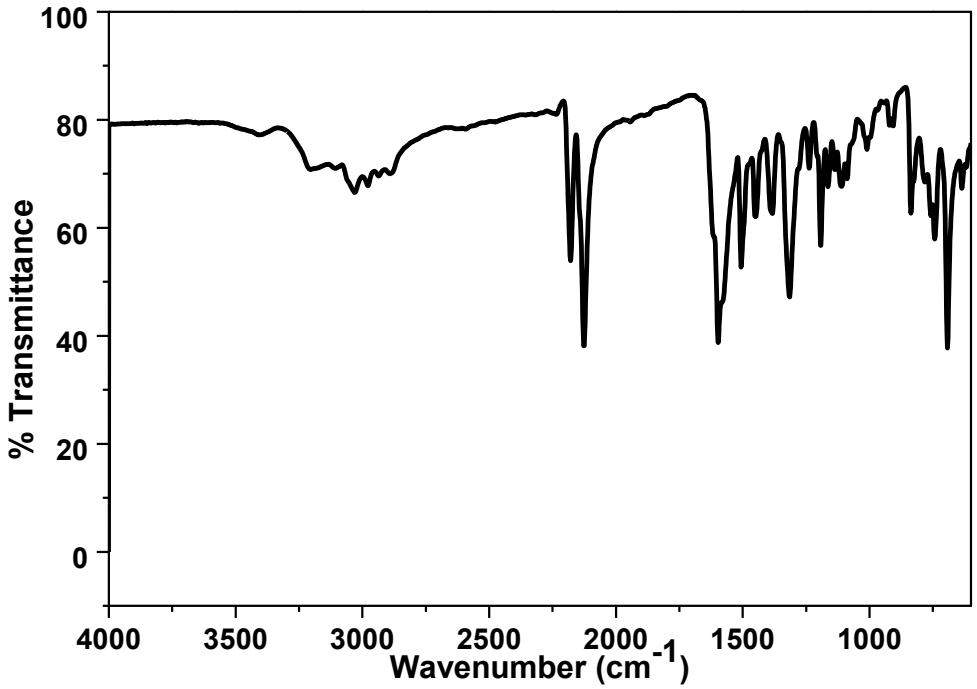

Figure D. 37 IR spectrum of compound **23**

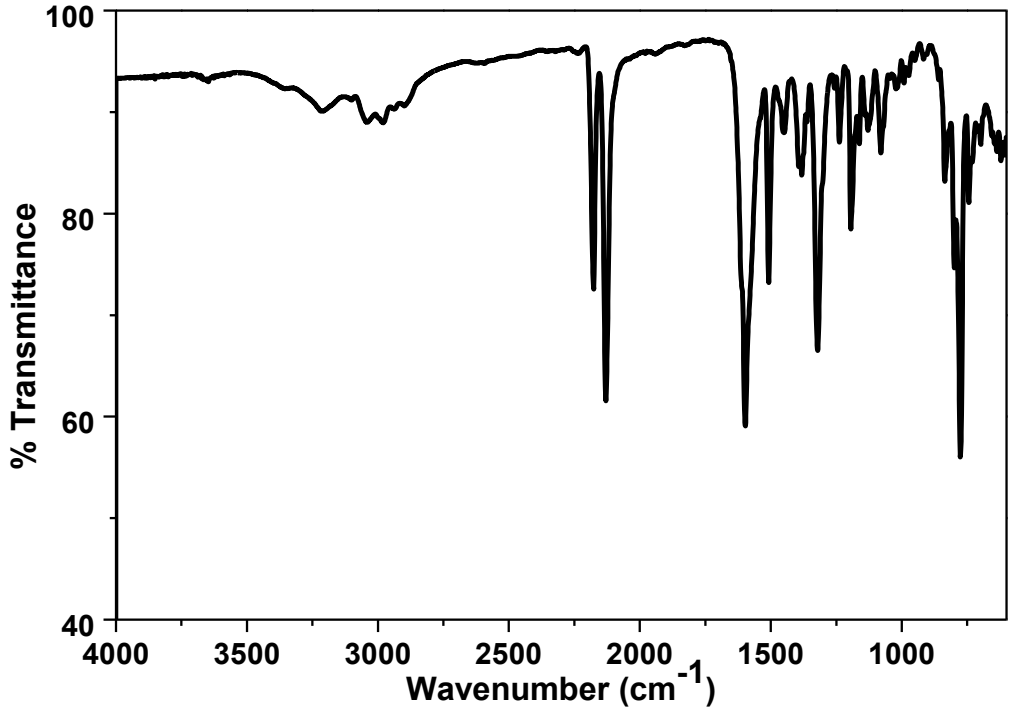

Figure D. 38 IR spectrum of compound **24**

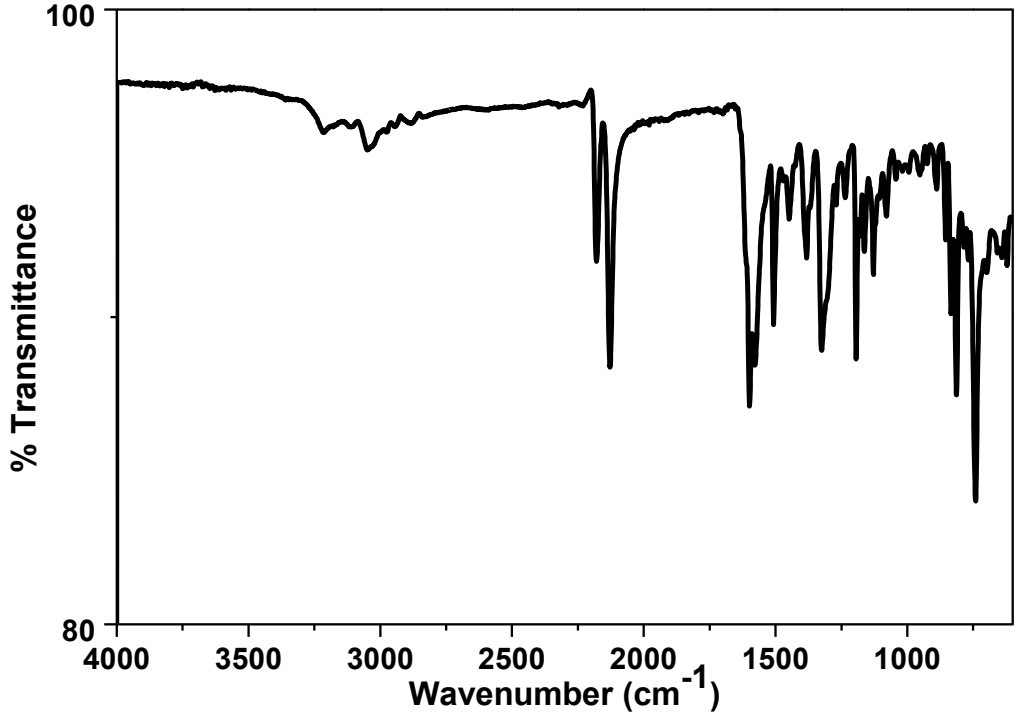

Figure D. 39 IR spectrum of compound **25**

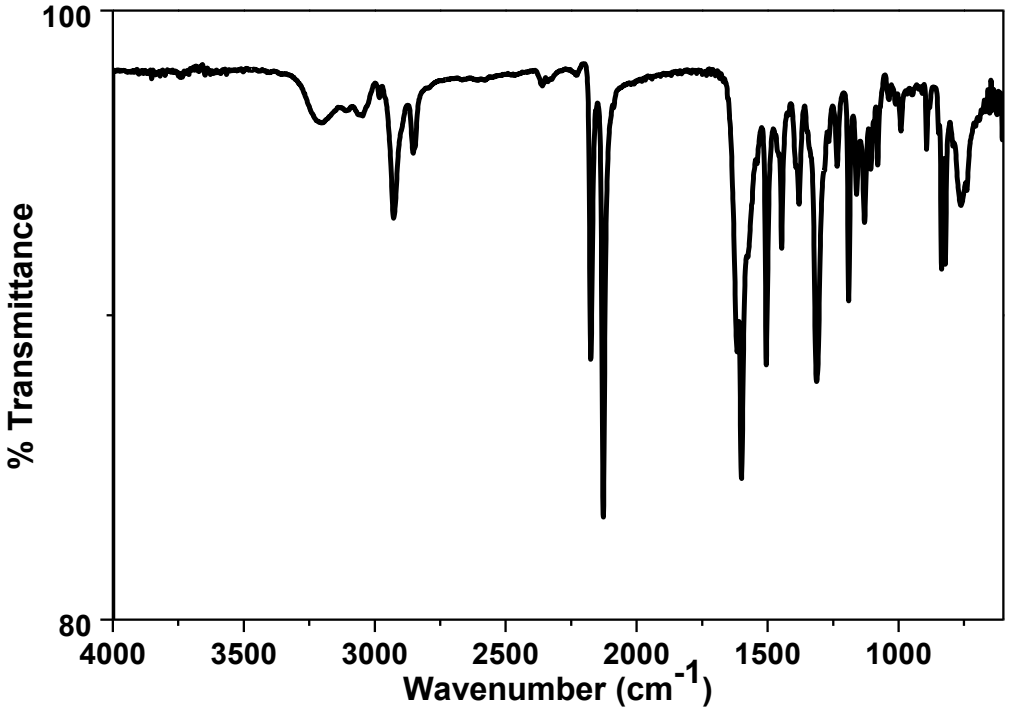

Figure D. 40 IR spectrum of compound **26**

8.14 HRMS spectra

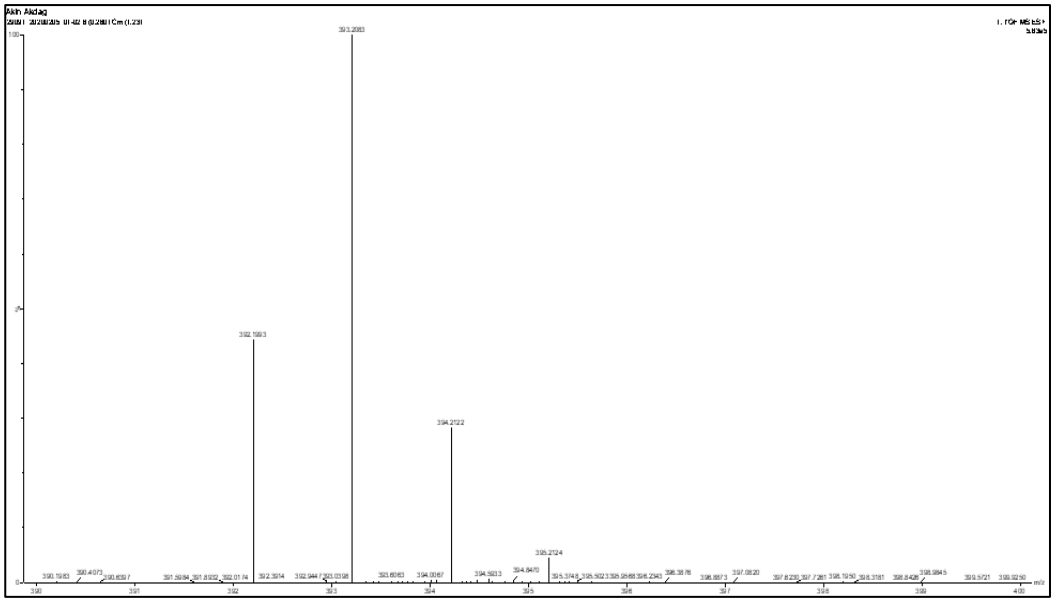

Figure D. 41 HRMS spectrum of compound **22**

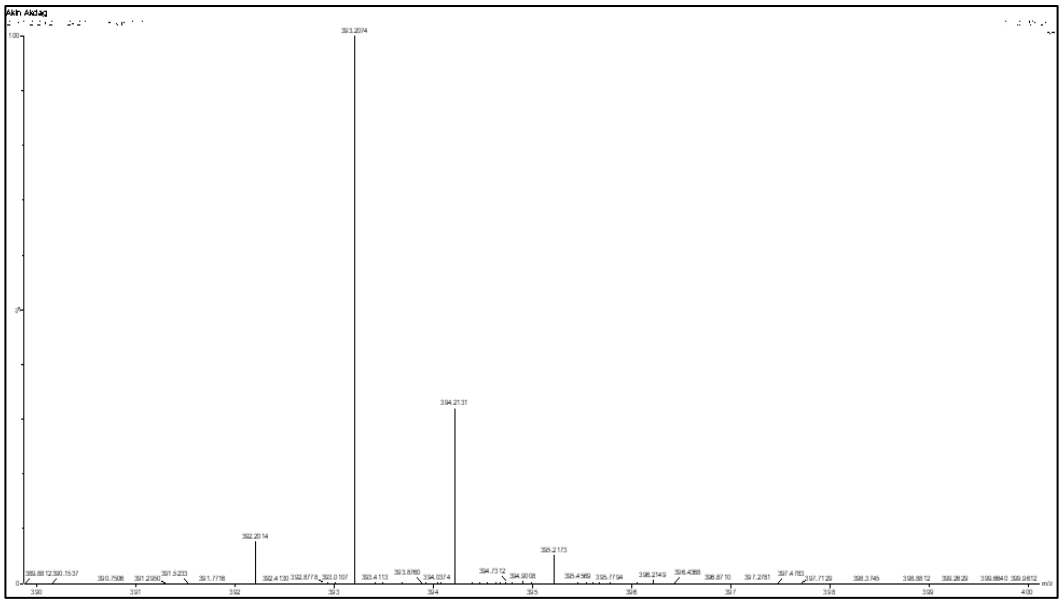

Figure D. 42 HRMS spectrum of compound **23**

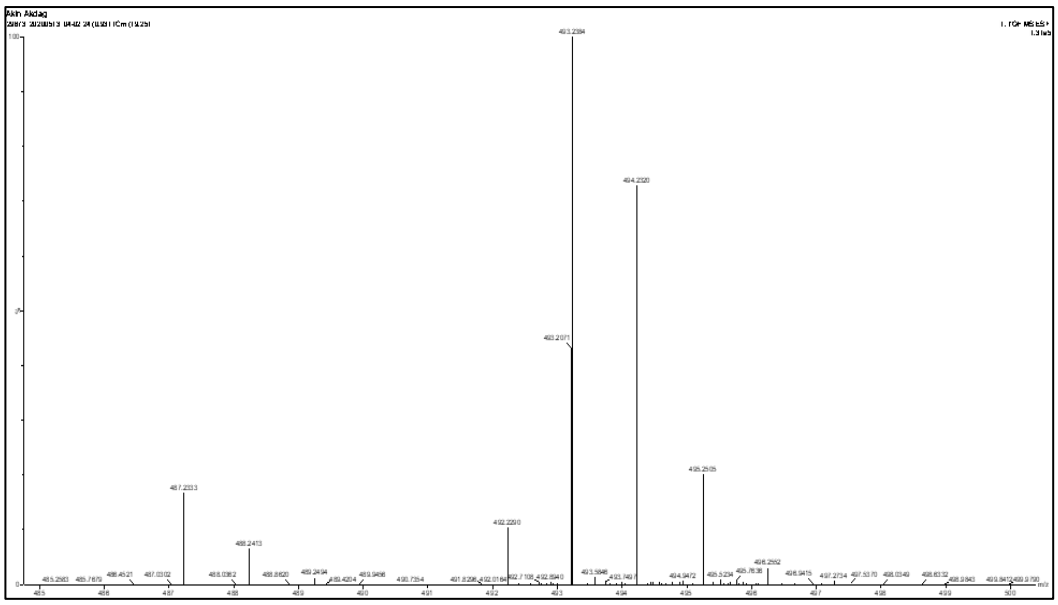

Figure D. 43 HRMS spectrum of compound **24**

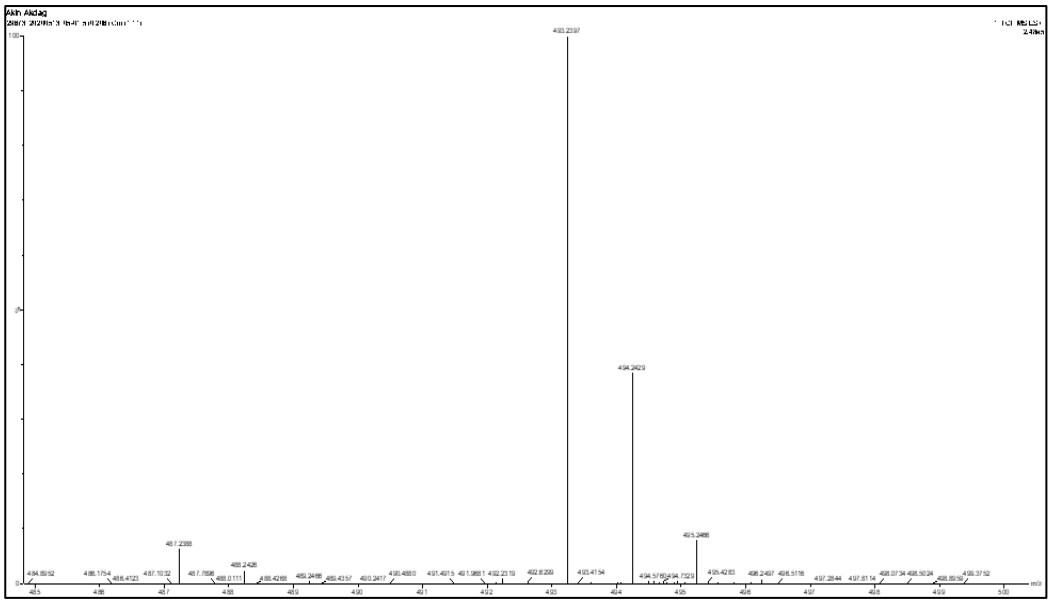

Figure D. 44 HRMS spectrum of compound **25**

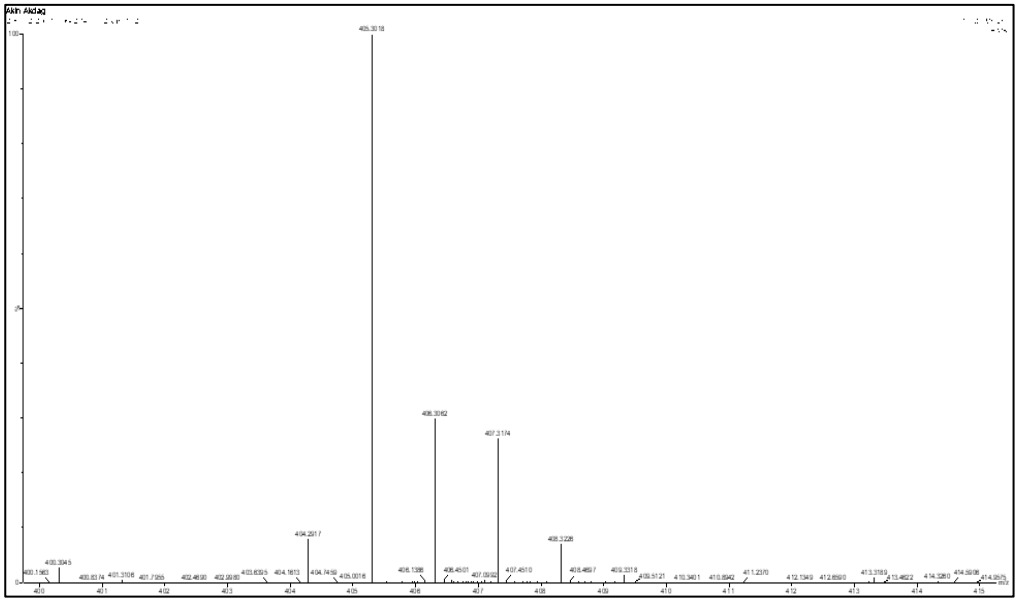

Figure D. 45 HRMS spectrum of compound **26**

8.15 Fluorescence Spectra

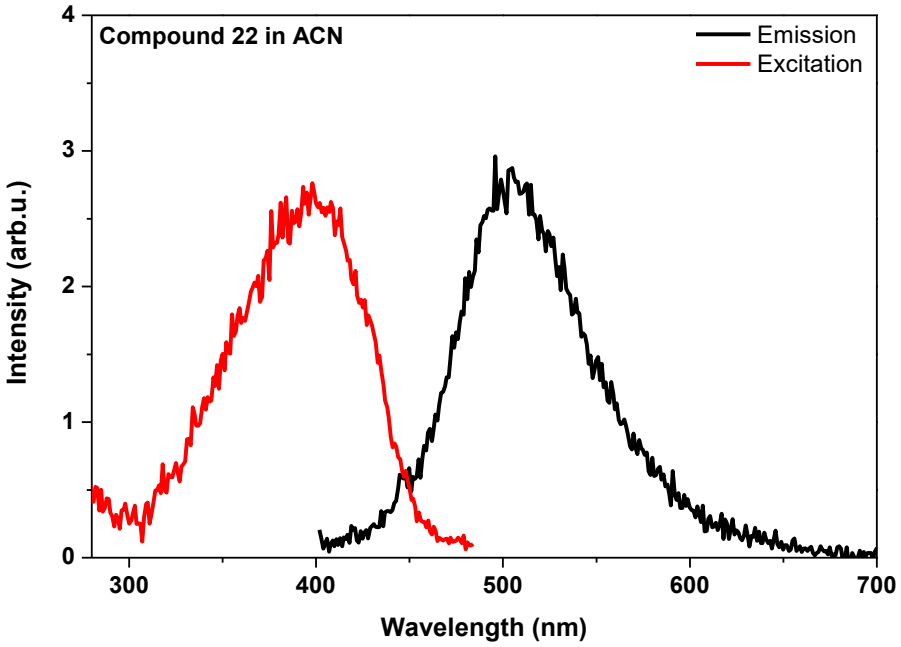

Figure D. 46 Fluorescence absorption and emission spectra of compound **22** in acetonitrile

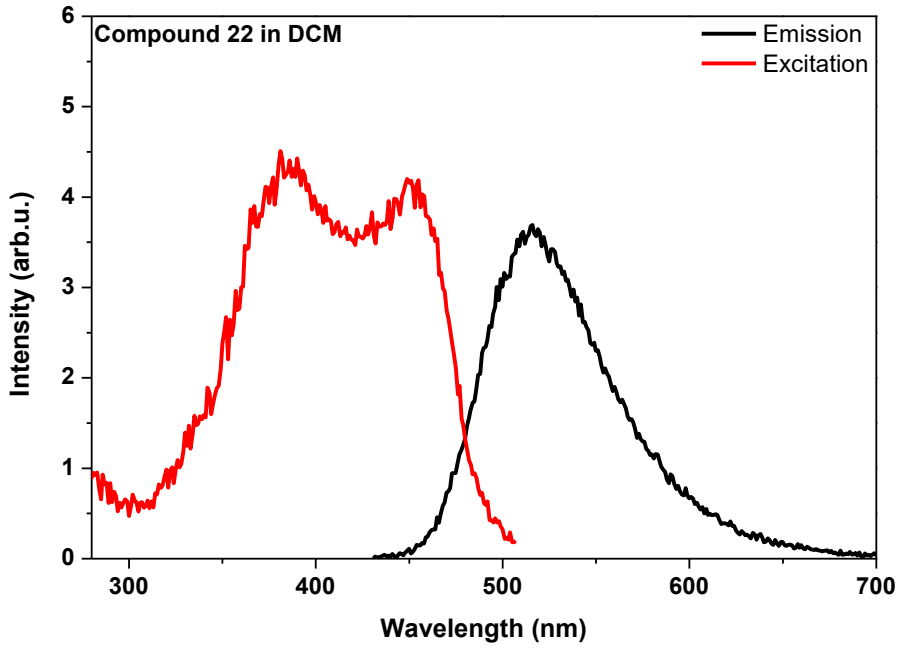

Figure D. 47 Fluorescence absorption and emission spectra of compound **22** in dichloromethane

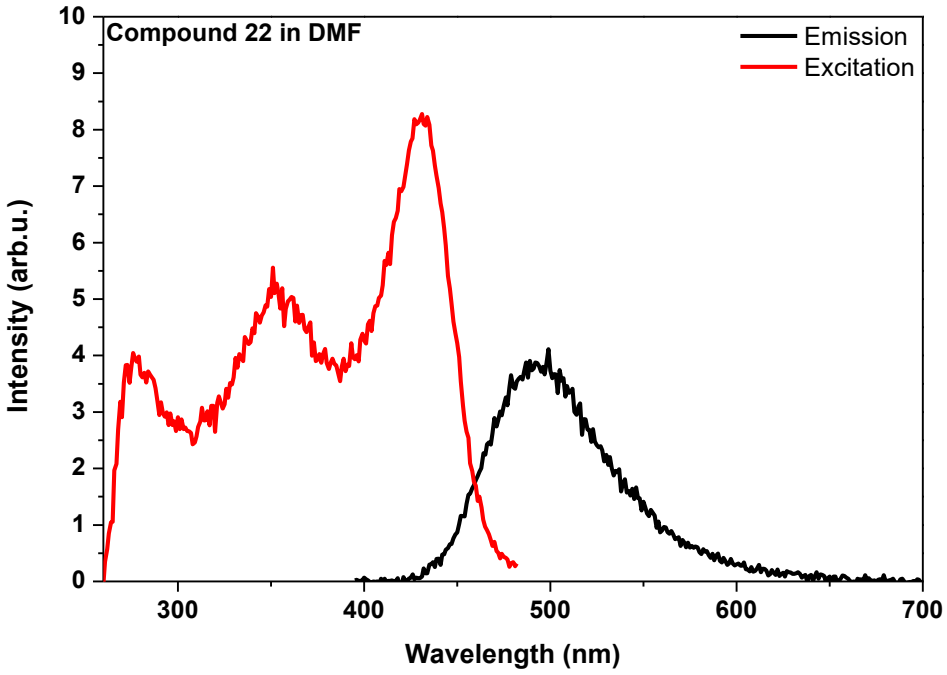

Figure D. 48 Fluorescence absorption and emission spectra of compound **22** in dimethylformamide

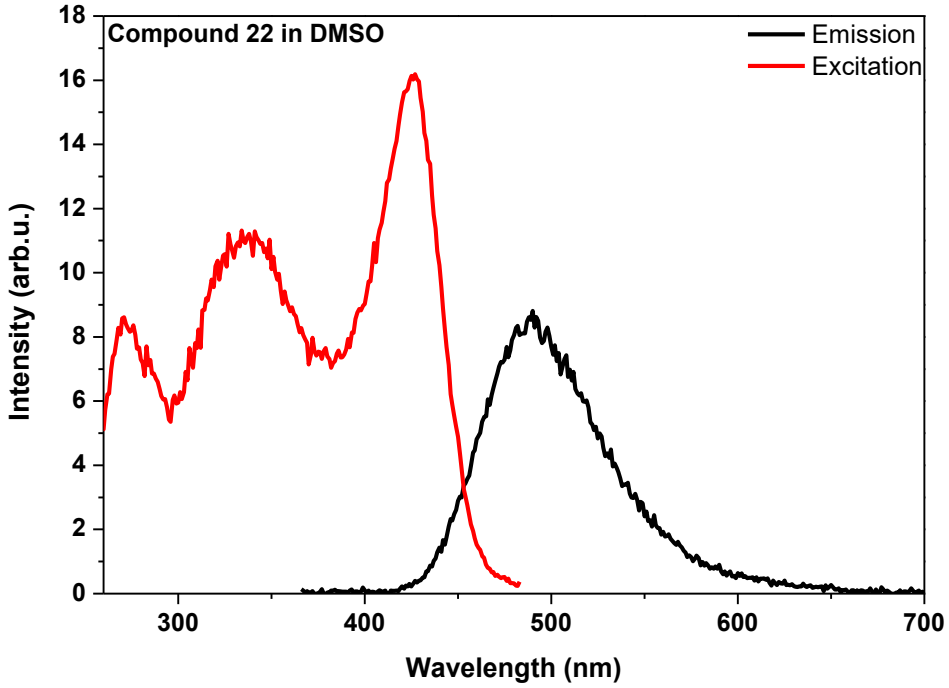

Figure D. 49 Fluorescence absorption and emission spectra of compound **22** in dimethylsulfoxide

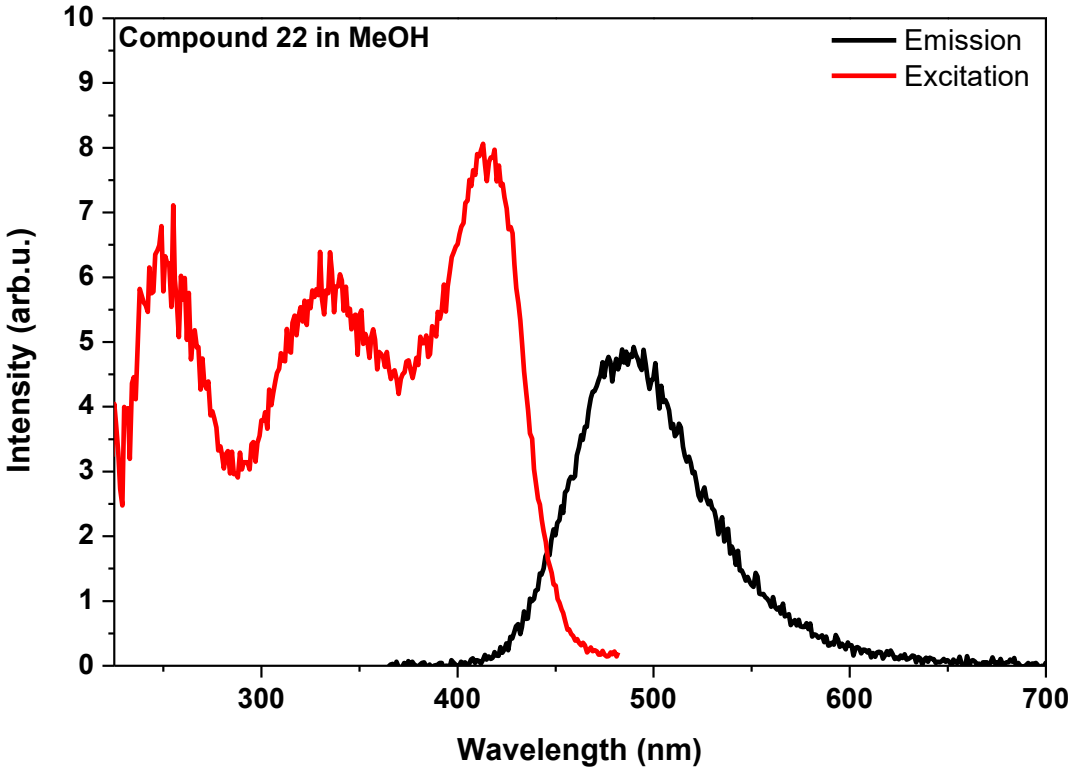

Figure D. 50 Fluorescence absorption and emission spectra of compound **22** in methanol

8.16 XY Coordinates of Optimized Structures

8.16.1 For 25-C1

C	2.976354	-2.758066	1.390960
C	2.877088	-1.339359	1.288366
C	3.880058	-0.647285	0.634989
C	5.003454	-1.312935	0.068443
C	5.090772	-2.740895	0.175726
C	4.047093	-3.435420	0.850122

C	1.673286	-0.595356	1.857014
C	1.413828	-0.889308	3.336627
N	0.463850	-0.894423	1.058908
C	-0.001400	-0.171059	0.001876
C	0.002887	1.252794	0.001023
C	-0.143749	2.004325	1.210621
C	-0.149792	3.375437	1.212350
C	0.011278	4.131061	-0.000557
C	0.168022	3.373182	-1.212613
C	0.153949	2.002127	-1.209379
C	0.015342	5.544344	-0.001342
C	-0.127273	6.279183	1.209368
N	-0.246905	6.851918	2.217514
N	-0.471165	-0.893001	-1.054043
C	-1.677933	-0.587081	-1.853649
C	-1.417474	-0.878379	-3.333598
C	-2.885464	-1.327565	-1.288262
C	-2.993179	-2.745041	-1.399011
C	-4.067137	-3.419268	-0.860607
C	-5.105802	-2.722656	-0.180671
C	-5.009945	-1.295872	-0.065109
C	-3.883488	-0.633506	-0.629366

C	0.162475	6.276999	-1.212835
N	0.285626	6.847940	-2.221574
H	1.860695	0.478615	1.740251
H	-0.297019	3.916356	2.149314
H	-0.310831	1.472310	2.149985
H	0.318395	3.912192	-2.150176
H	0.317989	1.468150	-2.148150
H	0.185578	-1.872197	1.073221
H	-0.199365	-1.872616	-1.066820
H	-1.861060	0.487356	-1.734345
H	-3.817958	0.454445	-0.533484
C	-6.044110	-0.589779	0.611052
C	-6.230870	-3.386316	0.382766
H	-4.137644	-4.506267	-0.957334
H	-2.220627	-3.312421	-1.926558
H	-2.313979	-0.651365	-3.929270
H	-0.583024	-0.267283	-3.709184
H	-1.163137	-1.937017	-3.504293
H	3.821010	0.441572	0.545382
C	6.042679	-0.608935	-0.602096
C	6.212718	-3.407797	-0.390092
H	4.111114	-4.523363	0.940528

H	2.199683	-3.323977	1.914069
H	2.312047	-0.667091	3.931507
H	0.582155	-0.276068	3.714928
H	1.156017	-1.947494	3.505033
C	7.117726	-1.284789	-1.140857
C	7.203929	-2.696404	-1.033791
H	6.278067	-4.496039	-0.305563
H	8.061833	-3.219085	-1.464030
H	7.909746	-0.732739	-1.652875
H	5.975861	0.479316	-0.683484
C	-7.122331	-1.262507	1.147339
C	-7.217015	-2.672929	1.032012
H	-5.970838	0.497569	0.698708
H	-7.910361	-0.708863	1.663773
H	-8.077376	-3.193073	1.460416
H	-6.302673	-4.473637	0.291883

8.16.2 For 25-C2

C	-6.894250	-0.373969	-0.753031
C	-7.825579	0.441731	-0.048890
C	-7.368536	-1.103921	-1.880316
N	-7.727658	-1.713188	-2.806296

N	-8.563683	1.118338	0.546959
C	-5.546141	-0.455708	-0.347344
C	-4.594716	-1.284022	-1.039272
C	-5.048951	0.284791	0.781761
C	-3.738787	0.204095	1.170541
C	-3.286022	-1.356713	-0.643548
C	-2.785614	-0.616788	0.479711
H	-4.938643	-1.877322	-1.888783
H	-2.621423	-2.034639	-1.185444
H	-5.737410	0.935381	1.324624
H	-3.414227	0.815795	2.016790
C	-1.427185	-0.697162	0.889218
N	-0.456677	-1.118268	0.026921
N	-1.068153	-0.363741	2.166181
H	-0.766384	-1.129316	-0.939043
H	-1.859751	-0.355132	2.797321
C	0.048503	0.514704	2.629843
C	0.551631	-2.145548	0.342416
H	-0.432043	1.116531	3.421313
C	1.170740	-0.267662	3.315927
C	0.495852	1.521885	1.574990
C	1.949581	-1.797446	-0.155199

C	0.092248	-3.507069	-0.214291
H	0.811345	-4.295487	0.052790
H	-0.894479	-3.782966	0.189562
H	0.028378	-3.479344	-1.314661
C	1.811086	1.655992	1.174773
C	2.209463	2.649176	0.234090
C	1.219628	3.527678	-0.315762
C	-0.130272	3.374692	0.110567
C	-0.478444	2.409364	1.026482
H	2.585632	0.998326	1.571484
C	3.563130	2.796181	-0.178859
C	1.619235	4.517541	-1.255427
H	-0.892620	4.045158	-0.295232
H	-1.521094	2.325056	1.341680
C	3.920907	3.767563	-1.091525
C	2.940578	4.635951	-1.635070
H	4.318026	2.123936	0.237478
H	4.964606	3.871749	-1.398759
H	3.236625	5.401485	-2.356696
H	0.861013	5.186258	-1.671927
H	1.838644	0.421325	3.854526
H	0.743171	-0.967889	4.049103

H	1.783133	-0.841046	2.606798
H	0.580537	-2.220204	1.437490
C	3.052059	-2.354859	0.469180
C	4.375377	-2.129665	-0.000366
C	4.567052	-1.301343	-1.156455
C	3.421738	-0.734849	-1.780422
C	2.153436	-0.972013	-1.294943
H	2.917728	-2.995030	1.347419
C	5.516483	-2.697019	0.634841
C	5.889889	-1.074222	-1.630433
H	3.559612	-0.092641	-2.654121
H	1.299535	-0.500087	-1.784653
C	6.785213	-2.458300	0.150247
C	6.974307	-1.639380	-0.992982
H	5.371390	-3.329408	1.515153
H	7.652495	-2.901450	0.646066
H	7.985230	-1.459522	-1.367083
H	6.032335	-0.443640	-2.512262

8.16.3 For 25-C3

C	-1.847566	4.667054	-0.349857
C	-1.008576	5.802566	-0.168453

C	-3.241863	4.891395	-0.528136
N	-4.388055	5.045104	-0.674407
N	-0.295878	6.712282	-0.015708
C	-1.313617	3.358419	-0.346450
C	0.089588	3.115353	-0.147884
C	-2.142573	2.199959	-0.539708
C	-1.624880	0.930181	-0.517733
C	0.603905	1.844686	-0.142944
C	-0.229026	0.691397	-0.316239
H	-3.209026	2.344460	-0.724279
H	-2.290216	0.086956	-0.702875
H	1.672423	1.715313	0.051072
H	0.750483	3.968409	0.018323
C	0.328674	-0.618416	-0.337821
N	-0.340678	-1.751510	0.017149
N	1.610577	-0.786472	-0.765737
H	2.015920	0.003091	-1.256253
C	-1.347555	-1.974554	1.087153
H	0.058065	-2.607450	-0.347403
C	-1.154118	-1.047035	2.287834
H	-1.759127	-1.408776	3.131465
H	-0.100631	-1.052583	2.604996

H	-1.443425	-0.009782	2.075549
C	-2.780720	-2.066540	0.553752
H	-1.103014	-2.992121	1.442072
C	-3.848220	-1.434451	1.162241
C	-5.179102	-1.571997	0.672799
C	-5.418716	-2.392861	-0.477557
C	-4.307060	-3.040114	-1.086954
C	-3.034219	-2.882612	-0.588080
H	-3.696014	-0.796755	2.034517
C	-6.280166	-0.913073	1.287388
C	-6.747323	-2.527464	-0.966038
H	-4.478552	-3.669409	-1.964571
H	-2.202263	-3.390071	-1.083641
C	-7.558048	-1.061824	0.789293
C	-7.794130	-1.876765	-0.346154
H	-6.097732	-0.280469	2.160242
H	-8.394531	-0.546941	1.268086
H	-8.811144	-1.984559	-0.731272
H	-6.926225	-3.153897	-1.844185
C	2.524860	-1.903565	-0.476692
C	2.583994	-2.897737	-1.641885
C	3.874607	-1.333814	-0.048428

H	2.103300	-2.422786	0.400608
C	3.940429	-0.624184	1.188058
C	5.118889	-0.066245	1.626646
C	6.313035	-0.177335	0.858229
C	6.259840	-0.887285	-0.386199
C	5.022269	-1.453671	-0.808539
H	3.036173	-0.524943	1.795121
H	5.151289	0.470572	2.578497
C	7.548633	0.386389	1.279344
C	7.447137	-1.004948	-1.161088
H	5.011283	-1.993197	-1.757740
C	8.631512	-0.446653	-0.726220
C	8.683050	0.255166	0.504979
H	7.407613	-1.545884	-2.110638
H	9.536499	-0.543298	-1.331059
H	9.627098	0.693578	0.837651
H	7.585386	0.928415	2.228074
H	3.258716	-3.736158	-1.413122
H	1.585682	-3.311980	-1.854190
H	2.932545	-2.412103	-2.566074

8.16.4 For the complex between compound 25 and (*S*)-α-methylbenzyl amine

C	-6.027616	-3.724378	0.192824
C	-5.684250	-2.738875	1.095025
C	-4.318505	-2.465716	1.387303
C	-3.298780	-3.235022	0.732966
C	-3.687662	-4.245261	-0.191488
C	-5.020311	-4.483274	-0.456261
C	-1.933257	-2.965411	1.031139
C	-1.562652	-1.984711	1.933378
C	-2.585180	-1.226815	2.577223
C	-3.918481	-1.459684	2.312035
C	-0.086482	-1.698047	2.197065
C	0.258657	-1.586712	3.685175
N	0.323405	-0.477878	1.472932
C	1.001529	-0.419297	0.291239
C	2.044763	-1.345709	-0.023442
C	2.279095	-1.772354	-1.367649
C	3.265087	-2.675346	-1.678579
C	4.128999	-3.224285	-0.670114
C	3.898302	-2.784163	0.677733
C	2.897042	-1.895785	0.983093

C	5.152052	-4.150064	-0.988166
C	5.989370	-4.693211	0.025674
N	6.658516	-5.119633	0.880105
N	0.619226	0.569528	-0.553010
C	1.530181	1.366197	-1.395070
C	0.881908	1.666087	-2.750648
C	1.976603	2.631440	-0.667026
C	1.023604	3.599134	-0.233881
C	1.421184	4.745381	0.417833
C	2.797096	5.001549	0.679981
C	3.765288	4.033673	0.251772
C	3.316541	2.859355	-0.416942
C	3.243697	6.175096	1.348266
C	4.586884	6.384045	1.583993
C	5.544490	5.426975	1.162070
C	5.142784	4.278627	0.511523
C	5.371886	-4.565610	-2.330888
N	5.524787	-4.886370	-3.441490
H	2.424721	0.756406	-1.567850
H	3.394091	-3.003288	-2.712078
H	1.622131	-1.411299	-2.162685
H	4.550829	-3.158819	1.469000

H	2.785797	-1.559699	2.016329
H	-0.316858	0.974369	-0.375898
H	-0.244319	0.341070	1.673475
H	0.494659	-2.521347	1.763727
H	-1.164251	-3.558445	0.527343
H	-4.689471	-0.877945	2.825197
H	-2.315496	-0.459702	3.308249
H	-0.074794	-2.486078	4.224352
H	1.344479	-1.480335	3.823051
H	-0.222307	-0.713916	4.154964
H	4.062750	2.125572	-0.736207
H	0.678519	5.479885	0.742245
H	-0.040428	3.428494	-0.418060
H	1.573708	2.243157	-3.381676
H	0.624997	0.733262	-3.275849
H	-0.038653	2.260455	-2.636825
H	2.503555	6.911855	1.672740
H	4.918699	7.289766	2.097776
H	6.605614	5.603331	1.354982
H	5.880517	3.540055	0.186386
H	-2.911216	-4.832557	-0.688904
H	-5.305560	-5.262178	-1.167577

H	-7.079496	-3.926712	-0.023432
H	-6.459549	-2.157058	1.601204
N	-2.275088	1.443874	-0.072398
H	-2.418019	2.310222	0.451338
H	-2.697587	0.706899	0.500003
C	-2.991251	1.532231	-1.366662
C	-4.413094	2.071705	-1.236208
C	-2.933224	0.174416	-2.072490
H	-2.430327	2.256645	-1.981903
C	-5.399416	1.367634	-0.523546
C	-6.692973	1.878819	-0.398381
C	-7.026806	3.104250	-0.985868
C	-6.057198	3.812885	-1.698692
C	-4.761939	3.298353	-1.820078
H	-5.160083	0.404380	-0.063853
H	-7.447860	1.315674	0.156679
H	-8.039864	3.502599	-0.888947
H	-6.307536	4.770164	-2.163116
H	-4.008781	3.859540	-2.381767
H	-3.467535	-0.599669	-1.497817
H	-3.399189	0.233561	-3.067033
H	-1.889609	-0.153676	-2.191909

8.16.5 For the complex between compound 25 and (*R*) -*α*-methylbenzyl amine

C	4.900541	-3.176699	0.137255
C	4.366900	-2.403833	-0.908182
C	5.247923	-1.640185	-1.686981
C	6.623712	-1.646230	-1.433417
C	7.140526	-2.417649	-0.389573
C	6.272834	-3.183599	0.397082
C	2.868020	-2.399053	-1.204072
H	2.693183	-1.636499	-1.981665
N	2.035924	-2.007654	-0.045362
N	-0.699050	-0.609827	-0.547593
C	-1.726176	-1.174758	-1.441439
C	-2.419542	-2.370153	-0.793530
C	-1.672282	-3.503336	-0.357782
C	-2.298285	-4.586869	0.217813
C	-3.710533	-4.610576	0.397078
C	-4.472293	-3.474107	-0.033939
C	-3.791049	-2.371545	-0.623198
C	-5.883913	-3.484920	0.145312
C	-6.513376	-4.568873	0.721428
C	-5.759951	-5.692872	1.145859

C	-4.389618	-5.712358	0.987213
C	-0.903989	0.390159	0.341163
C	-1.787574	1.486555	0.084599
C	-1.941961	2.028731	-1.228511
C	-2.767631	3.097248	-1.476884
C	-3.537485	3.712944	-0.431735
C	-3.389944	3.155791	0.884194
C	-2.545698	2.100682	1.128348
C	-4.395323	4.810827	-0.685689
C	-4.535153	5.341918	-1.997959
N	-4.625762	5.753669	-3.085187
N	-0.216521	0.295323	1.515313
C	0.391505	1.415671	2.263959
C	0.227347	1.190035	3.768624
C	1.837618	1.625918	1.823922
C	2.161919	2.680705	0.990234
C	3.489349	2.884326	0.518836
C	4.516122	1.963616	0.913906
C	4.165388	0.886293	1.775895
C	2.869921	0.725089	2.220942
C	3.831381	3.970340	-0.335090
C	5.127287	4.137217	-0.777098

C	6.141554	3.225547	-0.387101
C	5.842402	2.162126	0.439186
C	-5.140345	5.416408	0.364024
N	-5.737256	5.890247	1.246576
C	-1.115506	-1.510474	-2.806116
H	-2.486420	-0.398883	-1.587647
H	-2.835753	3.506659	-2.486860
H	-1.346666	1.618136	-2.047828
H	-3.979273	3.578937	1.700217
H	-2.494088	1.685527	2.137932
H	0.145776	-1.186542	-0.403534
H	0.216197	-0.608970	1.682997
H	-0.170080	2.314152	1.983766
H	1.384780	3.383797	0.676396
H	4.945714	0.187793	2.089933
H	2.640744	-0.099392	2.902512
H	0.686134	2.016269	4.331714
H	-0.838453	1.133256	4.035806
H	0.705292	0.253649	4.099644
H	-4.380899	-1.507815	-0.944568
H	-1.712265	-5.450078	0.546082
H	-0.585594	-3.511312	-0.474976

H	-1.888715	-1.908552	-3.479439
H	-0.677639	-0.611986	-3.267977
H	-0.324159	-2.271542	-2.720411
H	-3.806895	-6.578038	1.314299
H	-6.271117	-6.545237	1.600412
H	-7.598223	-4.564722	0.853244
H	-6.463914	-2.617550	-0.181322
H	3.049249	4.672728	-0.635367
H	5.377691	4.976044	-1.431261
H	7.164042	3.370793	-0.744641
H	6.621115	1.456274	0.739816
H	2.070876	-2.745787	0.662038
H	2.454583	-1.184930	0.397729
C	2.393779	-3.748595	-1.752532
H	4.851914	-1.028055	-2.502645
H	7.291936	-1.043126	-2.053362
H	8.214843	-2.424897	-0.189077
H	6.668554	-3.793400	1.213519
H	4.239829	-3.787434	0.760431
H	2.968520	-4.028113	-2.647529
H	2.529855	-4.550747	-1.007738
H	1.327570	-3.711482	-2.023117

CURRICULUM VITAE

PERSONAL INFORMATION

Surname, Name: Tan, Duygu
Nationality: Turkish (TC)
Date and Place of Birth: 3 August 1986, Ankara
Marital Status: Married
Phone: +90 507 271 10 26
email: duyguaksakaltan@gmail.com

EDUCATION

Degree	Institution	Year of Graduation
MS	METU Chemistry	2013
BS	METU Secondary Science and Mathematics Education	2010
High School	Hasan Ali Yücel Anatolian Teacher's High School, Ankara	2004

WORK EXPERIENCE

Year	Place	Enrollment
January 2019- June 2019	METU, Department of Chemistry	Research Assistant
2015-2019	METU Central Laboratory	Research Assistant
2010-2015	METU, Department of Chemistry	Research Assistant

FOREIGN LANGUAGES

Advanced English, Beginner French

PUBLICATIONS

1. Tan, D & Akdag, A. Synthesis of new flexible coumarin dimers for sodium and potassium differentiation *J Fluoresc*. 2020, 30(1), 27-34. doi:10.1007/s10895-020-02492-4.
2. Dogan, O., & Tan, D. Enantioselective Direct Aldol Reactions Promoted by Phosphine Oxide Aziridinyl Phosphonate Organocatalysts. *Tetrahedron: Asymmetry,* 2015, 26 (23), 1348-1353. doi:10.1002/chin.201616025.